Title
Reduction Chemistry of Rare-Earth Metal Complexes: Toward New Reactivity and Properties

Author
Huang, Wenliang

Publication Date
2013

Peer reviewed|Thesis/dissertation

UNIVERSITY OF CALIFORNIA

Los Angeles

Reduction Chemistry of Rare-Earth Metal Complexes: Toward New Reactivity and Properties

A dissertation submitted in partial satisfaction of the requirements for the degree Doctor of Philosophy in Chemistry

by

Wenliang Huang

2013

ABSTRACT OF THE DISSERTATION

Reduction Chemistry of Rare-Earth Metal Complexes:

Toward New Reactivity and Properties

by

Wenliang Huang

Doctor of Philosophy in Chemistry

University of California, Los Angeles, 2013

Professor Paula L. Diaconescu, Chair

Rare-earths are a group of metals with fascinating physical properties and intriguing chemical reactivity. Organometallic rare-earth chemistry is of particular interest because of the increasing number of their applications in industry and consumer goods as well as the importance of understanding their physical and chemical properties. Despite the dominance of the trivalent oxidation state, recently, low-valent organometallic rare-earth compounds were characterized and showed interesting reactivity toward various molecules. The theme of this thesis is the reduction chemistry of rare-earth metal complexes. By utilizing an electronically and geometrically flexible ferrocene diamide ligand (NN^{TBS} = $fc(NSi^tBuMe_2)_2$, fc =1,1′-

ferrocenediyl), unprecedented reactivity was discovered together with the synthesis and characterization of a series of rare-earth metal arene complexes. The fruitful reduction chemistry allowed: (1) the discovery of a new aromatic C-H and C-F bond activation mechanism for rare-earths; (2) the synthesis of the first scandium naphthalene complex and a reactivity study on P_4 activation by rare-earth arene complexes; (3) the isolation and characterization of a 6C, 10π-electron aromatic system stabilized by coordination to rare-earth metal ions. Recently, an improved method to access paramagnetic rare-earth starting materials for organometallic chemistry was developed in order to study the physical and chemical properties of paramagnetic rare-earth biphenyl complexes.

The dissertation of Wenliang Huang is approved.

Bruce S. Dunn

Neil K. Garg

Richard B. Kaner

Paula L. Diaconescu, Committee Chair

University of California, Los Angeles

2013

DEDICATION

Dedicated to my beloved grandpa, who passed away in the third year of my PhD.

Rest in peace, and you will always be with us.

Below are words in my native language to express my love to the person to whom this thesis is dedicated to.

“大大，我爱你，愿主与你同在。”

TABLE OF CONTENTS

List of Charts, Figures, Equations, Schemes, and Tables

Lists of Charts

List of Figures

List of Equations

List of Schemes

Lists of Tables

PREFACE

Thanks to all who have helped, encouraged, supported, and inspired me during my PhD time.

Chemistry! I feel I have so much to share on it. My chemistry course started in the ninth grade much later than mathematics and physics. My first major science competition award was in chemistry, which helped me get admitted to an elite class in one of the best high schools in China. The elite class was designed to train students in a specific course to win the International Olympiad in math, physics, chemistry, biology, and computer science. At that time, the winners of regional science competitions were granted admission to the top universities in China. Thousands of students participated in those competitions to fight for a small number of positions. Fortunately, I won the national first prize in chemistry and got admitted to one of the best universities in China, Peking University. Nowadays, the high school science competition system is blamed for killing the real interest of young students and squeezing their leisure time. In my opinion, if you participate in the competition only for the sake of admission to university, it is not worth it and most likely you will not succeed; however, if you participate because you are interested, you can really benefit a lot from the numerous resources provided by the system. I was able to listen to lectures taught by distinguished professors, get access to college level textbooks, and, perhaps particularly important for chemistry, perform sophisticated chemical experiments, such as the synthesis and analysis of aspirin that required both organic synthesis and analytical measurements. While preparing for those competitions, I met Professor Zipeng Yao, who guided me into the world of chemistry. Overall, I built up a strong chemistry background that benefits me even now.

However, my road since then was not smooth at all. In my first year at Peking University, I was ambitious to get a triple major in math, physics, and chemistry because my dream was to establish chemistry the way mathematicians and physicists established math and physics. That only resulted in a low GPA. I realized that I had to have a more realistic goal. In my second year, I joined a computational chemistry group led by Professor Yun-dong Wu. It was there that I first encountered organometallic chemistry. My project was to study the mechanism of the Pauson-Khand reaction by DFT calculations. I have to admit that the project itself did not go too well: the proposed mechanism based on my calculations led to a highly stable intermediate, which should have but was never observed experimentally. That was a dead end. What I learned from that experience was that experiment not theory is the soul of chemistry.

Disappointed by the failed project and the decadent atmosphere in the graduate school, I was pessimistic about my future when I applied for a PhD in chemistry. Fortunately, UCLA gave me an offer at the last minute. I had no idea what field I wanted to pursue. Then came the big moment. After the new student orientation, I was waiting outside Professor Diaconescu's office to ask about my performance in the entrance exam since she was the inorganic graduate student advisor at the time. Just out of curiosity, I started to look at the papers stuck to the board outside her office. Suddenly, I realized that this is the chemistry I dreamed to do. When it was my turn, I told her that I would like to join her group to do the organometallic chemistry.

Here come my five years of PhD in Paula's group. I would like to say that together we climbed high mountains and crossed large seas. There were definitely some bad moments, particularly in my first two years. There were more sweet moments. A particular one that I will remember forever is: When I identified the two products in the benzene activation reaction to be scandium hydride and scandium phenyl, I was very excited about it and planned to tell the good

news to Paula in the weekly individual meeting. She looked blue and tired at the meeting, so I told her my research news was going to cheer her up. And it did cheer her up. Not only was that the best moment during my PhD, the chemistry we discussed that day also became the theme of my PhD thesis.

During my PhD, I worked on several projects involving collaborations. Dr. Thibault Cantat at CEA, France, helped me a lot with computational studies; Dr. Jeffrey T. Miller at Argonne National Laboratory obtained important information for my compounds using his expertise in X-ray absorption near edge structure spectroscopy; Professor Muralee Murugesu at University of Ottawa is collaborating with us on a single-molecule magnet project. Without those excellent collaborators, I could not achieve as much as I had. In my last year of PhD, Professor Karsten Meyer at Friedrich-Alexander-University Erlangen-Nuremberg invited me for an academic visit, where I studied the EPR and Mössbauer spectra of several compounds and learned about the German culture. Thank you, Karsten. The list goes on and on and I need to stop at some point. In the end, I would like to thank all my committee members for supervising my research and academic growth.

Although research composed the majority of my life during my PhD period, I believe that maintaining a balance life is essential to have a successful career. In reality, my life was a mess before my wife (at that time my girlfriend) Lanfeng decided to quit her master program and come to the U.S. to accompany me. We got married in Las Vegas in February 2009. Together we got through a lot of difficult times. Things turned out to move in a positive direction recently. Two years before my graduation, she got a Master's degree in accounting and found a job in the well-known accounting firm KPMG. We have done a lot travelling, especially road trips, these

years. When I encountered problems, I often turned to her for advice. Not being a scientist, her perspective always gives me refreshing ideas.

Although I do not consider myself a very social person, I have still made some friends at UCLA and I am grateful for their friendship. My labmate, Erin Broderick, shared a glove-box with me for three years. She was the ideal labmate I could imagine to have. Even after she graduated, we kept in touch. My former roommate, Hexiang Deng, was a graduate student in Professor Omar Yaghi's group. Besides being an outstanding scientist, he was also a good friend to me. He is now a full professor in Wuhan University in China under a program for talented young investigators. I am a heavy user of the nuclear magnetic resonance (NMR) spectrometers and the X-ray crystallography instrument. Bob Taylor, who is in charge of the NMR facility, and Saeed Khan, who is in charge of the X-ray crystallography laboratory, helped me a lot with setting up elaborate NMR experiments and solving difficult molecular structures, respectively, and they also taught me a lot about the basics of each instrument. I had a good time in the Department of Chemistry here. I would like to acknowledge the following people Ricky Ruiz, Dr. Johnny Pang, Dr. Ignacio Martini, Dr. Jane Strouse, and Dr. Dafni Amirsakis and thank them for their help and advice.

Lastly but most important, I would like to thank my family. Without their full support, I cannot imagine finishing my PhD. My parents always encouraged me to pursue my dream. Recently, they visited Los Angeles and attended my graduation ceremony. I lived with my grandparents in my childhood and I love them as much as I love my parents. Two years ago, my grandpa passed away. I was not able to be with him at his last moment. I was terribly sorry when I heard it on the phone. This is my biggest regret. Rest in peace, grandpa! I love you and will always remember your advice to be an honest and kindly man.

VITA

EDUCATION

B.Sc. Chemistry Peking University 2008

AWARDS

2013 UCLA, Inorganic Chemistry Dissertation Award

2012 UCLA, Dissertation Year Fellowship

2011 UCLA, The Ernest F. Hare, Jr. Memorial Scholarship

2010 UCLA, Excellence in Second Year Academics and Research Award

2008 Peking University, Graduate with honor

2006 Peking University, Wu-Si Scholarship

2004 Peking University, First Freshmen Scholarship

2004 First Prize in Chinese National Chemistry Olympic Competition

PUBLICATIONS

1. *P_4 Activation by Lanthanum and Lutetium Naphthalene Complexes Supported by a Ferrocene Diamide Ligand*, Huang, W.; Diaconescu, P. L. *Eur. J. Inorg. Chem.* **2013**, *22-23*, 4090.

2. *Synthesis and Characterization of Paramagnetic Lanthanide Benzyl Complexes*, Huang, W.; Upton, B. M.; Khan, S. I.; Diaconescu, P. L. *Organometallics* **2013**, *32*, 1379.

3. *A Six-carbon, 10π-electron Aromatic System Supported by Group 3 Metals*, Huang, W.; Dulong, F.; Wu, T.; Khan, S. I.; Miller, J. T.; Cantat, T.; Diaconescu, P. L. *Nat. Commun.* **2013**, *4*, 1448.

4. *P_4 activation by Group 3 Metal Arene Complexes*, Huang, W.; Diaconescu, P. L. *Chem. Commun.* **2012**, *48*, 2216.

5. *Visible-Light-Induced Reversible C-C Bond Formation of an Imidazole-derived Scandium Complex*, Huang, W.; Diaconescu, P. L. *Inorg. Chim. Acta* **2012**, *380*, 274.

6. *Inverted Sandwiches of Scandium Arene Complexes Supported by a Ferrocene Diamide Ligand*, Huang, W.; Khan, S. I.; Diaconescu, P. L. *J. Am. Chem. Soc.* **2011**, *133*, 10410.

7. *Transmetalation Reactions of a Scandium Complex Supported by a Ferrocene-Diamide Ligand*, Huang, W.; Carver, C. T.; Diaconescu, P. L. *Inorg. Chem.* **2011**, *50*, 978.

8. *Group 3 Metal Complexes of Radical-Anionic 2,2'-Bipyridyl Ligands*, Williams, B. N.; Huang, W.; Miller, K. L.; Diaconescu, P. L. *Inorg. Chem.* **2010**, *49*, 11493.

CONFERENCE PRESENTATIONS

04/2013 The 245th ACS National Meeting, New Orleans, LA

03/2012 The 243rd ACS National Meeting, San Diego, CA

03/2011 The 241st ACS National Meeting, Anaheim, CA

03/2010 The 239th ACS National Meeting, San Francisco, CA

07/2012 Organometallic Chemistry Gordon Research Seminar & Conference, Newport, RI

07/2011 Organometallic Chemistry Gordon Research Seminar & Conference, Newport, RI

TEACHING EXPERIENCE AT UCLA

Organometallic Chemistry lecture, General Chemistry lecture, Organometallic Chemistry laboratory, Advanced Organic Chemistry laboratory, General Chemistry laboratory, Biochemistry laboratory

CHAPTER 1: INTRODUCTION

1.1 Rare-earth metals and their applications in industry and consumer goods

Rare-earths is a collective name for a group of elements whose physical and chemical properties are similar and encompass scandium, yttrium, and all the lanthanides. Because of their similar properties, they usually are found in minerals together. Such minerals were first discovered in the late 18th century.[1] Not until the great English physicist Henry Gwyn Jeffreys Moseley used X-ray spectroscopy to assign atomic numbers was the exact number of lanthanides determined to be 15. He also pointed out the absence of element 61, which was later discovered from the fission products of uranium fuel irradiated in a graphite reactor and was named promethium. Even Nature could only separate the rare-earths into two sub-groups: light elements (including Sc, La, Ce, Pr, Nd, Pm, Sm, Eu, and Gd) and heavy elements (including Tb, Dy, Ho, Er, Tm, Yb, Lu, and Y). The rare-earths in the same sub-group usually coexist in minerals. Unlike other metals, which are usually found concentrated in several types of minerals, rare-earths are highly dispersed in the Earth's crust and very few minerals (previously called "earths") contain a high concentration of these elements. Therefore, the term "rare earth" was coined to describe them. However, their actual abundance is much higher compared to that of noble metals and similar to that of some major industrial metals such as cobalt, nickel, and copper.[2]

The two opposite sides, their relative abundance and the difficulty in separating individual rare-earths from the already less concentrated minerals, set up a challenging area for generations of chemists and engineers. How to extract these elements from certain minerals and then to separate them into individual metals are still ongoing projects. The lack of economic and

environmental benign processes limits the production of rare-earths and makes research into the properties of their compounds an imperative.

In spite of the strenuous processes to obtain pure rare-earths, they are essential to numerous industrial applications and consumer goods. For example, rare-earths are heavily used in fuel-efficient hybrid cars. In a leading model of hybrid car, 1 kilogram of neodymium was required for building the electric motor, while 10 to 15 kilograms of lanthanum was used for the battery.[3] The number of applications of rare-earths is expected to explode in the future because of their unique physical properties, especially magnetism and luminescence. Lanthanide single molecule magnets are superior to transition metal counterparts because of the larger single ion anisotropy (large J values for lanthanides).[4] Lanthanide luminescence arises from the f-f transitions of the lanthanide ions and has high potential in hybrid materials for the use of lasers and chemical sensors[5] as well as in biomedical analyses and imaging.[6] The active research on fundamental rare-earth chemistry will undoubtedly enhance our understanding of these fascinating elements and their complexes, and, in turn, will improve the quality of human life in the future.

1.2 Organometallic chemistry of rare-earth metals

In the periodic table, the rare-earths are placed between alkaline earth and group 4 metals. As a consequence, four of them, scandium, yttrium, lanthanum, and lutetium, are also classified as group 3 metals. Unlike transition metals that usually have multiple common oxidation states, most rare-earths only have one common oxidation state, +3. Another significant difference between rare-earths and transition metals is that the valence electrons of the former are f electrons, which are barely affected by the ligand field, while the ligand field has a major

influence for the d electrons of the latter. Rare-earths also differ from main group metals, such as group 13 elements, in part because of their empty d orbitals available for ligand coordination. Therefore, rare-earth metal chemistry stands on its own ground and provides unique opportunities for synthetic chemists.

As an interdisciplinary field, the development of organometallic chemistry exploded during the middle of the 20th century, after the milestone discovery of ferrocene (Chart 1-1).[7] Its rapid growth can be recognized by the awardees of the Noble Prize in Chemistry with contributions to organometallic chemistry, including but not limited to: 1963: K. Ziegler and G. Natta, 1973: E. O. Fischer and G. Wilkinson, 1979: H. C. Brown and G. Wittig, 1994: G. A. Olah, 2001: W. S. Knowles, R. Noyori, and K. B. Sharpless, 2005: Y. Chauvin, R. H. Grubbs, and R. R. Schrock, and 2010: R. F. Heck, E.-i. Negishi, and A. Suzuki. The development of organometallic chemistry led to numerous industrial applications, including alkene polymerization using Zieglar-Natta catalysts and ring-opening polymerization based on alkene metathesis. "Genuine" organometallic compounds are those containing metal-carbon bonds. However, organometallic chemistry generally covers any compounds containing metal-element bonds that are of largely covalent character and behave similarly to metal-carbon bonds. For example, amides are similar to cyclopentadienyl (Cp) ligands because they have similar covalent character and basicity.[8]

Not surprisingly, organometallic rare-earth chemistry also had a golden time in the decades after the discovery ferrocene. π Ligands were found to bind rare-earth ions strongly (Chart 1-1).[9] The most popular π ligands are cyclopentadienyl and its derivatives. Binary rare-earth cyclopentadienyl complexes, Cp_3M, were made first,[10] followed by the metallocenes Cp_2MX[11] and half-sandwich $CpMX_2$ complexes[12] (M = rare-earth metals) with X being a

monoanionic ligand. Substituted cyclopentadienyls were next developed in order to adjust their electronic and steric properties. The most important substituted-Cp ligand is pentamethylcyclopentadienyl ($(\eta^5\text{-}C_5Me_5)^-$, commonly referred to as Cp^*), which is more electron donating and more sterically demanding than the non-substituted cyclopentadienyl. Brintzinger and Bercaw pioneered the Cp^* chemistry for group 4 metals.[13,14] Evans,[15] Watson,[16] and Tilley and Anderson[17] were among the first to synthesize Cp^*_2LnX complexes for different lanthanides. Rare-earths are highly electropositive elements and prefer ionic binding similar to alkali and alkali earth metals. As a consequence, rare-earth metal-carbon bonds are highly polarized with a significant amount of negative charge built up on carbon. Because Cp^- is a 5C, 6π-electron aromatic system, cyclopentadienyl ligands can readily diffuse the negative charge through resonance. Therefore, compared to σ bound ligands, cyclopentadienyl binds tightly to rare-earth metals and usually serves as a good ancillary ligand facilitating many reactivity studies on organometallic rare-earth chemistry.[18-20] Until recently, the majority of that chemistry was based on cyclopentadienyl and substituted-cyclopentadienyl as supporting ligands. The coordination chemistry of other π ligands, such as the cyclooctatetraene dianion ($(\eta^8\text{-}C_8H_8)^{2-}$, commonly referred to as OCT^{2-}) that is made famous by the molecule uranocene,[21] and of heterocycles, such as boratabenzene $(\eta^6\text{-}C_5H_5BR)^-$[22] and tetramethylphospholyl $(\eta^5\text{-}C_4Me_4P)^-$,[23] has also been explored (Chart 1-1).[9,24] They behave similarly to cyclopentadienyl but the number of their rare-earth metal complexes is far less because of their relative inaccessibility and difficult modification.

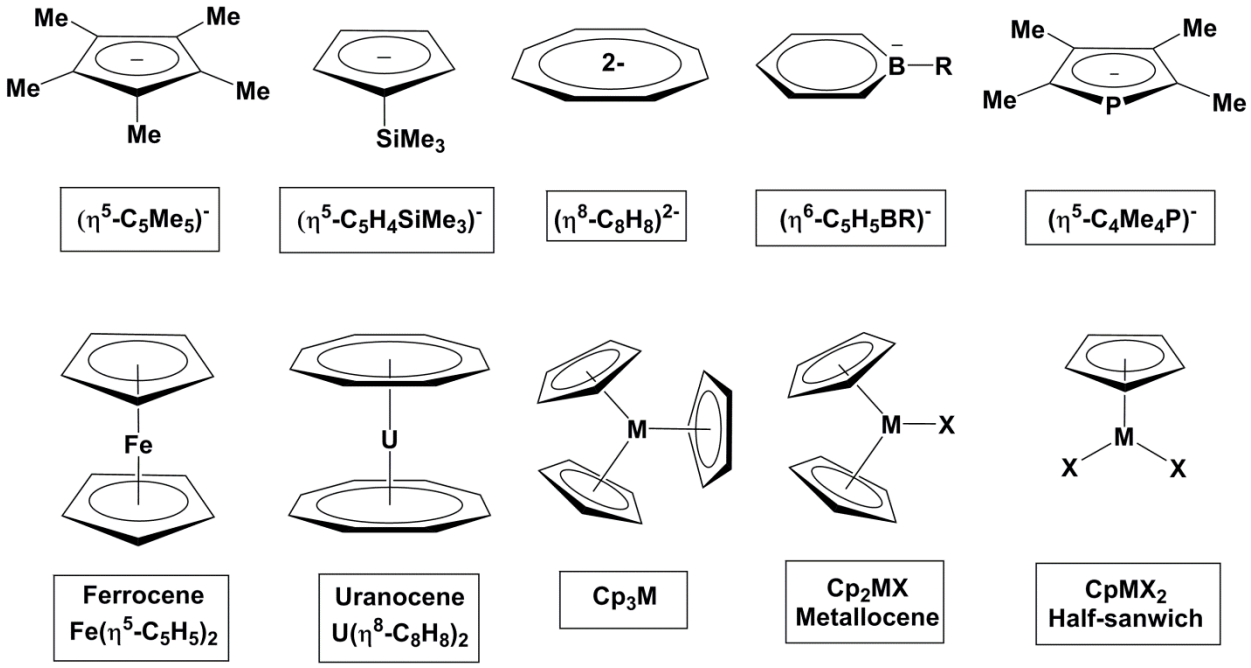

Chart 1-1: Important organometallic complexes and selected π ligands for organometallic rare-earth complexes (abbreviations are the same as in text).

In the last two decades, well defined ancillary ligands other than the aforementioned π ligands have been developed by various groups (Chart 1-2). They are usually electron rich and sterically demanding to compensate the high Lewis acidity and high coordination number of rare-earth ions. Fryzuk and co-workers are pioneers in this area: by combining soft phosphine donors and a hard amide donor, a series of multidentate amidophosphine ligands has been made and incorporated into the coordination sphere of group 3 metals, including the tridentate $N(SiMe_2CH_2P^iPr_2)_2$,[25] tetradentate ($PhP[CH_2(SiMe_2)N(SiMe_2)CH_2]_2PPh$) ($P_2N_2^{2-}$),[26] and, recently, the tetradentate $fc(NP^iPr_2)_2$.[27] Arnold introduced porphyrins as supporting ligands for group 3 metals,[28] and, later, synthesized bis(amidinate) scandium complexes as counterparts of Cp^*_2M.[29] Piers used bulky β-diketiminato ligands to obtain scandium dialkyl[30] and cationic

monoalkyl species,[31] and developed a salicylaldiminato ligand to afford group 3 metal hydrides upon hydrogenation by H_2.[32] Takats introduced the sterically demanding pyrazolylborate ligands (scorpionate) to rare-earth chemistry,[33] specifically for low-valent lanthanide chemistry.[34] Scott achieved the synthesis of triamidoamine complexes of rare-earths using the simple $N(CH_2CH_2NSiMe_3)_3$ ligand.[35] Bercaw introduced the neutral 1,4,7-trimethyl-1,4,7-triazacyclononane (TACN) on group 3 metals[36] that was later modified by Mountford with a monoanionic pendant arm as an anchor.[37] Gade and Mountford also developed a series of diamidopyridine and diamidoamine ligands with flexible backbones for the synthesis of scandium alkyl or aryl complexes.[38] Recently, Mindiola incorporated a pincer-type, rigid tridentate PNP ligand, $N(2\text{-}P^iPr_2\text{-}4\text{-methylphenyl})_2$, on scandium and isolated a rare scandium methylidene complex,[39] and, later, a scandium phosphinidene complex.[40] Chen developed a series of tridentate monoanionic[41] or dianionic[42] β-diketiminato ligands and was able to characterize an unsupported scandium terminal imide.[43] Cavell,[44] Le Floch,[45] and Liddle[46] have synthesized formal rare-earth metal carbene complexes by incorporating carbene in the framework of a chelating bis(iminophosphorano)methylene (N_2C^{2-}) ligand or bis(diphenylthiophosphinoyl)methylene (S_2C^{2-}) ligand. The formal carbene ligand can be viewed as an ancillary ligand because of the stabilization caused by the delocalization of π electrons in the metallocycles.

Our group previously synthesized group 3 metal monoalkyl complexes supported by ferrocene-diamide ligands[47,48] and studied their reactivity toward various organic substrates, including aromatic N-heterocycles[49,50] and other unsaturated substrates.[51] The 1,1′-ferrocenediyl diamide ligands have the general formula $fc(NR)_2$; the system studied the most by us has R = Si^tBuMe_2,[52] while other versions, such as R = $SiMe_3$,[53] $SiPhMe_2$,[54] adamantyl,[55] 2,4,6-

trimethylphenyl, and 3,5-dimethylphenyl,[56] have been explored only briefly. Group 3 metal alkyl complexes supported by a pincer-type pyridine-diamide ligand, 2,6-bis(2,6-di-iso-propylanilidomethyl)pyridine (N_2N^{py}),[57] were also synthesized for a reactivity comparison study.[58]

The continuous development of ancillary ligands has focused on nitrogen donors in the field of organometallic rare-earth chemistry, as shown in the special issue "Recent Advances in f-Element Organometallic Chemistry" appeared in *Organometallics* in 2013.[59] Although the non-cyclopentadienyl organometallic chemistry of rare-earths has been relatively underdeveloped, more than two thirds of the research articles in that issue used ancillary ligands other than cyclopentadienyl and its derivatives.

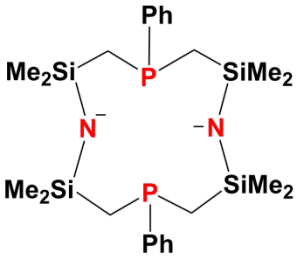

$N_2P_2^{2-}$
Fryzuk

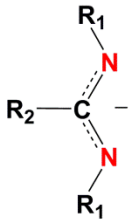

Bis(amidinate)
Arnold

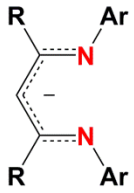

β-Diketiminate
Piers

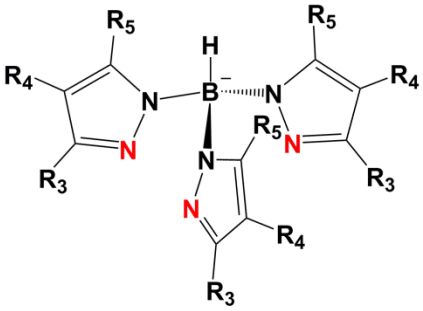

$(Tp^{R3,R4,R5})^-$
Takats

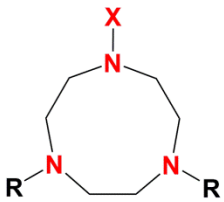

X = pendant arm donor

TACN
Bercaw and Mountford

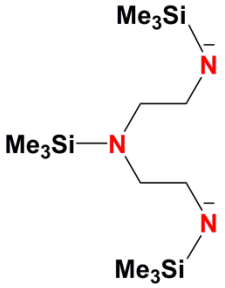

Diamidoamine
Gade and Mountford

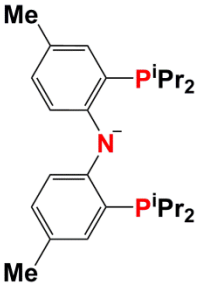

Pincer-type PNP^-
Mindiola

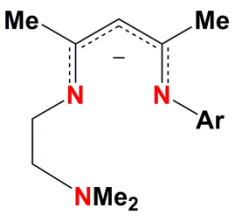

Tridentate β-Diketiminate
Chen

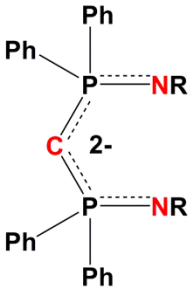

N_2C^{2-}
Cavell and Liddle

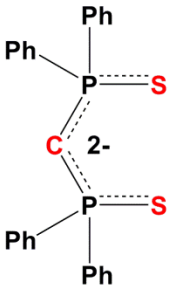

S_2C^{2-}
Le Floch

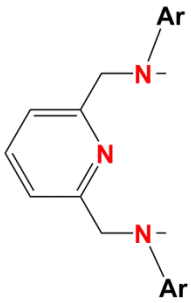

$(N_2N^{py})^{2-}$
Diaconescu

$[fc(NR)_2]^{2-}$
Diaconescu

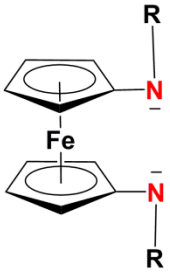

R = Si^tBuMe_2, $SiMe_3$, $SiPhMe_2$, adamantyl, 2,4,6-$C_6H_2Me_3$, and 3,5-$C_6H_3Me_2$

NN^{TBS}: R = Si^tBuMe_2
NN^{MES}: R = 2,4,6-$C_6H_2Me_3$

Chart 1-2: Well defined ancillary ligands developed or introduced by various groups (abbreviations are the same as in text) to organometallic rare-earth chemistry. The coordinating atoms are highlighted in red.

1.3 Low-valent organometallic rare-earth chemistry

As mentioned previously, rare-earth chemistry differs mainly from transition metal chemistry in that most rare-earth metals are redox inactive under ordinary conditions. However, a few lanthanides can also support the +2 or +4 oxidation state. Lanthanide chemistry in the +4 oxidation state is limited to cerium(IV) compounds.[60] On the other hand, the chemistry of low-valent lanthanides is more nuanced than that of high-valent compounds.[61] Table 1-1 lists the ionic radii for M^{3+} [62] and the spectroscopically estimated values for $E^0(M^{3+}/M^{2+})$.[63]

Table 1-1: Ionic radii for M^{3+} (effective ionic radii are listed) and spectroscopically estimated values for $M^{3+/2+}$ (all values referenced to the normal hydrogen electrode, values in brackets are experimentally determined, NA = not applicable).

Element	R (Å)	$E^0(M^{3+}/M^{2+})$ (V)
Sc	0.74	NA
Y	0.90	NA
La	1.03	-3.1
Ce	1.02	-3.2
Pr	0.99	-2.7
Nd	0.98	-2.6
Pm	0.97	-2.6
Sm	0.96	-1.6 (-1.5)
Eu	0.95	-0.3 (-0.3)
Gd	0.94	-3.9

Tb	0.92	-3.7
Dy	0.91	-2.6
Ho	0.90	-2.9
Er	0.89	-3.1
Tm	0.88	-2.3 (-2.2)
Yb	0.87	-1.1 (-1.1)
Lu	0.86	NA

An interesting study, although not directly relevant to organometallic rare-earth chemistry, found that most LnI_2 could be synthesized using solid state techniques with two different types of structures: those with a $[Xe]d^0f^n$ configuration and those with a $[Xe]d^1f^{n-1}$ configuration.[64] The former (including NdI_2, SmI_2, EuI_2, DyI_2, TmI_2, and YbI_2) are genuine $(M^{2+})(I^-)_2$ salts, while the latter (the rest of LnI_2) should be viewed as $(M^{3+})(I^-)_2(e^-)$ due to their metallic character (the valence d electron is not localized on the metal but in the conduction band). This phenomenon is well correlated to the spectroscopic estimated values of $M^{3+/2+}$: the salt-like LnI_2 are those of rare-earths having smaller values for the $M^{3+/2+}$ reduction potential, while the metallic LnI_2 are those with a $M^{3+/2+}$ reduction potential close to or lower than -3.0 V (the alkali metals have the $M^{1+/0}$ reduction potentials around -3.0 V). These characteristics are also reflected in the organometallic chemistry of these elements: Eu(II) is so stable that it is just as common as Eu(III) in organometallic rare-earth chemistry.[9,65] Indeed, no homoleptic Eu(III) alkyl complexes have been reported yet,[65] likely because the alkyl group is readily oxidized by Eu(III). Yb(II) is also common.[9,65] A major breakthrough in this field was the isolation of organo-samarium(II) complexes. Divalent samarium complexes, such as Cp^*_2Sm, are strong reductants. For example, Cp^*_2Sm could reduce N_2 to form the first dinitrogen complex of an f element, $(Cp^*_2Sm)_2(\mu\text{-}\eta^2\text{:}\eta^2\text{-}N_2)$ (Chart 1-3).[66] The synthesis of molecular thulium, dysprosium,

and even neodymium(II) complexes could be achieved from the corresponding metal diiodides with the appropriate ligands.[61] Cyclopentadienyls with bulky substituents like trimethylsilyl or *tert*-butyl, such as 1,3-$(Me_3Si)_2C_5H_3$, $Me_3SiC_5H_4$, and their *tert*-butyl counterparts, proved to be successful in isolating relatively stable divalent rare-earth metal complexes. Some of them were crystallographically characterized, including $[1,3\text{-}(Me_3Si)_2C_5H_3]_2Tm(THF)$[67] and $[(1,2,4\text{-}{}^tBu_3C_5H_2)_2Dy(\mu\text{-}Z)K(18\text{-crown-}6)]$ (Z = I, BH_4, Br),[68] while others were proposed as reaction intermediates.[69]

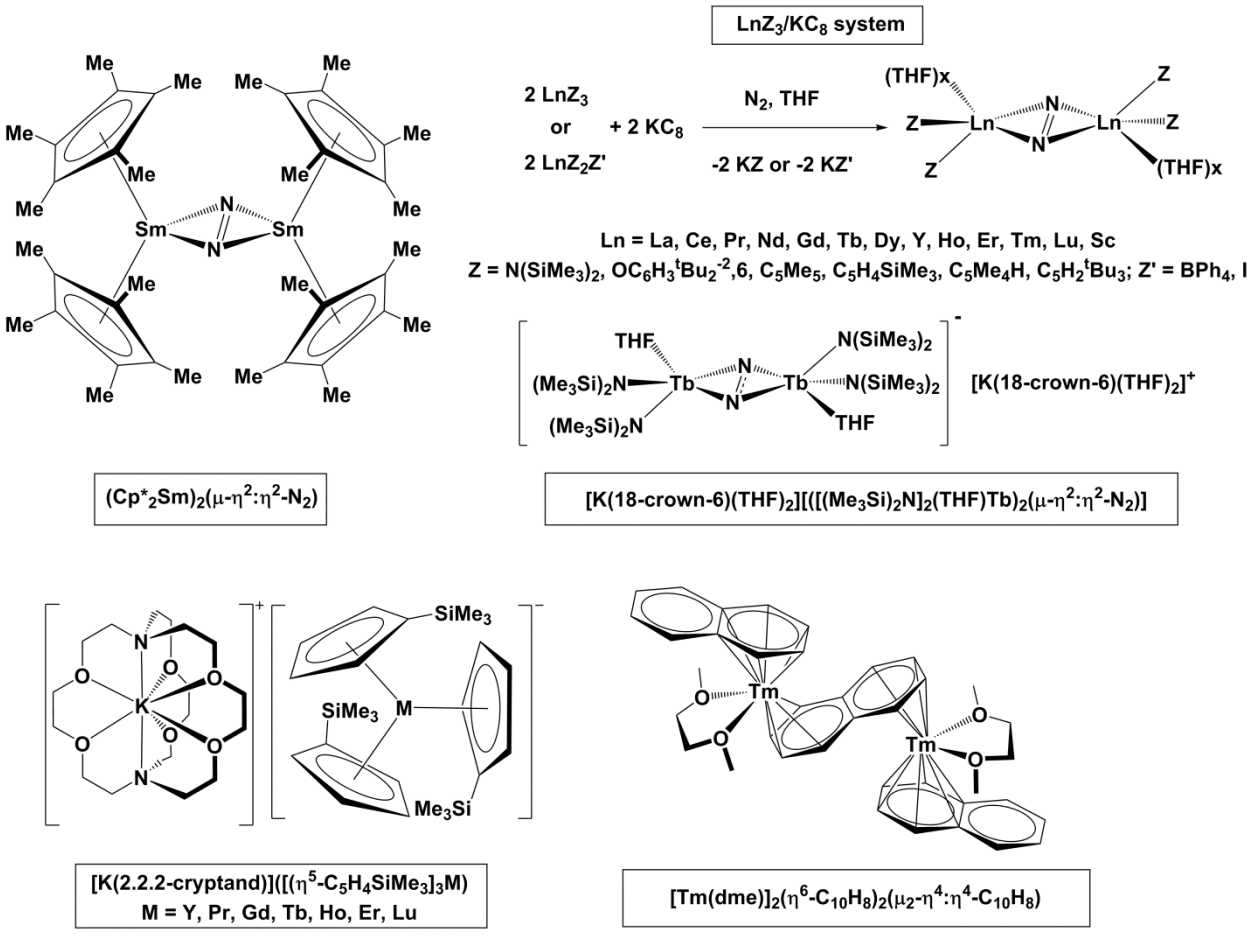

Chart 1-3: Selected examples of low-valent organometallic rare-earth compounds and chemically relevant systems.

Besides isolable divalent rare-earth metal complexes, systems that behave as M(II) are usually included with low-valent organometallic rare-earth compounds.[61] Perhaps the most famous is the LnZ_3/KC_8 system developed by Evans. X may be various monoanionic ligands, including amides, aryloxides, and cyclopentadienyls and Ln may be any rare-earth metal (Chart 1-3). This system can reduce dinitrogen to form $(N_2)^{2-}$.[70,71] Recently, lanthanide complexes of the radical trianion $(N_2)^{3-}$ have been isolated and characterized crystallographically.[72] It is important to note that some lanthanide $(N_2)^{3-}$ complexes behave as single molecule magnets due to the spin exchange between Ln ions and $(N_2)^{3-}$,[73] and one of them, $[K(18\text{-crown-}6)(THF)_2][([(Me_3Si)_2N]_2(THF)Tb)_2(\mu\text{-}\eta^2\text{:}\eta^2\text{-}N_2)]$ (Chart 1-3), is the current record holder for exhibiting magnetic hysteresis at the highest temperature (14 K).[74]

In 2008, Lappert isolated the first compound in a series of metal complexes with an ambiguous electronic structure: $[K(18\text{-crown-}6)(Et_2O)]([1,3\text{-}(Me_3Si)_2C_5H_3]_3La)$.[75] The authors proposed that it contains a lanthanum(II) ion. Recently, Evans extended this chemistry to almost all the lanthanides (Chart 1-3).[76-78]

Rare-earth metal arene complexes also play an important role in low-valent organometallic chemistry.[79] In these compounds, the metal is usually found in the +3 oxidation state, while the additional electrons rest in the π^* orbitals of the arene ligand. Because of the high energy of these orbitals, such complexes can serve as strong reductants. Fryzuk synthesized arene-bridging complexes of yttrium and lutetium supported by the cyclic P_2N_2 ligand: the biphenyl complexes were obtained through C-C bond formation,[26] while the fused-arene complexes by KC_8 reduction.[80] A triple decker binary thulium(III) naphthalene dianion complex $[Tm(dme)]_2(\eta^6\text{-}C_{10}H_8)_2(\mu_2\text{-}\eta^4\text{:}\eta^4\text{-}C_{10}H_8)$ (Chart 1-3) isolated from the reaction of TmI_2 and

lithium naphthalenide in 1,2-dimethoxyethane (dme) solution highlighted the rich potential of molecules formed from rare-earth ions and anionic arene ligands.[81]

Overall, low-valent organometallic rare-earth chemistry is a fast developing field with a lot of recent exciting discoveries.[71] Although cyclopentadienyl ligands feature prominently, non-cyclopentadienyl ligands have not been explored in detail in this respect.[61] The present thesis details our efforts to explore the reduction chemistry of rare-earth metal complexes supported by 1,1′-ferrocenediyl diamide ligands.

1.4 References

(1) Gschneidner, K. A.; Capelle, J. *1787-1987 Two hundred Years of Rare Earths*; Rare-earth Information Center, 1987.

(2) Haxel, G. B.; Hedrick, J. B.; Orris, G. J. *Rare Earth Elements--Critical Resources for High Technology*. 2002. http://pubs.usgs.gov/fs/2002/fs087-02.

(3) Gorman, S.; Elsner, A.; Milliken, M. *As hybrid cars gobble rare metals, shortage looms*. 2009. URL: http://www.reuters.com/article/2009/08/31/us-mining-toyota-idUSTRE57U02B20090831.

(4) Woodruff, D. N.; Winpenny, R. E. P.; Layfield, R. A. *Chem. Rev.* **2013**, *113*, 5110.

(5) Binnemans, K. *Chem. Rev.* **2009**, *109*, 4283.

(6) Bünzli, J.-C. G. *Chem. Rev.* **2010**, *110*, 2729.

(7) Wilkinson, G.; Rosenblum, M.; Whiting, M. C.; Woodward, R. B. *J. Am. Chem. Soc.* **1952**, *74*, 2125.

(8) Bordwell, F. G. *Acc. Chem. Res.* **1988**, *21*, 456.

(9) Bombieri, G.; Paolucci, G. In *Handbook on the Physics and Chemistry of Rare Earths*; Karl A. Gschneidner, Jr., LeRoy, E., Eds.; Elsevier: 1998, p 265.

(10) Wilkinson, G.; Birmingham, J. M. *J. Am. Chem. Soc.* **1954**, *76*, 6210.

(11) Maginn, R. E.; Manastyrskyj, S.; Dubeck, M. *J. Am. Chem. Soc.* **1963**, *85*, 672.

(12) Manastyrskyj, S.; Maginn, R. E.; Dubeck, M. *Inorg. Chem.* **1963**, *2*, 904.

(13) Bercaw, J. E.; Marvich, R. H.; Bell, L. G.; Brintzinger, H. H. *J. Am. Chem. Soc.* **1972**, *94*, 1219.

(14) Manriquez, J. M.; Bercaw, J. E. *J. Am. Chem. Soc.* **1974**, *96*, 6229.

(15) Wayda, A. L.; Evans, W. J. *Inorg. Chem.* **1980**, *19*, 2190.

(16) Watson, P. L.; Whitney, J. F.; Harlow, R. L. *Inorg. Chem.* **1981**, *20*, 3271.

(17) Tilley, T. D.; Andersen, R. A. *Inorg. Chem.* **1981**, *20*, 3267.

(18) Ephritikhine, M. *Chem. Rev.* **1997**, *97*, 2193.

(19) Evans, W. J.; Davis, B. L. *Chem. Rev.* **2002**, *102*, 2119.

(20) Arndt, S.; Okuda, J. *Chem. Rev.* **2002**, *102*, 1953.

(21) Streitwieser, A.; Mueller-Westerhoff, U. *J. Am. Chem. Soc.* **1968**, *90*, 7364.

(22) Putzer, M. A.; Rogers, J. S.; Bazan, G. C. *J. Am. Chem. Soc.* **1999**, *121*, 8112.

(23) Nief, F.; Ricard, L. *J. Chem. Soc., Chem. Commun.* **1994**, 2723.

(24) Edelmann, F. T.; Freckmann, D. M. M.; Schumann, H. *Chem. Rev.* **2002**, *102*, 1851.

(25) Fryzuk, M. D.; Giesbrecht, G.; Rettig, S. J. *Organometallics* **1996**, *15*, 3329.

(26) Fryzuk, M. D.; Love, J. B.; Rettig, S. J. *J. Am. Chem. Soc.* **1997**, *119*, 9071.

(27) Halcovitch, N. R.; Fryzuk, M. D. *Organometallics* **2013**, DOI: 10.1021/om400353h.

(28) Arnold, J.; Hoffman, C. G.; Dawson, D. Y.; Hollander, F. J. *Organometallics* **1993**, *12*, 3645.

(29) Hagadorn, J. R.; Arnold, J. *Organometallics* **1996**, *15*, 984.

(30) Hayes, P. G.; Piers, W. E.; Lee, L. W. M.; Knight, L. K.; Parvez, M.; Elsegood, M. R. J.; Clegg, W. *Organometallics* **2001**, *20*, 2533.

(31) Hayes, P. G.; Piers, W. E.; McDonald, R. *J. Am. Chem. Soc.* **2002**, *124*, 2132.

(32) Emslie, D. J. H.; Piers, W. E.; MacDonald, R. *J. Chem. Soc., Dalton Trans.* **2002**, 293.

(33) Marques, N.; Sella, A.; Takats, J. *Chem. Rev.* **2002**, *102*, 2137.

(34) Hasinoff, L.; Takats, J.; Zhang, X. W.; Bond, A. H.; Rogers, R. D. *J. Am. Chem. Soc.* **1994**, *116*, 8833.

(35) Roussel, P.; W. Alcock, N.; Scott, P. *Chem. Commun.* **1998**, 801.

(36) Hajela, S.; Schaefer, W. P.; Bercaw, J. E. *J. Organomet. Chem.* **1997**, *532*, 45.

(37) Bylikin, S. Y.; Robson, D. A.; Male, N. A. H.; Rees, L. H.; Mountford, P.; Schroder, M. *J. Chem. Soc., Dalton Trans.* **2001**, 170.

(38) Ward, B. D.; Dubberley, S. R.; Maisse-Francois, A.; Gade, L. H.; Mountford, P. *J. Chem. Soc., Dalton Trans.* **2002**, 4649.

(39) Scott, J.; Fan, H.; Wicker, B. F.; Fout, A. R.; Baik, M.-H.; Mindiola, D. J. *J. Am. Chem. Soc.* **2008**, *130*, 14438.

(40) Wicker, B. F.; Scott, J.; Andino, J. G.; Gao, X.; Park, H.; Pink, M.; Mindiola, D. J. *J. Am. Chem. Soc.* **2010**, *132*, 3691.

(41) Xu, X.; Chen, Y.; Zou, G.; Sun, J. *Dalton Trans.* **2010**, *39*, 3952.

(42) Lu, E.; Gan, W.; Chen, Y. *Dalton Trans.* **2011**, *40*, 2366.

(43) Lu, E.; Li, Y.; Chen, Y. *Chem. Commun.* **2010**, *46*, 4469.

(44) Aparna, K.; Ferguson, M.; Cavell, R. G. *J. Am. Chem. Soc.* **2000**, *122*, 726.

(45) Cantat, T.; Jaroschik, F.; Nief, F.; Ricard, L.; Mezailles, N.; Le Floch, P. *Chem. Commun.* **2005**, 5178.

(46) Mills, D. P.; Soutar, L.; Lewis, W.; Blake, A. J.; Liddle, S. T. *J. Am. Chem. Soc.* **2010**, *132*, 14379.

(47) Diaconescu, P. L. *Acc. Chem. Res.* **2010**, *43*, 1352.

(48) Diaconescu, P. L. *Comments Inorg.Chem.* **2010**, *31*, 196.

(49) Carver, C. T.; Diaconescu, P. L. *J. Am. Chem. Soc.* **2008**, *130*, 7558.

(50) Miller, K. L.; Williams, B. N.; Benitez, D.; Carver, C. T.; Ogilby, K. R.; Tkatchouk, E.; Goddard, W. A.; Diaconescu, P. L. *J. Am. Chem. Soc.* **2009**, *132*, 342.

(51) Carver, C. T.; Diaconescu, P. L. *J. Alloys Compd.* **2009**, *488*, 518.

(52) Carver, C. T.; Monreal, M. J.; Diaconescu, P. L. *Organometallics* **2008**, *27*, 363.

(53) Monreal, M. J.; Carver, C. T.; Diaconescu, P. L. *Inorg. Chem.* **2007**, *46*, 7226.

(54) Duhović, S.; Diaconescu, P. L. *Polyhedron* **2013**, *52*, 377.

(55) Wong, A. W.; Miller, K. L.; Diaconescu, P. L. *Dalton Trans.* **2010**, *39*, 6726.

(56) Lee, J. A.; Williams, B. N.; Ogilby, K. R.; Miller, K. L.; Diaconescu, P. L. *J. Organomet. Chem.* **2011**, *696*, 4090.

(57) Guerin, F.; McConville, D. H.; Vittal, J. J. *Organometallics* **1995**, *14*, 3154.

(58) Jie, S.; Diaconescu, P. L. *Organometallics* **2010**, *29*, 1222.

(59) Marks, T. J. *Organometallics* **2013**, *32*, 1133.

(60) Nair, V.; Balagopal, L.; Rajan, R.; Mathew, J. *Acc. Chem. Res.* **2003**, *37*, 21.

(61) Nief, F. In *Handbook on the Physics and Chemistry of Rare Earths*; Karl A. Gschneidner, Jr., Bünzli, J.-C. G., Vitalij, K. P., Eds.; Elsevier: 2010, p 241.

(62) Shannon, R. *Acta Cryst.* **1976**, *A32*, 751.

(63) Nugent, L. J.; Baybarz, R. D.; Burnett, J. L.; Ryan, J. L. *J. Phys. Chem.* **1973**, *77*, 1528.

(64) Meyer, G.; Gerlitzki, N.; Hammerich, S. *J. Alloys Compd.* **2004**, *380*, 71.

(65) Zimmermann, M.; Anwander, R. *Chem. Rev.* **2010**, *110*, 6194.

(66) Evans, W. J.; Ulibarri, T. A.; Ziller, J. W. *J. Am. Chem. Soc.* **1988**, *110*, 6877.

(67) Evans, W. J.; Allen, N. T.; Ziller, J. W. *Angew. Chem. Int. Ed.* **2002**, *41*, 359.

(68) Jaroschik, F.; Nief, F.; Le Goff, X.-F.; Ricard, L. *Organometallics* **2007**, *26*, 1123.

(69) Jaroschik, F.; Momin, A.; Nief, F.; Le Goff, X.-F.; Deacon, G. B.; Junk, P. C. *Angew. Chem. Int. Ed.* **2009**, *48*, 1117.

(70) Evans, W. J.; Lee, D. S.; Johnston, M. A.; Ziller, J. W. *Organometallics* **2005**, *24*, 6393.

(71) Evans, W. J. *Inorg. Chem.* **2007**, *46*, 3435.

(72) Evans, W. J.; Fang, M.; Zucchi, G. l.; Furche, F.; Ziller, J. W.; Hoekstra, R. M.; Zink, J. I. *J. Am. Chem. Soc.* **2009**, *131*, 11195.

(73) Rinehart, J. D.; Fang, M.; Evans, W. J.; Long, J. R. *Nat. Chem.* **2011**, *3*, 538.

(74) Rinehart, J. D.; Fang, M.; Evans, W. J.; Long, J. R. *J. Am. Chem. Soc.* **2011**, *133*, 14236.

(75) Hitchcock, P. B.; Lappert, M. F.; Maron, L.; Protchenko, A. V. *Angew. Chem. Int. Ed.* **2008**, *47*, 1488.

(76) MacDonald, M. R.; Ziller, J. W.; Evans, W. J. *J. Am. Chem. Soc.* **2011**, *133*, 15914.

(77) MacDonald, M. R.; Bates, J. E.; Fieser, M. E.; Ziller, J. W.; Furche, F.; Evans, W. J. *J. Am. Chem. Soc.* **2012**, *134*, 8420.

(78) MacDonald, M. R.; Bates, J. E.; Ziller, J. W.; Furche, F.; Evans, W. J. *J. Am. Chem. Soc.* **2013**, *135*, 9857.

(79) Bochkarev, M. N. *Chem. Rev.* **2002**, *102*, 2089.

(80) Fryzuk, M. D.; Jafarpour, L.; Kerton, F. M.; Love, J. B.; Rettig, S. J. *Angew. Chem. Int. Ed.* **2000**, *39*, 767.

(81) N. Bochkarev, M.; L. Fedushkin, I.; A. Fagin, A.; Schumann, H.; Demtschuk, J. *Chem. Commun.* **1997**, 1783.

CHAPTER 2: PREVIOUS STUDIES OF METAL COMPLEXES SUPPORTED BY FERROCENE-BASED DIAMIDE LIGANDS AND DEVELOPMENT OF NEW RARE-EARTH STARTING MATERIALS

2.1 Advantages of 1,1′-ferrocenediyl diamide ligands

In 2000, Arnold reported a reliable synthesis of 1,1′-diaminoferrocene[1] and introduced the trimethylsilyl silylated version fc($NHSiMe_3$)$_2$ ($H_2(NN^{TMS})$) on group 4 metals, titanium and zirconium, to afford metal dimethyl and dibenzyl complexes (NN^{TMS})$TiMe_2$ and (NN^{TMS})$ZrBn_2$ (Bn = CH_2Ph) (Chart 2-1).[2] [(NN^{TMS})ZrBn][(μ-Bn)B(C_6F_5)$_3$] could be obtained by treating (NN^{TMS})$ZrBn_2$ with 1 equivalent of B(C_6F_5)$_3$ and was studied in olefin polymerization.[3] Our group first introduced the 1,1′-ferrocenediyl diamide ligands to uranium and reported (NN^{TBS})$_2$U (NN^{TBS} = 1,1′-fc(NSi^tBuMe_2)$_2$) and its one electron oxidation product [(NN^{TBS})$_2$U][BPh_4] in 2007. The redox process was studied in detail and it was found that the electron communication between two iron centers was mediated by uranium in the mix-valent (Fe(II) and Fe(III)) complex, [(NN^{TBS})$_2$U][BPh_4].[4] At the time, it was also observed that the *tert*-butyldimethylsilyl version, 1,1′-fc($NHSi^tBuMe_2$)$_2$ ($H_2(NN^{TBS})$), was easier to handle because of its improved solubility and gave better results in crystallization. As a consequence, later efforts focused on this particular ligand platform. Group 3 metal monoalkyl complexes with the general formula (NN^{TBS})M(CH_2Ar)(THF) (M = Sc[5] and Lu:[6] Ar = 3,5-$C_6H_3Me_2$; M = Y[7] and La:[8] Ar = C_6H_5) and the uranium dialkyl complex (NN^{TBS})UBn_2[9] were successfully synthesized. The electron donating 1,1′-ferrocenediyl group[10] makes the amide donor bind strongly to the highly electropositive group 3 metals and uranium(IV) ion. By using NN^{TBS} as the ancillary ligand for d^0f^n metal alkyl complexes, the C-H bond activation of aromatic heterocycles,[11] successive C-C

bond coupling,[6,12-14] dearomatization of aromatic heterocycles,[8] and the unprecedented ring-opening of 1-methylimidazole,[7,15] 1-methylbenzimidazole,[16] or other aromatic heterocycles[17] were observed and studied.[18,19]

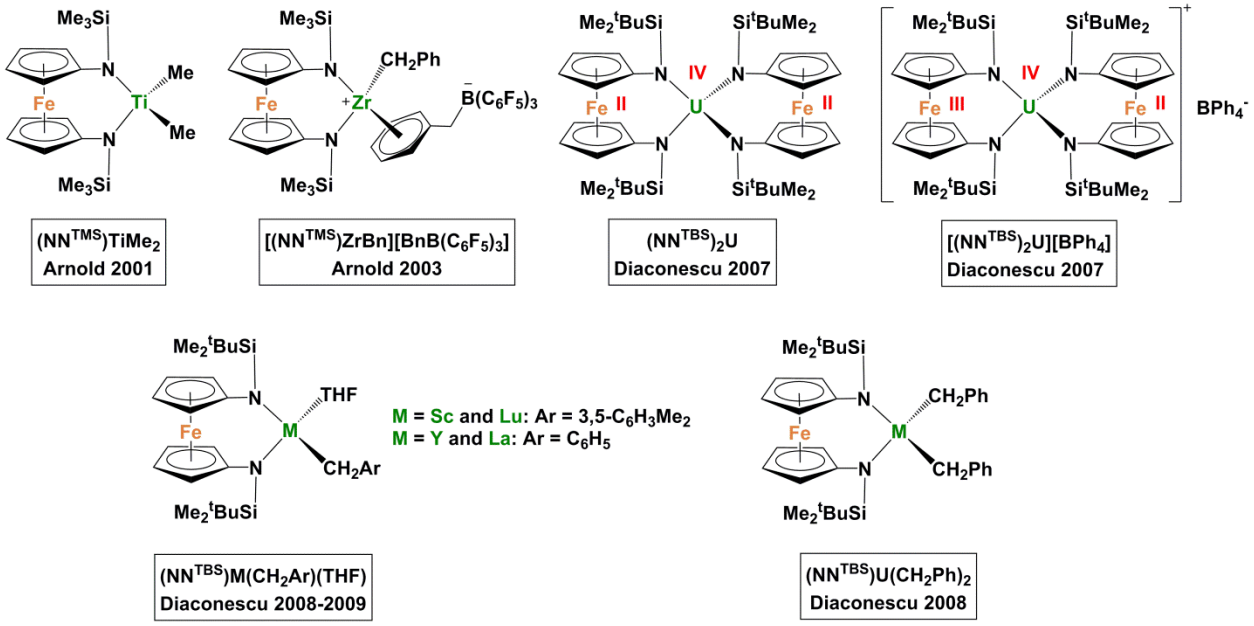

Chart 2-1: Group 4, uranium, and group 3 metal complexes supported by 1,1′-ferrocenediyl diamide ligands.

It is likely that the ferrocene backbone has a specific role in facilitating the unique reactivity observed by our group. When the electron rich iron center of ferrocene and the electropositive metal ion are brought into close proximity, a donor-acceptor interaction may take place between iron and the metal.[20] This type of Lewis acid-Lewis base interaction was observed previously with both electrophilic early and late transition metals (Chart 2-2): Seyferth suggested a weak, dative Fe to Pd bond in the compound $[Fe(\eta^5\text{-}C_5H_4S)_2]Pd(PPh_3)$;[21] Akabori later provided a comprehensive study based on $[M(\eta^5\text{-}C_5H_4O)_2]M'(PPh_3)$ (M = Fe or Ru, M′ = Pd or

Ni) that supported a dative M-M′ interaction;[22] Arnold suggested a dative Fe to Ti bond based on the short Fe-Ti distance in $([(NN^{TMS})Ti(\mu\text{-}Cl)]_2)[B(C_6F_5)_4]_2$.[23] More interestingly, Arnold observed that the Fe-Ti distance in a series of compounds with the same NN^{TMS} ligand varied according to the electrophilicity of the titanium center: Fe-Ti distance is 3.32 Å in the neutral dialkyl complex $(NN^{TMS})TiMe_2$, but it shortens to 3.07 Å in the Lewis acid adduct $[(NN^{TMS})TiMe][(\mu\text{-}Me)B(C_6F_5)_3]$ and reaches the shortest 2.49 Å in the chloride bridging dicationic complex $([(NN^{TMS})Ti(\mu\text{-}Cl)]_2)[B(C_6F_5)_4]_2$. Our group observed a similar trend for group 3 metal complexes supported by the NN^{TBS} ligand: the Fe-Sc distance is 3.16 and 2.80 Å in $(NN^{TBS})Sc(CH_2C_6H_3Me_2\text{-}3,5)(THF)$ and $[(NN^{TBS})Sc(\mu\text{-}Cl)]_2$, respectively.[5] A similar Fe-M distance shortening was observed upon one electron oxidation of $(NN^{TBS})_2U$.[4] Recently, our group also reported a dative Fe-Ru interaction in $[Fe(\eta^5\text{-}C_5H_4NH)_2]Ru(PPh_3)_2$ and characterized it by spectroscopic methods and DFT calculations.[24]

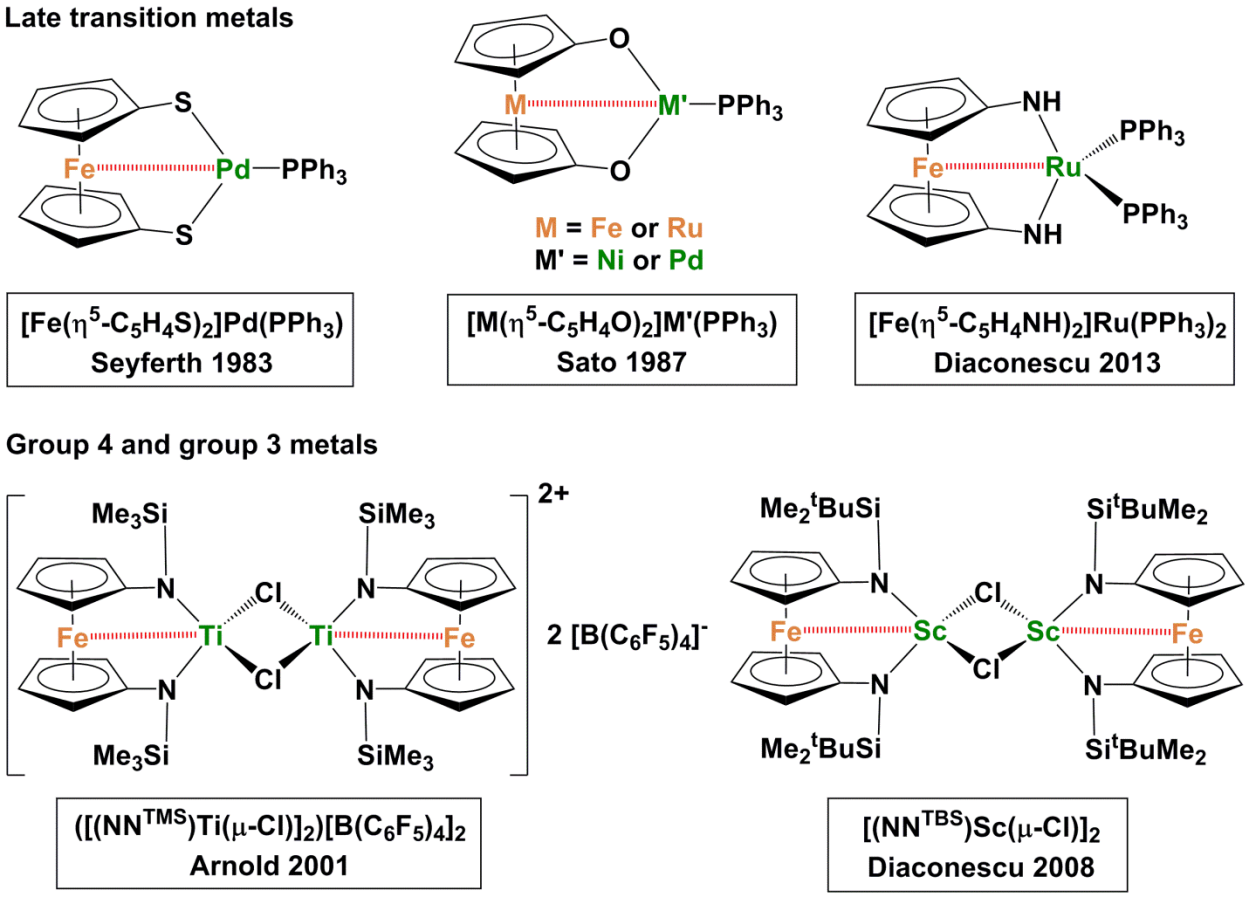

Chart 2-2: Organometallic complexes containing dative iron-metal bonds (which are indicated as red dashed lines).

Besides the weak Fe-M interaction, ferrocene-based ligands inherit the redox-active nature of ferrocene. The ferrocenium-ferrocene redox couple is usually reversible.[25] Therefore, the ferrocene unit can serve as a redox-switch providing an indirect control of active sites for polymerization or other chemical transformations.[26,27] Recently, our group reported a redox-switchable catalyst used for ring-opening polymerization and the synthesis of biodegradable materials.[28] This result highlighted the potential of the redox-active ferrocene backbone in tuning the reactivity of the metal center found in the vicinity of ferrocene. On the other hand, the

possibility to reduce ferrocene was evidenced by the reversible redox event observed for ferrocene in 1,2-dimethoxyethane at -3.45 V (referenced to ferrocene$^{+/0}$).[29] However, the extreme negative redox potential makes the assignment of this event to ferrocene$^{0/-}$ questionable. No other report of a reduced ferrocene species is known to us.

Based on our experimental observations and computational studies on the organometallic compounds supported by the 1,1′-ferrocenediyl diamide ligands, we attribute the following advantages/features to this type of ligands (Figure 2-1): (1) The redox-active ferrocene backbone serves as an electron reservoir; (2) The weak, dative iron-metal interaction stabilizes complexes of the Lewis acidic metal center, and, probably more important, this interaction is flexible since the barrier for the ferrocene unit to move toward or away from the metal center is low (nearly free rotation of C_{ipso}-N bonds); (3) The 1,1′-ferrocenediyl diamide blocks one side of the metal leaving the other side widely open for substrate coordination. This is particularly important when comparing it to substituted cyclopentadienyls. From our point of view, substituted cyclopentadienyls are usually sterically demanding, which facilitates the isolation of unstable compounds but hinders their reactivity.[30] The most common ferrocene diamide we used in the projects discussed herein is 1,1′-fc(NHSi^{t}BuMe$_2$)$_2$ (H_2(NN^{TBS})), although other derivatives such as 1,1′-fc(NHC$_6$H$_2$Me$_3$-2,4,6)$_2$ (H_2(NN^{MES})) were also explored.

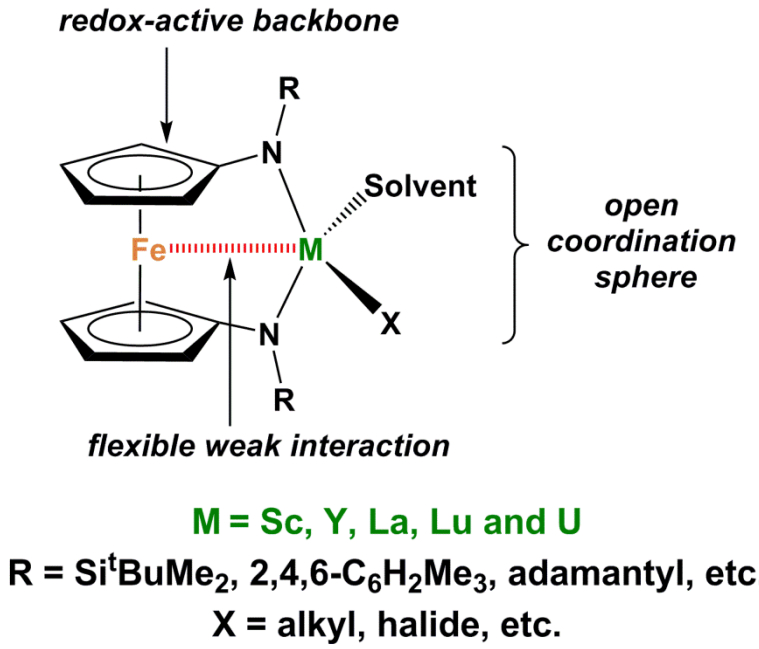

Figure 2-1: Advantages/features of 1,1′-ferrocenediyl diamide ligands to support electrophilic d^0f^n metals.

2.2 $(NN^{TBS})MI(THF)_2$ (M = Sc, Y, La, and Lu) as precursors for reduction chemistry

Initially, reduction chemistry was explored using the known scandium chloride $[(NN^{TBS})Sc(\mu\text{-}Cl)]_2$.[5] However, the reaction of $[(NN^{TBS})Sc(\mu\text{-}Cl)]_2$ and potassium graphite (KC_8) in common organic solvents such as hexanes, toluene, diethyl ether (Et_2O), tetrahydrofuran (THF) did not result in any products that could be identified. It was noted that either no reaction took place or that the reaction was not clean. We reasoned that the first step in those reactions is to break the Sc-Cl bond and eliminate KCl in order to allow a subsequent reaction to occur. Therefore, we hypothesized that the unsuccessful reaction of $[(NN^{TBS})Sc(\mu\text{-}Cl)]_2$ and KC_8 may be due to the high strength of the Sc-Cl bond that hinders the elimination of KCl. By replacing

chloride with iodide, the resulting Sc-I bond should be weaker and it is more likely to eliminate KI and facilitate a subsequent reaction.

$(NN^{TBS})ScI(THF)_2$ could be readily prepared from $(NN^{TBS})Sc(CH_2C_6H_3Me_2\text{-}3,5)(THF)$ on a gram scale. Heating $(NN^{TBS})Sc(CH_2C_6H_3Me_2\text{-}3,5)(THF)$ with 10 equivalents of iodomethane (MeI) in toluene for 24 hours led to complete conversion to $(NN^{TBS})ScI(THF)_2$ (Scheme 2-1).[31] The molecular structure of $(NN^{TBS})ScI(THF)_2$ is shown in Figure 2-2a. It was noted that prolong heating of the reaction mixture could lead to the addition of MeI across the Sc-N(amide) bond to afford a scandium diiodide complex $[Fe(\eta^5\text{-}C_5H_4NSi^tBuMe_2)(\eta^5\text{-}C_5H_4N(Me)(Si^tBuMe_2))]ScI_2$ (Figure 2-2b). The side reaction was more prominent for $(NN^{TBS})YBn(THF)$ and MeI, probably because the Y-N(amide) bond is more vulnerable to electrophilic attack by MeI. To avoid this complication, an alternative route was developed for the synthesis of all $(NN^{TBS})MI(THF)_2$ (M = Sc, Y, La, and Lu) based on the fact that Me_3SiI is more reactive than MeI.[32] Clean conversion to $(NN^{TBS})MI(THF)_2$ was achieved by stirring 2 equivalents of Me_3SiI and $(NN^{TBS})M(CH_2Ar)(THF)$ in toluene at 25 °C for 1 hour; the bulky trimethylsilyl group also prevents the electrophilic attack on the M-N(amide) bond.[33] $(NN^{TBS})MI(THF)_2$ is barely soluble in saturated hydrocarbons, but readily soluble in aromatic solvents and ethers. Except for $(NN^{TBS})ScI(THF)_2$, which crystallized in the space group C2/c, all other $(NN^{TBS})MI(THF)_2$ crystallized in the same space group, P-1, and differed only slightly in structural parameters. In all $(NN^{TBS})MI(THF)_2$ structures, the rare-earth ion is coordinated by two nitrogen, two oxygen, and one iodide, while the ferrocene backbone sits oppositely to iodide. If taking iron into account, the metal center is in a pseudo-octahedral geometry. As expected, the Fe-M interaction is in the "off" mode (indicated by the long Fe-M distance) in the presence of two coordinating THF molecules, which supply enough electron density to the metal center.

M = Sc, Ar = 3,5-$C_6H_3Me_2$, RI = MeI
i: Toluene, 85 °C, 24 hours
M = Sc, Y, La and Lu, Ar = 3,5-$C_6H_3Me_2$ or C_6H_5, RI = Me_3SiI
ii: Toluene, 25 °C, 1 hour

Scheme 2-1: Synthesis of $(NN^{TBS})MI(THF)_2$ (M = Sc, Y, La, and Lu): method i only worked for $(NN^{TBS})ScI(THF)_2$; method ii is general for all $(NN^{TBS})MI(THF)_2$.

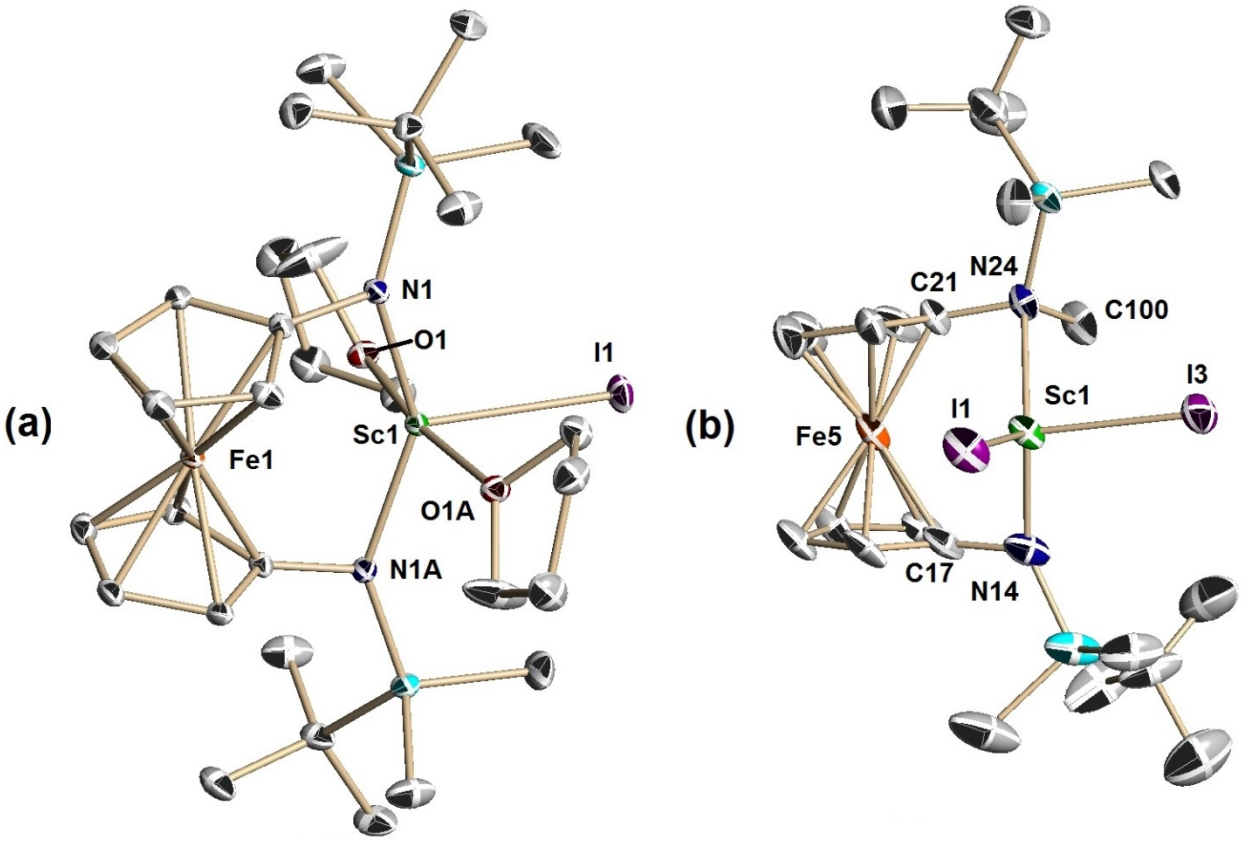

Figure 2-2: Molecular structures of $(NN^{TBS})ScI(THF)_2$ (a) and $[Fe(\eta^5\text{-}C_5H_4NSi^tBuMe_2)(\eta^5\text{-}C_5H_4N(Me)(Si^tBuMe_2))]ScI_2$ (b). Thermal ellipsoids are drawn at the 50% probability level.

Hydrogen atoms are omitted for clarity. Selected distances [Å] and angles [°] (errors in brackets): (a) $(NN^{TBS})ScI(THF)_2$: Sc1-I1 2.857(1), Sc1-N1 2.101(2), Sc1-O1 2.216(2), Sc1-Fe1 3.140(1); N1-Sc1-N1A 144.1(1), O1-Sc1-O1A 170.6(1), N1-Sc1-O1 92.7(1), Fe1-Sc1-I1 180.0. (b) $[Fe(\eta^5\text{-}C_5H_4NSi^tBuMe_2)(\eta^5\text{-}C_5H_4N(Me)(Si^tBuMe_2))]ScI_2$: Sc1-I1 2.778(1), Sc1-I3 2.784(1), Sc1-N14 2.012(1), Sc1-N24 2.323(1), N24-C100 1.515(1), Sc1-Fe5 2.919(1), I1-Sc1-I3 96.9(1), I3-Sc1-Fe5 158.3(1), Fe5-Sc1-I1 104.4(1) (sum of the last three angles is 359.6), N14-Sc1-N24 127.0(1).

After obtaining the molecular structures of $(NN^{TBS})MI(THF)_2$, we performed a molecular orbital analysis by using DFT calculations (Figure 2-3). Since we were going to explore the reduction chemistry of $(NN^{TBS})MI(THF)_2$, the LUMO of each compound is of particular interest. To our surprise, the LUMO of different metal iodides is not the same, although HOMO and HOMO-1 are always the 3d orbitals of iron. For $(NN^{TBS})ScI(THF)_2$, the LUMO is localized on the 3d orbital of scandium, while the LUMO+1 is the π^* orbital of the ferrocene backbone; however, for $(NN^{TBS})YI(THF)_2$, both the LUMO and LUMO+1 are the π^* orbitals of the ferrocene backbone. These unexpected results suggested the possibility of involvement of the ferrocene backbone in electron transfer processes: an electron may be first delivered to the ferrocene unit and then intramolecularly transferred to the rare-earth metal to activate the substrate. However, due to the heterogeneous nature of reductions with KC_8, we were unable to study this process in more detail.

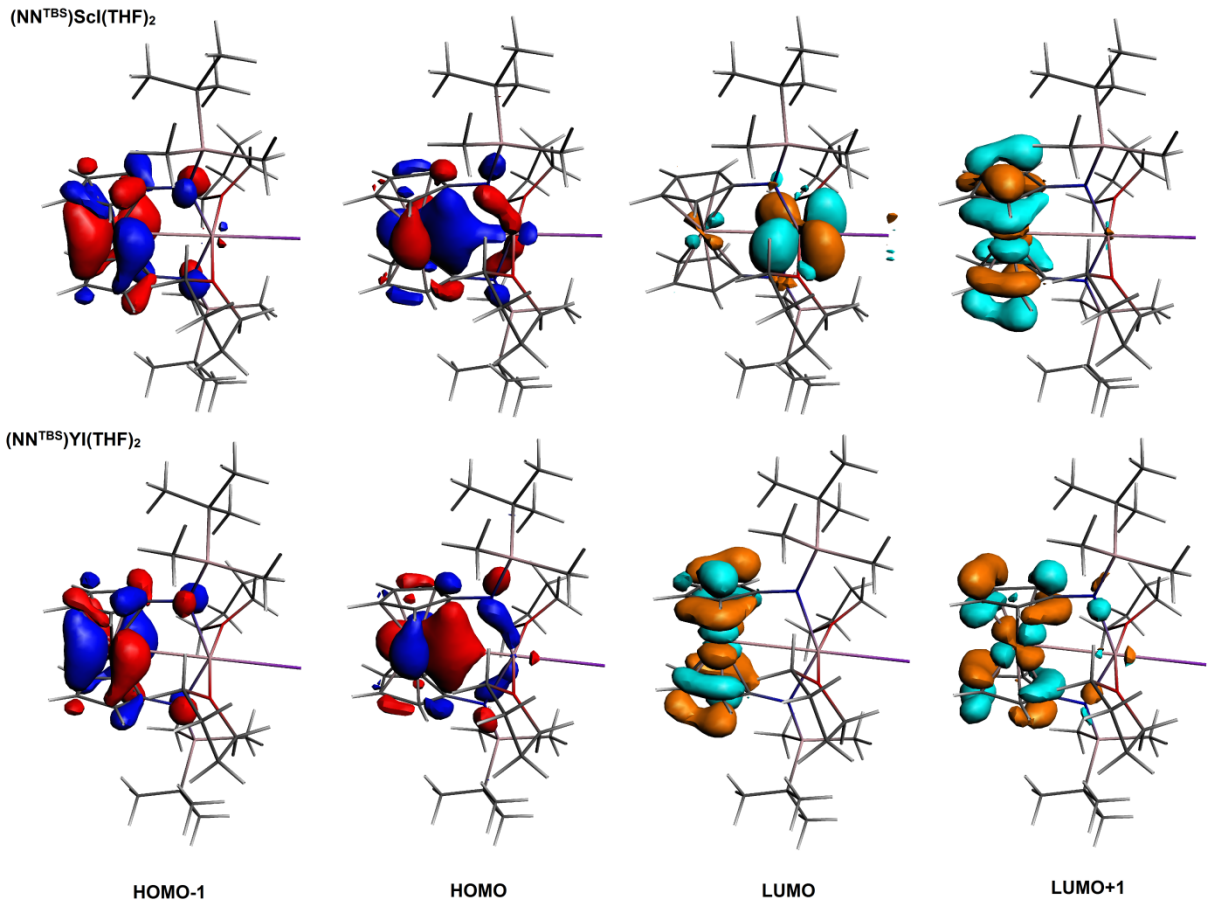

Figure 2-3: Selected molecular orbitals for $(NN^{TBS})ScI(THF)_2$ and $(NN^{TBS})YI(THF)_2$. Top: $(NN^{TBS})ScI(THF)_2$; bottom: $(NN^{TBS})YI(THF)_2$. Hydrogen atoms are omitted for clarity.

2.3 Reaction conditions for reduction chemistry

We observed that reaction conditions are crucial to the outcome of reduction chemistry. The choice of reductants is of great importance since the reducing power determines whether the reaction is thermodynamically favorable. The reducing power of common reductants was measured by electrochemical methods.[25] However, it is important to note that some heterogeneous reductants, most prominently, alkali metals or their equivalents, may initiate a reduction reaction that is beyond their redox potential. For example, the redox couple benzene$^{0/-}$

was measured to be -3.42±0.05 V versus SCE[34] and is much lower than $Na^{+/0}$ at -2.59 V versus SCE;[25] however, the well-known Birch reduction involves electron transfer from sodium metal to benzene as the first step.[35] Solvent plays an important role in reduction chemistry as well. For homogeneous reductants, for instance, alkali metal naphthalenides, the solvent can influence both the thermodynamics and kinetics of the reaction by its coordination to the metal ion and its relative permittivity.[36] For heterogeneous reductants, the solvent effect is more subtle but can still be prominent. As a typical heterogeneous reductant, KC_8 forms a suspension in common organic solvents such as *n*-pentane, Et_2O, and THF.[37] However, the reaction of KC_8 with acidic protons (water, methanol, and other alcohols) in different solvents resulted in different amount of evolved hydrogen gas. It was suggested that this difference in reactivity was caused by the fact that the suspensions formed by KC_8 in *n*-pentane and Et_2O are not as well dispersed as those formed in THF.[37]

Reductants: Potassium graphite (commonly referred to as KC_8) was discovered to be the most potassium rich form of a series of graphite intercalation compounds with potassium.[38] A space-filling model of KC_8 is shown in Figure 2-4.

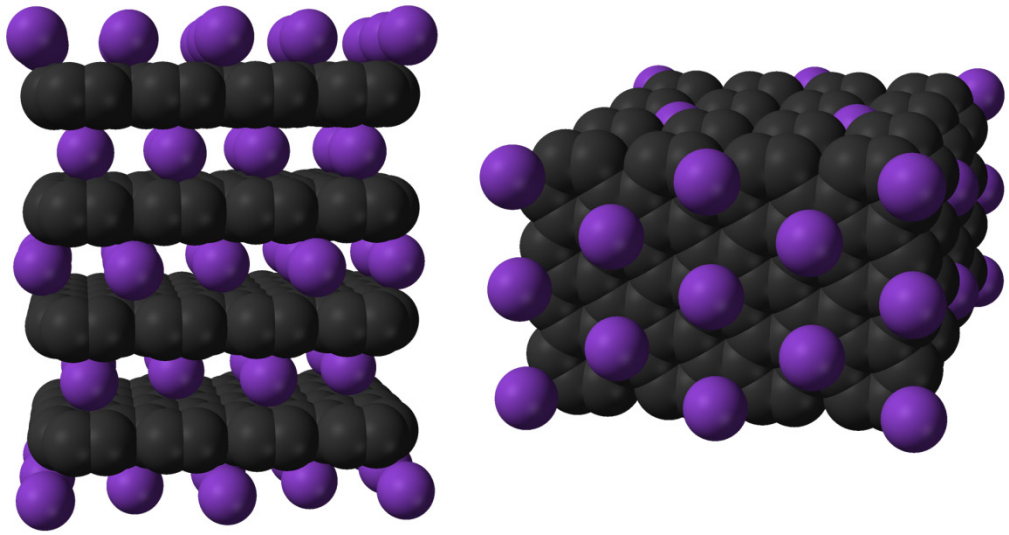

Figure 2-4: Space-filling model of KC_8: left, side view; right, top view. Use granted by Ben Mills from the Wikimedia Commons.

KC_8 is probably the most widely used reductant in low-valent organometallic rare-earth chemistry.[39] The system composed of trivalent lanthanide precursors LnZ_3 (Z represents a monoanionic ligand) and KC_8 developed by Evans proved successful in reducing dinitrogen to form stable lanthanide dinitrogen complexes with the general formula $(Z_2Ln)_2(\mu\text{-}\eta^2\text{:}\eta^2\text{-}N_2)$.[40] In addition, KC_8 was used in obtaining a series of divalent lanthanide complexes [K(2.2.2-cryptand)][$(C_5H_4SiMe_3)_3Ln$] (also see Chart 1-3).[41] The strategy of using KC_8 as a reductant was also employed in main group chemistry to obtain structurally fascinating and fundamentally important molecules, such as L:B(H)=B(H):L[42] and L:Si=Si:L[43] (L = :C[N(2,6-^{i}Pr$_2$C$_6$H$_3$)CH]$_2$) containing a B=B bond and a Si=Si bond, respectively, although similar molecules, L:B(Br)=B(Br):L and L:B≡B:L, could also be prepared using sodium naphthalenide as a reductant by another group.[44] The potential of using KC_8 as a reductant in organic synthesis or transformation has been explored.[37] It was concluded that, as a reducing agent, it behaved similar

or poorly compared to its homogeneous analogue sodium naphthalenide but it had the advantage that it did not form any soluble by-products. It was realized that this advantage is particularly important in organometallic chemistry.[45-47]

We also chose KC_8 as the default reductant in our studies for the following reasons: (1) The reducing power of potassium graphite is superior. Thermodynamically, it is considered as the equivalent of potassium;[48,49] kinetically, it can form suspensions in common organic solvents so it has a greatly increased surface area compared to metallic potassium.[50] (2) The by-products of KC_8 reduction are graphite and potassium halide salt that are not soluble in the organic solvents and can be readily removed by filtration. (3) Professor Richard B. Kaner's laboratory (University of California, Los Angeles) prepares high quality KC_8 by mixing a stoichiometric amount of potassium and graphite (usually 1μm in particle size) and milling the mixture at high temperature under an inert atmosphere. They usually prepare batches of 12 to 24 grams of KC_8 that they donate to our laboratory. Since the mixing of potassium and graphite takes place inside an inert-atmosphere glove-box at room temperature, and the reaction vessel is made of a metal alloy, this synthetic method is safer and more efficient than the traditional methods based on Schlenk techniques.[47] It is important to note that the mechanism and activity of KC_8 remains a mystery to synthetic chemists; however, we made some effort to understand the role of KC_8 in our system. This work is included in Chapter 3 section 3.2.3.

Besides KC_8, we also tested other reductants, including sodium (mirror) and sodium amalgam. Details regarding their activity and comparison to KC_8 are included in Chapter 3 section 3.2.2.1. Homogeneous reductants are usually preferred for reaction mechanistic studies. However, none of the homogeneous reductants had the required reducing power to reproduce the

results observed by us with KC_8.[25] Although sodium or lithium naphthalenide are strong reductants, they are not innocent in our system (see Chapter 4).

Solvent and atmosphere: Although it was previously reported that KC_8 suspensions in *n*-pentane, Et_2O, and THF are stable at room temperature for at least 24 hours,[37] we found that, in our system, the outcome of a certain reaction was highly dependent on the solvent used. In addition, we found that the stoichiometric addition of the coordinating solvent THF could change reactivity when keeping other parameters constant. Details are included in Chapter 3 section 3.2.1.

The gas atmosphere under which reactions are conducted becomes relevant under strong reducing conditions. Evans showed that LnZ_3/KC_8 system readily reduced N_2 from the N_2 atmosphere[40] and it was necessary to perform the reactions under argon in order to obtain divalent lanthanide triscyclopentadienyl complexes $[K(2.2.2\text{-cryptand})][(C_5H_4SiMe_3)_3Ln]$.[41] We also explored the influence of different gas atmospheres (N_2, Ar, H_2, and reduced pressure) on the outcome of a reaction. Details are included in Chapter 3 section 3.2.2.1.

2.4 Experimental section

Experimental details for the synthesis and characterizations of $(NN^{TBS})MI(THF)_2$

Method i: Synthesis of $(NN^{TBS})ScI(THF)_2$.[31] $(NN^{TBS})Sc(CH_2C_6H_3Me_2)(THF)$ (0.737 g, 1.09 mmol) was dissolved in 5 mL of toluene in a Schlenk tube and excess MeI (1.750 g, 12.30 mmol) was added. The mixture was stirred at 85 °C for 24.5 h. THF (2 mL) was added to the mixture before removing the volatiles under reduced pressure. The remaining yellow solid was extracted with diethyl ether and layered with *n*-pentane. Yellow crystals were formed after storing the solution overnight at -35 °C. The solvent was decanted and the crystals washed with

cold *n*-pentane. Yield: 0.561 g, 68.1%. Single crystals suitable for X-ray diffraction were grown from a dilute diethyl ether solution layered with *n*-pentane. ^{1}H NMR (500 MHz, C_6D_6) δ, ppm: 4.04 and 3.33 (s, 8H, C*H* on Cp rings), 3.97 (s, 8H, CH_2O), 1.41 (s, 8H, CH_2CH$_2$), 0.99 (s, 18H, SiCCH_3), 0.41 (s, 12H, SiCH_3). ^{13}C NMR (126 MHz, C_6D_6) δ, ppm: 101.9 (*C*N on Cp rings), 71.7, 69.3, and 68.4 (*C*H on Cp rings and *C*H$_2$O), 27.9 (SiC*C*H$_3$), 25.2 (*C*H$_2$CH$_2$O), 20.5 (Si*C*CH$_3$), and -1.6 (Si*C*H$_3$). Anal. (%): Calcd. for $C_{30}H_{54}N_2FeIO_2ScSi_2$: C, 47.50; H, 7.17; N, 3.69. Found: C, 47.62; H, 7.25; N, 3.54.

Method ii:[51] **Synthesis of (NN^{TBS})YI(THF)$_2$.** 1.0000 g of YBn$_3$(THF)$_3$ (1.723 mmol) and 0.7684 g of H$_2$(NN^{TBS}) (1.728 mmol) were dissolved in THF separately and placed in a dry ice/acetone bath for 10 min prior to mixing. After mixing, the solution was stirred at 0 °C (using an ice bath) for 30 min. The volatiles were then removed under reduced pressure. The resulting yellow solid was extracted with a minimum amount of toluene and the solution filtered through Celite. 0.6916 g of Me$_3$SiI (3.456 mmol) was added to the aforementioned toluene solution. The mixture was stirred at 25 °C for 1 hour. 5 mL of THF was added to the solution to quench the extra Me$_3$SiI. The volatiles were removed under reduced pressure. The remaining orange solids were dissolved in a minimum amount of diethyl ether, layered with *n*-pentane, and stored at -35 °C. Orange crystals formed after three days at -35 °C, 0.7540 g. The mother liquor was then dried under reduced pressure and washed with hexanes. A yellow powder was collected on a medium frit after an extensive hexanes wash, 0.3340 g. Total yield: 1.0880 g, 78.4%. ^{89}Y NMR (29.4 MHz, C_4D_8O, 25 °C) δ, ppm: 369.6. ^{89}Y NMR (29.4 MHz, C_4D_8O, -44 °C) δ, ppm: 369.9. ^{1}H NMR (500 MHz, C_6D_6, 25 °C) δ, ppm: 4.07 and 3.10 (b, 8H, C*H* on Cp rings), 4.06 (b, 8H, CH_2O), 1.40 (m, 8H, CH_2CH$_2$), 1.02 (s, 18H, SiCCH_3), and 0.44 (s, 12H, SiCH_3). ^{13}C NMR (126 MHz, C_6D_6, 25 °C) δ, ppm: 102.9 (*C*N on Cp rings), 72.6 (*C*H$_2$O), 67.6, and 67.1 (*C*H on Cp

rings), 28.0 (SiCCH_3), 25.0 (CH_2CH_2O), 20.6 (SiCCH$_3$), and -1.0 (SiCH_3). Anal. (%): Calcd. for $C_{30}H_{54}N_2FeIO_2Si_2Y$: C, 44.90; H, 6.78; N, 3.49. Found: C, 44.70; H, 6.56; N, 3.47.

Synthesis of (NN^{TBS})ScI(THF)$_2$. 0.7500 g of $Sc(CH_2C_6H_3Me_2\text{-}3,5)_3(THF)_2$ (1.372 mmol) and 0.6100 g of $H_2(NN^{TBS})$ (1.372 mmol) were dissolved in toluene separately and placed in a dry ice/acetone bath for 10 min prior to mixing. After mixing, the solution was stirred at 0 °C (using an ice bath) for 1 h. The volatiles were then removed under reduced pressure. The resulting yellow solid was extracted with toluene and the solution filtered through Celite. 0.5490 g of Me_3SiI (2.744 mmol) was added to the aforementioned toluene solution. The mixture was stirred at 25 °C for 2 h. 5 mL of THF was added to the solution to quench the extra Me_3SiI. The volatiles were removed under reduced pressure. The remaining orange solids were dissolved in a minimum amount of diethyl ether, layered with *n*-pentane, and stored at -35 °C. Orange crystals formed after three days at -35 °C, 0.5596 g. The mother liquor was then dried under reduced pressure and washed with hexanes. A yellow powder was collected on a medium frit after an extensive hexanes wash, 0.1991 g. Total yield: 0.7587 g, 72.9%.

Synthesis of (NN^{TBS})LaI(THF). 1.0501 g of $LaBn_3(THF)_3$ (1.670 mmol) and 0.7427 g of $H_2(NN^{TBS})$ (1.671 mmol) were dissolved in THF separately and placed in a dry ice/acetone bath for 10 min prior to mixing. After mixing, the solution was stirred at 0 °C (using an ice bath) for 30 min. The volatiles were then removed under reduced pressure. The resulting yellow solid was extracted with a minimum amount of toluene and the solution filtered through Celite. 0.6685 g of Me_3SiI (3.341 mmol) was added to the aforementioned toluene solution. The mixture was stirred at 25 °C for 1 h. 5 mL of THF was added to the solution to quench the extra Me_3SiI. The volatiles were removed under reduced pressure. The remaining yellow solids were dispersed in hexanes. A yellow powder was collected on a medium frit after an extensive hexanes wash.

Yield: 1.1650 g, 89.4%. Different from other (NN^{TBS})$MI(THF)_2$, the molecular formula of the product was determined by ^{1}H NMR spectroscopy as (NN^{TBS})La(THF). ^{1}H NMR (500 MHz, C_4D_8O, 25 °C) δ, ppm: 4.23 (s, 4H) and 3.13 (t, 4H), both belong to C*H* on Cp, 0.75 (s, 18H, $C(CH_3)_3$), and 0.16 (s, 12H, $SiCH_3$). ^{13}C NMR (126 MHz, C_4D_8O, 25 °C) δ, ppm: 103.0 (*C*N), 67.5, and 66.6 (*C*H on Cp), 27.7 ($C(CH_3)_3$), 20.5 ($C(CH_3)_3$) and -2.2 ($SiCH_3$). Anal. (%): Calcd. for $C_{26}H_{46}IFeLaN_2OSi_2$: C, 40.01; H, 5.94; N, 3.59. Found: C, 40.04; H, 5.81; N, 3.15.

Synthesis of (NN^{TBS})LuI(THF)$_2$. 0.9800 g of $LuBn_3(THF)_3$ (1.474 mmol) and 0.6550 g of $H_2(NN^{TBS})$ (1.473 mmol) were dissolved in THF separately and placed in a dry ice/acetone bath for 10 min prior to mixing. After mixing, the solution was stirred at 0 °C (using an ice bath) for 30 min. The volatiles were then removed under reduced pressure. The resulting yellow solid was extracted with a minimum amount of toluene and the solution filtered through Celite. 0.5900 g of Me_3SiI (2.949 mmol) was added to the aforementioned toluene solution. The mixture was stirred at 25 °C for 1 h. 5 mL of THF was added to the solution to quench the extra Me_3SiI. The volatiles were removed under reduced pressure. The remaining orange solids were dissolved in a minimum amount of diethyl ether, layered with *n*-pentane, and stored at -35 °C. Orange crystals formed after three days at -35 °C, 0.7488 g. The mother liquor was then dried under reduced pressure and washed with hexanes. A yellow powder was collected on a medium frit after an extensive hexanes wash, 0.3430 g. Total yield: 1.0918 g, 83.3%. ^{1}H NMR (500 MHz, C_6D_6, 25 °C) δ, ppm: 4.15 (m, 8H, CH_2O), 4.03 and 3.18 (s, 8H, C*H* on Cp), 1.42 (m, 4H, CH_2CH_2O), 1.01 (s, 18H, $C(CH_3)_3$), and 0.42 (s, 12H, $SiCH_3$). ^{13}C NMR (126 MHz, C_6D_6, 25 °C) δ, ppm: 102.4 (*C*N), 73.0, 67.3, and 67.2 (CH_2O and *C*H on Cp), 28.1 ($C(CH_3)_3$), 25.0 (CH_2CH_2O), 20.8 ($C(CH_3)_3$) and 0.8 ($SiCH_3$). Anal. (%): Calcd. for $C_{30}H_{54}IFeLuN_2O_2Si_2$: C, 40.55; H, 6.13; N, 3.15. Found: C, 40.93; H, 6.19; N, 3.06.

2.5 References

(1) Shafir, A.; Power, M. P.; Whitener, G. D.; Arnold, J. *Organometallics* **2000**, *19*, 3978.

(2) Shafir, A.; Power, M. P.; Whitener, G. D.; Arnold, J. *Organometallics* **2001**, *20*, 1365.

(3) Shafir, A.; Arnold, J. *Organometallics* **2003**, *22*, 567.

(4) Monreal, M. J.; Carver, C. T.; Diaconescu, P. L. *Inorg. Chem.* **2007**, *46*, 7226.

(5) Carver, C. T.; Monreal, M. J.; Diaconescu, P. L. *Organometallics* **2008**, *27*, 363.

(6) Carver, C. T.; Benitez, D.; Miller, K. L.; Williams, B. N.; Tkatchouk, E.; Goddard, W. A.; Diaconescu, P. L. *J. Am. Chem. Soc.* **2009**, *131*, 10269.

(7) Carver, C. T.; Diaconescu, P. L. *J. Am. Chem. Soc.* **2008**, *130*, 7558.

(8) Miller, K. L.; Williams, B. N.; Benitez, D.; Carver, C. T.; Ogilby, K. R.; Tkatchouk, E.; Goddard, W. A.; Diaconescu, P. L. *J. Am. Chem. Soc.* **2009**, *132*, 342.

(9) Monreal, M. J.; Diaconescu, P. L. *Organometallics* **2008**, *27*, 1702.

(10) Sauro, V. A.; Workentin, M. S. *Can. J. Chem.* **2002**, *80*, 250.

(11) Williams, B. N.; Benitez, D.; Miller, K. L.; Tkatchouk, E.; Goddard, W. A.; Diaconescu, P. L. *J. Am. Chem. Soc.* **2011**, *133*, 4680.

(12) Carver, C. T.; Williams, B. N.; Ogilby, K. R.; Diaconescu, P. L. *Organometallics* **2010**, *29*, 835.

(13) Monreal, M. J.; Diaconescu, P. L. *J. Am. Chem. Soc.* **2010**, *132*, 7676.

(14) Williams, B. N.; Huang, W.; Miller, K. L.; Diaconescu, P. L. *Inorg. Chem.* **2010**, *49*, 11493.

(15) Monreal, M. J.; Khan, S.; Diaconescu, P. L. *Angew. Chem. Int. Ed.* **2009**, *48*, 8352.

(16) Miller, K. L.; Carver, C. T.; Williams, B. N.; Diaconescu, P. L. *Organometallics* **2010**, *29*, 2272.

(17) Duhović, S.; Monreal, M. J.; Diaconescu, P. L. *Inorg. Chem.* **2010**, *49*, 7165.

(18) Diaconescu, P. L. *Acc. Chem. Res.* **2010**, *43*, 1352.

(19) Diaconescu, P. L. *Comments Inorg.Chem.* **2010**, *31*, 196.

(20) Bauer, J.; Braunschweig, H.; Dewhurst, R. D. *Chem. Rev.* **2012**, *112*, 4329.

(21) Seyferth, D.; Hames, B. W.; Rucker, T. G.; Cowie, M.; Dickson, R. S. *Organometallics* **1983**, *2*, 472.

(22) Akabori, S.; Kumagai, T.; Shirahige, T.; Sato, S.; Kawazoe, K.; Tamura, C.; Sato, M. *Organometallics* **1987**, *6*, 2105.

(23) Shafir, A.; Arnold, J. *J. Am. Chem. Soc.* **2001**, *123*, 9212.

(24) Green, A. G.; Kiesz, M. D.; Oria, J. V.; Elliott, A. G.; Buechler, A. K.; Hohenberger, J.; Meyer, K.; Zink, J. I.; Diaconescu, P. L. *Inorg. Chem.* **2013**, *52*, 5603.

(25) Connelly, N. G.; Geiger, W. E. *Chem. Rev.* **1996**, *96*, 877.

(26) Gregson, C. K. A.; Gibson, V. C.; Long, N. J.; Marshall, E. L.; Oxford, P. J.; White, A. J. P. *J. Am. Chem. Soc.* **2006**, *128*, 7410.

(27) Yoon, H. J.; Kuwabara, J.; Kim, J.-H.; Mirkin, C. A. *Science* **2010**, *330*, 66.

(28) Broderick, E. M.; Guo, N.; Vogel, C. S.; Xu, C.; Sutter, J.; Miller, J. T.; Meyer, K.; Mehrkhodavandi, P.; Diaconescu, P. L. *J. Am. Chem. Soc.* **2011**, *133*, 9278.

(29) Ito, N.; Saji, T.; Aoyagui, S. *J. Organomet. Chem.* **1983**, *247*, 301.

(30) Evans, W. J.; Davis, B. L. *Chem. Rev.* **2002**, *102*, 2119.

(31) Huang, W.; Khan, S. I.; Diaconescu, P. L. *J. Am. Chem. Soc.* **2011**, *133*, 10410.

(32) Olah, G. A.; Narang, S. C. *Tetrahedron* **1982**, *38*, 2225.

(33) Huang, W.; Diaconescu, P. L. *Chem. Commun.* **2012**, *48*, 2216.

(34) Mortensen, J.; Heinze, J. *Angew. Chem. Int. Ed.* **1984**, *23*, 84.

(35) Zimmerman, H. E. *Acc. Chem. Res.* **2011**, *45*, 164.

(36) Zandstra, P. J.; Weissman, S. I. *J. Am. Chem. Soc.* **1962**, *84*, 4408.

(37) Bergbreiter, D. E.; Killough, J. M. *J. Am. Chem. Soc.* **1978**, *100*, 2126.

(38) Rüdorff, W.; Schulze, E. *Z. Anorg. Allg. Chem.* **1954**, *277*, 156.

(39) Nief, F. In *Handbook on the Physics and Chemistry of Rare Earths*; Gschneidner, K. A., Bünzli, J.-C. G., Vitalij, K. P., Eds.; Elsevier: 2010, p 241.

(40) Evans, W. J.; Lee, D. S.; Johnston, M. A.; Ziller, J. W. *Organometallics* **2005**, *24*, 6393.

(41) MacDonald, M. R.; Bates, J. E.; Ziller, J. W.; Furche, F.; Evans, W. J. *J. Am. Chem. Soc.* **2013**, *135*, 9857.

(42) Wang, Y.; Quillian, B.; Wei, P.; Wannere, C. S.; Xie, Y.; King, R. B.; Schaefer, H. F.; Schleyer, P. v. R.; Robinson, G. H. *J. Am. Chem. Soc.* **2007**, *129*, 12412.

(43) Wang, Y.; Xie, Y.; Wei, P.; King, R. B.; Schaefer, H. F.; von R. Schleyer, P.; Robinson, G. H. *Science* **2008**, *321*, 1069.

(44) Braunschweig, H.; Dewhurst, R. D.; Hammond, K.; Mies, J.; Radacki, K.; Vargas, A. *Science* **2012**, *336*, 1420.

(45) Jensen, K. A.; Nygaard, B.; Elisson, G.; Nielsen, P. H. *Acta Chem. Scand.* **1965**, *19*, 768.

(46) Ungurenasu, C.; Palie, M. *J. Chem. Soc., Chem. Commun.* **1975**, 388a.

(47) Schwindt, M. A.; Lejon, T.; Hegedus, L. S. *Organometallics* **1990**, *9*, 2814.

(48) Ebert, L. B. *Carbon* **1985**, *23*, 585.

(49) Ebert, L. B.; Mills, D. R.; Garcia, A. R.; Scanlon, J. C. *Mater. Res. Bull.* **1985**, *20*, 1453.

(50) Weitz, A.; Rabinovitz, M. *Synthetic Metals* **1995**, *74*, 201.

(51) Huang, W.; Dulong, F.; Wu, T.; Khan, S. I.; Miller, J. T.; Cantat, T.; Diaconescu, P. L. *Nat. Commun.* **2013**, *4*, 1448.

CHAPTER 3: REDUCTIVE CLEAVAGE OF AROMATIC C-H AND C-F BONDS

3.1 Introduction

The carbon-hydrogen (C-H) bond is the most common chemical bond. It is also one of the strongest single bonds and almost non-polar. Although it is difficult to achieve selective functionalization of C-H bonds, these processes are highly desirable from an economical point of view.[1,2] In nature, C-H bond functionalization is achieved by certain enzymes to form a hydroxyl group.[3,4] Organometallic compounds have been found particularly useful in mediating C-H activation.[5] Four types of mechanisms (Scheme 3-1) have been widely accepted for the C-H activation reaction involving organometallic complexes: oxidative addition with electron-rich, low-valent late transition metals,[1] electrophilic activation with electron-deficient late transition metals,[6] 1,2-CH addition across a metal-element multiple bond,[7] and σ-bond metathesis with polarized metal-carbon bonds.[8] It has long been thought that oxidative addition is common for late transition metals while σ-bond metathesis is dominant for early transition metals and rare-earth metals.[9] Recently, examples of electron-deficient, late transition metals mediated C-H activation have been reported that cannot be rationalized by an oxidative addition mechanism. Experimental and computational studies suggest a pseudo-σ-bond metathesis mechanism.[6,10] Such discoveries blurry the line between early and late transition metals. However, to date, the metal-centered oxidative addition mechanism is found exclusively with late transition metals.[9]

***Oxidative addition*: typical for low valent late transition metal complexes**

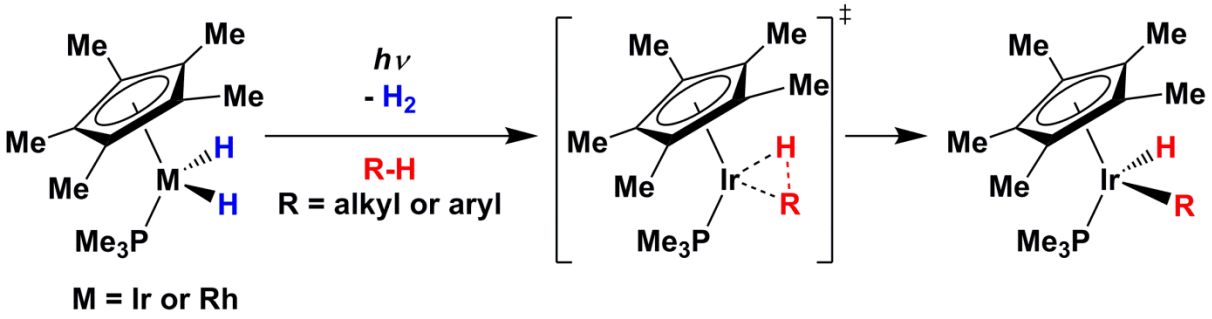

M = Ir or Rh

***σ-complex-assisted metathesis (σ-CAM)* mediated by electrophilic late transition metals**

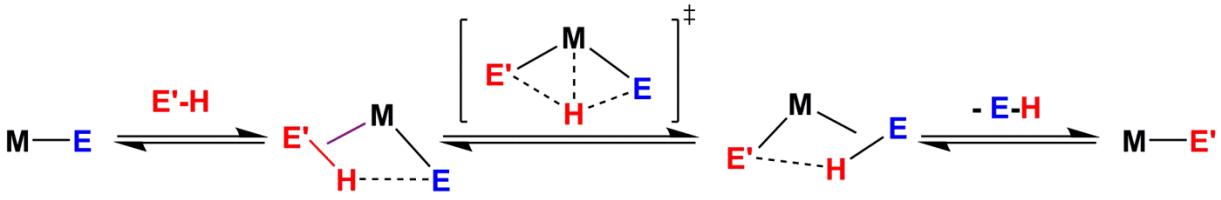

***1,2-Addition*: [2π+2σ] cycloaddition**

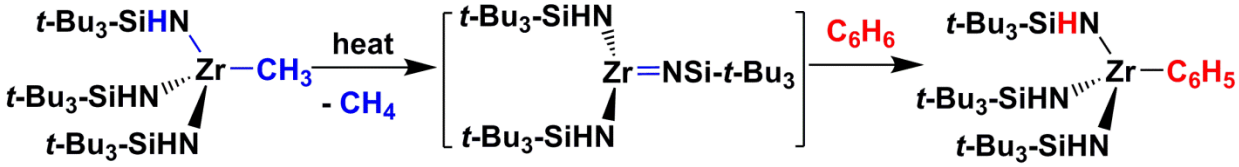

***σ-Bond metathesis*: typical for high valent d^0f^n metal complexes**

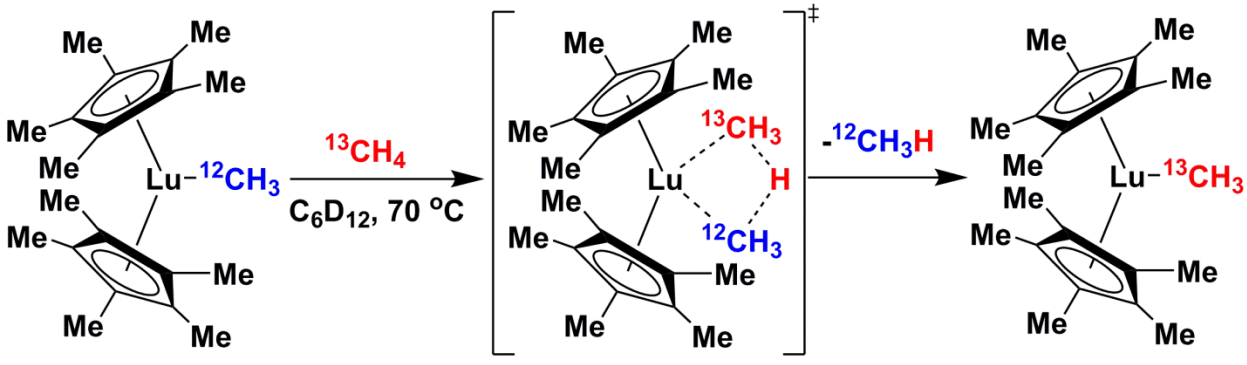

Scheme 3-1: Four types of C-H activation mechanisms involving organometallic complexes (from top to bottom): oxidative addition, σ-CAM, 1,2-addition, and σ-bond metathesis. The alkyl or hydride that was eliminated from the metal complexes is highlighted in **blue**; the alkyl and hydride that was activated by the metal complexes is highlighted in **red**.

3.2 Aromatic C-H bond activation

Herein we discuss a new type of C-H bond activation mediated by rare-earth metal complexes that cannot be classified as σ-bond metathesis. This reaction is closely related to oxidative addition in that its products are a metal hydride and a metal aryl complex. Because it requires reducing agents while the oxidation state of metal centers involved stays the same, we propose the term "reductive cleavage" for this type of C-H activation. We think that this reductive cleavage is a counterpart for rare-earth metals to the oxidative addition mechanism found with late transition metals. In addition to C-H activation, we extend the reductive cleavage to C-F activation (discussed in section 3.3).

Addition of 1.8 equivalents of KC_8 to a benzene solution of $(NN^{TBS})ScI(THF)_2$ (NN^{TBS} = 1,1′-fc(NSi^tBuMe_2)$_2$) resulted in no immediate color change (Scheme 3-2). However, after 2 hours of stirring at 25 °C, the characteristic golden brown color of KC_8 disappeared and the black graphite precipitated out. After a standard work-up to remove insoluble matter and volatiles, an orange solid was obtained. The ^{1}H NMR spectrum of the solid suggested that two products were obtained in a 1:1 scandium molar ratio that were separated based on their different solubilities.

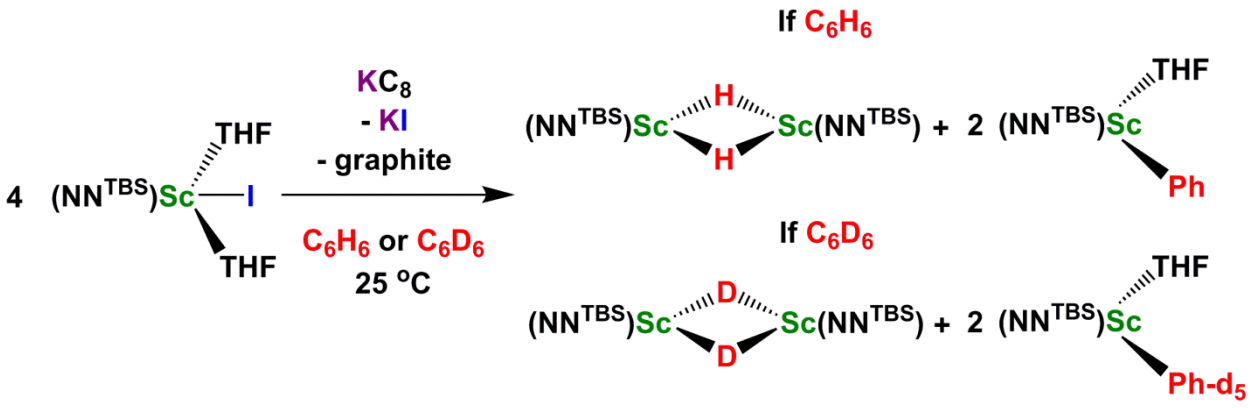

Scheme 3-2: Reaction of $(NN^{TBS})ScI(THF)_2$ and KC_8 in neat C_6H_6 or C_6D_6.

X-ray crystallography unambiguously established one of the products to be a scandium hydride, $[(NN^{TBS})Sc(THF)](\mu\text{-}H)_2[Sc(NN^{TBS})]$ (Figure 3-1a). The coordination of the THF molecule is labile: a THF-free version $[(NN^{TBS})Sc(\mu\text{-}H)]_2$ was obtained after recrystallization of the crude product from a toluene solution layered with *n*-pentane as indicated by ^{1}H NMR spectroscopy. The other product, a scandium phenyl complex, $(NN^{TBS})Sc(C_6H_5)(THF)$, was characterized by its independent synthesis from $(NN^{TBS})ScI(THF)_2$ and phenyl lithium (PhLi); the crystal structure of the analogous $(NN^{TBS})Sc(p\text{-}Me\text{-}C_6H_4)(THF)$ is shown in Figure 3-1b. The reaction between $(NN^{TBS})ScI(THF)_2$ and KC_8 could also be carried out in benzene-d_6 instead of benzene. Monitoring by ^{1}H NMR spectroscopy showed the formation of the corresponding deuterated products $[(NN^{TBS})Sc(\mu\text{-}D)]_2$ (the coordinating THF molecule is omitted since it is labile) and $(NN^{TBS})Sc(C_6D_5)(THF)$, which were also probed by ^{2}H NMR spectroscopy to confirm the presence of the deuteride and perdeuterated phenyl group (Figure 3-2). This experiment confirmed that the hydride and phenyl ligands originated from the C-H bond cleavage of benzene.

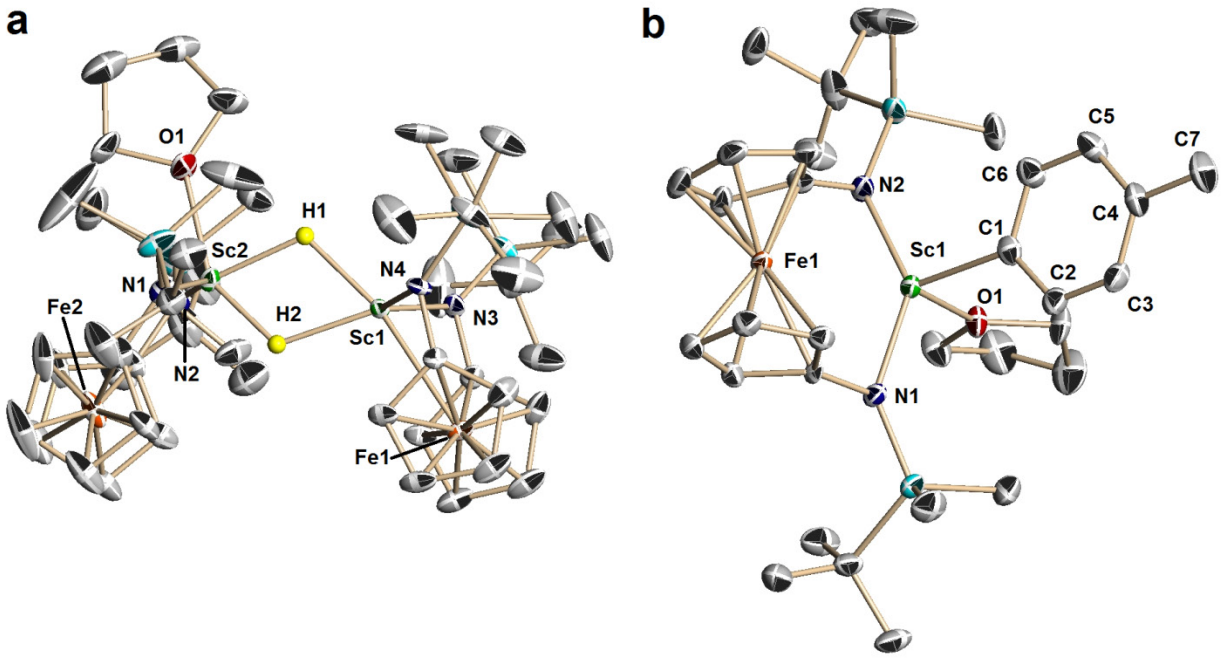

Figure 3-1: Molecular structures of [(NN^{TBS})Sc(THF)](μ-H)$_2$[Sc(NN^{TBS})] (a) and (NN^{TBS})Sc(*p*-Me-C$_6$H$_4$)(THF) (b). Thermal ellipsoids are drawn at the 50% probability level (except for hydrides). Hydrogen atoms except hydride ligands were omitted for clarity. Selected distances [Å] and angles [°] (errors in brackets): (a) [(NN^{TBS})Sc(THF)](μ-H)$_2$[Sc(NN^{TBS})]: Sc1-Sc2 3.278(2), Sc1-N3 2.093(4), Sc1-N4 2.063(5), Sc1-Fe1 2.800(2), Sc2-N1 2.072(5), Sc2-N2 2.063(5), Sc2-O1 2.196(4), Sc2-Fe2 3.279(2); N3-Sc1-N4 115.3(2), N1-Sc2-N2 133.0(2), Fe1-Sc1-Sc2 133.9(1), Fe2-Sc2-Sc1 121.8(1), O1-Sc2-Sc1 113.0(1). (b) (NN^{TBS})Sc(*p*-Me-C$_6$H$_4$)(THF): Sc1-C1 2.250(3), Sc1-N1 2.065(3), Sc1-N2 2.072(3), Sc1-O1 2.163(2), Sc1-Fe1 3.026(1), C1-C2 1.412(5), C2-C3 1.395(5), C3-C4 1.394(5), C4-C7 1.511(5), C4-C5 1.395(5), C5-C6 1.404(5), C6-C1 1.408(5); N1-Sc1-N2 137.5(1), C1-Sc1-O1 98.0 (1), O1-Sc1-Fe1 152.8(1) C1-Sc1-Fe1 109.2(1) (sum of the last three angles is 360.0), C2-C1-C6 114.4(3).

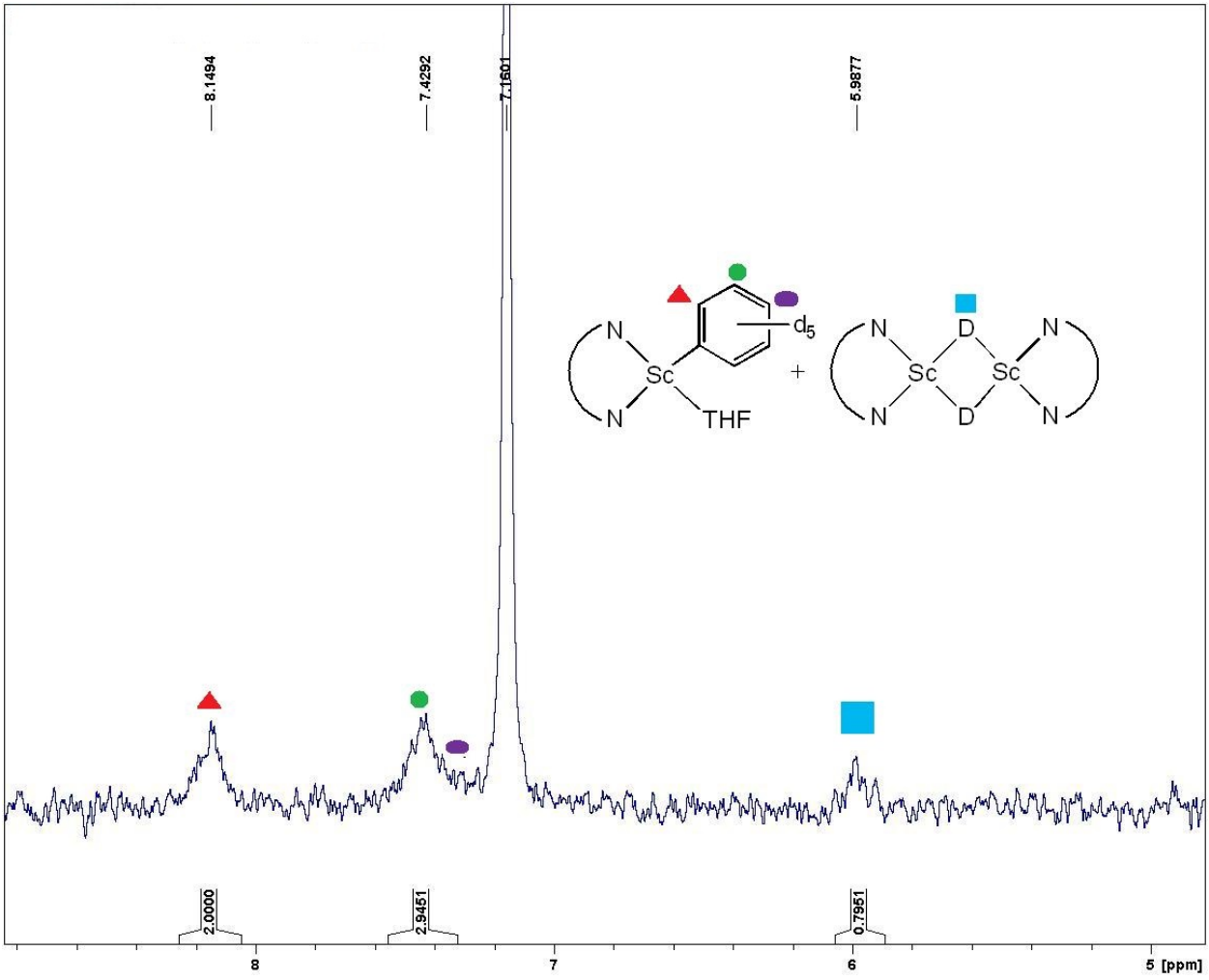

Figure 3-2: ^{2}H NMR spectrum of the crude products from the reaction of $(NN^{TBS})ScI(THF)_2$ and KC_8 in neat C_6D_6 (obtained in C_6H_6 and referenced to residue C_6D_6).

We propose the following mechanism (Scheme 3-3): the reduction of $(NN^{TBS})ScI(THF)_2$ with KC_8 in the presence of benzene leads to $[(NN^{TBS})Sc]_2(\mu\text{-}C_6H_6)$ (intermediate **I**) featuring a benzene dianion bridging two Sc(III) centers. Intermediate **I** undergoes C-H bond cleavage to give a bridging hydride-aryl dinuclear complex, $[(NN^{TBS})Sc](\mu\text{-}C_6H_5)(\mu\text{-}H)[Sc(NN^{TBS})]$ (**II**). Ligand redistribution from **II** accounts for the formation of the observed products, $[(NN^{TBS})Sc(\mu\text{-}H)]_2$ and $(NN^{TBS})Sc(C_6H_5)(THF)$.

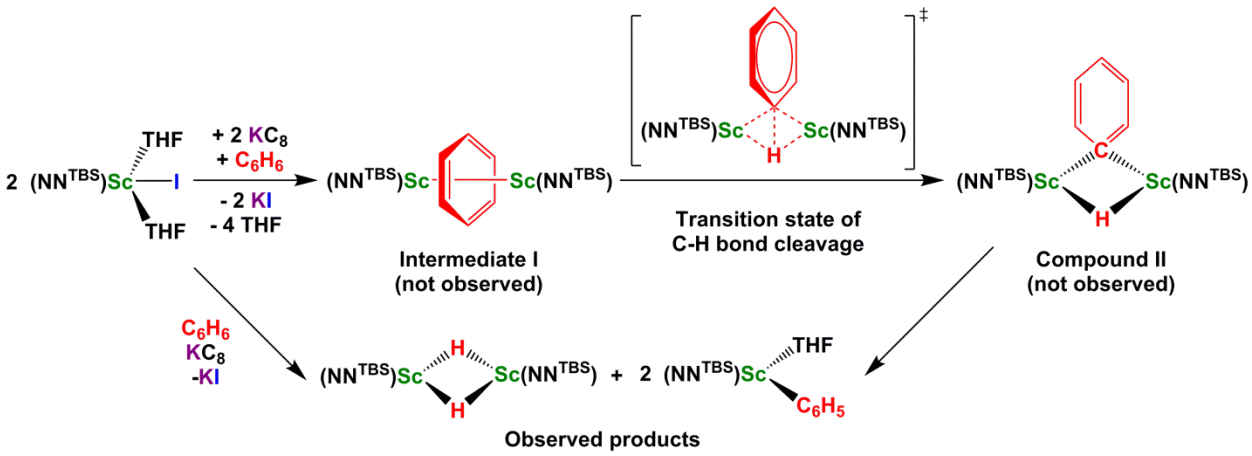

Scheme 3-3: Proposed mechanism for C-H activation of benzene by the $(NN^{TBS})ScI(THF)_2/KC_8$ system.

Support for the existence of intermediate **I** comes from Lappert's work, who studied intensively benzene reduction by alkali metals with or without the presence of lanthanide complexes (Chart 3-1). He reported the isolation of a benzene dianion supported by rare earth metals in the heterometallic compounds $[K(18\text{-crown-}6)][(\eta^5\text{-}1,3\text{-}(SiMe_3)_2\text{-}C_5H_3)_2Ln(\mu_2\text{-}\eta^6\text{:}\eta^4\text{-}C_6H_6)]$ (Ln = La, Ce, and Nd) from a mixture of $La(\eta^5\text{-}1,3\text{-}(SiMe_3)_2\text{-}C_5H_3)_3$, excess potassium metal (mirror), and 18-crown-6 in benzene. The benzene dianion is in a boat conformation and is best described as a 1,4-cyclohexa-2,5-dienyl ligand, although no further reactivity to form metal hydride and/or phenyl products has been reported.[11] Starting from a different substituted cyclopentadienyl complex, $La(\eta^5\text{-}1,3\text{-}(CMe_3)_2\text{-}C_5H_3)_3$, a planar bridging benzene ligand was found in the complex $[K(18\text{-crown-}6)(\eta^2\text{-}C_6H_6)_2][(\eta^5\text{-}1,3\text{-}(CMe_3)_2\text{-}C_5H_3)_2La]_2(\mu_2\text{-}\eta^6\text{:}\eta^6\text{-}C_6H_6)$. It was proposed that the complex contains two lanthanum(II) ions and a benzene monoanion.[12] In a subsequent article,[13] Lappert showed that the toluene radical anion could be obtained directly from potassium metal, 18-crown-6, and toluene in a THF solution. The corresponding benzene

radical anion could not be obtained probably due to its high reactivity, but, instead, the radical coupled dimer $[K(18\text{-crown-}6)]_2(\mu\text{-}\eta^5\text{:}\eta^5\text{-}C_6H_6\text{-}C_6H_6)$ was isolated. It is important to note that Lappert suggested that the dimer readily dissociated to $C_6H_6^{\bullet-}$ in solution.[13] However, no evidence for C-H bond activation was found in that system. In our case, monitoring the reaction in benzene-d_6 by ^{1}H NMR spectroscopy did not allow the observation of species other than the starting material, $(NN^{TBS})ScI(THF)_2$, and the products, $[(NN^{TBS})Sc(\mu\text{-}H)]_2$ and $(NN^{TBS})Sc(C_6H_5)(THF)$.

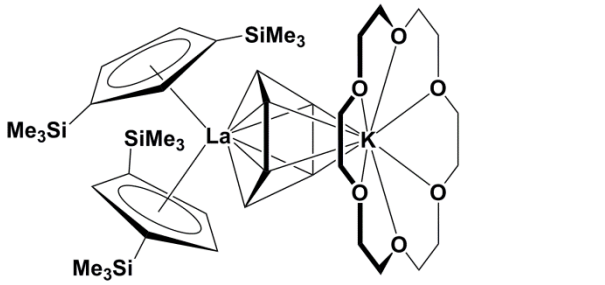

$[K([18]\text{-crown-}6)][(\eta^5\text{-}1,3\text{-}(SiMe_3)_2\text{-}C_5H_3)_2Ln(\mu_2\text{-}\eta^6\text{:}\eta^4\text{-}C_6H_6)]$

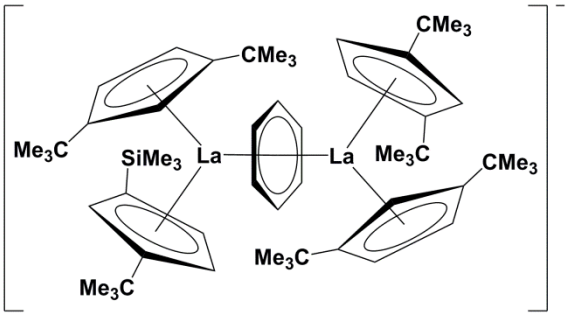

$([(\eta^5\text{-}1,3\text{-}(CMe_3)_2\text{-}C_5H_3)_2La]_2(\mu_2\text{-}\eta^6\text{:}\eta^6\text{-}C_6H_6))^-$

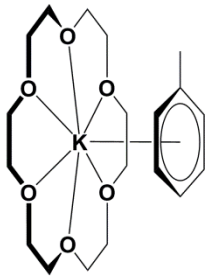

$K(18\text{-crown-}6)(\eta^6\text{-}C_6H_5Me)$

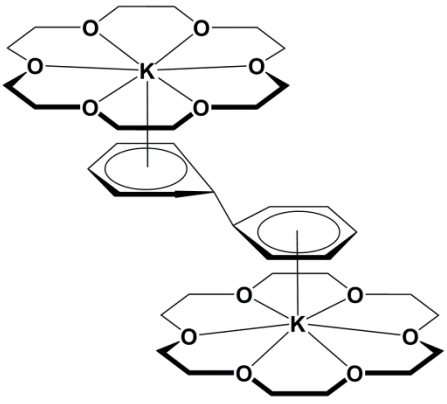

$[K(18\text{-crown-}6)]_2(\mu\text{-}\eta^5\text{:}\eta^5\text{-}C_6H_6\text{-}C_6H_6)$

Chart 3-1: Crystallographically characterized potassium and/or lanthanum stabilized reduced benzene moieties by Lappert (the counter cation without close contact to the reduced arene is omitted for clarity).

DFT calculations (collaboration with Dr. Thibault Cantat at CEA, France) support the proposed mechanism (Figure 3-3). The bridging benzene ligand in intermediate **I** $[(NN^{TBS})Sc]_2(\mu\text{-}C_6H_6)$ has a distorted structure and it is best described as $\mu\text{-}\eta^6\text{:}\eta^2\text{-}C_6H_6$ with one scandium ion (Sc_1) binding to all six carbon atoms (Sc_1-C distances range from 2.573 to 2.764 Å in **I**) and the other scandium ion (Sc_2) binding tightly only to two adjacent carbon atoms (2.281 and 2.305 Å). This asymmetry is more prominent in the calculated transition state: the scandium-carbon(phenyl) bond is almost formed (the red solid line in Figure 3-3, the Sc_1-C distance was calculated to be 2.21 Å, while in $(NN^{TBS})Sc(p\text{-}Me\text{-}C_6H_4)(THF)$ the Sc-C_{aryl} distance is 2.250(3) Å), while Sc_2 binds mainly to the π electrons of benzene. The Fe-Sc distances also experience a different amount of change: Sc_1-Fe_1 (see Figure 3-3 for labeling) is 2.90 Å (0.20 Å shorter than in intermediate **I**), while Sc_2-Fe_2 only shows a minimum amount of change (2.99 Å in the transition state and 3.04 Å in intermediate **I**). The asymmetry in the transition state indicates that the two scandium ions play different roles in activating the C-H bond. In the product, compound **II**, the geometric difference between the two scandium ions diminishes and they bind equally to the bridging hydride and phenyl ligand.

A low activation barrier of 17.5 kcal/mol was found for the C-H cleavage step. This value is consistent with the experimental observations that the C-H activation step is not rate-determining, i.e. the rate-determining step is either the formation of intermediate **I** or prior to it, since **I** is not observed. A comparison between a singlet and a triplet reaction coordinate, with

the latter involving unpaired electrons, was also undertaken. The activation barrier was calculated to be even lower than for the singlet coordinate, at 16.8 kcal/mol, but the triplet state of intermediate **I** was found to be 7.8 kcal/mol higher in energy than the corresponding singlet state. Although iron may play a role in the C-H cleavage step, it is unlikely that intermediates and transition states with unpaired electrons are involved, i.e. iron(I) species.

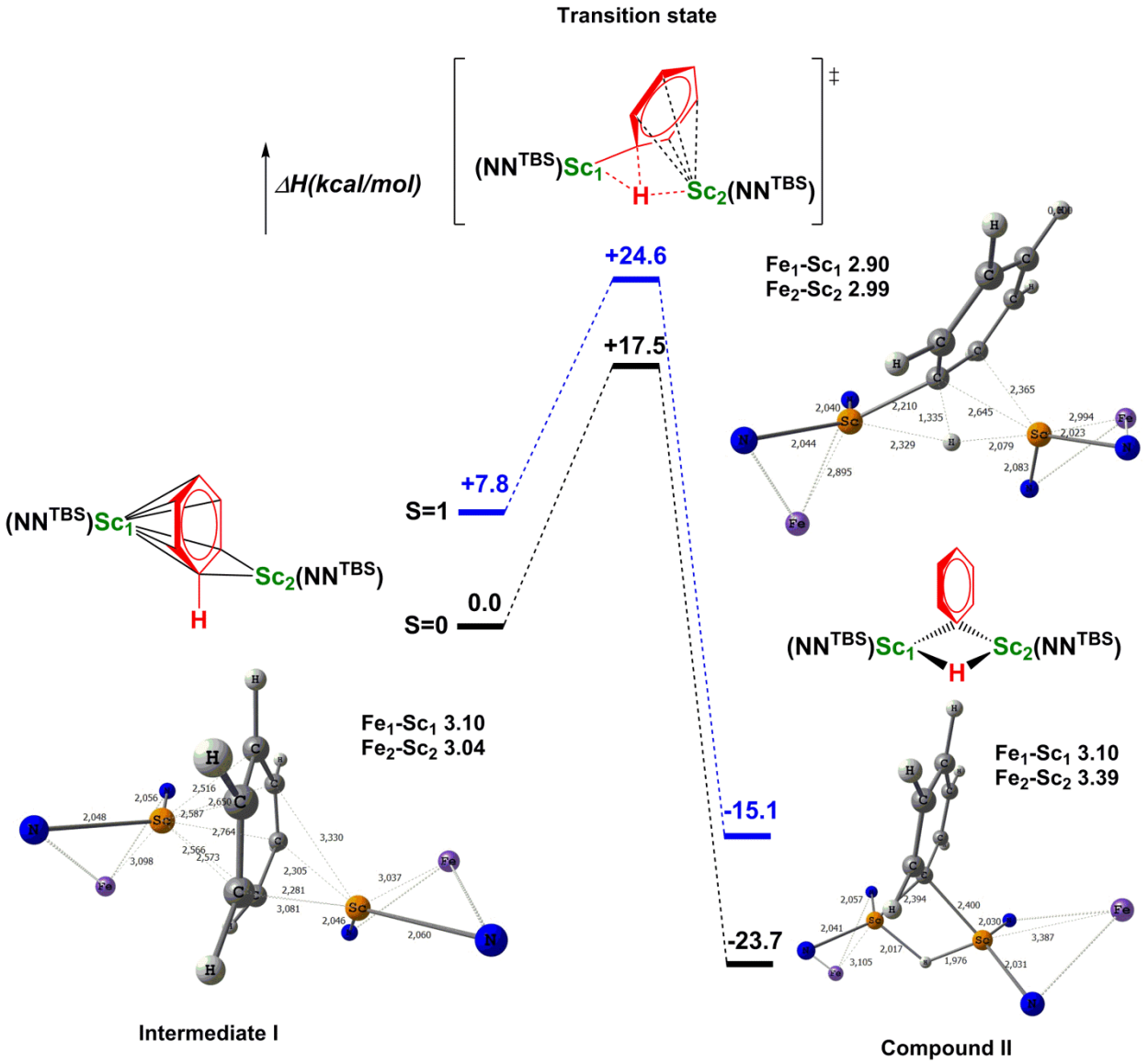

Figure 3-3: DFT calculation results for the C-H bond cleavage step of benzene activation. Relative energies (kcal/mol) for intermediate **I**, the transition state, and compound **II** are shown in the graph (singlet in black and triplet in blue). The calculated structures are shown with numbers indicating selected interatomic distances (in Å) (Sc in orange, Fe in purple, N in blue, and C and H in grey).

3.2.1 Generality of the reductive cleavage of aromatic C-H bonds

Since rare earth metals usually have similar chemical reactivity, it was not surprising that the analogues $(NN^{TBS})YI(THF)_2$, $(NN^{TBS})LuI(THF)_2$, and $(NN^{TBS})ErI(THF)_2$ (see Chapter 6 for the synthesis of $(NN^{TBS})ErI(THF)_2$) delivered C-H bond cleavage under the same reaction conditions, with the formation of the corresponding metal hydride and phenyl complexes (Figure 3-4). However, the largest analogue, $(NN^{TBS})LaI(THF)$, did not deliver the formation of lanthanum hydride and phenyl products. Currently, we do not fully understand the failure of $(NN^{TBS})LaI(THF)_2/KC_8$ system.

While most rare earth metals worked, ligand choice seemed to be critical: only complexes with ferrocene-based amide ligands, NN^{TBS} and NN^{MES} (NN^{MES} = 1,1′-fc[N(Mesityl)]$_2$, Mesityl = $C_6H_2Me_3$-2,4,6), showed C-H activation reactivity. Neither the pincer-type pyridine-diamide ligand, 2,6-bis(2,6-di-iso-propylanilidomethyl)pyridine, N_2N^{py}, nor bis(trimethylsilyl)amide scandium complexes delivered the C-H activation of benzene. The necessity of using 1,1′-ferrocenediyl diamide ligands echoes the important role of the ferrocene backbone suggested by DFT calculations.

After we achieved C-H activation of benzene by $(NN^{TBS})ScI(THF)_2/KC_8$ system, we revisited the reaction of $[(NN^{TBS})Sc(\mu\text{-}Cl)]_2$ and KC_8 in benzene. $(NN^{TBS})ScCl(THF)_2$ was

freshly prepared by dissolving $[(NN^{TBS})Sc(\mu\text{-}Cl)]_2$ in a small amount of THF and then removing the volatiles under reduced pressure (the presence of the coordinating THF molecules was confirmed by ^1H NMR spectroscopy). $(NN^{TBS})ScCl(THF)_2/KC_8$ system was also able to reductive cleavage the C-H bond of benzene. Although the reaction was messier compared to $(NN^{TBS})ScI(THF)_2/KC_8$ system, this result highlighted the role of coordinating molecules in the reduction chemistry.

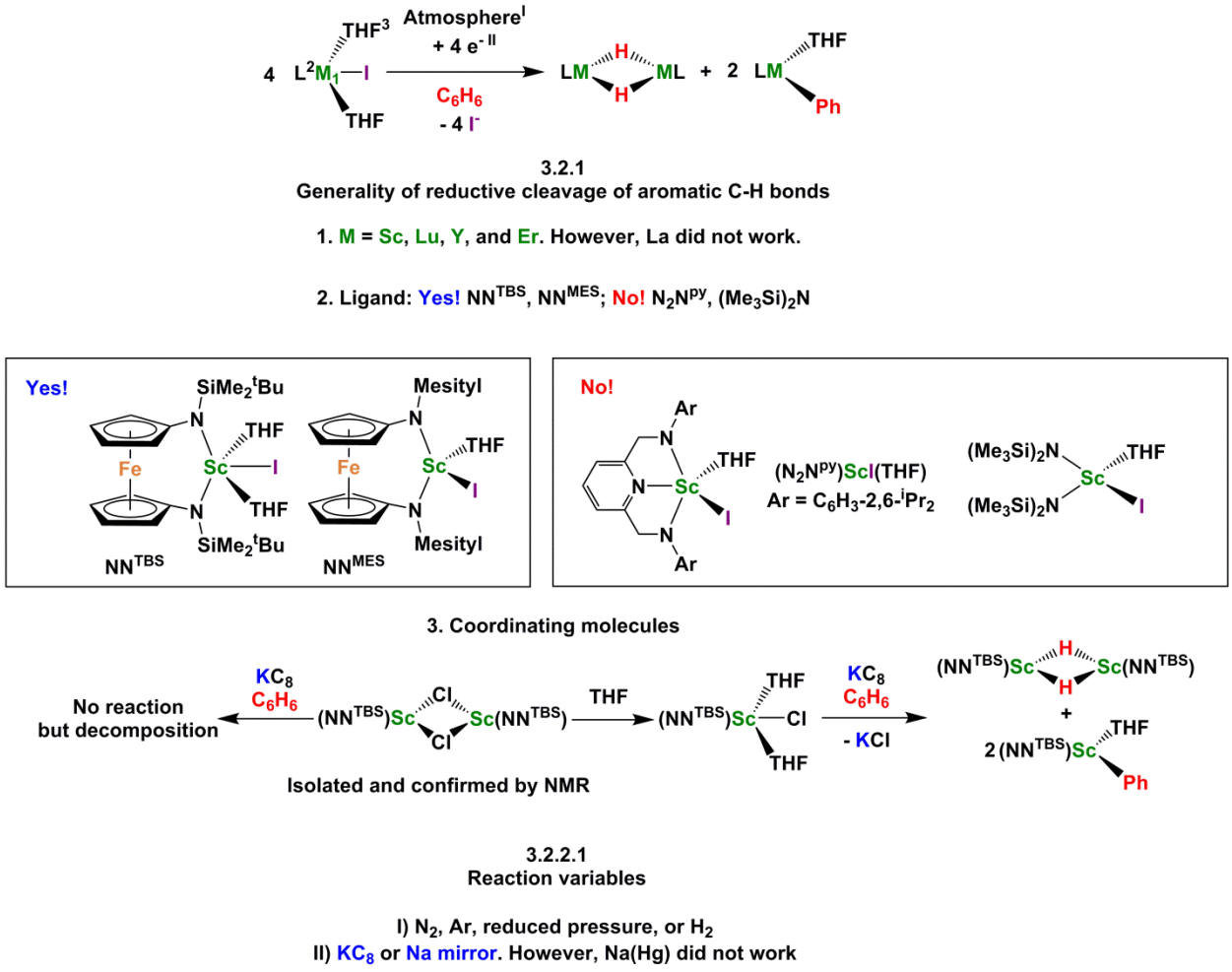

Figure 3-4: Generality of reductive cleavage of aromatic C-H bonds and reaction variables.

3.2.2 Mechanistic study

3.2.2.1 Variables: Since the observation of the dianionic benzene intermediate **I** eluded us, we turned to study the reaction further by changing reaction variables (Figure 3-4). The first variable was the gas atmosphere. Evans and co-workers have shown that the common products when treating Ln(III) precursors with strong reducing agents under an N_2 atmosphere are N_2^{2-} containing complexes.[14] All our reactions were carried out under an N_2 atmosphere. In order to eliminate the possibility that N_2^{2-} serves as a catalyst or intermediate, we performed a reaction under argon or under reduced pressure and found that the C-H activation reaction proceeded similarly. This observation does not support the involvement of N_2^{2-} in the C-H activation reactions.

In order to test whether the C-H activation could proceed through a σ-bond metathesis mechanism, we carried reactions under H_2. The presence of H_2 would favor the formation of $[(NN^{TBS})Sc(\mu\text{-}H)]_2$ if the reaction followed a σ-bond metathesis mechanism,[15] but our studies did not show different results when reactions were carried out under H_2. Therefore, the σ-bond metathesis mechanism does not apply.

The second variable explored was reducing agents. We decided to determine whether the C-H bond reductive cleavage is limited to KC_8 as the electron source. We found out that sodium mirror worked just as well as KC_8. However, when sodium amalgam was used, no reactivity was observed even at a high sodium concentration (2%). The incapacity of sodium amalgam to effect a reaction may be explained by its weaker reducing power (-1.96 V vs. NHE (Normal Hydrogen Electrode)) compared to sodium and KC_8 (ca. -2.7 to -3.0 V vs. NHE).[16]

3.2.2.2 Kinetic isotope effects: In order to learn more about the reaction mechanism, we determined the *inter*molecular and *intra*molecular kinetic isotope effects (KIEs) using a 1:1

mixture of benzene and benzene-d_6, and 1,3,5-trideuterobenzene, respectively (Scheme 3-4). We first determined that the products $[(NN^{TBS})Sc(\mu\text{-}H)]_2$ and $(NN^{TBS})Sc(C_6H_5)(THF)$ did not undergo any scrambling with benzene or benzene-d_6 at 25 °C or higher temperatures. The *inter*molecular KIE was found to be 1.0 indicating that the C-H bond cleavage step is not rate-determining, consistent with other experimental observations and results derived from DFT calculations. For comparison, the KIE was 2.8 for the σ-bond metathesis reaction of $(Cp^*\text{-}d_{15})_2ScCH_3$ with C_6H_6 and C_6D_6 at 80 °C.[15] The *intra*molecular KIE using 1,3,5-trideuterobenzene was found to be 4.2. The fact that the *inter*molecular and *intra*molecular KIEs were found to be different indicates that the C-H bond cleavage does not occur from the direct insertion of a metal species into the C-H bond of benzene but rather from an intermediate containing both the metal and benzene.[17] This result is important since it supports the proposed benzene dianion intermediate **I**, $[(NN^{TBS})Sc]_2(\mu\text{-}C_6H_6)$.

3.2.2.3 Toluene regioselectivity: We also studied whether the reaction shows any regioselectivity if toluene is used. Toluene contains four different C-H bonds: *ortho*-, *meta*-, *para*-, and benzylic C-H bonds. In the reaction of scandium alkyl complexes and toluene that follows the σ-bond metathesis mechanism, Bercaw found no selectivity for the *meta*- and *para*-positions and suggested that there was no involvement of the π system of arene in σ-bond metathesis.[15] However, regioselectivity was found in the reaction of $(NN^{TBS})ScI(THF)_2$ and KC_8 in toluene. A product distribution of 6:1 for $(NN^{TBS})Sc(m\text{-}Me\text{-}C_6H_4)(THF)$ versus $(NN^{TBS})Sc(o\text{-}Me\text{-}C_6H_4)(THF)$ was obtained, without any $(NN^{TBS})Sc(p\text{-}Me\text{-}C_6H_4)(THF)$ or $(NN^{TBS})Sc(CH_2C_6H_5)(THF)$ formation observed. These experimental results agreed with DFT calculations that showed that the C-H activation of the *ortho*- and *meta*-positions had similar activation barriers (14.5 kcal/mol) and were 3.1 kcal/mol lower than the barrier for the *para*-

position (17.6 kcal/mol); all those barriers were much lower than that for the benzylic position (50.4 kcal/mol). The preference for the *meta*-C-H activation observed experimentally is likely due to steric hindrance since the less hindered $(NN^{TBS})LuI(THF)_2/KC_8$ system gave a 1:1 ratio of $(NN^{TBS})Lu(m\text{-}Me\text{-}C_6H_4)(THF)$ versus $(NN^{TBS})Lu(o\text{-}Me\text{-}C_6H_4)(THF)$. This selectivity disfavors a σ-bond metathesis mechanism as well as a radical mechanism, and is reminiscent of the 2,5-selectivity observed for Birch reductions of arenes with electron donating alkyl substituents.[18]

3.2.2.4 C-H activation from a dianionic naphthalene complex: Since intermediate **I** could not be observed, we decided to probe whether a similar reaction would take place from an analogous dianionic naphthalene complex $[(NN^{TBS})Lu(THF)]_2(\mu\text{-}\eta^4\text{:}\eta^4\text{-}C_{10}H_8)$ (**Lu_2-naph**, see Chapter 4 for synthesis). Although the two $(NN^{TBS})Lu(THF)$ moieties sit oppositely on two different phenyl rings in the solid state as determined by X-ray crystallography, the variable temperature ^1H NMR spectroscopic study of **Lu_2-naph** in toluene-d_8 showed that this complex displays fluxional behavior in solution.[19] Therefore, we hypothesized that, in solution, the two lutetium ions may coordinate to the same phenyl ring and enable the C-H bond activation reaction. To our delight, heating a benzene-d_6 solution of **Lu_2-naph** at 50 °C led to clean C-H bond cleavage of naphthalene exclusively at the α-position to form $[(NN^{TBS})Lu(THF)(\mu\text{-}H)]_2$ and $(NN^{TBS})Lu(\alpha\text{-}C_{10}H_7)(THF)$ in a 1:1 lutetium molar ratio. The analogous reaction with $[(NN^{TBS})Sc]_2(\mu\text{-}\eta^4\text{:}\eta^4\text{-}C_{10}H_8)$ (**Sc_2-naph** see Chapter 4) only led to trace amounts of $[(NN^{TBS})Sc(\mu\text{-}H)]_2$ and $(NN^{TBS})Sc(\alpha\text{-}C_{10}H_7)(THF)$. Those results were attributed to the lack of fluxional behavior of **Sc_2-naph** in solution and to the instability of the products $[(NN^{TBS})Sc(\mu\text{-}H)]_2$ and $(NN^{TBS})Sc(\alpha\text{-}C_{10}H_7)(THF)$ at 85 °C. For the larger rare-earth ions, no C-H bond activation of naphthalene was observed from **Y_2-naph** and **La_2-naph** but rather decomposition to unidentified species. The lack of C-H bond activation reactivity for the yttrium and lanthanum

analogues is probably due to the weaker Lewis acidity of those ions compared to that of scandium and lutetium.[20] The unambiguous C-H bond activation of naphthalene from **Lu_2-naph** strongly supports the proposed mechanism involving a bridging arene dianionic intermediate.

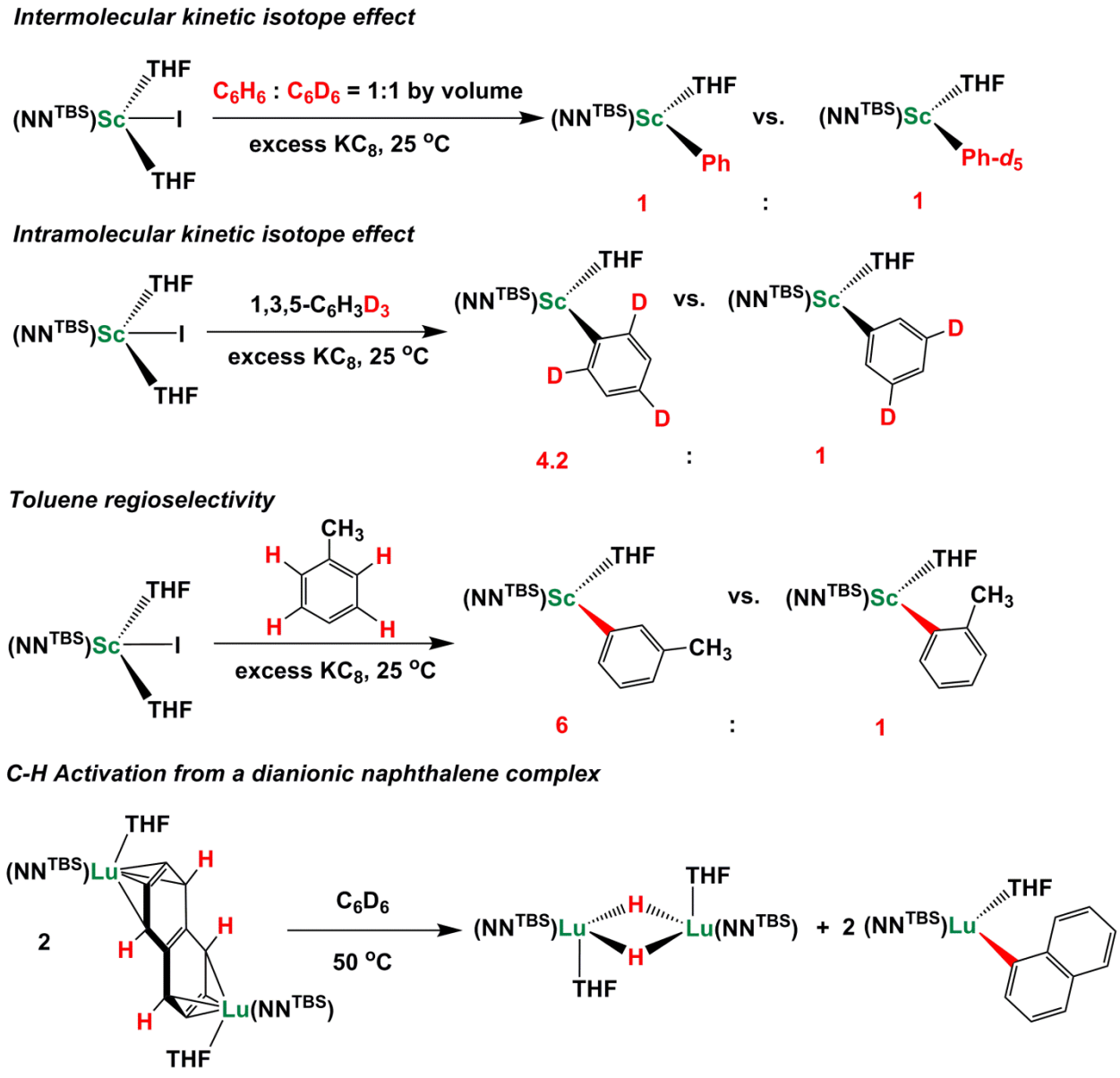

Scheme 3-4: Mechanistic studies: *inter*- and *intra*molecular KIEs, toluene regioselectivity, and C-H activation from a dianionic naphthalene complex.

3.2.3 Kinetics studies:

$(NN^{TBS})ScI(THF)_2/KC_8$ system in benzene: Although the heterogeneous nature of KC_8 precludes any quantitative kinetics studies, we aimed to understand the kinetics of the reductive cleavage reaction qualitatively. We considered several reaction variables: temperature, stirring rate, solution volume, amount of $(NN^{TBS})ScI(THF)_2$, amount of KC_8, and benzene percentage. By keeping the temperature, stirring rate, solution volume, and amount of $(NN^{TBS})ScI(THF)_2$ constant, we studied the effects of KC_8 and benzene percentage using the conversion of $(NN^{TBS})ScI(THF)_2$ as a probe.

The decay of $(NN^{TBS})ScI(THF)_2$ was found to be linear under all conditions, i.e., there was no observed dependence of the reaction rate on the concentration of $(NN^{TBS})ScI(THF)_2$. Since no estimation of the concentration nor degree of activity of KC_8 is available, this does not necessary mean that the reductive cleavage of C-H bonds is zero-order in $(NN^{TBS})ScI(THF)_2$. However, it strongly suggests that the first electron transfer step is heterogeneous in nature. The amount of KC_8 (the reactions were set up in parallel) was found to affect the reaction rate greatly: changing the amount of KC_8 by a factor of four resulted in the reaction rate increasing by nine times while keeping other reaction variables constant. Two reasons may account for the positive effect of the KC_8 amount: (1) increased surface area as a consequence of more KC_8 present; (2) increased amount of the more active K^0 species.[21] However, since the decay of $(NN^{TBS})ScI(THF)_2$ remained constant the latter is likely not important. The benzene percentage also affected the reaction rate. The reaction of $(NN^{TBS})ScI(THF)_2/KC_8$ in 1:9 benzene:hexanes was much slower than in neat benzene. However, besides the concentration of benzene, the relative permittivity and how well dispersed KC_8 in a certain organic solvent[22] may also be the reason for the change in reaction rate.

C-H bond activation from $[(NN^{TBS})Lu(THF)]_2(\mu\text{-}\eta^4\text{:}\eta^4\text{-}C_{10}H_8)$: Lu_2-naph is slightly soluble in C_6D_6. This allowed a quantitative kinetics study on the C-H bond activation from **Lu_2-naph**. The decay of **Lu_2-naph** was used to probe the reaction rate. It was found that the reaction order in **Lu_2-naph** is 1.5. The Erying plot for three different reaction temperatures gave an activation barrier of 21.2 kcal/mol. Corresponding computational studies on naphthalene C-H activation from **Lu_2-naph** is underway in order to compare with the experimental activation barrier as well as to explain the regio-selective C-H activation at α-position of naphthalene.

3.3 Aromatic C-F bond activation

Despite the fact that C-F bonds are relatively rare in nature,[23] fluorinated organic molecules have been found to exhibit remarkable changes in their physical properties, chemical reactivity, and biological activity compared to their hydrocarbon counterparts.[24,25] The interest in fluorine chemistry in recent years resulted in a constantly increasing number of fluorine-containing pharmaceutical drugs and agrochemicals[26] and the development of methods to introduce fluorine into organic substrates.[27,28] However, the combustion products of fluorine-containing molecules are usually greenhouse gases.[29] Therefore, it is necessary to develop methods to transform C-F bonds into other C-X bonds, preferably C-H bonds.[30] However, because of the strength of C-F bond as well as the relatively small size of the fluorine atom, transformations of C-F bonds are difficult to achieve and only a few examples of lanthanide and group 4 metal complexes are known to mediate C-F bond cleavage stoichiometrically or catalytically.[30] Given the high activity of $(NN^{TBS})ScI(THF)_2/KC_8$ toward C-H bond cleavage of benzene, we decided to apply this system to a fluorinated benzene, C_6F_6.

Although C_6F_6 is incompatible with KC_8, we were able to optimize the reaction conditions to achieve clean C-F bond cleavage (Scheme 3-5). Analogous to benzene activation, $[(NN^{TBS})Sc(\mu\text{-}F)]_2$ and $(NN^{TBS})Sc(C_6F_5)(THF)$ were formed in a 1:1 scandium molar ratio. The two products were separated on the basis of their different solubilities. When the corresponding yttrium and lutetium systems were used, only $[(NN^{TBS})M(THF)(\mu\text{-}F)]_2$ was identified as the reaction product containing the NN^{TBS} ligand. By comparing the ^{19}F spectrum of the crude reaction mixture with literature values,[31] the by-product was confirmed to be octafluorobiphenylene. The by-product is likely formed by β-F elimination from $(NN^{TBS})M(C_6F_5)(THF)$ (M = Y and Lu). A similar process is known for $[\eta^5\text{-}1,3,4\text{-}(CMe_3)_3C_5H_2]_2Ce(C_6F_5)$ and is a consequence of the high electrophilicity of rare-earth ions.[32] In addition, aliquots taken during the early stages of the reaction contained an intermediate species as determined by NMR spectroscopy. In the case of $(NN^{TBS})Lu(C_6F_5)(THF)$, the process was slow enough to allow the identification of the intermediate species as $(NN^{TBS})Lu(C_6F_5)(THF)$. The absence of β-F elimination from $(NN^{TBS})Sc(C_6F_5)(THF)$ is probably due to steric hindrance at smaller scandium ion.

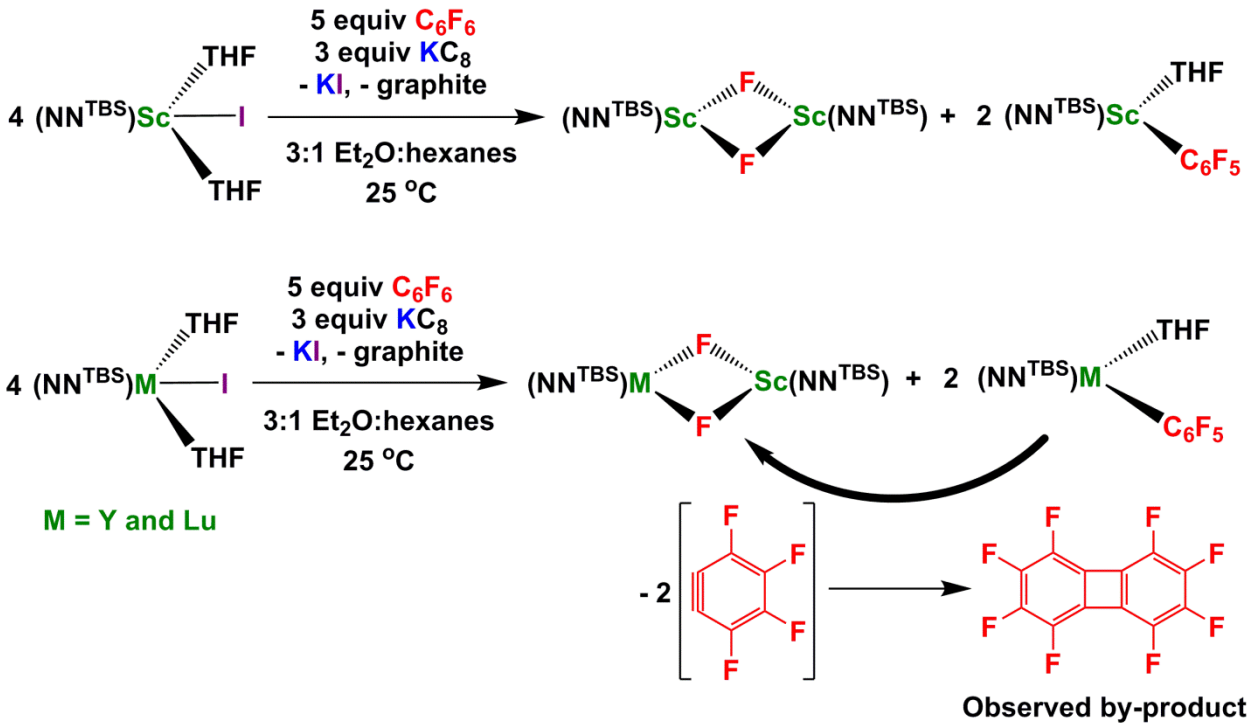

Scheme 3-5: Aromatic C-F bond cleavage of C_6F_6 by $(NN^{TBS})MI(THF)_2/KC_8$.

The rare-earth fluorides and $(NN^{TBS})Sc(C_6F_5)(THF)$ were characterized by X-ray crystallography (Figure 3-5) and ^1H and ^{19}F NMR spectroscopy. In the molecular structure of $[(NN^{TBS})Sc(THF)](\mu\text{-}F)_2[Sc(NN^{TBS})]$, the Fe-Sc distance is 2.840(2) Å. This is consistent with previous observations by our group on iron-metal distances.[33] For the molecular structure of $(NN^{TBS})Sc(C_6F_5)(THF)$, any agostic interaction between scandium and *ortho*-F could be excluded because of the long $Sc\text{-}F_{ortho}$ distance (3.33 and 3.43 Å); instead, a relative short Fe-Sc distance is observed at 3.027(1) Å. The ^{19}F NMR spectra for the metal fluorides exhibited a broad signal between -30 to -50 ppm. No $^{89}Y\text{-}^{19}F$ coupling could be interpreted. The broadness of the signal could be caused by restricted rotation of NN^{TBS} ligand indicated by ^1H NMR spectra. Three distinct multiplets were found in the ^{19}F NMR spectrum of $(NN^{TBS})Sc(C_6F_5)(THF)$ at -119, -155, and -161 ppm in a 2:1:2 ratio for *ortho*-, *para*-, and *meta*-F, respectively.

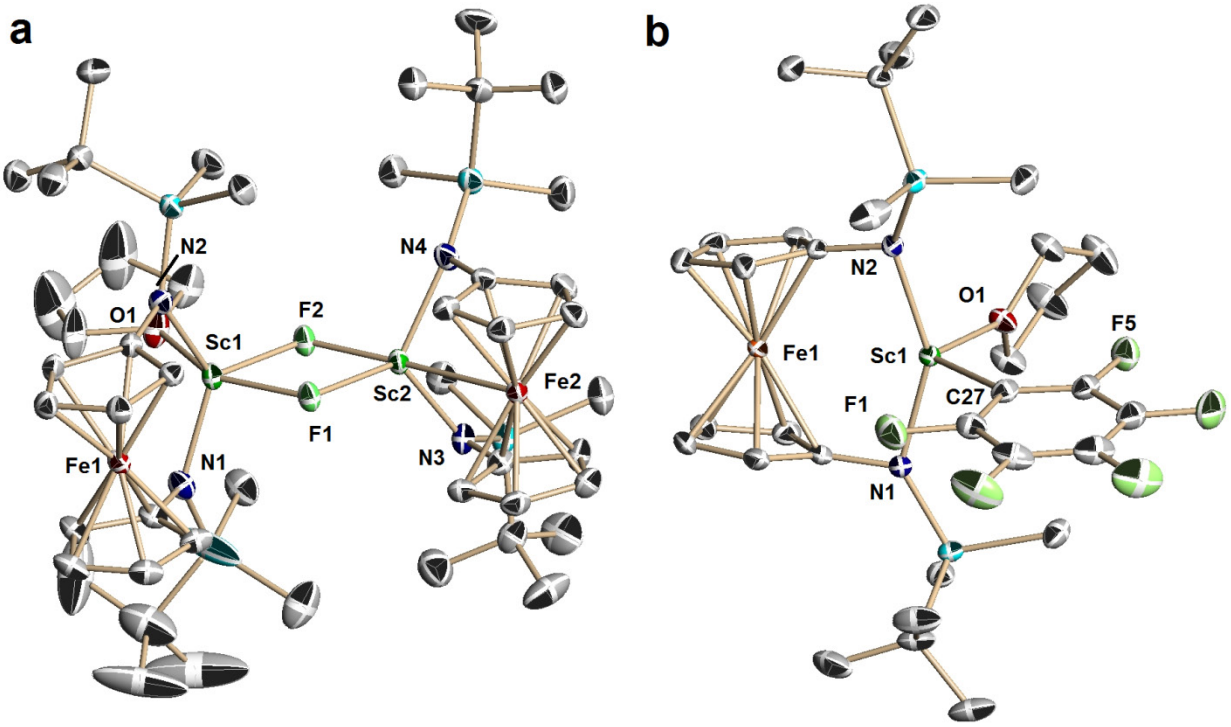

Figure 3-5: Molecular structures of $[(NN^{TBS})Sc(THF)](\mu\text{-}F)_2[Sc(NN^{TBS})]$ (only one of the two crystallographically independent molecules selected) (a) and $(NN^{TBS})Sc(C_6H_5)(THF)$ (b). Thermal ellipsoids are drawn at the 50% probability level. Hydrogen atoms were omitted for clarity. Selected distances [Å] and angles [°] (errors in brackets): (a) $[(NN^{TBS})Sc(THF)](\mu\text{-}F)_2[Sc(NN^{TBS})]$: Sc1-F1 2.090(4), Sc1-F2 2.083(5), Sc2-F1 2.036(5), Sc2-F2 2.045(5), Sc1-Sc2 3.310(2), Sc1-N1 2.055(7), Sc1-N2 2.050(8), Sc1-O1 2.200(6), Sc2-N3 2.058(8), Sc2-N4 2.065(8), Sc2-Fe2 2.840(2); Sc1-F1-Sc2 106.7(2), Sc1-F2-Sc2 106.6(2), N1-Sc1-N2 127.7(3), N3-Sc2-N4 114.5(3). (b) $(NN^{TBS})Sc(C_6F_5)(THF)$: Sc1-C1 2.308(1), Sc1-N1 2.046(1), Sc1-N2 2.058(1), Sc1-O1 2.145(1), Sc1-Fe1 3.027(1), Sc1-F1 3.429(1), Sc1-F5 3.335(1); N1-Sc1-N2 148.1(1), C27-Sc1-O1 110.9(1), O1-Sc1-Fe1 110.3(1) C1-Sc1-Fe1 138.8(1) (sum of the last three angles is 360.0).

It is noteworthy that the C-F activation of C_6F_6 could also be carried out cleanly in C_6D_6, a non-innocent solvent for the $(NN^{TBS})ScI(THF)_2/KC_8$ system. The preference for C-F bond activation over C-H bond (accurately, C-D bond) activation may be explained by the fact that C_6F_6 is more readily reduced compared to C_6D_6. However, although the proposed intermediate $[(NN^{TBS})Sc]_2(\mu\text{-}C_6F_6)$ should be more stable than intermediate **I**, $[(NN^{TBS})Sc]_2(\mu\text{-}C_6H_6)$, we did not observe it by NMR spectroscopy.

Interestingly, the C-F bond cleavage of C_6F_6 was also achieved using rare-earth naphthalene complexes as the reductant. $[(NN^{TBS})Sc(\mu\text{-}F)]_2$ and $(NN^{TBS})Sc(C_6F_5)(THF)$ were formed by heating **Sc_2-naph** and excess C_6F_6 (ca. 10 equiv) in C_6D_6 at 85 °C, while $[(NN^{TBS})M(THF)(\mu\text{-}F)]_2$ was the sole metal product at lower temperature for the reaction of **Y_2-naph** or **Lu_2-naph** and C_6F_6 (for Y, T = 25 °C; for Lu, T = 50 °C). In the lutetium reaction, $(NN^{TBS})Lu(C_6F_5)(THF)$ could be identified in the early stages of the reaction by NMR spectroscopy. Free naphthalene was also formed in the reaction. These results show that potassium is not necessary in promoting the C-F bond cleavage.

The C-F bond cleavage of C_6F_6 is particularly encouraging because it shows that the reductive cleavage in the presence of KC_8 is compatible with polar C-F bonds. In addition, it illustrates that the aromatic substrate does not have to be used as a solvent; a slight excess in a mixture of ethers and inert hydrocarbons will work as well.

To the best of our knowledge, the activation of aromatic C-H/F bonds by an early transition metal complex to form an equal molar mixture of metal hydride/fluoride and metal phenyl complexes is unprecedented.[9,30] The closest examples to our results are the oxidative addition of halogens and the reductive elimination of C-C bonds to form biphenyl on a d^0 Zr(IV) center supported by a redox active *ortho*-iminoquinone ligand reported by Heyduk.[34,35]

3.4 Experimental section

General reaction setup, monitoring, and work-up for benzene activation by the $(NN^{TBS})ScI(THF)_2/KC_8$ system (using the kinetics study as an example)**:** 0.1500 g of $(NN^{TBS})ScI(THF)_2$ (0.1977 mmol) and 0.0315 g of C_6Me_6 (as internal standard) were dissolved in 6.00 mL of C_6H_6. An initial aliquot was taken before the addition of 0.0429 g of KC_8 (1.605 equiv). Every half an hour afterwards, a 0.20 mL of aliquot was taken and volatiles were removed under reduced pressure. The remaining solid was extracted by C_6D_6 and filtered through Celite before it was examined by ^1H NMR spectroscopy. The two products, $[(NN^{TBS})Sc(\mu\text{-}H)]_2$ and $(NN^{TBS})Sc(C_6H_5)(THF)$, were identified by their characteristic proton chemical shifts. Similar procedures applied for toluene or benzene-d_6 activation. C-H activations from rare-earth naphthalene complexes were usually set up in a J-Young tube using C_6D_6 as the solvent and monitored by ^1H NMR spectroscopy. For the reactions ran under a gas atmosphere other than N_2, KC_8 was added to a frozen benzene solution of $(NN^{TBS})ScI(THF)_2$ in a Schlenk tube sealed by a Teflon cap. The Schlenk tube was taken out of the glove-box and linked to a Schlenk line while keeping the solution frozen with a dry ice/isopropanol bath. The Schlenk tube was evacuated for 5 min and then the desired gas was filled into the tube. From that point, the benzene solution was allowed to thaw and the reaction mixture was stirred for a designated time under the desired gas atmosphere.

Regarding the separation of $[(NN^{TBS})Sc(\mu\text{-}H)]_2$ and $(NN^{TBS})Sc(C_6H_5)(THF)$, since $[(NN^{TBS})Sc(\mu\text{-}H)]_2$ is far less soluble in hexanes than $(NN^{TBS})Sc(C_6H_5)(THF)$, it could be obtained pure after washing the crude reaction mixture with hexanes. However, due to the high solubility of $(NN^{TBS})Sc(C_6H_5)(THF)$ in common organic solvents, it could not be isolated pure from this reaction. Instead, all scandium, yttrium, and lutetium aryl complexes were

independently synthesized from $(NN^{TBS})MI(THF)_2$ and the corresponding aryl lithium (see below).

Synthesis of LiC_6H_5: 0.5000 g iodobenzene (2.451 mmol) was dissolved in Et_2O and placed in an ice bath at 0 °C. 0.94 mL of 2.6 M n-butyl lithium (1 equiv) was added drop-wisely. The mixture was allowed to stir at 0 °C for 30 min. Volatiles were removed under reduced pressure. The remaining solid was first washed with hexanes and then extracted by Et_2O. The volatiles were removed again and the remaining solid was dried under reduced pressure for 2 hours. The empirical molecular formula was determined by reaction with $(NN^{TBS})ScI(THF)_2$ to be $C_6H_5Li(OEt_2)_{0.31}$ (molecular weight = 106.9 g/mol). Yield: 0.2266 g, 86.5%.

Synthesis of other aryl lithium (Li(*p*-Me-C_6H_4), Li(*m*-Me-C_6H_4), Li(*o*-Me-C_6H_4), Li(α-$C_{10}H_7$), and Li(β-$C_{10}H_7$) is in analog to that of LiC_6H_5 (from *p*-I-C_6H_4Me, *m*-I-C_6H_4Me, *o*-I-C_6H_4Me, α-bromonaphthalene, and β-bromonaphthalene, respectively).

Synthesis of $(NN^{TBS})Sc(o\text{-}Me\text{-}C_6H_5)(THF)$: 0.1000 g of $(NN^{TBS})ScI(THF)_2$ (0.1318 mmol) was dissolved in 4 mL of Et_2O. 0.0141 g Li(*o*-Me-C_6H_5) (1 equiv) was dissolved in 1 mL of Et_2O and drop-wisely added to the $(NN^{TBS})ScI(THF)_2$ solution at 25 °C. The reaction mixture was allowed to stir at 25 °C for one hour. The volatiles were removed under reduced pressure. The remaining yellow solid was extracted into hexanes and then the volatiles were removed under reduced pressure. Same procedure was repeated with *n*-pentane. The remaining solid was dissolved in minimum amount of *n*-pentane and stored in a -35 °C freezer. Orange solid precipitated out after several days. Yield: 0.0556 g, 64.8%. Anal. (%): Calcd. for $C_{33}H_{53}FeN_2OScSi_2$: C, 60.91; H, 8.21; N, 4.30. Found: C, 60.52; H, 8.17; N, 3.85.

Synthesis of $(NN^{TBS})Sc(C_6H_5)(THF)$, $(NN^{TBS})Y(C_6H_5)(THF)$, $(NN^{TBS})Lu(C_6H_5)(THF)$, $(NN^{TBS})Sc(m\text{-}Me\text{-}C_6H_4)(THF)$, $(NN^{TBS})Sc(o\text{-}Me\text{-}C_6H_4)(THF)$, $(NN^{TBS})Lu(p\text{-}Me\text{-}C_6H_4)(THF)$,

$(NN^{TBS})Lu(m\text{-}Me\text{-}C_6H_4)(THF)$, $(NN^{TBS})Lu(o\text{-}Me\text{-}C_6H_4)(THF)$, $(NN^{TBS})Lu(\alpha\text{-}C_{10}H_7)(THF)$, $(NN^{TBS})Lu(\beta\text{-}C_{10}H_7)(THF)$ is in analogous to that of $(NN^{TBS})Sc(o\text{-}Me\text{-}C_6H_5)(THF)$. Note: some rare-earth aryl complexes were contaminated by the formation of ate complex. For example, $[(NN^{TBS})Lu(\beta\text{-}C_{10}H_7)(\mu\text{-}\beta\text{-}C_{10}H_7)][Li(THF)]$ was crystallized from the crude product instead of $(NN^{TBS})Lu(\beta\text{-}C_{10}H_7)(THF)$ in the reaction of $(NN^{TBS})LuI(THF)_2$ and $Li(\beta\text{-}C_{10}H_7)$.

C-F bond activation of C_6F_6 by $(NN^{TBS})ScI(THF)_2/KC_8$: 0.2030 g $(NN^{TBS})ScI(THF)_2$ (0.2676 mmol) and 0.2480 g C_6F_6 (4.981 equiv) were weighed in a scintillation vial (20 mL) and were dissolved in 6.0 mL of Et_2O. 2.0 mL of hexanes was added. 0.1065 g KC_8 (2.944 equiv) was added to the solution. The mixture was allowed to stir at 25 °C for 2.5 hours before the volatiles were removed under reduced pressure. The crude products were determined to be $[(NN^{TBS})Sc(\mu\text{-}F)]_2$ and $(NN^{TBS})Sc(C_6F_5)(THF)$ in 1:1 scandium molar ratio. The crude products were extracted first by hexanes then by toluene. $(NN^{TBS})Sc(C_6F_5)(THF)$ crystallized as pale yellow crystals from the hexanes extraction. Yield: 0.0535 g, 27.5% (theoretical maximum yield is 50%). Anal. (%): Calcd. $C_{32}H_{46}F_5FeN_2OScSi_2$: C, 52.89; H, 6.38; N, 3.85. Found: C, 53.35; H, 6.60; N, 3.48. $[(NN^{TBS})Sc(\mu\text{-}F)]_2$ crystallized as yellow crystals from the toluene extraction layered with *n*-pentane. Yield: 0.0372 g, 27.5% (theoretical maximum yield is 50%).

3.5 References

(1) Bergman, R. G. *Science* **1984**, *223*, 902.

(2) Labinger, J. A.; Bercaw, J. E. *Nature* **2002**, *417*, 507.

(3) Ortiz de Montellano, P. R. *Chem. Rev.* **2009**, *110*, 932.

(4) Shaik, S.; Cohen, S.; Wang, Y.; Chen, H.; Kumar, D.; Thiel, W. *Chem. Rev.* **2009**, *110*, 949.

(5) Shilov, A. E.; Shul'pin, G. B. *Chem. Rev.* **1997**, *97*, 2879.

(6) Perutz, R. N.; Sabo-Etienne, S. *Angew. Chem., Int. Ed.* **2007**, *46*, 2578.

(7) Cummins, C. C.; Baxter, S. M.; Wolczanski, P. T. *J. Am. Chem. Soc.* **1988**, *110*, 8731.

(8) Watson, P. L.; Parshall, G. W. *Acc. Chem. Res.* **1985**, *18*, 51.

(9) Balcells, D.; Clot, E.; Eisenstein, O. *Chem. Rev.* **2010**, *110*, 749.

(10) Boutadla, Y.; Davies, D. L.; Macgregor, S. A.; Poblador-Bahamonde, A. I. *Dalton Trans.* **2009**, 5820.

(11) Cassani, M. C.; Gun'ko, Y. K.; Hitchcock, P. B.; Lappert, M. F.; Laschi, F. *Organometallics* **1999**, *18*, 5539.

(12) Cassani, M. C.; Duncalf, D. J.; Lappert, M. F. *J. Am. Chem. Soc.* **1998**, *120*, 12958.

(13) Hitchcock, P. B.; Lappert, M. F.; Protchenko, A. V. *J. Am. Chem. Soc.* **2000**, *123*, 189.

(14) Evans, W. J. *Inorg. Chem.* **2007**, *46*, 3435.

(15) Thompson, M. E.; Baxter, S. M.; Bulls, A. R.; Burger, B. J.; Nolan, M. C.; Santarsiero, B. D.; Schaefer, W. P.; Bercaw, J. E. *J. Am. Chem. Soc.* **1987**, *109*, 203.

(16) Connelly, N. G.; Geiger, W. E. *Chem. Rev.* **1996**, *96*, 877.

(17) Jones, W. D.; Feher, F. J. *J. Am. Chem. Soc.* **1986**, *108*, 4814.

(18) Zimmerman, H. E. *Acc. Chem. Res.* **2011**, *45*, 164.

(19) Huang, W.; Diaconescu, P. L. *Eur. J. Inorg. Chem.* **2013**, n/a.

(20) Tsuruta, H.; Imamoto, T.; Yamaguchi, K. *Chem. Commun.* **1999**, *0*, 1703.

(21) Ebert, L. B.; Mills, D. R.; Garcia, A. R.; Scanlon, J. C. *Mater. Res. Bull.* **1985**, *20*, 1453.

(22) Bergbreiter, D. E.; Killough, J. M. *J. Am. Chem. Soc.* **1978**, *100*, 2126.

(23) Gribble, G. W. *Chemosphere* **2003**, *52*, 289.

(24) Smart, B. E. In *Organofluorine Chemistry: Principles and Commercial Applications*; Banks, R. E., Smart, B. E., Tatlow, J. C., Eds.; Plenum Press: New York, 1994; Chapter 3, p 57.

(25) Hiyama, T., Ed. *Organofluorine Compounds Chemistry and Applications*; Springer: New York, 2000.

(26) Lemal, D. M. *J. Org. Chem.* **2004**, *69*, 1.

(27) Singh, R. P.; Shreeve, J. n. M. *Acc. Chem. Res.* **2003**, *37*, 31.

(28) Grushin, V. V. *Acc. Chem. Res.* **2010**, *43*, 160.

(29) Shine, K. P.; Sturges, W. T. *Science* **2007**, *315*, 1804.

(30) Klahn, M.; Rosenthal, U. *Organometallics* **2012**, *31*, 1235.

(31) Gardner, D. V.; McOmie, J. F. W.; Albriksten, P.; Harris, R. K. *J. Chem. Soc. C* **1969**, 1994.

(32) Maron, L.; Werkema, E. L.; Perrin, L.; Eisenstein, O.; Andersen, R. A. *J. Am. Chem. Soc.* **2005**, *127*, 279.

(33) Carver, C. T.; Monreal, M. J.; Diaconescu, P. L. *Organometallics* **2008**, *27*, 363.

(34) Blackmore, K. J.; Ziller, J. W.; Heyduk, A. F. *Inorg. Chem.* **2005**, *44*, 5559.

(35) Haneline, M. R.; Heyduk, A. F. *J. Am. Chem. Soc.* **2006**, *128*, 8410.

CHAPTER 4: SYNTHESIS OF RARE-EARTH FUSED-ARENE COMPLEXES AND THEIR REACTIVITY TOWARD P_4 ACTIVATION

4.1 Introduction

While we were studying the mechanism of C-H bond activation of benzene by the $(NN^{TBS})ScI(THF)_2/KC_8$ system, we tried to isolate or observe an arene dianion as an intermediate for aromatic C-H bond activation. Fused arenes such as naphthalene and anthracene have a more accessible reduction potential compared to benzene.[1] We rationalized that a naphthalene dianion or an anthracene dianion would be stabilized by rare-earth ions and allow its isolation. Indeed, we successfully prepared $[(NN^{TBS})Sc]_2(\mu\text{-}\eta^4\text{:}\eta^4\text{-}C_{10}H_8)$,[2] $[(NN^{TBS})Sc]_2(\mu\text{-}\eta^6\text{:}\eta^6\text{-}C_{14}H_{10})$,[2] and $[(NN^{TBS})M(THF)]_2(\mu\text{-}\eta^4\text{:}\eta^4\text{-}C_{10}H_8)$[3,4] (M = Y, La, and Lu). In addition to studying the C-H activation from these rare-earth naphthalene complexes (see Chapter 3), we employed them in white phosphorus (P_4) activation.[3,4] Chapter 4 will focus on the synthesis and characterization of these rare-earth fused-arene complexes and their reactivity toward P_4 activation.

4.2 Scandium fused-arene complexes: synthesis, characterization, and reactivity

Rare-earths complexes of reduced arenes have been long targeted because of their fundamental importance and their potential to be multi-electron sources for reduction chemistry.[5] Arenes have outstanding stability due to their aromaticity; however, the accessibility of both their π and π^* orbitals allows them to serve as multi-electron neutral or anionic ligands. Rare-earths, because of their large ionic radii and high positive charges, can have high coordination numbers without sacrificing the strength of interactions with a ligand. Therefore, neutral arenes

and arene anions serve as excellent ligands for rare-earth ions.[5] The first authentic arene-lanthanide complex was reported in 1986,[6] containing a neutral C_6Me_6 ligand. With the development in low valent rare-earth chemistry, a few rare-earth reduced arene complexes have been reported in the last two decades. Among them, reduced-naphthalene complexes are the most studied and have been synthesized and characterized for most rare-earths.[5]

However, rare-earth reduced naphthalene complexes were missing examples of scandium reduced naphthalene compounds. The synthesis of scandium arene complexes has been limited to the co-condensation of scandium metal vapors and benzene derivatives with bulky substituents (1,3,5-*t*-$Bu_3C_6H_3$)[7] or heteroaromatic hydrocarbons (2,4,6-*t*-$Bu_3C_5H_2N$ and 2,4,6-*t*-$Bu_3C_3P_3$) to give sandwich formal zero-valent scandium arene complexes;[8-10] the gas-phase reaction of scandium ion with benzene and its derivatives led to products that could only be characterized by mass spectrometry.[11] On the other hand, a series of neutral arene scandium(III) complexes supported by β-diketiminato ligands have been isolated and structurally characterized.[12,13] This highlighted the strong Lewis acidity of scandium(III). Although binuclear inverted sandwiches of yttrium and lutetium naphthalene complexes with the general formula $[(P_2N_2)Ln]_2$(μ-arene) (P_2N_2 = (PhP[CH_2($SiMe_2$)N($SiMe_2$)CH_2]$_2$PPh), also see Chart 1-2, arene = $C_{10}H_8$ or α-Me-$C_{10}H_7$; Ln = Y / Lu) could be prepared by the reaction of a mixture of potassium graphite (KC_8) and naphthalene or α-methylnaphthalene with the yttrium complex $[(P_2N_2)Y)_2(\mu\text{-}Cl)_2]$ or its lutetium analogue[14] and homoleptic or mixed-halide naphthalene complexes of larger lanthanides are known,[15-20] no scandium naphthalene complexes had been reported prior to our work. Similarly, no scandium complex with another fused arene, such as anthracene, was known, although reduced-anthracene complexes with other rare-earths are common.[5]

We rationalized that the lack of scandium reduced arene complexes may be related to the unique characteristics of scandium. Scandium(III) is the smallest among rare-earths: its ionic radius of 0.74 Å is 0.12 Å smaller than that of lutetium(III).[21] The large difference in ionic radius between scandium and other rare-earths leads to special properties and reactivity of scandium complexes.[22,23] For example, scandium(III) prefers σ binding to π binding. This is best illustrated by the product from the co-condensation of scandium metal and 1,3,5-*t*-$Bu_3C_6H_3$.[7] While other rare-earths gave the formally zero-valent sandwich complexes (1,3,5-*t*-$Bu_3C_6H_3$)Ln (Ln = Y, La, Pr, Nd, Sm, Gd, Tb, Dy, Ho, Er, and Lu),[24] in the case of scandium, a second product arising from the insertion of scandium into the C–H bond of the *tert*-butyl groups was also been observed.[7]

Upon addition of 1.2 equiv KC_8 to a pre-mixed THF solution of $(NN^{TBS})ScI(THF)_2$ (NN^{TBS} = 1,1′-fc($NHSi^tBuMe_2$)$_2$) and 0.5 equiv naphthalene (Scheme 4-1a), an immediate color change from yellow to dark purple was observed; for comparison, in the absence of $(NN^{TBS})ScI(THF)_2$, the KC_8/naphthalene mixture has a dark green color in THF, typical for alkali metal naphthalenides.[1] The reaction mixture was allowed to stir at 25 °C for 1.5 hours, and then the volatiles were removed under reduced pressure to get a dark red solid. Interestingly, when extracting the dark red solid with toluene, the toluene solution turned to an intense blue color. Single crystals suitable for X-ray crystallography were grown from a toluene solution after storing at -35 °C for several days. The solid-state molecular structure unambiguously established that the product was the first scandium naphthalene complex, $[(NN^{TBS})Sc]_2(\mu\text{-}\eta^4\text{:}\eta^4\text{-}C_{10}H_8)$ (**Sc_2-naph**) (Figure 4-1a).[2] To explore further the scope of the scandium arene synthesis, anthracene was employed as well. 1.5 equiv KC_8 was added to a pre-mixed THF solution of $(NN^{TBS})ScI(THF)_2$ and 0.5 equiv anthracene at -78 °C and the reaction mixture was allowed to

stir at -78 °C for 2 h. After a similar work-up as for **Sc_2-naph**, the corresponding scandium complex of reduced anthracene could be crystallized from hexanes and isolated in 70% yield (Scheme 4-1b). Single crystals suitable for X-ray crystallography were grown from a concentrated diethyl ether solution stored at -35°C for a week. The molecular structure of $[(NN^{TBS})Sc]_2(\mu\text{-}\eta^6\text{:}\eta^6\text{-}C_{14}H_{10})$ (**Sc_2-anth**) is shown in Figure 4-1b.

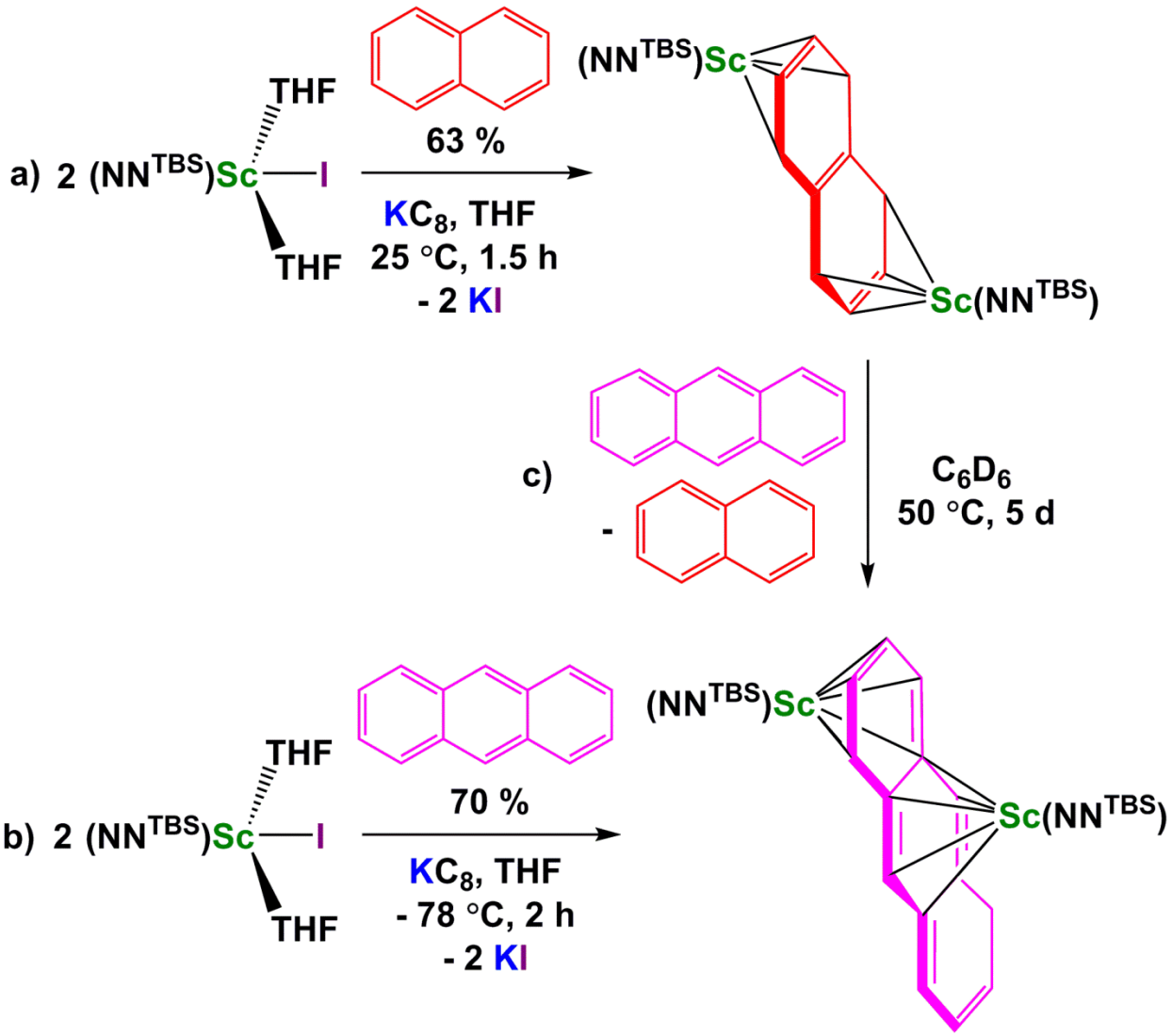

Scheme 4-1: a) Synthesis of **Sc_2-naph**, yield: 63%; b) synthesis of **Sc_2-anth**, yield: 70%; c) conversion of **Sc_2-naph** to **Sc_2-anth**.

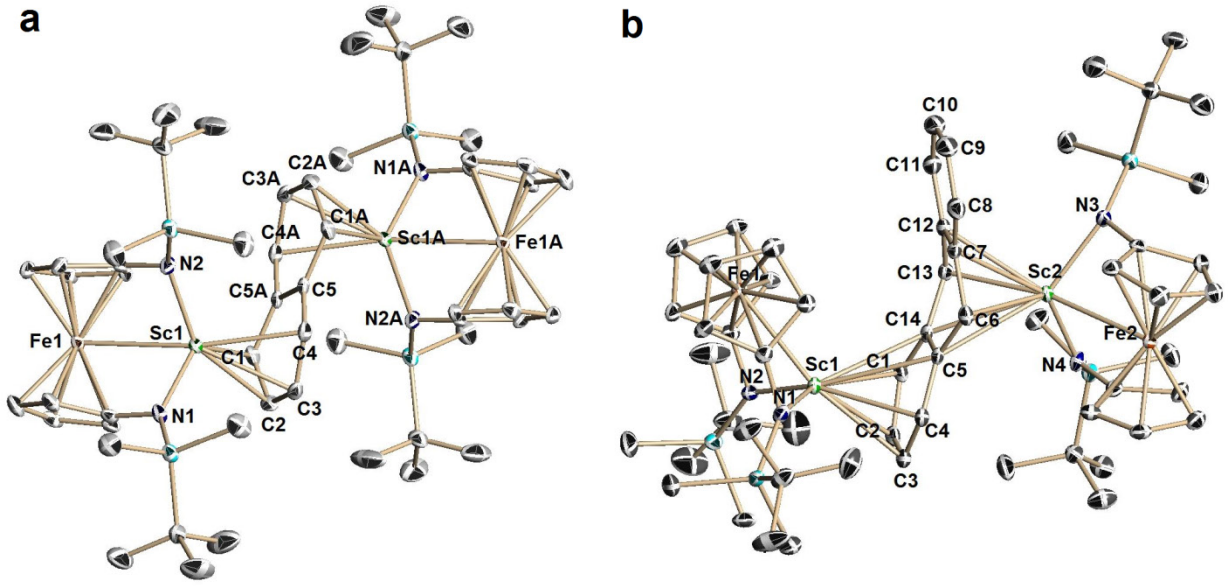

Figure 4-1: Molecular structures of **Sc_2-naph** (a) and **Sc_2-anth** (b). Thermal ellipsoids are drawn at the 50% probability level. Hydrogen atoms are omitted for clarity. Selected distances [Å] and angles [°]: (a) **Sc_2-naph**: Sc1-N1 2.056(4), Sc1-N2 2.090(4), Sc1-C1 2.511(4), Sc1-C2 2.503(4), Sc1-C3 2.506(5), Sc1-C4 2.536(5), Sc1-Fe1 2.831(1), C1-C5A 1.421(6), C1-C2 1.428(7), C2-C3 1.368(7), C5-C5A 1.445(9); N1-Sc1-N2 110.6(2), Fe1-Sc1-C1 105.1(1), Fe1-Sc1-C4 167.0(1), C5A-C1-C2 120.3(4), C1-C2-C3 118.9(4), C2-C3-C4 119.6(4), C3-C4-C5 120.9(4), C4-C5-C5A 117.0(5). (b) **Sc_2-anth**: Sc1-N1 2.057(3), Sc1-N2 2.061(3), Sc1-Fe1 2.743(1) Sc2-N3 2.072(3), Sc2-N4 2.078(3), Sc2-Fe2 2.851(1), Sc1-C1 2.583(3), Sc1-C2 2.523(3), Sc1-C3 2.543(3), Sc1-C4 2.605(3), Sc1-C14 2.833(3), Sc2-C5 2.844(3), Sc2-C6 2.442(3), Sc2-C7 2.679(3), Sc2-C12 2.707(3), Sc2-C13 2.464(3), Sc2-C14 2.863(3), C14-C1 1.403(4), C1-C2 1.428(5), C2-C3 1.385(5), C5-C14 1.452(4), C5-C6 1.436(4), C6-C7 1.470(4), C7-C12 1.416(4), C7-C8 1.411(5), C8-C9 1.394(5), C9-C10 1.397(6); N1-Sc1-N2 112.0(1), N3-Sc2-N4 114.3(1), Fe1-Sc1-C1 121.1(1), Fe2-Sc2-C6 101.3(1), Fe2-Sc2-C13 167.6(1), C4-C5-C6 124.6(3), C6-C7-C8 123.6(3).

The molecular structure of **Sc_2-naph** is reminiscent of previously reported yttrium naphthalene complexes.[14] The naphthalene is distorted from planarity with C2/C3 and C2A/C3A bending in opposite directions from the plane composed of the other six carbon atoms (ca. 20° torsion angle). The C-C bonds within the naphthalene are best described as two isolated double bonds (C2=C3 and C2A=C3A), with short distances averaging 1.37 Å, and a 6C, 8π-electron system for the six co-planar center carbon atoms. Each scandium ion binds η^4 to C1 through C4 (or C1A through C4A) with similar distances averaging 2.51 Å. These features are also reminiscent of the lithium naphthalene dianion $[Li(TMEDA)]_2(\mu\text{-}\eta^4\text{:}\eta^4\text{-}C_{10}H_8)$ (TMEDA = tetramethylethylenediamine).[25]

Despite the structural parameters common with previously reported rare-earth or alkali metal naphthalene dianion complexes, **Sc_2-naph** features a short Fe-Sc distance of 2.83 Å, which is significantly shorter than that of $(NN^{TBS})ScI(THF)_2$ (3.12 Å) and among the shortest Fe-Sc distances observed by our group with the NN^{TBS} ligand,[26,27] indicating a relatively strong interaction between scandium and iron that might be essential to the stability of **Sc_2-naph**. Geometrically, with the short Fe-Sc distance, the scandium ion is sterically protected by the shielding of the ferrocene backbone. An even shorter Fe-Sc distance of 2.74 Å was observed in **Sc_2-anth**. When using $[(Me_3Si)_2N]_2ScI(THF)$ in place of $(NN^{TBS})ScI(THF)_2$, no formation of a scandium naphthalene complex was observed. This highlighted the advantages of the NN^{TBS} ligand in stabilizing highly electrophilic scandium(III).

The solid-state molecular structure of **Sc_2-anth** is similar to that of $[(P_2N_2)_2Y)_2(\mu\text{-}C_{14}H_{10})$,[14] featuring an unsymmetrical coordination mode. The two scandium ions are η^6-bound on opposite sides of the middle and an outer ring. ^{1}H NMR spectroscopy, however, indicated that the solution structure of **Sc_2-anth** is symmetrical at 25 °C in C_6D_6. In order to study the

dynamics of **Sc_2-anth** in solution, a variable temperature NMR experiment was performed (Figure 4-2). Cooling a toluene-d_8 solution of **Sc_2-anth** from room temperature resulted in broadening of the peaks; coalescence took place at -15 °C; further cooling led to the appearance of new, sharp peaks, which are well correlated with the unsymmetrical molecular structure obtained by X-ray crystallography. Similar fluxional behavior has been reported for $[(P_2N_2)_2Y)_2(\mu\text{-}C_{14}H_{10})$.[14]

Conversion of **Sc_2-naph** to **Sc_2-anth** could also be achieved: heating a 1:1 mixture of **Sc_2-naph** and anthracene at 50 °C in C_6D_6 for five days led to the complete conversion to **Sc_2-anth** and free naphthalene (Scheme 4-1c). No significant decomposition of either **Sc_2-naph** or **Sc_2-anth** was observed after heating at 70 °C in C_6D_6 for one day; however, both decomposed rapidly in THF at 70 °C, leading to free naphthalene and anthracene as well as an intractable mixture of scandium products.

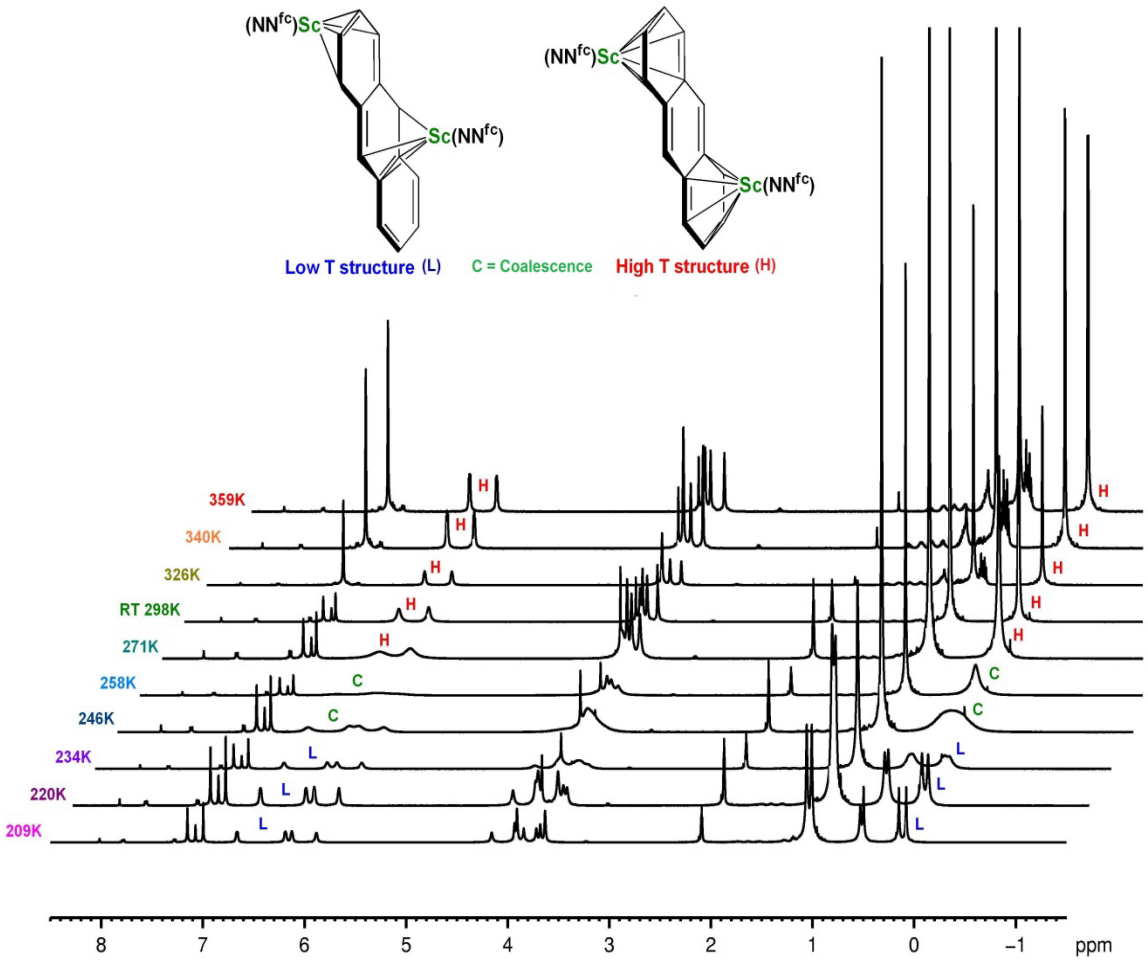

Figure 4-2: Variable temperature ^{1}H NMR spectra of **Sc_2-anth** in aromatic solvents (209 K to 298 K in C_7D_8; 326 K to 359 K in C_6D_6). NN^{fc} = NN^{TBS}. Peaks corresponding to low T and high T structures are labeled and highlighted with **L** and **H**. The coalescence peaks were labeled and highlighted with **C**.

Rare-earth arene complexes are considered to be good precursors for difficult-to-synthesize rare-earth metal compounds;[5] therefore, we became interested in exploring the reactivity of **Sc_2-naph**. The addition of 2,2′-bipyridine to a C_6D_6 solution of **Sc_2-naph** was associated with an immediate color change from dark blue to dark green (Scheme 4-2a). The formation of the previously characterized bipyridyl radical anion complex (NN^{TBS})Sc(2,2′-

bipyridine)[28] was confirmed by ^{1}H NMR spectroscopy. The fast and clean reaction with 2,2′-bipyridine illustrated that **Sc_2-naph** could serve as an excellent two-electron reductant.

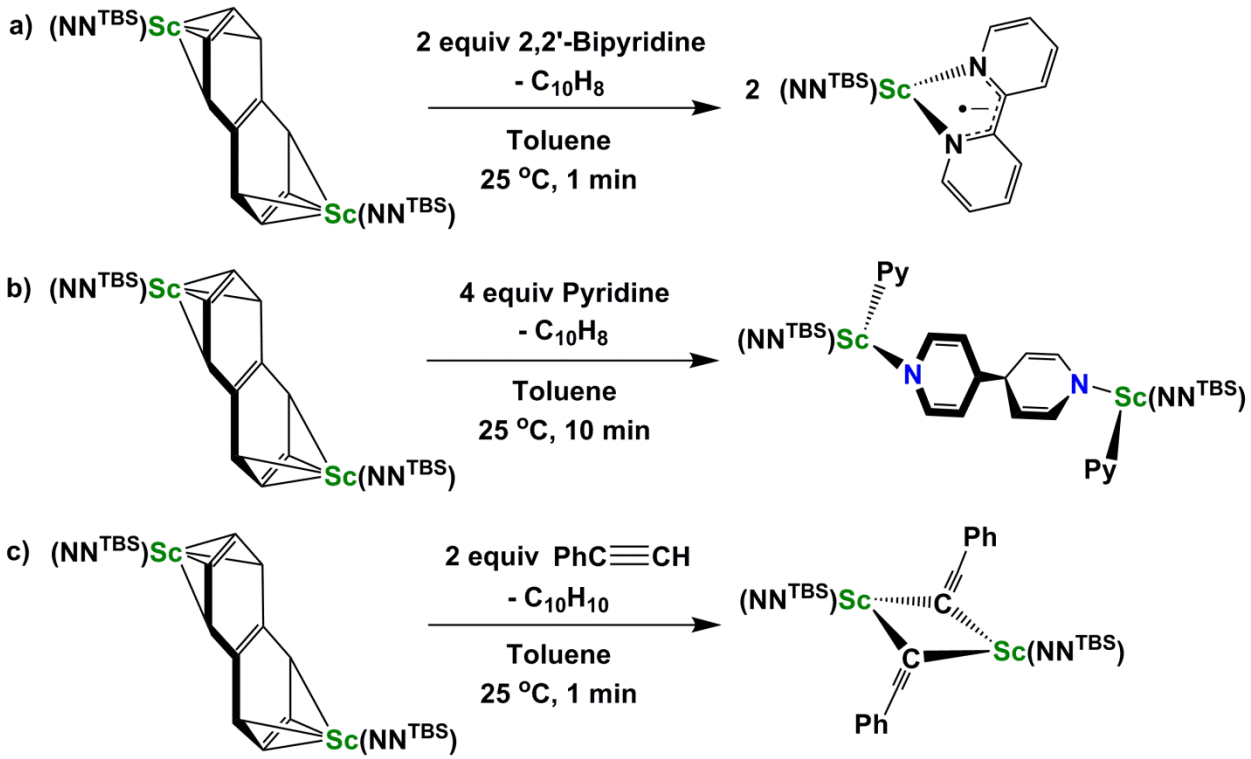

Scheme 4-2: a) Reaction of **Sc_2-naph** with 2 equiv 2,2′-bipyridine to form (NN^{TBS})Sc(2,2′-bipyridine) with the elimination of free naphthalene; b) reaction of **Sc_2-naph** with 4 equiv pyridine to form [(NN^{TBS})Sc(NC_5H_5)]$_2$[μ-(NC_5H_5-C_5H_5N)] with the elimination of free naphthalene; c) reaction of **Sc_2-naph** with 2 equiv phenylacetylene to form [(NN^{TBS})Sc(μ-CCPh)]$_2$ with the elimination of dihydronaphthalene.

Hessen showed that the scandium complex of the 2,2′-bipyridyl radical anion could be readily accessed from a reduced 1,3-diene scandium complex;[29] however, the reaction of rare-earth arene complexes with pyridine was not known. The reaction of **Sc_2-naph** with excess

pyridine was attempted (Scheme 4-2b). The color of the solution changed immediately from dark blue to pale yellow upon the addition of excess pyridine. X-ray crystallography corroborated the isolation of a rare, reductively 4,4′-C-C coupled diamide linker that bridges the two scandium ions in the complex $[(NN^{TBS})Sc(NC_5H_5)]_2[\mu\text{-}(NC_5H_5\text{-}C_5H_5N)]$. A similar reduction was reported in the reactions of divalent thulium complexes with pyridine.[30,31] The reduced nature of the diamide linker is supported by the metrical parameters of $[(NN^{TBS})Sc(NC_5H_5)]_2[\mu\text{-}(NC_5H_5\text{-}C_5H_5N)]$: the two carbons at the 4 and 4′ positions are sp^3 hybridized (average bond angles 111° and average bond distances 1.53 Å to the neighboring carbon atoms); the average distance between scandium and the amide nitrogen is 2.10 Å, 0.14 Å shorter than the Sc-$N_{pyridine}$ distance, and close to the average distance of scandium and the ferrocene diamide nitrogen, 2.08 Å. These structural features are comparable to those of previously reported thulium complexes.[30,31]

Another common substrate used with rare-earth arene complexes is phenylacetylene.[5] The reaction of **Sc_2-naph** with 2 equiv phenylacetylene led to the immediate formation of $[(NN^{TBS})Sc(\mu\text{-}CCPh)]_2$ (Scheme 4-2c) presumably from protonation of naphthalene dianion since a mixture of dihydronaphthalene isomers was observed as by-products. X-ray crystallography confirmed the isolation of the phenylacetylide bridging dimer with short Fe-Sc and Sc-Sc distances. The average Fe-Sc distance is 2.89 Å, close to that of **Sc_2-naph**, indicating a relatively strong Fe-Sc interaction. The Sc-Sc distance is 3.45 Å, close to the sum of covalent radii of 3.40 Å.[32] The relatively short Sc-Sc distance likely does not indicate any bonding interaction between them but is rather a consequence of the small size of the acetylide anion.

In order to understand the electronic structure of **Sc_2-naph**, DFT calculations were carried out on the full molecule and the optimized structural parameters matched well with those of the solid-state structure. The results indicate that **Sc_2-naph** bears a similar electronic structure

to that of other rare-earth naphthalene complexes.[5] As expected, the HOMO is comprised mostly of naphthalene orbitals, consistent with its dianionic nature (Figure 4-3a). Charge calculations showed that the negative charge is mainly localized on C1 and C4 (average -0.30), while C5 has the least (-0.07), and C2 and C3 are in the middle (average -0.14), confirming the η^4 coordination mode observed in the solid state. More interestingly, the nearly degenerate HOMO-1 (Figure 4-3b) and HOMO-2 showed some orbital mixing between the 3d orbitals of iron and scandium together with the 2p orbitals of nitrogen and carbon of the NN^{TBS} ligand. This iron-scandium interaction is also supported by the Mayer bond order of 0.41, which is larger than the average Mayer bond order of the Sc-C1 and Sc-C4 bonds (0.24). Mulliken charges were also calculated with Sc being +1.02 and Fe being -0.04. The highly positive charge on scandium and slightly negative charge on iron indicates that the interaction between scandium and iron is mainly electrostatic, with iron serving as a donor and scandium being the acceptor. DFT calculations were also carried out on **Sc_2-anth**. The orbital mixing between the 3d orbitals of scandium and of iron was found in HOMO-1 and HOMO-3. The calculated Mayer bond orders for the Fe-Sc interactions are 0.44 and 0.41, for the outer ring bound to Sc (Sc1 in Figure 4-1b) and the middle ring bound to Sc (Sc2), respectively. Mulliken charges for Sc1, Sc2, Fe1, and Fe2 are +1.04, +1.07, -0.05 and -0.05, respectively, similar to the values in **Sc_2-naph**. The orbital mixing and calculated bond orders together with the short Fe-Sc distances determined by X-ray crystallography support the existence of a relatively strong interaction between iron and scandium, likely essential to the stability of **Sc_2-naph** and **Sc_2-anth**.

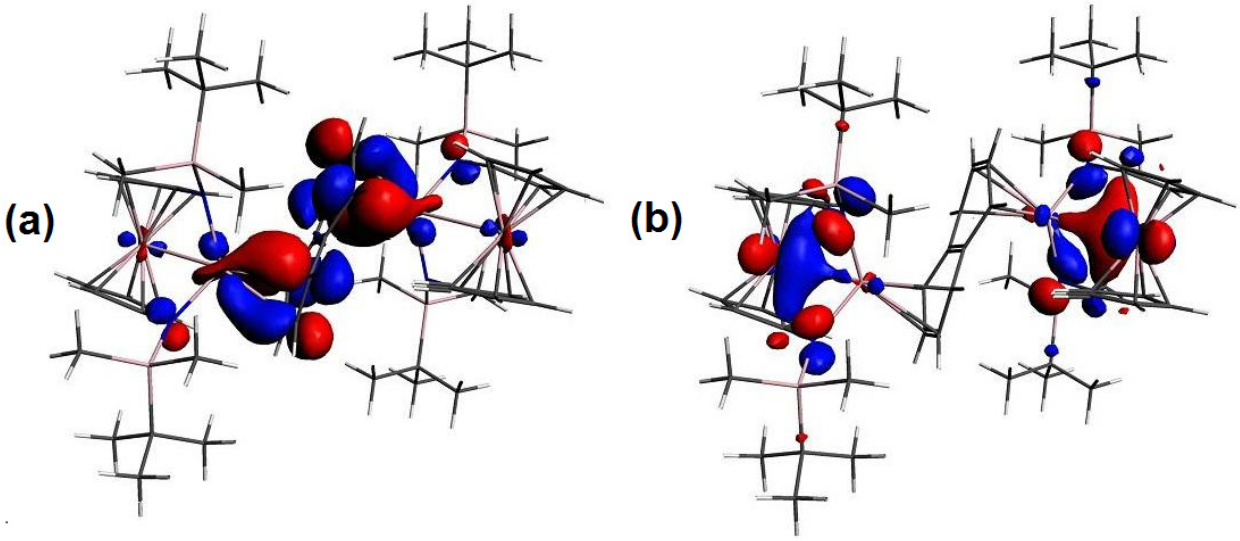

Figure 4-3: Selected molecular orbitals of **Sc_2-naph**: (a) HOMO; (b) HOMO-1.

4.3 P_4 activation by rare-earth arene complexes

4.3.1 P_4 activation by scandium arene complexes

White phosphorous (P_4) activation has been long targeted by synthetic chemists.[33-35] Unlike main group elements and late-transition metals,[34,35] the number of P_n-containing early transition metal complexes formed from direct P_4 activation is much smaller.[33,36-39] Among early transition metals, group 3 metals together with lanthanides are more Lewis acidic, leading to a more pronounced mismatch in binding between their ions and P-anions.[40-42] There was no report of a P_n-containing group 3 metal complex prior to our study; two samarium[43,44] and a few actinide complexes have been reported;[45,46] all known examples of lanthanide and actinide mediated P_4 activation involved low-valent metal complexes. As discussed in section 4.2, the scandium naphthalene complex **Sc_2-naph** was found to be an excellent two-electron reductant toward a variety of substrates. Therefore, we decided to investigate the reactivity of **Sc_2-naph**

toward P_4. It is worth noting that late transition metal arene complexes have also been used for P_4 activation recently.[47]

The reaction of **Sc_2-naph** and P_4 took place smoothly at ambient conditions and was accompanied by the generation of free naphthalene (Scheme 4-3). The reaction could be readily monitored by its gradual color change from dark blue to orange, which corresponded to the conversion of **Sc_2-naph** to the product $[(NN^{TBS})Sc]_4(\mu_4\text{-}\eta^2\text{:}\eta^2\text{:}\eta^2\text{:}\eta^2\text{-}P_8)$ (**Sc_4P_8**).[3]

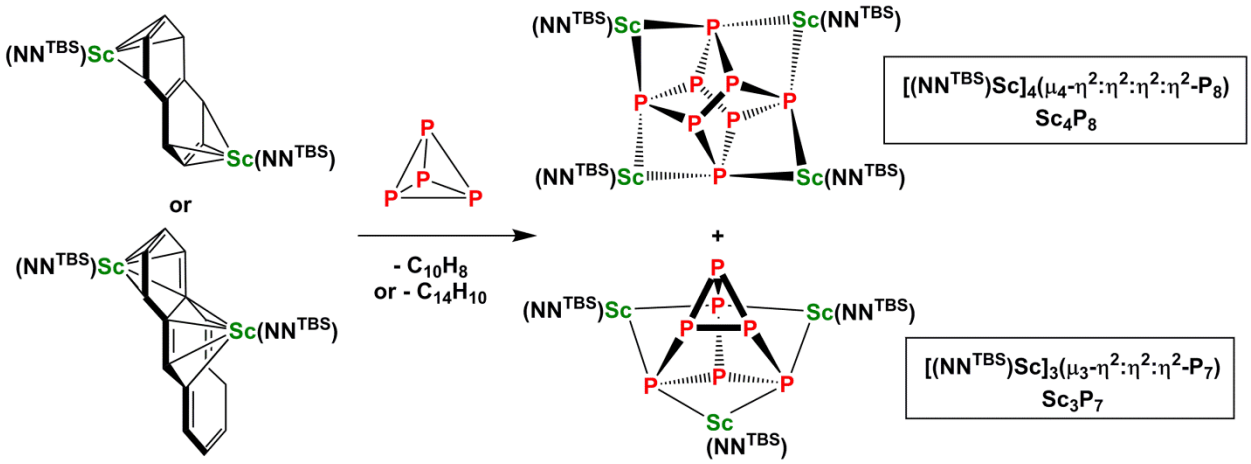

Scheme 4-3: Reactions of **Sc_2-naph** and **Sc_2-anth** with P_4 to form $[(NN^{TBS})Sc]_4(\mu_4\text{-}\eta^2\text{:}\eta^2\text{:}\eta^2\text{:}\eta^2\text{-}P_8)$ (**Sc_4P_8**) and $[(NN^{TBS})Sc]_3(\mu_3\text{-}\eta^2\text{:}\eta^2\text{:}\eta^2\text{-}P_7)$ (**Sc_3P_7**) with the elimination of free naphthalene or anthracene.

The molecular structure of **Sc_4P_8** (Figure 4-4a) can be described as having a realgar-type P_8 unit in the center and four $[(NN^{TBS})Sc]$ fragments at the corners, each binding to two anionic phosphorus atoms. A structural feature worth mentioning is the short Fe-Sc distance of 2.80 Å, likely playing a role in stabilizing the structural motif of **Sc_4P_8**. This feature was observed in **Sc_2-naph** (Fe-Sc: 2.83 Å) as well and considered to be essential to the stability of the scandium

naphthalene complex. The P_8 unit has local C_{2v} symmetry, which leads to two distinct types of P-atoms: P_{inner} (P2, P3, P5, and P6) and P_{corner} (P1, P4, P7 and P8). The average P_{inner}-P_{inner} distance is 2.31 Å, 0.11 Å longer than that of P_{inner}-P_{corner}. This elongation might be caused by the ring strain and/or the electron repulsion between two lone pairs on each P_{inner} atom. The average P_{inner}-P_{corner} distance of 2.20 Å is close to the P-P interatomic distance in P_4 (2.21 Å)[48] or a recent updated gas phase value 2.1994(3).[49] The structure of the P_8 unit resembles that of $(Cp^*_2Sm)_4P_8$.[43] The P_8 unit has been previously observed in some late transition metal complexes, which were obtained from the photolysis reaction of P_4 with cyclopentadienyl iron or iridium carbonyl species,[50,51] and in the tricyclic [3.3.0.0^{3,7}]octaphosphane.[52]

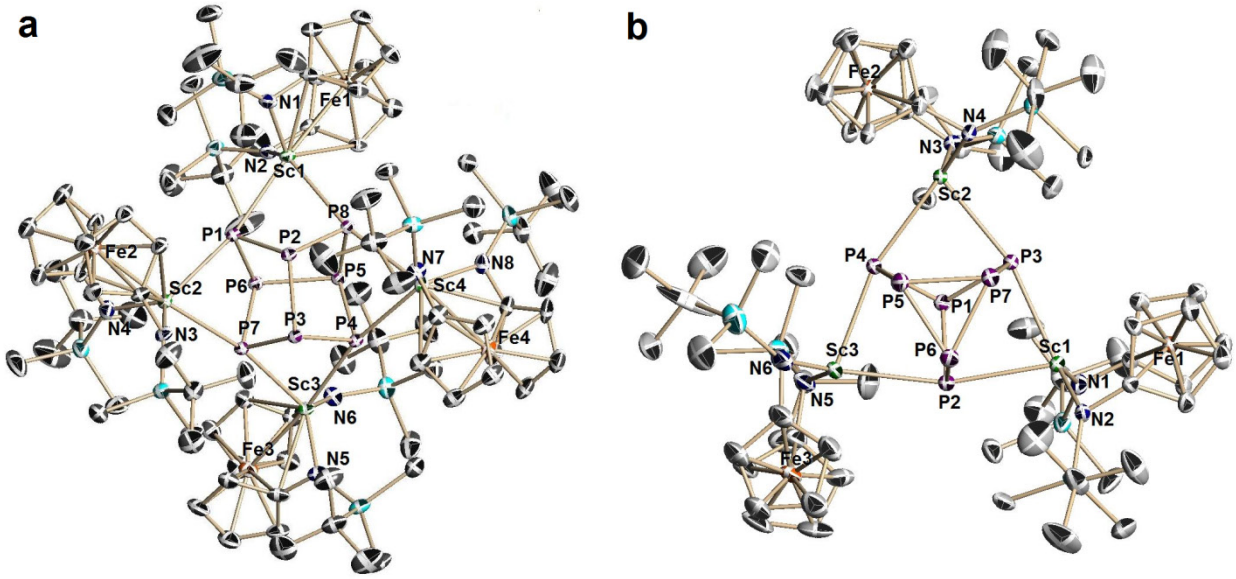

Figure 4-4: Molecular structures of $[(NN^{TBS})Sc]_4(\mu_4\text{-}\eta^2\text{:}\eta^2\text{:}\eta^2\text{:}\eta^2\text{-}P_8)$ (a) and $[(NN^{TBS})Sc]_3(\mu_3\text{-}\eta^2\text{:}\eta^2\text{:}\eta^2\text{-}P_7)$ (b). Thermal ellipsoids are drawn at the 50% probability level. Hydrogen atoms are omitted for clarity. Selected distances [Å] and angles [°]: (a) $[(NN^{TBS})Sc]_4(\mu_4\text{-}\eta^2\text{:}\eta^2\text{:}\eta^2\text{:}\eta^2\text{-}P_8)$: P1-P2 2.203(2), P1-P6 2.205(2), P2-P3 2.306 (2), P2-P8 2.206(2), P3-P4 2.207(2), P3-P7 2.207(2), P4-P5 2.198(2), P5-P6 2.308(2), P5-P8 2.201(2), P6-P7 2.205(2), Sc1-P1 2.780(2),

Sc1-P8 2.762(2), Sc1-N1 2.037(6), Sc1-N2 2.065(5), Sc1-Fe1 2.792(2), Sc2-Fe2 2.823(2), Sc3-Fe3 2.813(2), Sc4-Fe4 2.791(2), P1-Sc1-P8 70.1(1), P1-Sc1-Fe1 175.2(1), P8-Sc1-Fe1 106.3(1), P2-P1-P6 98.5(1), P1-P2-P8 92.4(1), P1-P2-P3 101.8(1). (b) $[(NN^{TBS})Sc]_3(\mu_3\text{-}\eta^2\text{:}\eta^2\text{:}\eta^2\text{-}P_7)$: P1-P2 2.197(2), P1-P3 2.204(2), P1-P4 2.196(2), P2-P6 2.197(2), P3-P7 2.197(2), P4-P5 2.194(2), P5-P6 2.226(2), P5-P7 2.234(2), P6-P7 2.228(2), Sc1-P2 2.730(2), Sc1-P3 2.747(2), Sc1-N1 2.028(4), Sc1-N2 2.072(4), Sc1-Fe1 2.803(1), Sc2-Fe2 2.788(1), Sc3-Fe3 2.824(1), P2-P1-P3 99.9(1), P1-P2-P6 100.7(1), P5-P6-P2 103.9(1), P5-P6-P7 60.2(1), N1-Sc1-N2 116.8(2), P2-Sc1-P3 75.9(1), P2-Sc1-Fe1 179.1(1), P3-Sc1-Fe1 104.1(1).

Sc_4P_8 was also characterized by ^{1}H, ^{13}C, and ^{31}P NMR spectroscopy. Although the solid-state structure has only C_2 symmetry, the ^{1}H spectrum of **Sc_4P_8** shows only two singlets for the *tert*-butyl groups indicating that all four $[(NN^{TBS})Sc]$ fragments are equivalent in solution at the NMR timescale. Cooling down the solution to -80 °C (in toluene-d_8) did not lead to splitting of the *tert*-butyl peaks. This suggests that the free rotation of (NN^{TBS}) ligand be fast even at low temperature. The ^{31}P NMR spectrum features an AA'A"A'"MM'M"M'" spin system. The ^{31}P NMR spectrum and the simulation are shown in Figure 4-5. The four P_{corner} atoms give rise to the A part of the spectrum at δ = 96.2 ppm. The M part arises from the four P_{inner} atoms at δ = 45.7 ppm. The $^{1}J_{Pcorner\text{-}Pinner}$ and $^{1}J_{Pinner\text{-}Pinner}$ were found to be similar at 255 Hz. One remarkable feature is that the long range coupling constant $^{3}J_{P1\text{-}P4}$ is 20 Hz larger than $^{2}J_{P1\text{-}P3}$, $^{2}J_{P1\text{-}P7}$, and $^{2}J_{P2\text{-}P5}$ which are ranging from -10 to -15 Hz. Likely caused by the quadrupolar broadening introduced by the 7/2 spin of ^{45}Sc, the A part of the spectrum is significantly broader than the simulation, while the M part shows a good match.

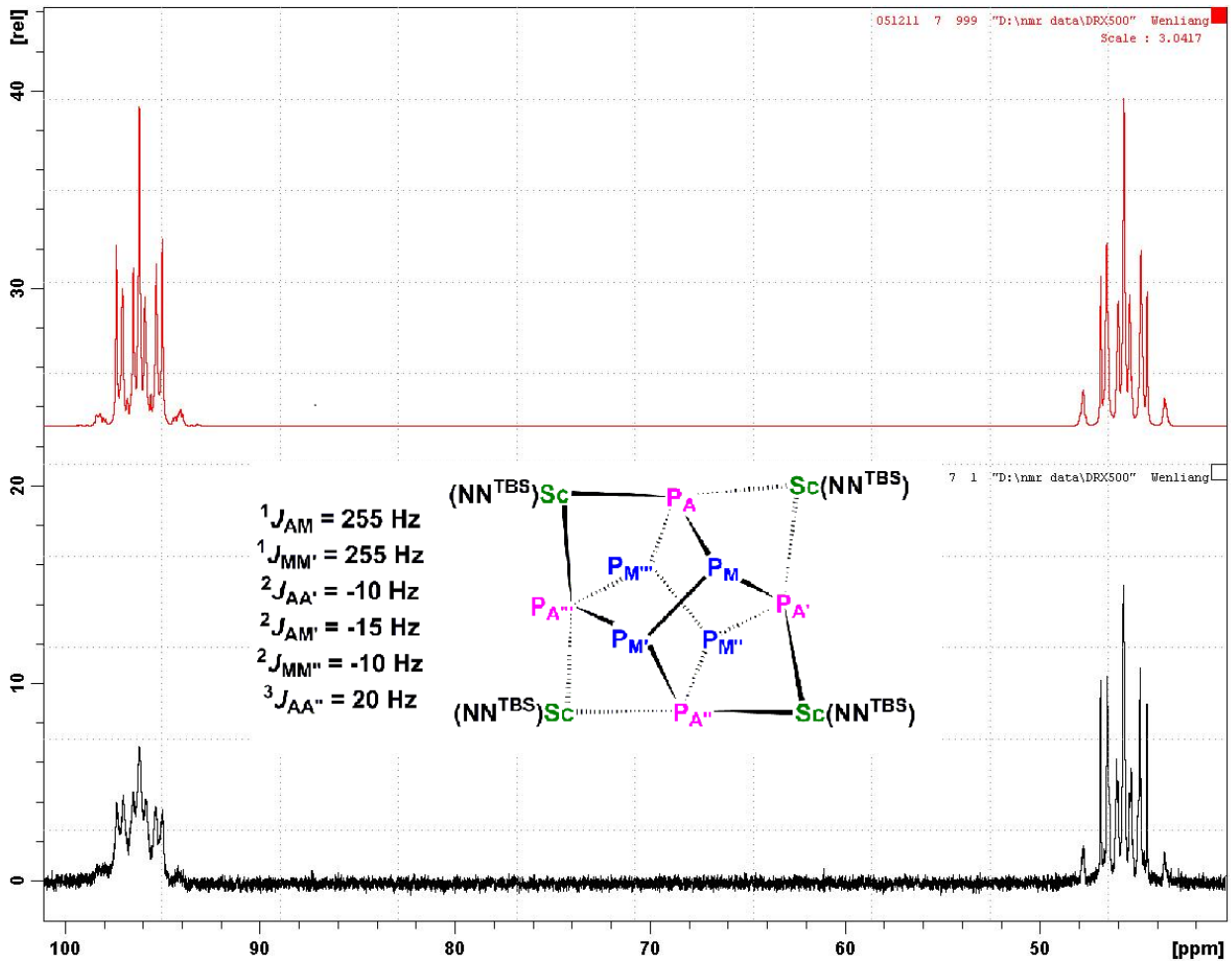

Figure 4-5: Bottom: ^{31}P NMR spectrum of **Sc$_4$P$_8$** (203 MHz, C_6D_6, 25 °C). Top: simulation performed with Topspin^{TM} software.

Although **Sc$_4$P$_8$** could be isolated cleanly, an extra set of peaks was present in the ^{1}H and ^{31}P NMR spectra of the crude products, indicating the presence of another P-containing species. It was found that the two products could be readily separated based on their different solubilities: the second product was mainly found in the *n*-pentane extraction of the crude product while **Sc$_4$P$_8$** was barely soluble in *n*-pentane. X-ray crystallography confirmed the isolation of the first early transition metal P_7 compound, $[(NN^{TBS})Sc]_3(\mu_3\text{-}\eta^2\text{:}\eta^2\text{:}\eta^2\text{-}P_7)$ (**Sc$_3$P$_7$**) (Figure 4-4b). The

observation of multiple products from direct P_4 activation is common due to the high reactivity of the P_4 molecule.[33-35] We found that the product distribution could be tuned by either changing the stoichiometry of P_4 or using a different arene starting material: employing 1.0 equiv or a sub-stoichiometric amount of P_4 favored the formation of **Sc_4P_8**; using excess P_4 or the less reactive but more labile **Sc_2-anth** (as indicated by its fluxitional behavior in solution) favored the formation of **Sc_3P_7**. Moreover, we noted that all phosphorous atoms originated from P_4 are converted to either **Sc_4P_8** or **Sc_3P_7** without any P-containing side-products when we monitored the NMR scale reaction quantitatively by ^{31}P NMR and ^{1}H spectroscopy.

Sc_3P_7 was the first example of a Zintl-type P_7^{3-} compound formed directly from P_4 activation without using an alkali metal or its equivalent as reducing agents.[35,47,53-55] Three types of phosphorous atoms are present in **Sc_3P_7**: P_{apex} (P1), P_{edge} (P2, P3, P4), and P_{bottom} (P5, P6, P7). The difference in P-P distances is smaller than that in **Sc_4P_8**, with almost identical P_{apex}-P_{edge} and P_{edge}-P_{bottom} distances of 2.20 Å and a slightly longer P_{bottom}-P_{bottom} distance of 2.23 Å. The P_7^{3-} unit in **Sc_3P_7** resembles that of the solid-state structure of Li_3P_7, although in the latter case, the difference in P-P distances is larger. Similarly to **Sc_4P_8**, **Sc_3P_7** also bears a short Fe-Sc distance of 2.80 Å.

The solution ^{1}H NMR spectrum of **Sc_3P_7** showed broad peaks for the NN^{TBS} ligand at 25 °C likely due to restricted rotation. The ^{31}P NMR spectrum showed three sets of peaks, at δ = +23.1 -118.9, and -131.4 ppm, in a 3:1:3 ratio, featuring an AA'A"MM'M"X spin system similar to the previously reported Li_3P_7, Fe_3P_7 and P_7R_3 (R = silyl or alkyl) cases.[56,57] The A part of the spectrum arises from three P_{edge} atoms centered at δ = 23.1 ppm. The three P_{bottom} atoms give rise to the M part of the spectrum at δ = -131.4 ppm, while the P_{apex} atom appears at δ = -118.9 ppm as the X part. Although the P-P distances determined by X-ray crystallography are similar; the

$^1J_{PP}$ values vary a lot: $^1J_{Papex\text{-}Pedge}$ is the smallest, at 195 Hz, the $^1J_{Pbottom\text{-}Pbottom}$ is in the middle, at 230 Hz, and $^1J_{Papex\text{-}Pbottom}$ is the largest, at 320 Hz. $^2J_{P1\text{-}P5}$ and $^2J_{P2\text{-}P3}$ are remarkably high, at -55 and -53 Hz, respectively, while $^2J_{P2\text{-}P5}$ is moderate at -12 Hz. Similarly to **Sc_4P_8**, the A part of the experimental spectrum shows significant broadness compared to the simulated spectrum, while the M and X part show good matches.

DFT calculations were carried out on model molecules of **Sc_4P_8** and **Sc_3P_7** (Si^tBuMe_2 substituents were replaced by $SiMe_3$) in order to understand their electronic structures. The two polyphosphide complexes exhibit mostly ionic interactions between the metal and the polyphosphide anion as described for $(Cp^*_2Sm)_4P_8$.[43] The examination of bonding orbitals with the same symmetry, HOMO-15 for **Sc_4P_8** and HOMO-18 for **Sc_3P_7** (Figure 4-6), revealed some overlapping between the 3d orbitals of scandium and the 3p orbitals of phosphorous. In addition, the calculated Mayer bond order for Sc-P is 0.53 and 0.51 for **Sc_4P_8** and **Sc_3P_7**, respectively. DFT calculations also support the existence of an iron-scandium interaction: Mayer bond orders of Fe-Sc interaction were found to be 0.44 and 0.42 for **Sc_4P_8** and **Sc_3P_7**, respectively.

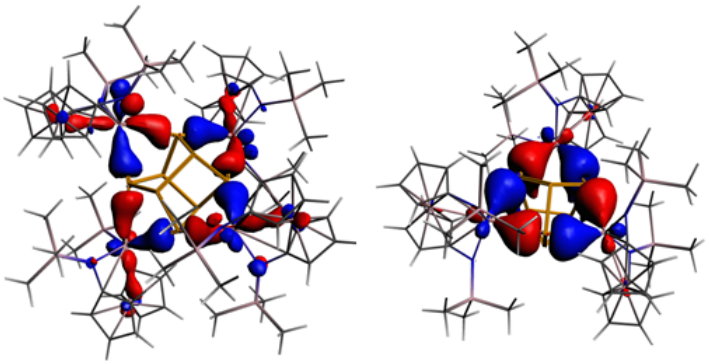

HOMO-15 for P_8 **HOMO-18 for P_7**

Figure 4-6: Selected molecular orbitals of **Sc_4P_8** and **Sc_3P_7**. Left: HOMO-15 for **Sc_4P_8**; right: HOMO-18 for **Sc_3P_7**.

4.3.2 Yttrium, lanthanum, and lutetium naphthalene complexes: synthesis, characterization, and reactivity toward P_4 activation

The success of direct P_4 activation by scandium arene complexes encouraged us to extend this chemistry to other rare-earths such as yttrium, lanthanum, and lutetium. We also hypothesized that, by changing the rare-earth ions, different product distribution from P_4 activation may be observed. The yttrium, lanthanum, and lutetium naphthalene complexes were prepared by a similar protocol to that of **Sc_2-naph** (Scheme 4-4a). Different from **Sc_2-naph**, which does not coordinate THF, the other rare-earth naphthalene complexes were synthesized with the general formula of $[(NN^{TBS})M(THF)]_2(\mu\text{-}\eta^4\text{:}\eta^4\text{-}C_{10}H_8)$ (**M_2-naph**, M = Y, La, and Lu).[3,4] The larger ionic radii for those rare-earths compared to scandium are likely to be responsible for the presence of a coordinating THF that could not be removed under reduced pressure or by crystallization. With the complete series of diamagnetic rare-earth naphthalene complexes supported by NN^{TBS} ligand, we were able to compare their physical properties. **Sc_2-naph** is a black solid barely soluble in hexanes but soluble in aromatic solvents. However, $[(NN^{TBS})Y(THF)]_2(\mu\text{-}\eta^4\text{:}\eta^4\text{-}C_{10}H_8)$ (**Y_2-naph**) is a dark-red solid barely soluble in hexanes, aromatic solvents, and diethyl ether, but only soluble in THF. While $[(NN^{TBS})Lu(THF)]_2(\mu\text{-}\eta^4\text{:}\eta^4\text{-}C_{10}H_8)$ (**Lu_2-naph**) has similar physical properties to **Y_2-naph**, $[(NN^{TBS})La(THF)]_2(\mu\text{-}\eta^4\text{:}\eta^4\text{-}C_{10}H_8)$ (**La_2-naph**), with the largest ionic radius of all rare-earths and same molecular formula as **Y_2-naph** and **Lu_2-naph**, has physical properties similar to **Sc_2-naph**: it is a black solid soluble in aromatic solvents and even slightly soluble in hexanes. These counterintuitive

phenomena educated us that it is not always correct that the properties of rare-earth metal complexes follow the trend of the size of the ions.

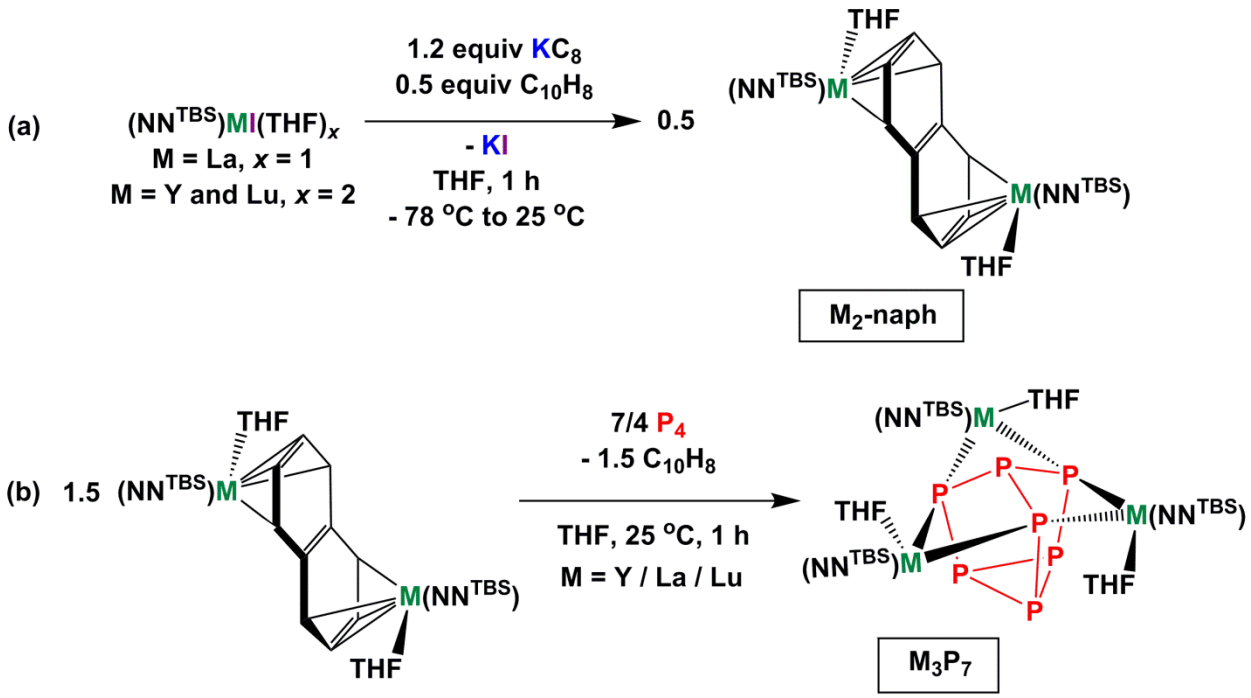

Scheme 4-4: (a) Synthesis of **M_2-naph** (M = Y, La, and Lu); (b) exclusive formation of $[(NN^{TBS})M(THF)]_3(\mu_3\text{-}\eta^2\text{:}\eta^2\text{:}\eta^2\text{-}P_7)$ (**M_3P_7**) from P_4 activation by employing **M_2-naph**.

All **M_2-naph** were characterized by ^1H and ^{13}C NMR spectroscopy, X-ray crystallography, and elemental analysis. While the proton chemical shifts of the scandium, yttrium, and lutetium naphthalene complexes were close to each other, the proton chemical shifts of the naphthalene fragment in **La_2-naph** were significantly upfield compared to the other three complexes. For those, the naphthalene fragments showed two sets of multiplets in the ^1H NMR spectra: one at ca. δ = 5 ppm and the other at δ = 4 ppm. For lanthanum, the corresponding proton chemical shifts were at δ = 4.3 and δ = 2.7 ppm, each shifted upfield by ca. 1 ppm.

However, the ^{13}C chemical shifts for **La_2-naph** were similar to those of other rare-earth naphthalene complexes. The reason for the unexpected proton upfield shift for the lanthanum naphthalene complex is not clear, especially since the ^{13}C chemical shifts were in the normal range.

Although **La_2-naph** crystallized in the space group *P*-1, different from **Y_2-naph** and **Lu_2-naph** that crystallized in the space group $P2_1/n$ and are isostructural, we found that **M_2-naph** (M = Y, La, and Lu) have similar structural parameters. Therefore, the molecular structure of **La_2-naph** is shown in Figure 4-7a as representative for **M_2-naph**. The C-C distances within the naphthalene fragment ranged from 1.37 to 1.45 Å in **La_2-naph**. The two lanthanum fragments are η^4-coordinated to opposite sides of the naphthalene ligand. The distances between lanthanum and the four coordinating carbon atoms were similar, ranging from 2.83 to 2.89 Å. Noteworthy, the Fe-La distance of 3.27 Å is 0.12 Å shorter than the sum of the covalent radii of iron and lanthanum.[32] On the contrary, the corresponding Y-Fe distance in yttrium analogue was 3.20 Å, which is close to the sum of metal covalent radii (3.22 Å). As mentioned, the THF free **Sc_2-naph** has a Fe-Sc distance of 2.83 Å, which is 0.19 Å shorter than the sum of the metal covalent radii. We previously proposed that the electron-rich iron in the ferrocene-based ligand could serve as a Lewis base to a highly Lewis acidic rare-earth metal centre.[58,59] This Lewis acid-base interaction is weak and may be disrupted by strong Lewis bases such as THF, as was in **Y_2-naph**, where the additional THF coordination cancelled the weak Fe-Y interaction and resulted in a long Fe-Y distance. However, in **La_2-naph**, the Fe-La interaction is maintained even with one coordinating THF. We attribute this phenomenon to the coordination unsaturation resulted from the large size of lanthanum(III) compared to yttrium(III).

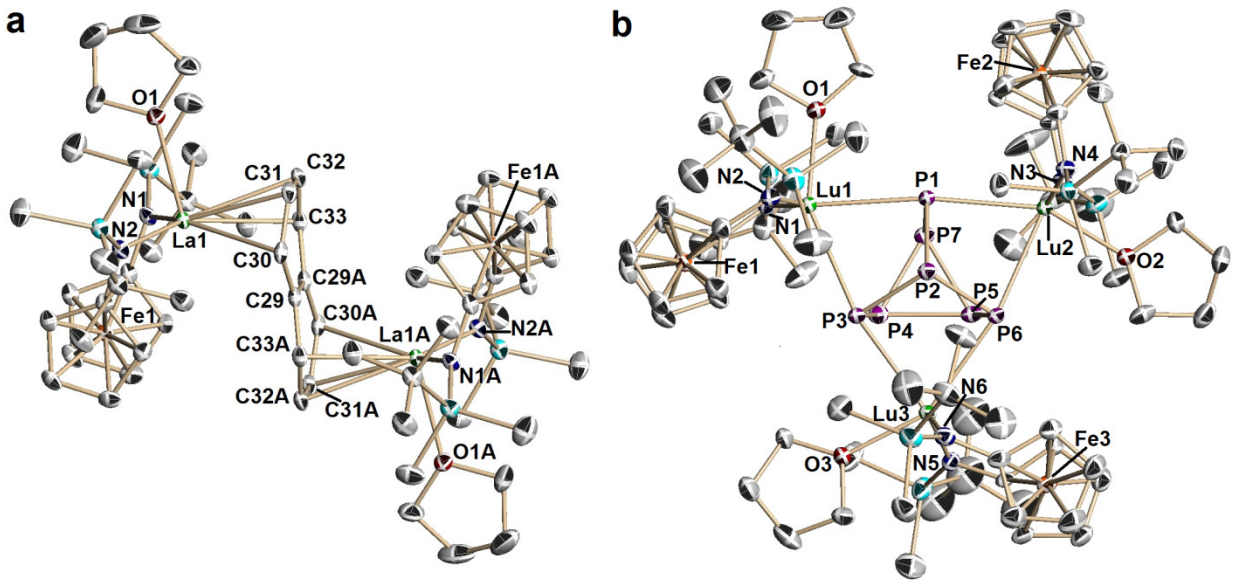

Figure 4-7: Molecular structure of **La_2-naph** (a) (only one of the two crystallographically independent molecules is shown here) and **Lu_3P_7** (b). Thermal ellipsoids are drawn at the 50% probability level. Hydrogen atoms are omitted for clarity. Selected distances [Å] and angles [°]: (a) **La_2-naph**: La1-N1 2.382(2), La1-N2 2.3672(2), La1-O1 2.5342(2), La1-Fe1 3.2659(4), La1-C30 2.891(2), La1-C31 2.841(2), La1-C32 2.827(2), La1-C33 2.865(2), C29-C29A 1.451(5), C29-C30 1.418(3), C30-C31 1.433(4), C31-C32 1.374(4), C32-C33 1.437(4), N1-La-N2 120.28(7), C29A-C29-C30 118.36(28), C29-C30-C31 121.00(22), C30-C31-C32 119.45(24), C31-C32-C33 119.76(23), C32-C33-C29A 120.55(22). (b) **Lu_3P_7**: Lu1-N1 2.184(5), Lu1-N2 2.178(5), Lu2-N3 2.187(5), Lu2-N4 2.170(5), Lu3-N5 2.197(5), Lu3-N6 2.165(5), Lu1-O1 2.298(4), Lu2-O2 2.290(4), Lu3-O3 2.316(4), Lu1-Fe1 3.320(1), Lu2-Fe2 3.265(1), Lu3-Fe3 3.372(1), Lu1-P1 2.862(2), Lu1-P3 2.947(2), Lu2-P1 2.865(2), Lu2-P6 2.897(2), Lu3-P6 2.876(2), Lu3-P3 2.910(2), P1-P2 2.178(2), P2-P3 2.183(2), P2-P6 2.188(2), P3-P4 2.180(3), P6-P5 2.180(2), P1-P7 2.183(2), P4-P5 2.246(2), P5-P7 2.224(2), P7-P4 2.228(2), N1-Lu-N2 127.43(19), N3-Lu2-N4 129.08(19), N5-Lu3-N6 125.10(20), P1-Lu1-P3 69.95(4), P1-Lu2-P6 70.37(4), P6-Lu3-P3 71.39(4), P1-P2-P3 99.56(8), P3-P2-P6 101.13(9), P1-P2-P6 99.02(8), P2-

P3-P4 100.56(9), P3-P4-P5 105.34(9), P4-P5-P7 59.79(7), P5-P7-P4 60.60(7), P7-P4-P5 59.61(7).

With **M_2-naph** in hand, we tested their reactivity toward P_4. Regardless of the stoichiometry of P_4 versus **M_2-naph**, a single product was formed with the general formula of $[(NN^{TBS})M(THF)]_3(\mu_3\text{-}\eta^2\text{:}\eta^2\text{:}\eta^2\text{-}P_7)$ (**M_3P_7**). This behavior was different from that of **Sc_2-naph**, which led to two different products, **Sc_4P_8** and **Sc_3P_7**. The exclusive formation of **M_3P_7** from **M_2-naph** raised an interesting question for the mechanism of P_4 activation by rare-earth arene complexes. It seems plausible that there are two competing reaction pathways: the first led to the formation of **M_4P_8** and the second led to the formation of **M_3P_7**. For scandium, the two pathways have similar reaction barriers so both products **Sc_4P_8** and **Sc_3P_7** were observed; for other rare-earths, the pathway to form **M_3P_7** is more favorable so **M_3P_7** formed exclusively in the reaction. However, the P_4 activation reactions were too fast even at low temperature to allow any characterization of the reaction intermediates.

With the accurate stoichiometry of P_4 (Scheme 4-4b), the reaction of **M_2-naph** and P_4 went to completion and naphthalene was the only by-product. ^{31}P NMR spectra of the crude reaction mixture showed peaks only for **M_3P_7**. Crystalline **M_3P_7** (M = Y, La, and Lu) were isolated in good yield after crystallization from various organic solvents. It was found that **La_3P_7** was more soluble than **Y_3P_7** and **Lu_3P_7** in common organic solvents: **La_3P_7** was soluble in hexanes and aromatic solvents, while **Y_3P_7** and **Lu_3P_7** was barely soluble in hexanes and slightly soluble in aromatic solvents. While the solubility of **Lu_3P_7** was similar to that of previously reported **Y_3P_7**, the solubility of **La_3P_7** was different but similar to that of the THF free compound

Sc_3P_7. The unexpected solubility properties of **M_3P_7** (M = Sc, Y, La, Lu) echo the different solubilities of **M_2-naph** described above.

The ^{31}P NMR spectrum of **Y_3P_7** is of some interest because of the presence of ^{89}Y-^{31}P coupling. It is best described as an AA'A"MM'M"XYY'Y" (Y = yttrium) spin system with A at δ = -21.1, M at δ = -130.3, and X at δ = -82.4 ppm. However, due to the peak broadening caused by ^{89}Y-^{31}P coupling and its poor solubility in aromatic solvent, the ^{31}P spectrum of **Y_3P_7** is poorly resolved. A tentative assignment of $^{1}J_{Y\text{-}P}$, $^{2}J_{Y\text{-}P}$, and $^{3}J_{Y\text{-}P}$ confirms that the coupling between ^{89}Y and ^{31}P nuclei is the cause of peak broadening. The coupling constants were estimated between 100 to 150 Hz for $^{1}J_{Y\text{-}P}$ and $^{2}J_{Y\text{-}P}$ and between -25 to -30 Hz for $^{3}J_{Y\text{-}P}$. The *J* values for ^{31}P-^{31}P coupling were found to be similar to those of **Sc_3P_7**.

The molecular structure of **Lu_3P_7** (Figure 4-7b) was selected to represent **M_3P_7**. While **Y_3P_7** is isostructural to **Lu_3P_7**, **La_3P_7** crystallized in a different space group, and two out of the three lanthanum ions were coordinated by diethyl ether instead of THF. Different batches of **La_3P_7** showed different ratios between THF and diethyl ether as coordinating solvent. Similar to **La_3P_7**, some batches of **La_2-naph** also had diethyl ether replacing THF. We attribute the lack of selectivity for coordinating solvent to the weaker Lewis acidity of lanthanum(III) compared to that of yttrium(III) and lutetium(III).[60]

Table 4-1: P-P distances of $\mathbf{M_3P_7}$ (unit: Å, error in brackets, all are average values). [a] Unlike other $\mathbf{M_3P_7}$, $\mathbf{Sc_3P_7}$ has no solvent molecule coordinating to scandium.

$\mathbf{M_3P_7}$	P_{apex}-P_{edge}	P_{edge}-P_{bottom}	P_{bottom}-P_{bottom}
$\mathbf{Sc_3P_7}$[a]	2.201(2)	2.197(2)	2.229(2)
$\mathbf{Lu_3P_7}$	2.183(2)	2.181(2)	2.233(2)
$\mathbf{Y_3P_7}$	2.188(2)	2.176(3)	2.238(2)
$\mathbf{La_3P_7}$	2.191(2)	2.161(2)	2.258(2)

All $\mathbf{M_3P_7}$ structures feature a central Zintl-type polyphosphide P_7^{3-} anion surrounded by three [(NN^{TBS})M(solvent)] fragments. Except for $\mathbf{Sc_3P_7}$, which does not coordinate any THF, all the other $\mathbf{M_3P_7}$ adopt similar coordination environment. The small ionic size of scandium may cause the difference. The lack of THF coordination in $\mathbf{Sc_3P_7}$ is compensated by a close contact between scandium and the ferrocene backbone, as shown by the short Fe-Sc distance of 2.80 Å, 0.22 Å shorter than the sum of the covalent radii of scandium and iron.[32] Despite this difference in coordination environment, P-P distances (listed in Table 4-1) show a clear trend: the larger the rare-earth ion, the shorter is the P_{edge}-P_{bottom} distance, which is accompanied by a slight lengthening of the other two types of P-P bonds. In alkali-earth metal stabilized P_7^{3-} compounds, the three distinguishable P-P bonds also have different distances, with the shortest being the P_{edge}-P_{bottom} and the longest being the P_{bottom}-P_{bottom} distance.[61] For instance, in Sr_3P_{14}, P_{apex}-P_{edge}, P_{edge}-P_{bottom}, and P_{bottom}-P_{bottom} are 2.21, 2.17, and 2.25 Å, respectively.[62] For $\mathbf{La_3P_7}$, the difference among the P-P distances is comparable to those of alkali earth P_7^{3-} binary complexes; for $\mathbf{Sc_3P_7}$, the difference among the P-P distances is at the minimum and is close to that observed for silyl substituted P_7R_3 compounds. For instance, in $P_7(SiMe_3)_3$, P_{apex}-P_{edge}, P_{edge}-P_{bottom}, and P_{bottom}-P_{bottom} distances are 2.180(4), 2.192(4), and 2.214(4) Å.[63] The P-P distances seem to be a

probe for the bonding character of M-P interaction: for covalent Si-P bond, the difference among three types of P-P bonds is the smallest; for highly ionic Sr-P interaction, the difference among three types of P-P bonds is the largest. If this illustration is correct, the trend observed for the P-P distances of **M_3P_7** complexes pointed out that the character of M-P bond varies for different rare-earth ions: the larger the rare-earth ion, the more ionic is the bond character.

4.3.3 Tautomerization of M_3P_7 studied by variable temperature NMR spectroscopy

P_7^{3-} is the major product of P_4 activation by strong reductants or nucleophiles as well as the "dead-end" of the decompositions of other polyphosphide species.[35,61] Intense experimental and theoretical studies have been performed on its alkali and alkali earth metal complexes. For example, Li_3P_7 was studied by variable temperature and 2D ^{31}P NMR spectroscopy,[64-66] and it was found that the ^{31}P NMR spectrum of Li_3P_7 in THF-d_8 is temperature dependent: at low temperature (-60 °C), three distinguishable signals were observed for the three different types of phosphorus atoms in P_7^{3-}; however, upon warming, coalescence took place and, eventually, at high temperature (50 °C) only one peak was observed. This phenomenon was attributed to a fluxional behavior of P_7^{3-}.[61] The free P_7^{3-} anion can tautomerize to essentially the same tautomer (there are 1680 of them)[64] by simultaneously breaking one P_{bottom}-P_{bottom} bond and forming a new P-P bond between two P_{edge} atoms right next to the two P_{bottom} atoms of the P-P bond that breaks. This tautomerization mechanism, which is analogous to bullvalene tautomerization,[67] was calculated to have a low energy barrier[68] and was further supported by a topology study.[69] Apparently, this tautomerization only takes place in highly ionic compounds like Li_3P_7 and Cs_3P_7;[70] no tautomerization was observed for silyl substituted P_7R_3 compounds.[61] Since the bonding character of rare-earth metals is in between ionic and covalent, and because of our

observations of different P-P distances among the four solid state molecular structures of $\mathbf{M_3P_7}$, we became interested in studying the solution behavior of $\mathbf{M_3P_7}$ (M = Sc, Y, La, and Lu).

The ^{31}P NMR spectra of $\mathbf{Sc_3P_7}$, $\mathbf{Y_3P_7}$, and $\mathbf{Lu_3P_7}$, at 25 °C in benzene-d_6 or toluene-d_8, were similar and showed three well resolved peaks that integrated to a 3:1:3 ratio, indicating that the tautomerization of the P_7^{3-} anion was frozen. However, the ^{31}P NMR spectrum (25 °C, benzene-d_6) of $\mathbf{La_3P_7}$ showed only one, broad signal centered at -75 ppm, similarly to Li_3P_7 in THF-d_8. Therefore, ^{31}P NMR spectra (Figure 4-8 left) were collected from -75 °C to 107 °C ($\mathbf{La_3P_7}$ was stable throughout the variable temperature measurement and at 85 °C for at least 24 h without any noticeable decomposition).

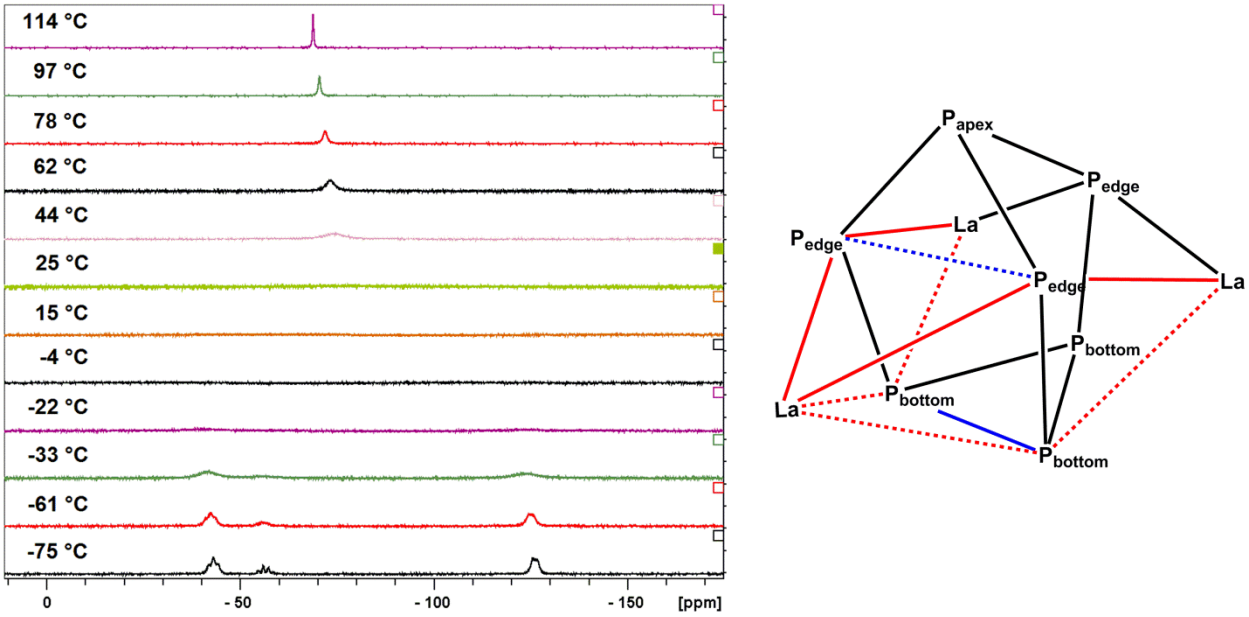

Figure 4-8: Left: Overlay of ^{31}P NMR spectra (toluene-d_8) of $\mathbf{La_3P_7}$ at different temperatures. Right: Proposed mechanism for valence tautomerization of P_7^{3-} in $\mathbf{La_3P_7}$. NN^{TBS} ligands and solvent molecules were omitted for clarity. The red solid line represents the La-P bond to break. The red dashed line represents the La-P bond to form. The blue solid line represents the P-P bond

to break. The blue dashed line represents the P-P bond to form. The black solid line represents the La-P and P-P bonds not affected by this particular tautomerization process.

The variable temperature ^{31}P NMR spectra clearly showed the fluxional behavior of P_7^{3-} in **La_3P_7** and a coalescence temperature comparable to that of Li_3P_7. However, surprisingly, this behavior took place in non-polar solvents (benzene-d_6 or toluene-d_8) for **La_3P_7**, while for Li_3P_7 it was only observed in polar and strongly coordinating solvents such as THF, DME (1,2-dimethoxyethane), and TMEDA (tetramethylethylenediamine); without a strongly coordinating solvent, Li_3P_7 decomposed. This difference suggests two possibilities that account for the fluxional behavior: (1) **La_3P_7** can dissociate to separate ion pairs in non-polar solvents, a behavior that would mimic that of Li_3P_7, and (2) the (NN^{TBS})La(THF) fragment can migrate rather easily from one phosphorous atom to another, allowing the valence tautomerization to occur. In the first case, a cationic (NN^{TBS})La(THF) species would have to be generated in a non-polar solvent. Although the ferrocene backbone of the NN^{TBS} ligand can provide some electronic stabilization and steric shielding, a coordination number of four (two nitrogen, one oxygen, and one ferrocene donor) for lanthanum is not reasonable especially in non-polar and weakly coordinating aromatic solvents. Therefore, we dismissed the idea of a separate ion pair in solution. The second possible mechanism for P_7^{3-} tautomerization in **La_3P_7** requires the simultaneous breaking and formation of four La-P bonds (Figure 4-8 right). The tautomerization involves one of the five-member rings of P_7^{3-}: a P_{bottom}-P_{bottom} bond breaks while a P_{edge}-P_{edge} bond forms; at the same time, the lanthanum fragment coordinated to that face migrates from two P_{edge} atoms to two P_{bottom} atoms. The other two lanthanum ions only break and form one La-P bond each. Such a process, together with the necessary breaking and formation of P-P bonds, is

made possible by the coordination of lanthanum to two neighbouring P_{edge} atoms and two neighbouring P_{bottom} atoms. To support this hypothesis, the average La-P_{edge} distance is 3.10 Å, while the average La-P_{bottom} distance is 3.54 Å. The 0.44 Å difference is smaller than the corresponding distance difference in the other $\mathbf{M_3P_7}$ (M = Sc: 0.67 Å, Lu: 0.57 Å, Y: 0.53 Å). If it is assumed that the metal-P distances vary linearly with the strength of the metal-P interaction, then it will be easier to form new metal-P bonds for $\mathbf{La_3P_7}$ than for $\mathbf{Y_3P_7}$ > $\mathbf{Lu_3P_7}$ > $\mathbf{Sc_3P_7}$. Consequently, we found that the tautomerization also took place in $\mathbf{Y_3P_7}$ but at a high temperature (coalescence temperature higher than 75 °C). Unfortunately, the low solubility of $\mathbf{Y_3P_7}$ in aromatic solvents and the high coalescence temperature prevented a detailed variable temperature ^{31}P NMR spectroscopy study for this complex.

4.3.4 Synthesis of organic P-containing compounds from P_4

Transferring the activated polyphosphide is essential to generate organophosphorus compounds. As a proof of concept, we tested the reactivity of the group 3 metal polyphosphide complexes with organic substrates. The reaction of $\mathbf{Sc_3P_7}$ or $\mathbf{Y_3P_7}$ (Equation 4-1) with 3 equiv Me_3SiI led to the formation of the corresponding rare-earth iodide and $P_7(SiMe_3)_3$,[3] as confirmed by ^{31}P NMR spectroscopy.[56] Since the only by-product is rare-earth iodide, which is used in synthesizing the rare-earth naphthalene complexes, a synthetic cycle for the transformation of P_4 to organophosphorus compounds was achieved.

Equation 1:

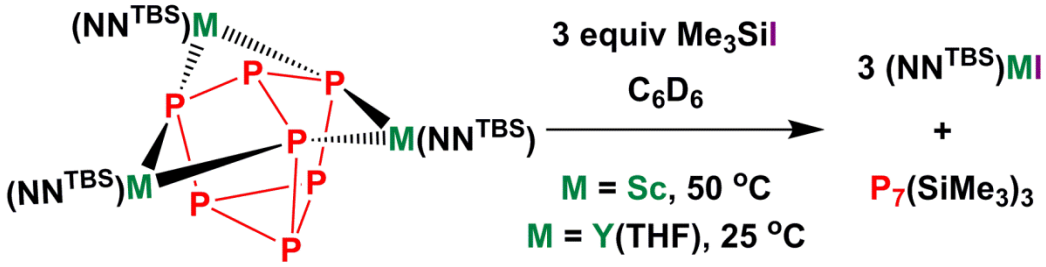

4.4 Experimental section

Synthesis of Sc_2-naph: $(NN^{TBS})ScI(THF)_2$ (0.363 g, 0.478 mmol) and 0.5 equiv naphthalene (0.0324 g, 0.253 mmol) were dissolved in 5 mL of THF. The solution was cooled down to -78 °C using a dry ice/acetone bath. Then KC_8 (0.080 g, 0.592 mmol) was added to the solution. The color immediately turned to dark red. The reaction mixture was allowed to stir at room temperature for 1.5 h. The solution was then filtered through Celite to get rid of graphite and KI. After removing volatiles under reduced pressure, the remaining dark-red oily solid was extracted with toluene and filtered through Celite again to get rid of residual KI. The toluene was removed under reduced pressure, resulting in a dark-blue solid. 5 mL of diethyl ether was added and the mixture was kept at -35 °C. After one day, the diethyl ether solution was filtered and **Sc_2-naph** was collected as a dark purple microcrystalline solid on the medium frit. Yield: 0.166 g, 62.9%. Single crystals suitable for X-ray diffraction were grown from a concentrated toluene solution. ^{1}H NMR (500 MHz, C_6D_6) δ, ppm: 5.06 and 4.02 (t, 8H, C*H* of naphthalene), 4.20, 4.11 and 3.99 (m, 16H, C*H* on Cp rings), 1.03 (s, 36H, SiCC*H*$_3$), and 0.35 and 0.16 (s, 24H, SiC*H*$_3$). ^{13}C NMR (126 MHz, C_7D_8) δ, ppm: 158.4, 120.3 and 95.0 (*C* and *C*H on naphthalene), 108.0 (CN on Cp rings), 71.7, 68.9, 68.6, and 59.6 (*C*H on Cp rings), 27.6 (SiC*C*H$_3$), -1.1 and -2.7 (Si*C*H$_3$), Si*C*CH$_3$ is likely overlapping with solvent C_7D_8 peak at 21. Anal. (%): Calcd. for $C_{54}H_{84}N_4Fe_2Sc_2Si_4$: C, 58.79; H, 7.67; N, 5.08. Found: C, 58.44; H, 7.50; N, 4.79.

Synthesis of Sc_2-anth: $(NN^{TBS})ScI(THF)_2$ (0.231 g, 0.304 mmol) and 0.5 equiv anthracene (0.030 g, 0.168 mmol) were dissolved in 5 mL of THF and cooled down to -78 °C with a dry ice/acetone bath for 15 min. 1.5 equiv KC_8 (0.062 g, 0.459 mmol) was then added to the solution. The color of solution immediately turned to dark purple. The reaction mixture was allowed to stir at -78 °C for 2 h. The THF solution was filtered through Celite to get rid of graphite and KI. Volatiles were removed under reduced pressure. The solid was then extracted with 10 mL of toluene and filtered through Celite again to get rid of residual KI. After removing toluene under reduced pressure, the crystalline purple solid was dissolved in a minimum amount of hexanes and kept at -35 °C for 3 days. The solution was decanted and the purple crystals were dried under reduced pressure to give **Sc_2-anth**. Yield: 0.122 g, 69.7%. Single crystals suitable for X-ray diffraction were grown from a concentrated diethyl ether solution. ^{1}H NMR (500 MHz, C_6D_6) δ, ppm: 6.36 and 6.09 (b, 8H, C*H* on the outer two rings of anthracene), 4.02, 3.00, 3.90, and 3.82 (s, 16H, C*H* on Cp rings), 3.98 (s, 2H, C*H* on center ring of anthracene), 0.97 (SiCC*H*$_3$), and 0.29 (SiC*H*$_3$). ^{13}C NMR (126 MHz, C_6D_6) δ, ppm: 127.9 overlapping with solvent C_6D_6 in regular ^{13}C NMR but showing up in DEPT135 ^{13}C NMR (*C*H on center ring of Anthracene), 123.0 (C on Anthracene), 106.9 (*C*N on Cp ring), 78.2, 69.0, and 61.4 (*C*H on Cp ring, the peak at 61.4 likely to be two peaks coincidently overlapping), 71.7 and 69.5 (*C*H on two outer rings of anthracene), 27.7 (SiC*C*H$_3$), 20.2 (Si*C*CH$_3$), -0.8 and 2.5 (Si*C*H$_3$). Anal. (%): Calcd. for $C_{58}H_{86}N_4Fe_2Sc_2Si_4$ with one molecule of hexanes (C_6H_{14}) per **Sc_2-anth** molecule: C, 62.02; H, 8.13; N, 4.52. Found: C, 62.63; H, 7.73; N, 4.60.

Conversion of Sc_2-naph to Sc_2-anth: **Sc_2-naph** (6.0 mg, 0.0054 mmol) and 1.6 equiv anthracene (1.6 mg, 0.0090 mmol) were dissolved in C_6D_6 in a J-Young tube. The mixture was heated at 50 °C and monitored by ^{1}H NMR spectroscopy. After 16 h, there was about 34%

conversion from **Sc_2-naph** to **Sc_2-anth**. As the transformation took place, the solution color gradually changed from dark blue to dark purple. The conversion reached completion after 5 days at 50 °C. Repeating the reaction with another batch of **Sc_2-naph** synthesized separately gave similar results: the conversion reached completion after four days at 70 °C.

Reaction of Sc_2-naph and 2,2′-bipyridine: Sc_2-naph (14.6 mg, 0.013 mmol) was dissolved in C_6D_6 in a J-Young tube and 2 equiv 2,2′-bipyridine (4.1 mg, 0.026 mmol) was added as a C_6D_6 solution. The color of the solution changed immediately from dark blue to green. ^{1}H NMR spectroscopy showed the complete consumption of **Sc_2-naph** and 2,2′-bipyridine with the generation of naphthalene and several broad peaks confirmed to be the corresponding 2,2′-bipyridine radical anion complex, which was synthesized and reported previously by our group.[28]

Synthesis of $[(NN^{TBS})Sc(NC_5H_5)]_2[\mu$-$(NC_5H_5$-$C_5H_5N)]$: Sc_2-naph (0.105 g, 0.0952 mmol) was dissolved in 10 mL of toluene and kept in a dry ice/acetone bath for 15 min. Excess pyridine (0.056 g, 0.708 mmol) was added and the mixture was warmed up to ambient temperature and stirred for 20 min. The color changed immediately from dark blue to yellow. After 20 min of stirring at ambient temperature, the volatiles were removed under reduced pressure. Single crystals suitable for X-ray diffraction were grown from a concentrated hexanes solution. After crystallization from a concentrated toluene solution layered with *n*-pentane, the product was isolated as yellow crystals. Yield: 0.060 g, 48.9%. ^{1}H NMR (300 MHz, C_6D_6) δ, ppm: 8.76 (d, *J* = 4.89, 4H, *o*-C*H* on coordinating pyridine) Hz, 7.56 (d, *J* = 7.68 Hz, 4H, NC*H*=CH on reductive coupled 4,4'-bipyridine fragment), 6.92 (t, 2H, *p*-C*H* on coordinating pyridine), 6.68 (t, *m*-C*H* on coordinating pyridine), 4.99 (d, J = 6.33 Hz, 4H, NCH=C*H* on reductive coupled 4,4'-bipyridine fragment), 4.02 and 3.80 (b, 16H, C*H* on Cp rings), 3.89 (s, 2H, C*H*-C*H* on reductive coupled 4,4'-bipyridine fragment), 0.94 (s, 36H, SiCCH_3), -0.20 (b, 24H,

SiCH_3). ^{13}C NMR (126 MHz, C_6D_6) δ, ppm: 150.2 (*o*-*C*H on coordinating pyridine), 139.7 (N*C*H=CH on reductive coupled 4,4'-bipyridine fragment), 136.2 (*p*-*C*H on coordinating pyridine), 125.0 (*m*-*C*H on coordinating pyridine), 107.9 (*C*N on Cp rings), 93.3 (NCH=*C*H on reductive coupled 4,4'-bipyridine fragment), 68.9 (b, *C*H on Cp rings), 45.2 (*C*H-*C*H on reductive coupled 4,4'-bipyridine fragment), 27.9 (SiC*C*H_3), 20.5 (Si*C*CH_3), -2.9 (b, Si*C*H_3). Anal. (%): Calcd. for $C_{64}H_{96}N_8Fe_2Sc_2Si_4$: C, 59.52; H, 7.49; N, 8.68. Found: C, 59.44; H, 7.55; N, 8.52.

Synthesis of [(NN^{TBS})Sc]$_2$(μ-CCPh)$_2$: Sc$_2$-naph (0.224 g, 0.203 mmol) was dissolved in 10 mL of toluene and kept in a dry ice/acetone bath for 15 min. 2 equiv phenylacetylene (0.049 g, 0.48 mmol) was added as a toluene solution and the mixture was warmed up to ambient temperature and stirred for 30 min. The color changed immediately from dark blue to green and finally to orange. After 30 min of stirring at ambient temperature, the volatiles were removed under reduced pressure. Single crystals suitable for X-ray diffraction were grown from a concentrated hexanes solution. The crude product was extracted in hexanes and diethyl ether. The hexanes extraction was kept at -35 °C. Crystals formed and were washed with cold *n*-pentane, yielding 0.032 g. The diethyl ether extraction was dried giving a yellow powder (0.073 g). Combined yield: 0.105 g, 43.9%.^{1}H NMR (500 MHz, C_6D_6) δ, ppm: 7.77 (d, *J* = 7.05 Hz, 4H, *o*-C*H* on phenyl rings), 7.03 (t, 4H, *m*-C*H* on phenyl rings), 6.98 (t, 2H, *p*-C*H* on phenyl rings), 4.10 and 3.89 (t, 16H, C*H* on Cp rings), 1.09 (s, 36H, SiCCH_3), 0.56 (s, 24H, SiCH_3). ^{13}C NMR (126 MHz, C_6D_6) δ, ppm: 132.9 (*o*-*C*H on phenyl), 130.2 and 128.7 (*p*-*C*H and *m*-*C*H on phenyl), 123.0 (*ipso*-*C* on phenyl), 105.1 (*C*N on Cp rings), 69.0 and 68.9 (*C*H on Cp rings), 28.3 (SiC*C*H_3), 20.5 (Si*C*CH_3), -0.8 (Si*C*H_3), the signals for the sp hybridized carbon atoms were not

identified in the spectrum. Anal. (%): Calcd. for $C_{60}H_{86}N_4Fe_2Sc_2Si_4$: C, 61.21; H, 7.36; N, 4.76. Found: C, 60.32; H, 7.26; N, 4.70.

Synthesis of Sc_4P_8 and Sc_3P_7: Sc_2-naph (0.316 g, 0.286 mmol) was dissolved in 15 mL of toluene in a Schlenk tube and P_4 (0.036 g, 0.291 mmol) was added as a 5 mL of toluene solution. The mixture was stirred at 25 °C for 22.5 h. The initial dark blue color turned to green after 15 min stirring. Then the color gradually changed from green to light green and finally to orange. After stirring, the volatiles were removed under reduced pressure. The resulting orange solid was extracted by pentane, diethyl ether and toluene. Based on ^{1}H NMR spectroscopy, pentane extraction was mostly **Sc_3P_7** while diethyl ether and toluene extraction contained mostly **Sc_4P_8**. **Sc_3P_7** was collected as orange micro-crystals precipitated from pentane. Yield: 0.100 g, 31.2 % (based on Sc). The diethyl ether and toluene extraction were combined and dried down under reduced pressure. The resulting yellow solid was further washed with pentane to get clean **Sc_4P_8**. Yield: 0.147 g, 46.8 %. **Sc_4P_8**: ^{1}H NMR (500 MHz, C_6D_6, 25 °C) δ, ppm: 4.65, 4.46, 4.07 4.03, 4.01, 3.96, 3.93, and 3.79 (m, 32H, C*H* on Cp rings), 1.20, and 1.19 (s, 72H, SiCCH_3), and 0.92, 0.37, 0.36, and 0.29 (s, 48H, SiCH_3). ^{13}C NMR (126 MHz, C_6D_6, 25 °C) δ, ppm: 107.4, and 105.7 (*C*N on Cp rings), 71.3, 71.1, 70.4, 70.1, 69.8, 66.5, and 64.3 (*C*H on Cp rings), 28.5, and 27.7 (SiC*C*H$_3$), 20.6, and 20.1 (Si*C*CH$_3$), and 2.0, 0.4, -1.2, and -1.3 (Si*C*H$_3$). ^{31}P NMR (122 MHz, C_6D_6, 25 °C) δ, ppm: 96.2 (m, 4P, P_{corner}), and 45.7 (m, 4P, P_{inner}). Anal. (%): Calcd. for $C_{88}H_{152}N_8Fe_4Sc_4Si_8P_8$ with half molecule of toluene: C, 48.97; H, 7.01; N, 4.99. Found: C, 48.76; H, 6.60; N, 5.19. **Sc_3P_7**: ^{1}H NMR (500 MHz, C_6D_6, 25 °C) δ, ppm: 4.62, 4.03, 3.88, and 3.83 (b, 24H, C*H* on Cp rings), 1.15 (s, 54H, SiCCH_3), and 0.72, and 0.35 (s, 12H, SiCH_3). ^{13}C NMR (126 MHz, C_6D_6, 25 °C) δ, ppm: 106.2 (*C*N on Cp rings), 71.3, 69.8, 67.2, and 66.0 (*C*H on Cp rings), 28.1 (SiC*C*H$_3$), 20.3 (Si*C*CH$_3$), and 0.2, and -0.3 (Si*C*H$_3$). ^{31}P NMR (122 MHz, C_6D_6,

25 °C) δ, ppm: 23.2 (m, 3P, P_{edge}), -118.9 (m, 1P, P_{apex}), and -131.4 (m, 3P, P_{bottom}). Anal. (%): Calcd. for $C_{66}H_{114}N_6Fe_3Sc_3Si_6P_7$ with one molecule of hexanes: C, 48.98; H, 7.31; N, 4.75. Found: C, 48.77; H, 7.29; N, 4.89.

Synthesis of Y_2-naph: $(NN^{TBS})YI(THF)_2$ (0.410 g, 0.511 mmol) and 0.5 equiv naphthalene (0.0350 g, 0.273 mmol) were dissolved in 10 mL of THF. The solution was cooled down to -78 °C using a dry ice/acetone bath. Then KC_8 (0.125 g, 0.925 mmol) was added to the solution. The color immediately turned to dark red. The reaction mixture was allowed to stir at room temperature for 2 h. 6 mL of hexanes was added to the reaction mixture to minimize the solubility of salt KI. The solution was then filtered through Celite. The solid left on Celite was washed with 4 mL THF/hexanes (3:1 ratio). After removing volatiles under reduced pressure, the remaining reddish-purple solid was transferred into a vial using 18 mL of THF. The THF was removed under reduced pressure, resulting in a reddish-purple solid. 6 mL of diethyl ether was added and the mixture was kept at -35 °C. After one day, the diethyl ether solution was filtered and **Y_2-naph** was collected as a reddish-purple solid on the medium frit. Yield: 0.214 g, 62.6 %. ^{1}H NMR (500 MHz, C_6D_6, 25 °C) δ, ppm: 5.09 and 3.94 (t, 8H, C*H* of naphthalene), 4.33, 4.13 and 3.87 (b, 24H, C*H* on Cp rings and CH_2O), 1.42 (b, 8H, CH_2CH_2O), 1.07 (s, 36H, SiCCH_3), and 0.22 and 0.13 (s, 24H, SiCH_3). ^{1}H NMR (500 MHz, C_4D_8O, 25 °C) δ, ppm: 5.01 and 3.66 (t, 8H, C*H* of naphthalene), 4.25, and 3.83 (b, 16H, C*H* on Cp rings), 0.73 (s, 36H, SiCCH_3), and -0.03 (s, 24H, SiCH_3). ^{13}C NMR (126 MHz, C_4D_8O, 25 °C) δ, ppm: 158.3, 118.3 and 94.3 (*C* and *C*H on naphthalene), 108.4 (*C*N on Cp rings), signals of *C*H on Cp rings were covered by solvent C_4D_8O peaks, 28.5 (SiC*C*H$_3$), 21.2 (Si*C*CH$_3$) and -1.7 (Si*C*H$_3$). Anal. (%): Calcd. for $C_{62}H_{100}N_4Fe_2O_2Si_4Y_2$: C, 55.77; H, 7.55; N, 4.20. Found: C, 55.22; H, 7.20; N, 4.53.

Synthesis of La_2-naph: (NN^{TBS})LaI(THF) (0.5326 g, 0.682 mmol) and naphthalene (0.0416 g, 0.325 mmol) were weighed in a scintillation vial. 10 mL of THF was added to make a yellow solution, which was cooled down to -78 °C with a dry ice / acetone bath. KC_8 (0.106 g, 0.784 mmol) was added to the solution. The reaction mixture was allowed to warm up to 25 °C and stirred for 3 h. The resulting dark red solution was filtered through Celite and dried under reduced pressure. The remaining red solid was dispersed in Et_2O and stored in a -35 °C freezer for 5 days. A blackcrystalline solid was collected on a medium frit after filtration. Yield: 0.289 g, 59.0%. ^{1}H NMR (500 MHz, C_6D_6, 25 °C) δ, ppm: 4.28 and 2.73 (br s, 4H each, C*H* on naphthalene fragement), 4.20 and 3.85 (br s, 8H each, C*H* on Cp rings), 4.09 (br s, 2H, CH_2O on THF), 3.61 (br s, 8H, CH_2O on Et_2O), 1.52 (br s, 2H, CH_2CH$_2$O on THF), 1.26 (m, 12H, CH_3CH$_2$O on Et_2O), 1.01 (s, 36H, (CH_3)$_3$C), and 0.30 (s, 24H, SiCH_3). ^{13}C NMR (126 MHz, C_6D_6, 25 °C) δ, ppm: 156.8, 122.0, 99.5, and 71.0 (*C* or *C*H on naphthalene fragment), 109.4 (CN on Cp rings), broad peaks around 66.8 (*C*H on Cp rings), 27.7 ((*C*H$_3$)$_3$C), 20.7 ((CH$_3$)$_3$*C*), and -2.4 (Si*C*H$_3$). An analytical pure sample was obtained by recrystallization from a concentrated hexanes solution in a -35 °C freezer for two days. Anal. (%): Calcd. for $C_{62}H_{100}N_4O_2Fe_2La_2Si_4$, Mw = 1435.354: C, 51.88; H, 7.02; N, 3.90. Found: C, 51.28; H, 7.05; N, 3.46.

Synthesis of Lu_2-naph: (NN^{TBS})LuI(THF)$_2$ (0.2005 g, 0.226 mmol) and naphthalene (0.0156 g, 0.122 mmol) were weighed in a scintillation vial. 6 mL of THF was added to make a yellow solution which was cooled down to -78 °C with a dry ice / acetone bath. KC_8 (0.451 g, 0.334 mmol) was added to the solution. The reaction mixture was allowed to warm up to 25 °C and stirred for 1 h. The resulting dark red solution was filtered through Celite and dried under reduced pressure. The remaining red solid was dispersed in Et_2O and stored in a -35 °C freezer

for 2 days. A red solid was collected on a medium frit after filtration. Yield: 0.0866 g, 51.1%. ^{1}H NMR (500 MHz, C_7D_8, 25 °C) δ, ppm: 5.17 and 4.23 (br s, 4H each, C*H* on naphthalene fragment), 3.96 and 3.87 (br s, 8H each, C*H* on Cp rings), broad peaks around 3.90 (br, 8H, CH_2O on THF), 1.42 (br s, 2H, CH_2CH$_2$O on THF), 1.07 (s, 36H, (CH_3)$_3$C), and 0.26 and 0.15 (s, 12H each, SiCH_3). ^{13}C NMR (126 MHz, C_7D_8, 25 °C) δ, ppm: 154.9, 117.8, and 95.2 (*C* or *C*H on naphthalene fragment), broad peaks around 68.8 (*C*H on Cp rings), 65.9 (*C*H$_2$O on THF), 28.1 ((*C*H$_3$)$_3$C), 25.7 (*C*H$_2$CH$_2$O on THF), and -1.0 and -2.8 (Si*C*H$_3$). Some peaks were missing due to low solubility of **Lu$_2$-naph** or may be masked by deuterated solvent peaks. Anal. (%): Calcd. for $C_{62}H_{100}N_4O_2Fe_2Lu_2Si_4$, Mw = 1507.476: C, 49.39; H, 6.69; N, 3.72. Found: C, 44.78; H, 6.04; N, 3.57. Although multiple samples were submitted for analysis all results were significantly low in carbon. It is possible that fine powders of **Lu$_2$-naph** are extremely air and moisture sensitive and decompose upon handling.

Synthesis of Y$_3$P$_7$: Y$_2$-naph (0.150 g, 0.112 mmol) was dissolved in 10 mL of THF and cooled down to -78 °C with a dry ice/acetone bath for 15 min. P_4 (0.0189 g, 0.153 mmol) was then added as a THF solution. The color of solution gradually changed from reddish-purple to orange. After stirring for 1 h at 25 °C, the volatiles were removed under reduced pressure. The resulting orange solid was washed with pentane until the pentane wash was very light yellow. **Y$_3$P$_7$** was isolated as a yellow powder. Yield: 0.106 g, 69.7%. ^{1}H NMR (500 MHz, C_6D_6, 25 °C) δ, ppm: 4.18, 3.94, and 3.41 (b, 24H, C*H* on Cp rings), 4.04 (b, 12H, CH_2O), 1.48 (b, 12H, CH_2CH$_2$), 1.19 (s, 54H, SiCCH_3), and 0.61, and 0.28 (s, 24H, SiCH_3). Due to low solubility of **Y$_3$P$_7$** in C_6D_6, the ^{13}C NMR experiment was performed at higher temperature (75 °C). The ^{1}H NMR spectrum at 75 °C is also included here since it was different from that at 25 °C. ^{1}H NMR (500 MHz, C_6D_6, 75 °C) δ, ppm: 4.13, 4.04, and 3.55 (b, 24H, C*H* on Cp rings), 3.95 (b, 12H,

CH_2O), 1.55 (b, 12H, CH_2CH$_2$), 1.13 (s, 54H, SiCCH_3), and 0.55, and 0.29 (s, 24H, SiCH_3). ^{13}C NMR (126 MHz, C_6D_6, 75 °C) δ, ppm: 106.1 (*C*N on Cp rings), 70.3, 69.1, and 66.4 (*C*H on Cp rings), 68.4 (*C*H$_2$O), 28.3 (SiC*C*H$_3$), 25.5 (*C*H$_2$CH$_2$O), 20.6 (Si*C*CH$_3$), and -0.5 (Si*C*H$_3$). ^{31}P NMR (122 MHz, C_6D_6, 25 °C) δ, ppm: -20.4 (b, 3P, P_{edge}), -81.8 (b, 1P, P_{cap}), and -130.4 (b, 3P, P_{bottom}). Anal. (%): Calcd. for $C_{78}H_{138}N_6Fe_3O_3P_7Si_6Y_7$ with one molecule of toluene, C_7H_8: C, 48.16; H, 6.94; N, 3.96. Found: C, 47.88; H, 6.99; N, 3.87.

Synthesis of La_3P_7: To a solution of **La_2-naph** (0.1584 g, 0.110 mmol) in 6 mL of THF, P_4 (0.0160 g, 0.129 mmol) was added. The color of the solution changed gradually from dark red to orange in 5 min. The reaction mixture was allowed to stir at 25 °C for 1 h. The volatiles were removed under reduced pressure. The resulting yellow-orange solid was extracted in hexanes. After storing in a -35 °C freezer for 6 days, yellow crystals formed and were isolated by decanting the mother liquor and washing with cold *n*-pentane. Yield: 0.0677 g, 42.3%. The formula of single crystals was found to be [(NN^{TBS})La(THF)][(NN^{TBS})La(OEt$_2$)]$_2$P$_7$. The 2:1 ratio of Et$_2$O:THF of that batch was confirmed by integration of the corresponding peaks in the ^{1}H NMR spectrum. However, a ^{1}H NMR spectrum of another batch, prepared independently, showed exclusively THF as the coordinating solvent molecule. ^{1}H NMR (500 MHz, C_7D_8, 25 °C) δ, ppm: broad peaks centered at 4.11, 3.81, and 3.28 (br, 24H total, C*H* on Cp rings), 3.97 (br s, 6H, C*H*$_2$O on THF), 3.56 (br s, 6H, C*H*$_2$O on Et$_2$O), 1.55 (br s, 6H, C*H*$_2$CH$_2$O on THF), 1.14 (br s, 9H, C*H*$_3$CH$_2$O on Et$_2$O), 1.10 (s, 54H, (C*H*$_3$)$_3$C), and 0.44 (br s, 36H, SiC*H*$_3$). ^{13}C NMR (126 MHz, C_7D_8, 25 °C) δ, ppm: 104.9 (*C*N on Cp rings), broad peaks centered at 69.2, 68.2, and 65.0 (*C*H on Cp rings), 28.0 ((*C*H$_3$)$_3$C), 25.3 ((CH$_3$)$_3$*C*), and -1.7 (Si*C*H$_3$). Anal. (%): Calcd. for $C_{78}H_{142}N_6O_3Fe_3La_3P_7Si_6$, Mw = 2181.620: C, 42.94; H, 6.56; N, 3.85. Found: C, 43.30; H, 6.75; N, 3.51.

Synthesis of Lu_3P_7. To a solution of **Lu_2-naph** (0.200 g, 0.133 mmol) in 12 mL of THF, P_4 (0.0227 g, 0.183 mmol) was added. The color changed gradually from dark red to orange in 10 min. The reaction mixture was allowed to stir at 25 °C for 1 h. The volatiles were removed under reduced pressure. The resulted yellow-orange solid was dissolved in 4 mL of toluene and layered with 2 mL of *n*-pentane. After storing in a -35 °C freezer for 2 days, yellow crystals formed and were isolated by decanting the mother liquor and washing with cold *n*-pentane. Yield: 0.109 g, 53.9%. ^{1}H NMR (500 MHz, C_7D_8, 25 °C) δ, ppm: 4.13, 4.07, 3.89, and 3.49 (s, 4H each, C*H* on Cp rings), 4.03 (br s, 12H, CH_2O on THF), 1.53 (br s, 12H, CH_2CH$_2$O on THF), 1.12 (s, 54H, (CH_3)$_3$C), and 0.56 and 0.25 (s, 12H each, SiCH_3). ^{13}C NMR (126 MHz, C_7D_8, 25 °C) δ, ppm: 103.8 (*C*N on Cp rings), 71.0, 67.6, and 65.3 (*C*H on Cp rings), 28.4 ((*C*H$_3$)$_3$C), 25.5 ((CH$_3$)$_3$*C*), and -0.4 and -0.5 (Si*C*H$_3$). Anal. (%): Calcd. for $C_{78}H_{138}N_6O_3Fe_3Lu_3P_7Si_6$ with one molecule of *n*-pentane, Mw = 2357.922: C, 42.28; H, 6.41; N, 3.56. Found: C, 41.93; H, 6.40; N, 3.52.

General reaction set-up for the reaction of M_3P_7 (M = Sc, Y) and Me_3SiI: 0.015 g **M_3P_7** was dissolved in C_6D_6 in a J-Young tube. Excess TMSI was added at room temperature and the reaction was monitored by ^{1}H NMR spectroscopy. For M = Sc, no obvious change was observed after 1 h at room temperature; so, the J-Young tube was heated at 50 °C. The transformation reached completion after 23 h at 50 °C with the formation of [(NN^{TBS})Sc(μ-I)]$_2$ and $P_7(SiMe_3)_3$, which was confirmed by ^{31}P NMR spectra. For M = Y, the transformation took place at 25 °C and reached completion after 9 h. The formation of [(NN^{TBS})Y(μ-I)]$_2$ and $P_7(SiMe_3)_3$ were confirmed by ^{1}H and ^{31}P NMR spectroscopy, respectively.

Note: The attempt to transfer the P_8^{4-} unit in **Sc_4P_8** with Me_3SiI was not successful. Even after prolonged heating (2 days) at 100 °C with excess Me_3SiI, **Sc_4P_8** remained intact.

4.5 References

(1) Connelly, N. G.; Geiger, W. E. *Chem. Rev.* **1996**, *96*, 877.

(2) Huang, W.; Khan, S. I.; Diaconescu, P. L. *J. Am. Chem. Soc.* **2011**, *133*, 10410.

(3) Huang, W.; Diaconescu, P. L. *Chem. Commun.* **2012**, *48*, 2216.

(4) Huang, W.; Diaconescu, P. L. *Eur. J. Inorg. Chem.* **2013**, *2013*, 4090.

(5) Bochkarev, M. N. *Chem. Rev.* **2002**, *102*, 2089.

(6) Cotton, F. A.; Schwotzer, W. *J. Am. Chem. Soc.* **1986**, *108*, 4657.

(7) Cloke, F. G. N.; Khan, K.; Perutz, R. N. *J. Chem. Soc., Chem. Commun.* **1991**, 1372.

(8) Cloke, F. G. N. *Chem. Soc. Rev.* **1993**, *22*, 17.

(9) Arnold, P. L.; Cloke, F. G. N.; Hitchcock, P. B.; Nixon, J. F. *J. Am. Chem. Soc.* **1996**, *118*, 7630.

(10) Arnold, P. L.; Cloke, F. G. N.; Nixon, J. F. *Chem. Commun.* **1998**, 797.

(11) Huang, Y.; Wise, M. B.; Jacobson, D. B.; Freiser, B. S. *Organometallics* **1987**, *6*, 346.

(12) Hayes, P. G.; Piers, W. E.; Parvez, M. *J. Am. Chem. Soc.* **2003**, *125*, 5622.

(13) Hayes, P. G.; Piers, W. E.; Parvez, M. *Chem. Eur. J.* **2007**, *13*, 2632.

(14) Fryzuk, M. D.; Jafarpour, L.; Kerton, F. M.; Love, J. B.; Rettig, S. J. *Angew. Chem. Int. Ed.* **2000**, *39*, 767.

(15) Arakawa, T.; Shimada, S.; Adachi, G.-Y.; Shiokawa, J. *Inorg. Chim. Acta.* **1988**, *145*, 327.

(16) Bochkarev, M. N.; Trifonov, A. A.; Fedorova, E. A.; Emelyanova, N. S.; Basalgina, T. A.; Kalinina, G. S.; Razuvaev, G. A. *J. Organomet. Chem.* **1989**, *372*, 217.

(17) Fedushkin, I. L.; Bochkarev, M. N.; Schumann, H.; Esser, L. *J. Organomet. Chem.* **1995**, *489*, 145.

(18) Fedushkin, I. L.; Nevodchikov, V. K.; Cherkasov, V. K.; Bochkarev, M. N.; Schumann, H.; Girgsdies, F.; Görlitz, F. H.; Kociok-Köhn, G.; Pickardt, J. *J. Organomet. Chem.* **1996**, *511*, 157.

(19) N. Bochkarev, M.; L. Fedushkin, I.; A. Fagin, A.; Schumann, H.; Demtschuk, J. *Chem. Commun.* **1997**, 1783.

(20) Evans, W. J.; Allen, N. T.; Ziller, J. W. *J. Am. Chem. Soc.* **2000**, *122*, 11749.

(21) Shannon, R. *Acta Cryst.* **1976**, *A32*, 751.

(22) Moeller, T.; Martin, D. F.; Thompson, L. C.; Ferrús, R.; Feistel, G. R.; Randall, W. J. *Chem. Rev.* **1965**, *65*, 1.

(23) Zimmermann, M.; Anwander, R. *Chem. Rev.* **2010**, *110*, 6194.

(24) Anderson, D. M.; Cloke, F. G. N.; Cox, P. A.; Edelstein, N.; Green, J. C.; Pang, T.; Sameh, A. A.; Shalimoff, G. *J. Chem. Soc., Chem. Commun* **1989**, 53.

(25) Melero, C.; Guijarro, A.; Yus, M. *Dalton Trans.* **2009**, 1286.

(26) Diaconescu, P. L. *Acc. Chem. Res.* **2010**, *43*, 1352.

(27) Huang, W.; Carver, C. T.; Diaconescu, P. L. *Inorg. Chem.* **2010**, *50*, 978.

(28) Williams, B. N.; Huang, W.; Miller, K. L.; Diaconescu, P. L. *Inorg. Chem.* **2010**, *49*, 11493.

(29) Beetstra, D. J.; Meetsma, A.; Hessen, B.; Teuben, J. H. *Organometallics* **2003**, *22*, 4372.

(30) Fedushkin, I. L.; Nevodchikov, V. I.; Bochkarev, M. N.; Dechert, S.; Schumann, H. *Russ. Chem. Bull.* **2003**, *52*, 154.

(31) Jaroschik, F.; Nief, F.; Le Goff, X.-F.; Ricard, L. *Organometallics* **2007**, *26*, 3552.

(32) Cordero, B.; Gomez, V.; Platero-Prats, A. E.; Reves, M.; Echeverria, J.; Cremades, E.; Barragan, F.; Alvarez, S. *Dalton Trans.* **2008**, *0*, 2832.

(33) Cossairt, B. M.; Piro, N. A.; Cummins, C. C. *Chem. Rev.* **2010**, *110*, 4164.

(34) Caporali, M.; Gonsalvi, L.; Rossin, A.; Peruzzini, M. *Chem. Rev.* **2010**, *110*, 4178.

(35) Scheer, M.; Balázs, G.; Seitz, A. *Chem. Rev.* **2010**, *110*, 4236.

(36) Hey, E.; Lappert, M. F.; Atwood, J. L.; Bott, S. G. *J. Chem. Soc., Chem. Commun* **1987**, 597.

(37) Scherer, O. J.; Swarowsky, M.; Swarowsky, H.; Wolmershäuser, G. *Angew. Chem. Int. Ed.* **1988**, *27*, 694.

(38) Chirik, P. J.; Pool, J. A.; Lobkovsky, E. *Angew. Chem. Int. Ed.* **2002**, *41*, 3463.

(39) Seidel, W. W.; Summerscales, O. T.; Patrick, B. O.; Fryzuk, M. D. *Angew. Chem. Int. Ed.* **2009**, *48*, 115.

(40) Masuda, J. D.; Jantunen, K. C.; Ozerov, O. V.; Noonan, K. J. T.; Gates, D. P.; Scott, B. L.; Kiplinger, J. L. *J. Am. Chem. Soc.* **2008**, *130*, 2408.

(41) Lv, Y.; Xu, X.; Chen, Y.; Leng, X.; Borzov, M. V. *Angew. Chem. Int. Ed.* **2011**, *50*, 11227.

(42) Cui, P.; Chen, Y.; Xu, X.; Sun, J. *Chem. Commun.* **2008**, 5547.

(43) Konchenko, S. N.; Pushkarevsky, N. A.; Gamer, M. T.; Köppe, R.; Schnöckel, H.; Roesky, P. W. *J. Am. Chem. Soc.* **2009**, *131*, 5740.

(44) Li, T.; Wiecko, J.; Pushkarevsky, N. A.; Gamer, M. T.; Köppe, R.; Konchenko, S. N.; Scheer, M.; Roesky, P. W. *Angew. Chem. Int. Ed.* **2011**, *50*, 9491.

(45) Scherer, O. J.; Werner, B.; Heckmann, G.; Wolmershäuser, G. *Angew. Chem. Int. Ed.* **1991**, *30*, 553.

(46) Stephens, F. H. Ph.D., Massachusetts Institute of Technology, 2004.

(47) Schnöckelborg, E.-M.; Weigand, J. J.; Wolf, R. *Angew. Chem. Int. Ed.* **2011**, *50*, 6657.

(48) Corbridge, D. E. C.; Lowe, E. J. *Nature* **1952**, *170*, 629.

(49) Cossairt, B. M.; Cummins, C. C.; Head, A. R.; Lichtenberger, D. L.; Berger, R. J. F.; Hayes, S. A.; Mitzel, N. W.; Wu, G. *J. Am. Chem. Soc.* **2010**, *132*, 8459.

(50) Barr, M. E.; Adams, B. R.; Weller, R. R.; Dahl, L. F. *J. Am. Chem. Soc.* **1991**, *113*, 3052.

(51) Scheer, M.; Becker, U.; Matern, E. *Chem. Ber.* **1996**, *129*, 721.

(52) Butts, C. P.; Green, M.; Hooper, T. N.; Kilby, R. J.; McGrady, J. E.; Pantazis, D. A.; Russell, C. A. *Chem. Commun.* **2008**, 856.

(53) Baudler, M.; Faber, W. *Chem. Ber.* **1980**, *113*, 3394.

(54) Fritz, G.; Schneider, H. W.; Hoenle, W.; von Schnering, H. G. *Z. Anorg. Allg. Chem.* **1990**, *585*, 51.

(55) Charles, S.; Fettinger, J. C.; Bott, S. G.; Eichhorn, B. W. *J. Am. Chem. Soc.* **1996**, *118*, 4713.

(56) Fritz, G.; Härer, J. *Z. Anorg. Allg. Chem.* **1983**, *500*, 14.

(57) Ahlrichs, R.; Fenske, D.; Fromm, K.; Krautscheid, H.; Krautscheid, U.; Treutler, O. *Chem. Eur. J.* **1996**, *2*, 238.

(58) Carver, C. T.; Monreal, M. J.; Diaconescu, P. L. *Organometallics* **2008**, *27*, 363.

(59) Monreal, M. J.; Diaconescu, P. L. *Organometallics* **2008**, *27*, 1702.

(60) Tsuruta, H.; Imamoto, T.; Yamaguchi, K. *Chem. Commun.* **1999**, *0*, 1703.

(61) Baudler, M.; Glinka, K. *Chem. Rev.* **1993**, *93*, 1623.

(62) Dahlmann, W.; Schnering, H. G. *Naturwissenschaften* **1972**, *59*, 420.

(63) Hönle, W.; Schnering, P. D. H. G. V. *Z. anorg. allg. Chem.* **1978**, *440*, 171.

(64) Baudler, M.; Temberger, H.; Faber, W.; Hahn, J. *Z. Naturjorsch.* **1979**, *34b*, 1690.

(65) Baudler, M.; Pontzen, T.; Hahn, J.; Temberger, H.; Faber, W. *Z. Naturjorsch.* **1980**, *35b*, 517.

(66) Baudler, M.; Hahn, J. *Z. Naturjorsch.* **1990**, *45b*, 1279.

(67) Schröder, G.; Oth, J. F. M.; Merényi, R. *Angew. Chem. Int. Ed.* **1965**, *4*, 752.

(68) Bōhm, M. C.; Gleiter, R. *Z. Naturjorsch.* **1981**, *36b*, 498.

(69) Randic, M.; Oakland, D. O.; Klein, D. J. *J. Comput. Chem.* **1986**, *7*, 35.

(70) Kraus, F.; Aschenbrenner, J. C.; Korber, N. *Angew. Chem. Int. Ed.* **2003**, *42*, 4030.

CHAPTER 5: SYNTHESIS AND CHARACTERIZATION OF RARE-EARTH BIPHENYL COMPLEXES: A 6C, 10π-ELECTRON AROMATIC SYSTEM

Special remarks: The research described in this chapter was achieved by collaboration with two outstanding research groups: (1) Florian Dulong[1] and Dr. Thibault Cantat[1] contributed with the density functional theory (DFT) calculations; (2) Dr. Tianpin Wu[2],[3] and Dr. Jeffrey T. Miller[2] contributed with the X-ray absorption near edge structure (XANES) spectroscopy results. Their contributions are essential to this research.

Affiliations for our collaborators:

[1] CEA, IRAMIS, SIS2M, CNRS UMR 3299 91191 Gif-sur-Yvette, France

[2] Chemical Sciences and Engineering Division, Argonne National Laboratory, Argonne, Illinois 60439

[3] Current affiliation: X-ray Science Division, Advanced Photon Source, Argonne National Laboratory, 9700 South Cass Avenue, Lemont, Illinois 60439

5.1 Introduction

Ever since Michael Faraday isolated benzene in 1825, aromaticity has become one of the most useful chemical concepts.[1] Its scope encompasses not only two-dimensional but also three-dimensional systems, and not only π but also σ orbitals.[2] Oftentimes, however, aromaticity is difficult to define and a host of geometric, energetic, and magnetic criteria has been proposed to evaluate its strength in series of compounds, with disputable success and always stimulating debate. As such, the classic aromaticity of annulene and benzenoid compounds (Chart 5-1) is still

best predicted and determined by the simple yet powerful Hückel's ($4n$+2) π-electron rule.[3] The later discovery of aromaticity in azulene reinforced Hückel's rule since the unfavorable charge separation in the system is compensated by the fulfillment of the ($4n$+2) π-electron requirement.[4,5] Besides the naturally occurring neutral aromatic species, the charged all-carbon systems that meet the ($4n$+2) π-electron rule have long been targeted by synthetic chemists. Cyclopentadienyl has been known to organic chemists by readily deprotonating 1,3-cyclopentadiene.[6] In 1954, Doering and Knox convincingly showed the structure of cycloheptatrienylium (tropylium) ion.[7] In 1960, Katz reported the first direct evidence for the presence of the flat cyclooctatetraene dianion in solution.[8,9] The electronic structure of metallocenes with the general formula of (η^7-C_7H_7)M(η^5-C_5R_5) (M = group 4 metals, R = H or Me) has been experimentally and computationally studied in detail, with strong debates over the charge of the C_7H_7 ligand.[10,11] However, no unambiguous evidence for $(C_7H_7)^{3-}$ has been presented so far. The last of the series, a benzene tetraanion that is predicted to be a 6C, 10π-electron aromatic system, stands as Mount Everest in synthetic chemistry.

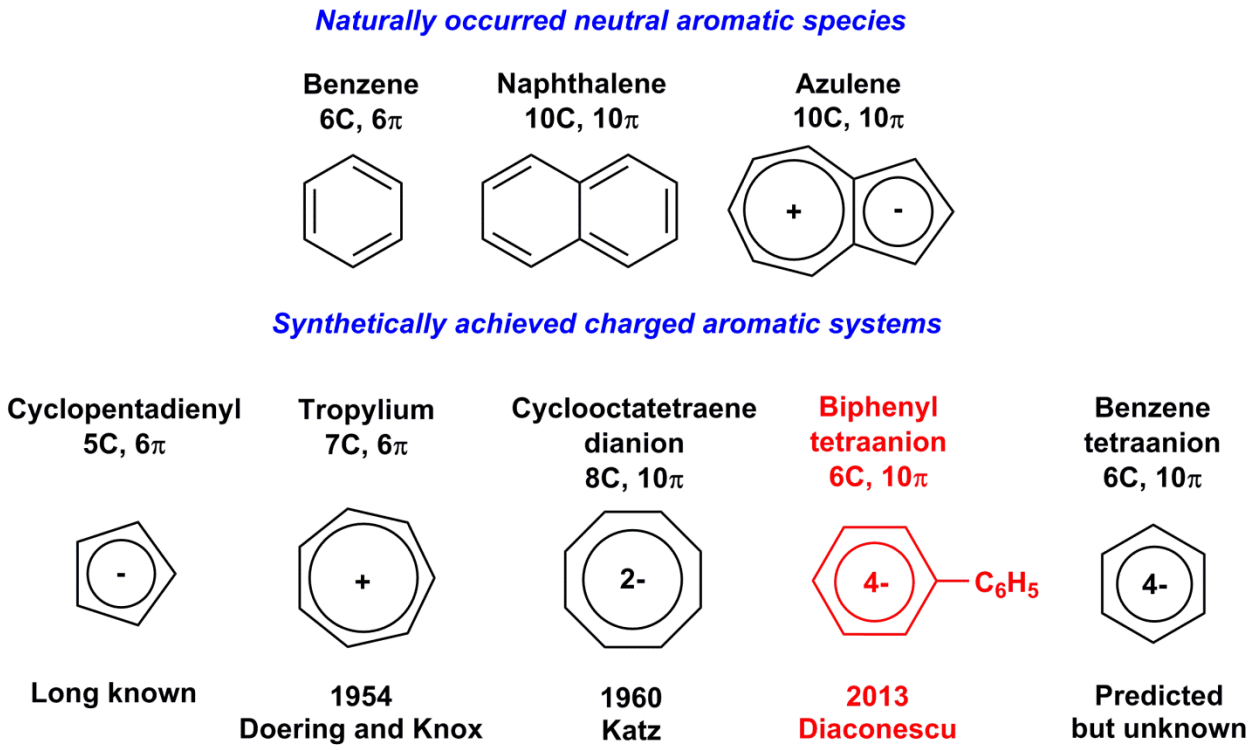

Chart 5-1: Examples of all-carbon aromatic systems: top, naturally occurring neutral aromatic species; bottom, synthetically achieved charge aromatic systems, all are known except for the benzene tetraanion.

The hypothetical $C_6H_6^{4-}$ was shown computationally[12] to have the largest orbital overlap and the strongest bonds compared to its 10π-electron heteroaromatic analogues.[13,14] Despite the successful synthesis of $S_3N_3^-$,[15] P_6^{4-},[16] and Te_6^{2+},[17] however, there are no reports of $C_6H_6^{4-}$ or its derivatives, likely due to its high negative charge. A successful approach to stabilize benzene polyanions relies on the use of lanthanides and actinides to support the highly reduced benzene ring by coordination. Lappert and co-workers reported the isolation of $[(Cp^{tt}{}_2La)_2(\mu\text{-}\eta^6\text{:}\eta^6\text{-}C_6H_6)]$ (Cp^{tt} = η^5-1,3-*t*-$Bu_2C_5H_3$), which was formulated as an ionic aggregate containing two La(II) ions and the benzene radical anion,[18] and $[K(18\text{-crown-6})][(Cp''_2Ln)(\mu\text{-}\eta^6\text{:}\eta^4\text{-}C_6H_6)]$ (Cp'' = η^5-

1,3-$(SiMe_3)_2C_5H_3$; Ln = La, Ce, Nd), containing Ln(III) and a benzene 1,4-dianion.[19] For actinides, several groups reported that benzene or its derivatives can serve as a bridging ligand between two uranium ions.[20-25] Magnetic susceptibility measurements, X-ray absorption near edge structure (XANES) spectroscopy, and density functional theory (DFT) studies showed that most of these complexes can be described as having a benzene (or a substituted benzene) dianion bridging two U(III) centers[21,25]. Liddle and coworkers suggested a $[toluene]^{4-}$ ligand in $[U(Ts^{Xy})]_2(\mu\text{-}\eta^6\text{:}\eta^6\text{-}C_6H_5Me)]$ (Ts^{Xy} = $HC(SiMe_2NAr)_3$; Ar=3,5-$Me_2C_6H_3$);[22,26] the evidence presented there, however, does not allow an irrefutable interpretation of its electronic structure, especially when taking the multiple accessible oxidation states for uranium into account.

We describe for the first time the isolation of tetraanionic, substituted benzenes, which are stabilized by coordination to group 3 metals and an aryl substituent. Overall, the energetic, structural, and magnetic data derived from experiments and theory for complexes incorporating these tetraanionic ligands point to the phenyl ring coordinated to the group 3 metal ions having a 10π-electron aromatic system. The nature of the benzene tetraanion and the aromaticity of the 6C, 10π-electron system are established based on X-ray crystallographic studies, multi-nuclei NMR spectroscopy, X-ray absorption spectroscopy, and density functional theory (DFT) calculations.

5.2 Synthesis and structural characterization of rare-earth biphenyl complexes

We previously reported that 1,1'-ferrocenediyl diamide ligand NN^{TBS} (NN^{TBS} = 1,1′-$fc(NSi^tBuMe_2)_2$)[27] can support rare-earth complexes of fused arenes[28] (see also Chapter 4) and have since focused on expanding this chemistry to non-fused benzenoid derivatives. Biphenyl was chosen because the two phenyl rings are only weakly conjugated[29] and it has a more accessible reduction potential than benzene ($[biphenyl]^{0/-}$ at -2.69 V, $[benzene]^{0/-}$ at -3.42 V, and

[naphthalene]$^{0/-}$ at -2.50 V; these values are referenced to the saturated calomel electrode (SCE) and were calculated from the references).[30,31] Addition of potassium graphite (KC_8) to a pre-mixed tetrahydrofuran (THF) solution of $(NN^{TBS})YI(THF)_2$ and biphenyl at -78 °C led to a dark purple solution upon warming to room temperature (Scheme 5-1). Dark crystals suitable for X-ray crystallography obtained after a standard work up allowed us to determine the molecular structure of the product as $[(NN^{TBS})Y]_2[K(toluene)]_2(\mu$-biphenyl) (**$Y_2K_2$-biph**) (Figure 5-1a). The two yttrium ions coordinate to opposite sides of the same phenyl ring in an η^6 fashion, while the two potassium ions coordinate to the other biphenyl ring in an η^6 fashion as well. Assuming that yttrium is Y(III) and potassium is K(I), the biphenyl ligand carries a 4- charge. XANES spectroscopy studies, commonly used to correlate the electronic structure of metal centers with formal oxidation states,[32] agree with the formulation of yttrium as Y(III) and of iron as Fe(II) in **Y_2K_2-biph**.

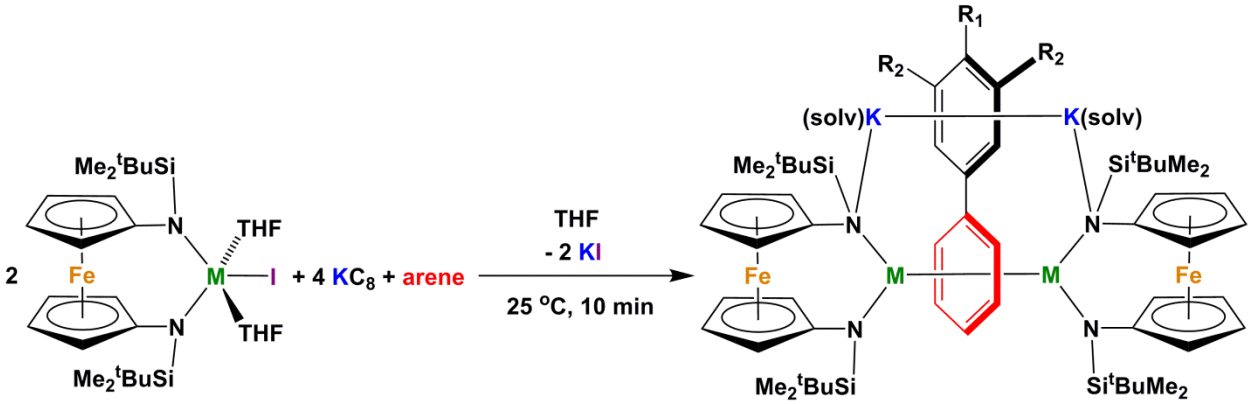

Scheme 5-1: Synthesis of quadruply reduced substituted benzene complexes **M_2K_2-biph** (M = Sc, Y, La, and Lu), **Y_2K_2-terph**, and **Lu_2K_2-TPB**.

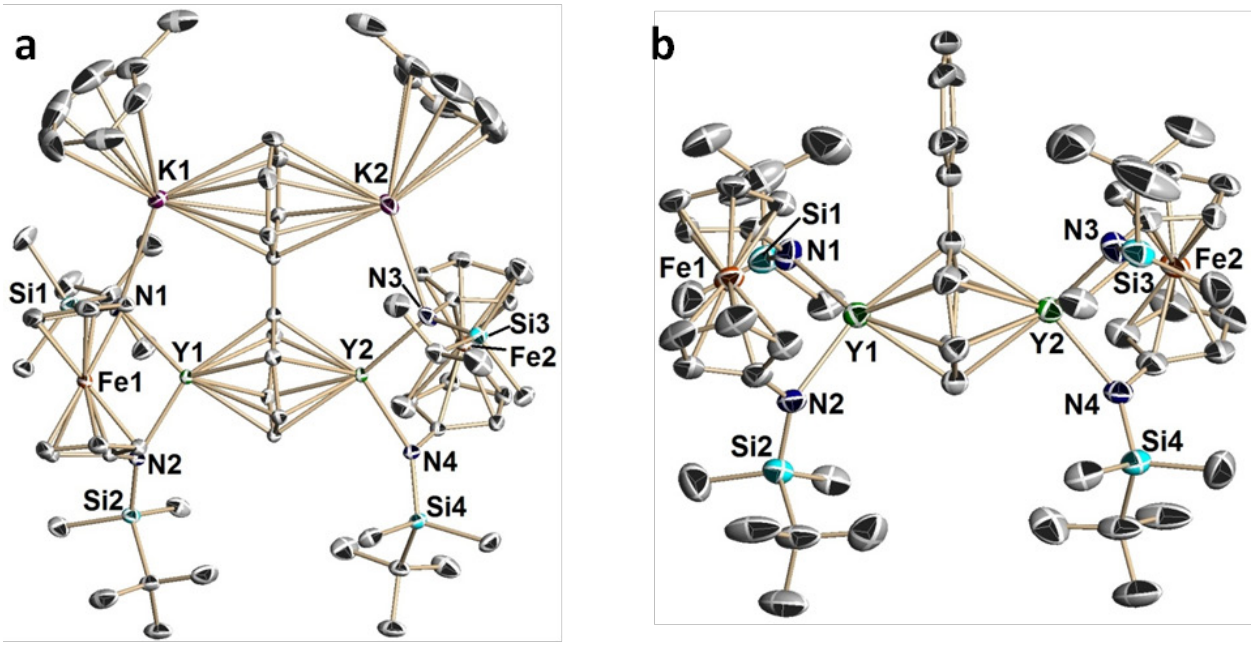

Figure 5-1: Thermal-ellipsoid (50% probability) representation of **Y_2K_2-biph** (a) and the anion of $[K(18\text{-crown-6})(THF)_{1.5}]_2[[(NN^{TBS})Y]_2(\mu\text{-biphenyl})]$ (**Y_2-biph-K_2-crown$_2$**) (b). Hydrogen and solvent atoms and disordered counter cations are omitted for clarity. Details of structural parameters are presented in Figure 5-3 and Table 5-2.

The unusual binding mode of biphenyl in **Y_2K_2-biph** with yttrium and potassium coordinating to different rings is of fundamental importance since it suggests that the two aromatic rings are not equivalent. This coordination mode is maintained in solution. The ^{1}H NMR spectra of **Y_2K_2-biph** at 25 ° C, -45 °C, or -89 °C in THF-d_8 all showed two distinct sets of signals for the phenyl rings. The ^{1}H NMR pattern for the ring coordinated to the yttrium centers is shifted upfield, while that for the other ring appears in the expected aromatic region (complete assignment of ^{1}H, ^{13}C chemical shifts is summarized in Table 5-1). In addition, $^{13}C[^{1}H]$ NMR spectroscopy showed that the signals for the *ortho*- and *meta*-carbon atoms of the ring coordinating to yttrium are triplets due to coupling to ^{89}Y;[33] the *para*- and *ipso*-carbon atoms,

being the farthest from the yttrium ions, are not coupled to them and appear as singlets. These findings are consistent with the fact that only one of the two phenyl rings is coordinated to both yttrium ions in a symmetrical fashion in solution.

It is worth mentioning that previously reported lanthanide arene complexes usually exhibit fluxional behavior in solution even when their solid-state structures indicate that the two metal centers coordinate in an asymmetric fashion, as reported for doubly reduced biphenyl yttrium complexes.[34] In our case, no fluxional behavior was observed in solution. In addition, the isolation of the 18-crown-6 version of **Y_2K_2-biph**, $[K(18\text{-crown-6})(THF)_{1.5}]_2[[(NN^{TBS})Y]_2(\mu\text{-biphenyl})]$ (**Y_2-biph-K_2-crown$_2$**), indicated that the coordination of potassium ions to the biphenyl ligand is not required to maintain the rigid structure. The solid-state molecular structure of **Y_2-biph-K_2-crown$_2$** (Figure 5-1b) showed the presence of separated ion pairs of $[[(NN^{TBS})Y]_2(\mu\text{-biphenyl})]^{2-}$ and two $[K(18\text{-crown-6})(THF)_{1.5}]^{+}$. The chemical shifts of the resonances in the ^{1}H and ^{13}C NMR spectra (THF-d_8, 25 °C and -45 °C) of **Y_2-biph-K_2-crown$_2$** were only slightly different from those of the corresponding resonances documented for **Y_2K_2-biph**, suggesting that **Y_2K_2-biph** is likely a separated ion pair in THF-d_8 solution as well. We also observed that **Y_2K_2-biph** formed exclusively even when sub-stoichiometric amounts of KC_8 were used, suggesting that the quadruply reduced biphenyl in **Y_2K_2-biph** is more stable than a doubly reduced yttrium biphenyl complex.[34] In addition, a comproportionation reaction between $(NN^{TBS})YI(THF)_2$ and **Y_2K_2-biph** did not occur to give a doubly reduced biphenyl complex. Attempts were made to oxidize selectively the quadruply reduced arene to a doubly reduced species but they failed (Scheme 5-2).

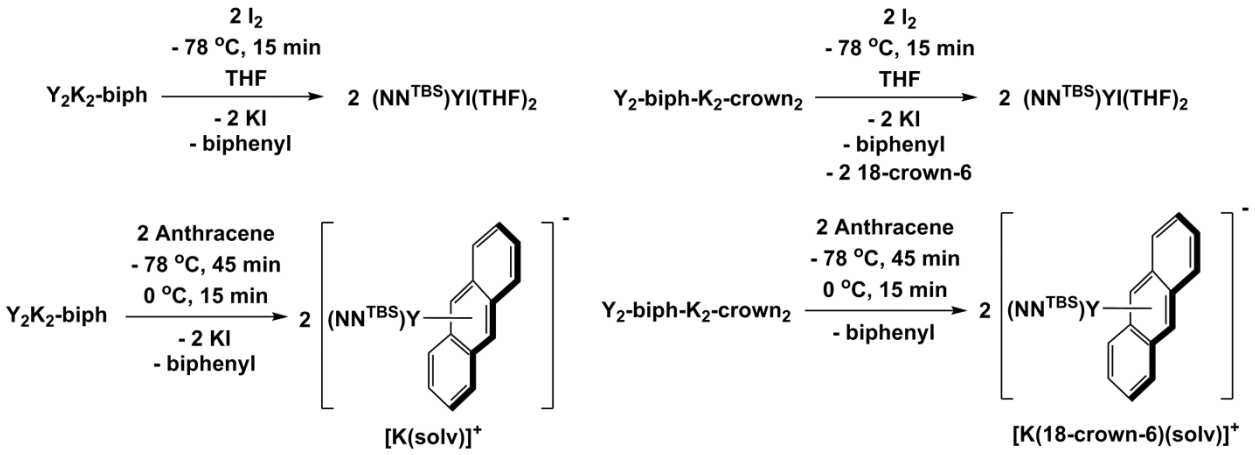

Scheme 5-2: Oxidation attempts involving **Y_2K_2-biph** and **Y_2-biph-K_2-crown$_2$** (sub-stoichiometric amount of oxidants were applied in all cases but only resulted in incomplete reaction with excess **Y_2K_2-biph** or **Y_2-biph-K_2-crown$_2$** left intact).

The synthesis of **Y_2K_2-biph** is not an isolated instance: other group 3 metals, namely, scandium, lanthanum, and lutetium form **Sc_2K_2-biph**, **La_2K_2-biph**, and **Lu_2K_2-biph**, respectively, following a synthetic protocol analogous to that for **Y_2K_2-biph** (Figure 5-1). However, for the smaller rare-earths, especially scandium, the yield of **Sc_2K_2-biph** (ca. 30%) was much lower than **Y_2K_2-biph** (ca. 60%). $[(NN^{TBS})Sc(\mu\text{-}H)]_2$ and $[(NN^{TBS})Sc(C_6H_4Ph)]$ could be identified in the ^{1}H NMR spectrum of the crude product, presumably from the C-H activation of biphenyl following a similar reductive cleavage mechanism as discussed in Chapter 3. Although the formation of **M_2K_2-biph** is fast (completed in less than 10 min at 25 °C), the side reaction of C-H activation of biphenyl is more prominent with the highly Lewis acidic scandium. This phenomenon was observed, to a lesser extent, in the synthesis of **Lu_2K_2-biph**.

The ^{1}H and ^{13}C NMR spectra and solid-state molecular structures of **M_2K_2-biph** (M = Sc, La, and Lu) reflect their similarity to **Y_2K_2-biph** (see Table 5-1 and Table 5-2). The generality of

this reduction reaction also applies to other non-fused arenes. When using *p*-terphenyl instead of biphenyl, $[(NN^{TBS})Y]_2[K(THF)_2]_2[\mu\text{-}(p\text{-terphenyl})]$ (**Y_2K_2-terph**) was obtained (Scheme 5-1). The solid-state molecular structure (Figure 5-2a) and solution ^1H and ^{13}C NMR spectra of **Y_2K_2-terph** (Table 5-1) showed that one of the end rings was bridging the two yttrium centers. 1,3,5-triphenylbenzene was also examined in the reaction with lutetium (Scheme 5-1). Compound $[(NN^{TBS})Lu]_2[K(THF)_2]_2[\mu\text{-}1,3,5\text{-}C_6H_3Ph_3]$ (**Lu_2K_2-TPB**, Ph = C_6H_5) is analogous to **Lu_2K_2-biph**, with one end ring coordinating to the two lutetium fragments (Figure 5-2b).

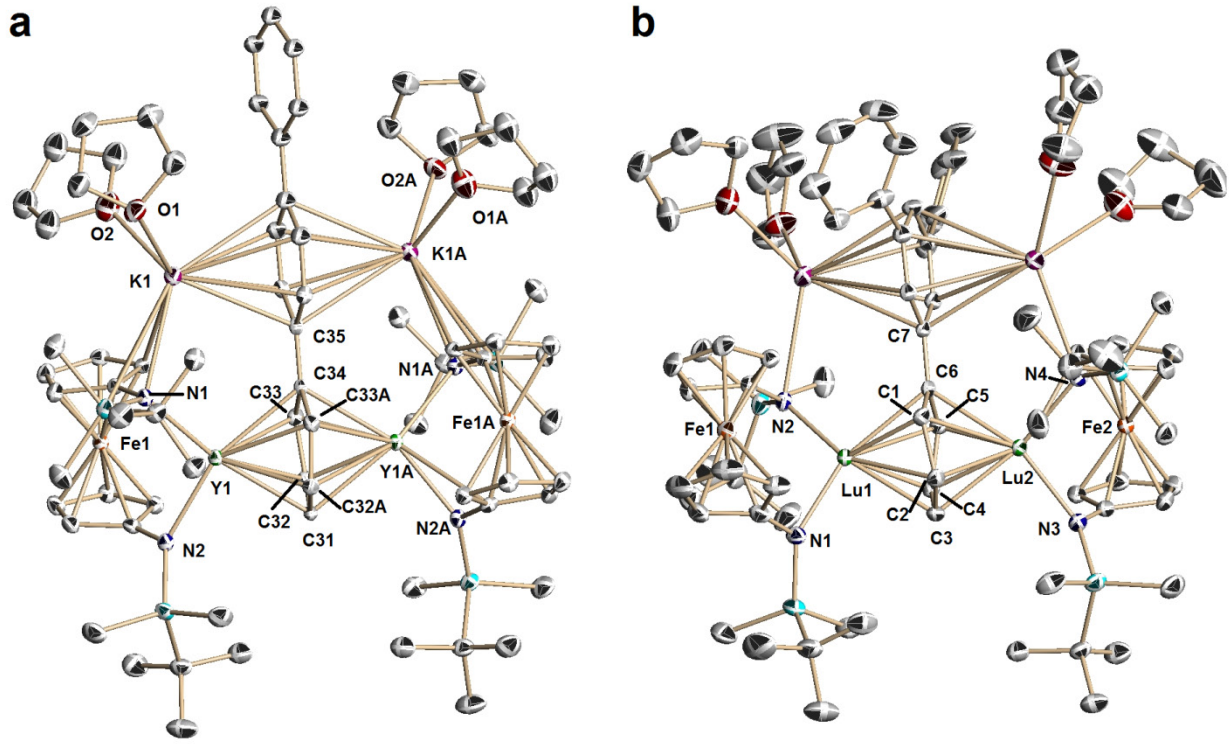

Figure 5-2: Thermal-ellipsoid (50% probability) representation of **Y_2K_2-terph** (a) and **Lu_2K_2-TPB** (b). Hydrogen and solvent atoms are omitted for clarity. Details of structural parameters are presented in Table 5-2.

The confirmed features of the bridging arenes, namely quadruple reduction, rigid coordination mode, and the relative stability over the doubly reduced complexes brought up the fundamental question of whether these species could be considered examples of a 6C, 10π-electron aromatic system according to Hückel's (4*n*+2) π-electron rule. Structurally, an ideal aromatic system exhibits similar bond lengths and planarity of the atoms involved in π conjugation. In $C_6H_6^{4-}$, because the two e_{2u} vacant orbitals (π_4 and π_5, Figure 5-4d) of benzene are filled, there is one net π bonding orbital. Compounds **M_2K_2-biph** (M = Y, Sc, and Lu), **Y_2-biph-K_2-crown$_2$**, **Y_2K_2-terph**, and **Lu_2K_2-TPB** exhibit similar C-C distances of the coordinated phenyl ring (average of 1.46 Å for **Y_2K_2-biph** and 1.47 Å for **Y_2-biph-K_2-crown$_2$** in Figure 5-3, see Table 5-2 for other complexes) that are significantly different and longer than those in neutral biphenyl (1.39 to 1.42 Å for intra-ring and 1.48 Å for inter-ring distances)[35] or the non-coordinated ring (1.41 Å for **Y_2K_2-biph** and 1.38 Å for **Y_2-biph-K_2-crown$_2$**). The average distance of 1.47 Å (**Y_2-biph-K_2-crown$_2$**) is the longest reported average C-C distance within a single benzene ring, and close to the value calculated for the elusive $C_6H_6^{4-}$ (1.507 Å; this value was found to be consistent with the presence of aromatic character; the calculated values for the electron-rich heteroaromatics were found to be higher than experimental values).[12] The fact that the C-C distances within the ring coordinated to yttrium of **Y_2K_2-biph** (1.49, 1.48, and 1.42 Å) or **Y_2-biph-K_2-crown$_2$** (1.50, 1.49, and 1.44 Å) are slightly different and that the values for the C_{ipso}-C_{ipso} distances and the C-C bonds in the non-coordinating ring vary may be explained by the localized molecular orbital model and corresponding drawing of resonance canonical structures[12] or by taking into account small contributions from other resonance structures (see Figure 5-5 and related text). All six C-C-C angles in the coordinated phenyl ring are close to 120°, which is the calculated value for the hypothetical $C_6H_6^{4-}$ with D_{6h} symmetry.[12] It was

noticed that the phenyl ring coordinated to yttrium exhibited a small torsion angle (defined by the atoms C_{24}, C_{25}, C_{25*}, and C_{24*}) of 11.4° (**Y_2K_2-biph**) or 12.4° (**Y_2-biph-K_2-crown$_2$**). This angle was slightly larger in **Sc_2K_2-biph** (20.4°) and **Lu_2K_2-biph** (19.7°). These distortions may be caused by a second-order Jahn-Teller effect that is well documented for reduced arenes.[36]

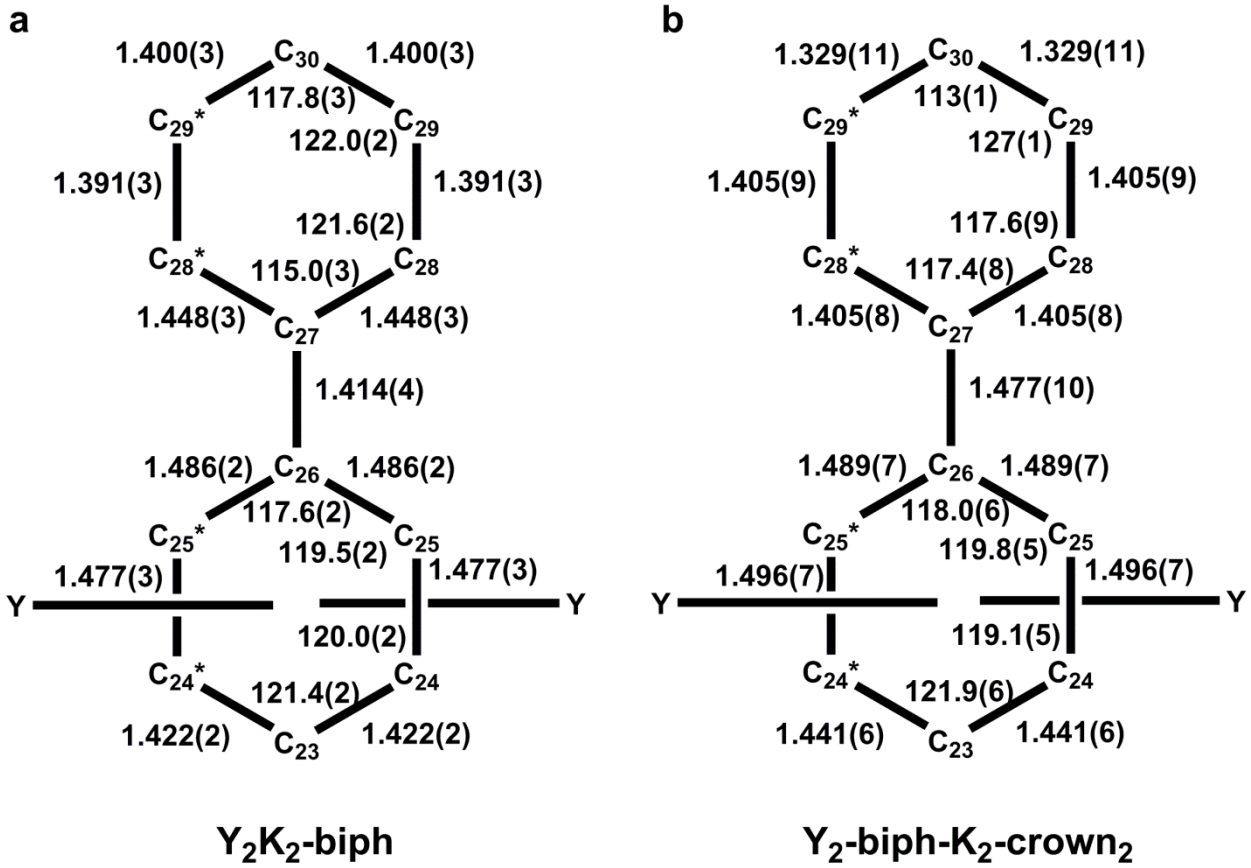

Figure 5-3: Metrical parameters for the biphenyl ligand in **Y_2K_2-biph** (a) and **Y_2-biph-K_2-crown$_2$** (b). Distances are in [Å] and angles in [°], with the errors showed in parentheses. For **Y_2-biph-K_2-crown$_2$**, C_{29} and C_{30} are disordered, therefore, the C_{29}-C_{30} distance and the C_{28}-C_{29}-C_{30} and C_{29}-C_{30}-C_{29}* angles are not reliable.

5.3 Electronic structures of the biphenyl tetraanion: a density functional theory study

Density functional theory (DFT) calculations showed that the optimized structures for the model dianion **2-Y^{2-}** (Si^{t}BuMe$_2$ was replaced by SiMe$_3$; potassium counter cations were omitted) of **Y$_2$K$_2$-biph** or **Y$_2$-biph-K$_2$-crown$_2$** are in excellent agreement with the experimental findings, with average C-C distances of 1.472-1.479 Å for the coordinated phenyl ring. The ground state was found to be a singlet, with no unpaired electrons on the yttrium ions and an iron(II) electronic configuration, in agreement with the oxidation states derived from the XANES measurements. As depicted in Figure 5-4, inspection of the Kohn-Sham frontier molecular orbitals confirms the presence of a benzene unit reduced by four electrons. Indeed, the highest occupied molecular orbital (HOMO) and HOMO-1 clearly result from the population of the two e_{2u} vacant orbitals (π_4 and π_5) of the benzene motif. The computed natural bond orbital (NBO) charges for the coordinated benzene ring (-1.90 to -1.95) and the uncoordinated phenyl group (-0.26 to -0.27) are significantly different. This confirms the experimental observation that negative charges are mainly localized on the coordinated phenyl ring, while the uncoordinated phenyl ring acts only as an electron withdrawing group. Importantly, the putative complex **5-Y^{2-}**, in which each yttrium ion is coordinated to a different benzene ring, could also be investigated computationally for comparison. HOMO and HOMO-1 of **5-Y^{2-}** (Figure 5-4f) establish that only one e_{2u} vacant orbital (π_5) on each ring is occupied, leaving two anti-aromatic 8π-electron ligands. The charge distribution in **5-Y^{2-}** is symmetrical, each ring bearing a charge of -1.05. More interestingly, the anti-aromatic character of **5-Y^{2-}** is attested by the 20.7 kcal/mol energy gap with respect to its more stable aromatic isomer **2-Y^{2-}**, in agreement with the absence of fluxionality established experimentally.

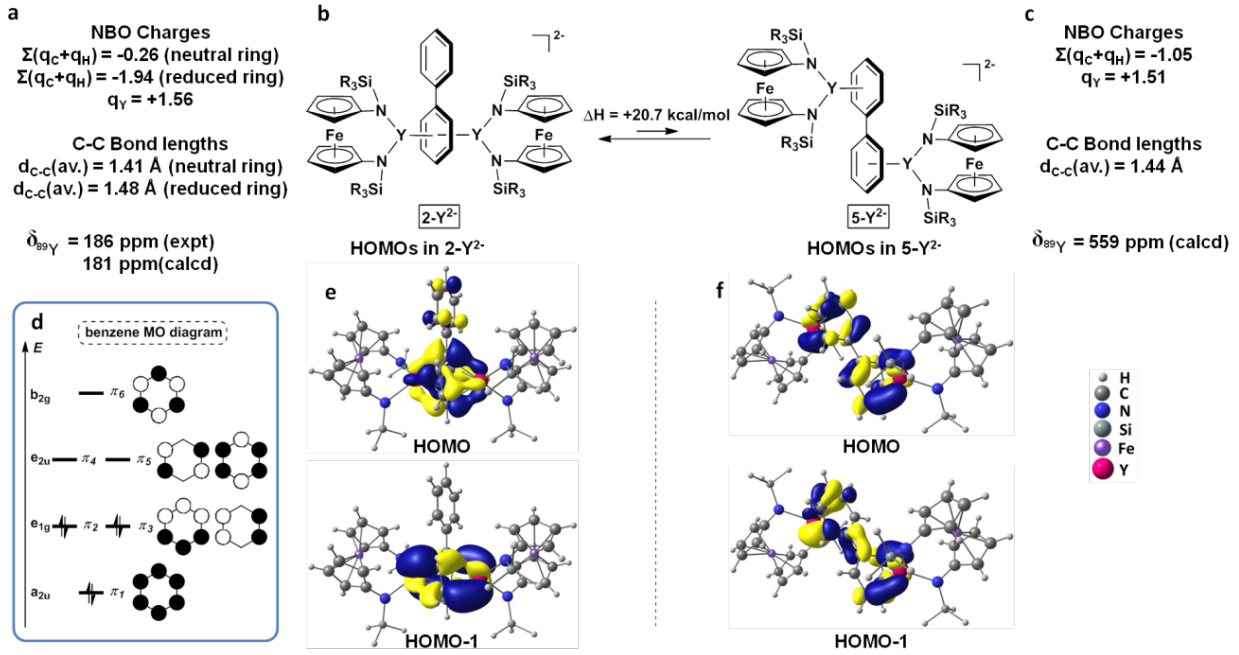

Figure 5-4: DFT calculations on the electronic structure, energetic, and magnetic properties of anions **2-Y^{2-}** (C_2 symmetry) and **5-Y^{2-}** (S_2 symmetry). (a) Calculated NBO charges for the tetraanionic biphenyl ligand and yttrium, C-C distances for the tetraanionic biphenyl ligand, and comparison between the experimental and calculated ^{89}Y chemical shift for **2-Y^{2-}**. (b) Equilibrium between the tetraanionic substituted benzene complex (**2-Y^{2-}**) and a hypothetical tetraanionic biphenyl complex, in which each ring coordinated to yttrium is dianionic (**5-Y^{2-}**). (c) Calculated NBO charges for the tetraanionic biphenyl ligand and yttrium, C-C distances for the tetraanionic biphenyl ligand, and calculated ^{89}Y chemical shift for **5-Y^{2-}**. (d) Frontier molecular orbitals in free benzene. (e) HOMO and HOMO-1 Kohn-Sham orbitals of **2-Y^{2-}**. (f) HOMO and HOMO-1 Kohn-Sham orbitals of **5-Y^{2-}**.

5.4 Experimental evidence for aromaticity of quadruply reduced phenyl ring: an ^{89}Y NMR spectroscopic study

Among experimental methods to determine aromaticity, chemical shifts of NMR active nuclei at specific positions are especially useful.[2,37] Fortunately, among rare-earths, yttrium has a 100% naturally abundant isotope with spin 1/2. Although ^{89}Y suffers from low sensitivity (1/133 of that of ^{13}C) and requires prolonged relaxation times in solution (typically over 300 seconds),[38] we obtained ^{89}Y chemical shifts for a series of compounds (Table 5-3) containing different groups, including halide, alkyl, and the aromatic anion Cp: $(NN^{TBS})YI(THF)_2$ (**Y-I**), $(NN^{TBS})Y(CH_2C_6H_5)(THF)_2$ (**Y-Bn**), and $(NN^{TBS})Y(Cp)(THF)$ (**Y-Cp**) together with **Y_2K_2-biph** and **Y_2K_2-terph**. We found that the value (in ppm) of the ^{89}Y chemical shift decreased in the series: **Y-Bn** (+436), **Y-I** (+370), **Y_2K_2-terph** (+213), **Y_2K_2-biph** (+189), **Y-Cp** (+69). This result confirms significant aromatic ring current effects of the phenyl ring coordinating to yttrium in **Y_2K_2-biph** and **Y_2K_2-terph** since ^{89}Y chemical shifts in **Y_2K_2-biph** and **Y_2K_2-terph** are different from **Y-Bn** and **Y-I**, but closer to **Y-Cp**, which contains the aromatic ligand Cp. The ^{89}Y downfield shifts of **Y_2K_2-biph** and **Y_2K_2-terph** compared to that of **Y-Cp** are expected because the net π bond order in the non-coordinating phenyl ring is 1, while in cyclopentadienyl the net π bond order is 2. Computational studies of NMR parameters have proved successful in the past for organometallic complexes, even for heavy atoms such as ^{89}Y.[39] The calculated ^{89}Y chemical shifts (in ppm) for **Y-Bn** (+451), **Y-I** (+350), **Y_2K_2-terph** (+212), **Y_2K_2-biph** (+181), and **Y-Cp** (+77) are in excellent agreement with the experimental values and allowed us to compute the ^{89}Y chemical shift of the anti-aromatic isomer **[5-Y]$^{2-}$** to be +559 ppm. This change ongoing from **Y_2K_2-biph** to **5-Y** corroborates the structural, electronic, and energetic data discussed above and points to the aromatic character of **Y_2K_2-biph**. The fact that **Y_2K_2-biph** and

Y_2K_2-terph have similar chemical shifts that are greatly different from those of **Y-I** and **Y-Cp** supports the assignment of a 6C, 10π-electron aromatic system for the yttrium-coordinated phenyl ring. Altogether, these results support the description of **Y_2K_2-biph** (and **Y_2K_2-terph**) as coordinated 6C, 10π-electron tetraanionic benzene ligands. The correct match of the trend of ^{89}Y chemical shifts found by us also demonstrates the potential of utilizing ^{89}Y NMR spectroscopy in characterizing aromatic currents in highly reduced π-conjugated systems.

5.5 Discussion on benzene tetraanions and aromaticity

The isolation of tetraanionic, substituted benzenes was possible because of their coordination to rare-earth ions. Based on experimental and computational data, we propose that the phenyl ring coordinated to the group 3 metal ions has a 10π-electron aromatic system. ^{89}Y NMR spectroscopy and DFT calculations of the tetraanionic biphenyl metal complexes were instrumental in understanding the proposed electronic structure. In addition to the group 3 metals, the phenyl substituents of the reduced benzene ring also have a stabilizing influence on the four-electron reduction state of the arene ligands.

Besides the structures described above, we also considered the possibility of two limit Lewis structures that may describe the distribution of the additional four electrons in the reduced arene ligands: a 7C, 10π-electron structure, in which a trianionic benzyl fragment is substituted by a pentadienyl anion, and the 6C, 10π-electron structure, discussed above, in which the four highest energy electrons are located on a single benzene ring and the phenyl substituent remains neutral (Figure 5-5). The two limit structures differ by the amount of electronic density located on the phenyl substituent. Model complexes **6-Y^{2-}** and **7-Y^{-}** illustrate each Lewis structure, respectively; their geometrical and electronic characteristics were investigated computationally

(Figure 5-5). While **6-Y^{2-}** has frontier molecular orbitals, bond lengths, and charge distributions similar to the **2-Y^{2-}** model, the computational data gathered for complex **7-Y^{-}** strongly differ from those of **2-Y^{2-}**. Indeed, the exocyclic C=C bond in **7-Y^{-}** is much shorter than in **2-Y^{2-}** (calculated values of 1.37 vs. 1.45 Å) and HOMO-1 is mostly located on the exocyclic C=C bond, leaving the π_5 orbital of the benzene ring vacant (Supplementary Figure S102). Additionally, the ^{89}Y chemical shift computed for **6-Y^{2-}** (117 ppm) is more shielded than the shift calculated for **7-Y^{-}** (311 ppm) and closer to **2-Y^{2-}** (181 ppm).

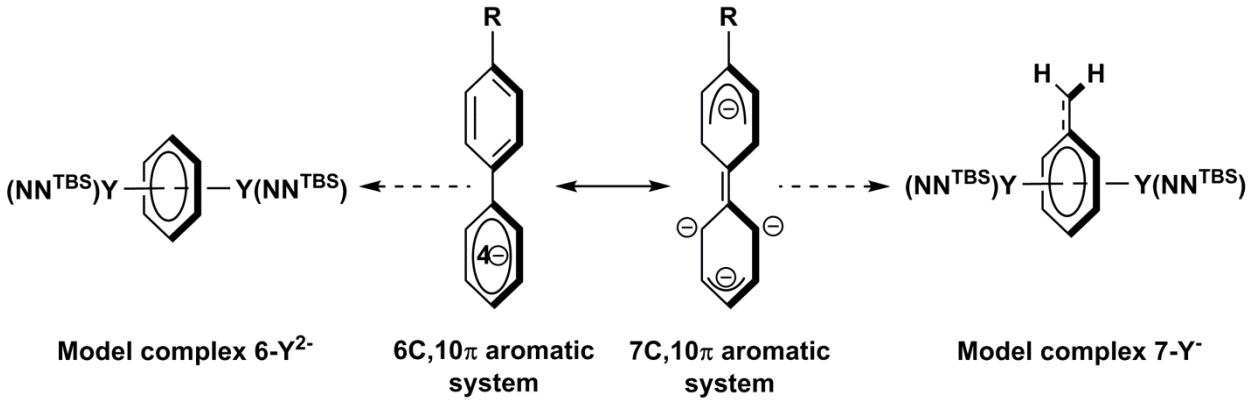

Figure 5-5: Possible Lewis structures for the tetraanionic ligands in **Y_2K_2-biph, Y_2-biph-K_2-crown$_2$**, and **Y_2K_2-terph** and drawing of model complexes **6-Y^{2-}** and **7-Y^{-}**.

An interesting analogy between the present work and two reports by Pierrefixe and Bickelhaupt[40,41] can be made: in those reports, it was shown that the regular structure of aromatics cores with equivalent partial double bonds (6C, 6π- and 10C, 10π-electron systems) stems from the σ skeleton and not from the π-electrons. Naphthalene prefers localized double bonds, a behavior that can be understood from the fact that the π overlap increases as the C-C bond becomes shorter and reaches its maximum at 0 Å. On the other hand, σ-bond overlap

achieves its optimum around 1.5 Å for all C-C bonds. Thus, the σ electrons are responsible for the highly symmetric structure. From this work, it follows that reducing the aromatic 6C, 6π-electron system towards the 6C, 10π-electron system weakens the bond localizing tendency of the π electrons because e^* type orbitals are being filled. Pierrefixe and Bickelhaupt illustrated that effect by going from benzene to planar cyclohexane (6C, 12π). Although the benzene tetraanion described by us is thermodynamically less stable and more reactive (it has to be stabilized through coordination) than benzene, according to the structural considerations described by Pierrefixe and Bickelhaupt, it shows higher aromaticity than benzene.

The benzene tetraanionic fragments reported here expand the series of all-carbon aromatic systems. Although $C_6H_6^{4-}$ in its free form may prove elusive to synthetic chemists, the examples reported here further our understanding of aromaticity and of the ability of metal complexes to stabilize reactive fragments.

5.6 Experimental section

Synthesis of [(NN^{TBS})M]$_2$[K(solvent)]$_2$(μ-biphenyl), M$_2$K$_2$-biph: The procedures for synthesizing arene-bridged complexes are similar and only that for **Y$_2$K$_2$-biph** is described below.

Synthesis of Y$_2$K$_2$-biph: 0.4680 g of **Y-I** (0.583 mmol) and 0.0450 g of biphenyl (0.292 mmol) were weighed in the same vial and dissolved in 8 mL of THF. The solution was placed in a dry ice/acetone bath for 10 min prior to the addition of 0.1890 g KC_8 (1.40 mmol). After the addition, the mixture was taken out from the dry ice/acetone bath and stirred at 25 °C for 10 min. Right after the addition, the solution color changed from bright yellow to dark. The solution was then filtered through Celite adding a small amount of Et_2O to help the transfer. The volatiles

were removed under reduced pressure. The remaining dark solids were dispersed in Et_2O, transferred to a vial, and stored at -35 °C for one day. Black microcrystals were collected on a medium frit. Yield: 0.2420 g, 57.6%. Single crystals suitable for X-ray crystallography were obtained from a THF solution layered with toluene and hexanes with a molecular formula of $[(NN^{TBS})Y]_2[K(toluene)]_2(\mu\text{-biphenyl})$.

^{89}Y NMR spectroscopy details: All ^{89}Y NMR spectra were measured on a Bruker AV600 spectrometer with a 5 mm broadband probe with z-gradient at frequency 29.40 MHz using C_4D_8O as a solvent. Two data collection settings were used: zg30 pulse grogram with d1 = 59 sec and ns = 1024 or more; zg90 pulse grogram with d1 = 300 sec and ns = 160 or more. ^{89}Y chemical shifts were referenced to YCl_3 in D_2O used as an external standard (0 ppm) at 25 °C. **Y-Bn**, **Y-I**, **$Y(CH_2C_6H_5)_3(THF)_3$**, **Y-Cp**, and **$Cp_3Y(THF)$** were measured at 25 °C; **Y_2K_2-biph** and **Y_2K_2-terph** were measured between -40 to -50 °C to avoid decomposition during data collection. A temperature dependence study was carried out for **Y-I** and **Y-Cp**. **Y-I**: 25 °C, +369.6 ppm; -44 °C, +369.9 ppm. **Y-Cp**: 25 °C, +68.8 ppm; -44 °C, +69.6 ppm. The study showed little temperature dependence of ^{89}Y chemical shifts.

5.7 Supplementary tables

Table 5-1: Summary of ^{1}H and ^{13}C NMR chemical shifts assignment for **M_2K_2-biph** (M = Sc, Y, La, and Lu, labelled as **Sc_2**, **Y_2**, **La_2**, and **Lu_2**, respectively, in the table), and **Y_2K_2-terph** (labelled as **$^tY_2$**), **Lu_2K_2-TPB** (labelled as **$^TLu_2$**), and **Y_2-biph-K_2-crown$_2$** (labelled as **Y_2C**) (all measured at -40 to -50 °C). **Note: same labelling system for other Tables.** T1-T6 for *p*-terphenyl and P1-P6 for 1,3,5-triphenylbenzene (the other equivalent ring was omitted for

clarity). The proton was labelled the same as the carbon attached to it (for example, H1 on C1). The values in purple for proton and in red for carbon are on the phenyl ring coordinated to rare-earth ions.

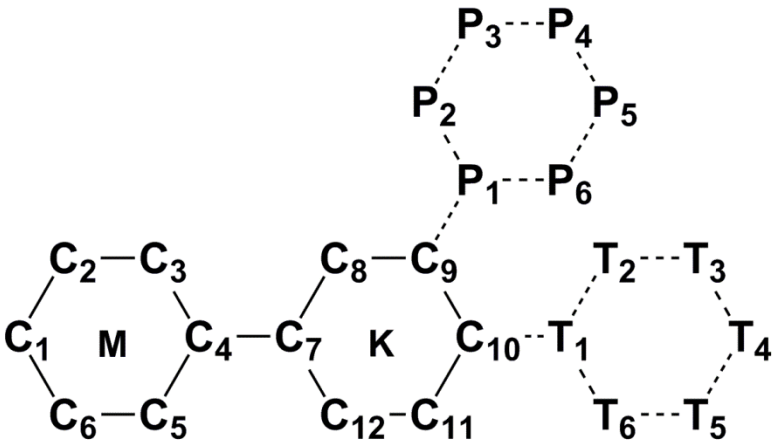

	Y_2	Sc_2	La_2	Lu_2	Y_2C	$^{t}Y_2$	$^{T}Lu_2$
H1	4.02	4.23	4.20	3.76	3.83	4.13	3.77
H2	3.85	4.17	3.89	3.59	3.76	3.82	3.77
H3	2.92	3.69	2.87	2.92	3.03	2.85	3.00
H8	6.06	6.53	5.81	6.03	6.27	5.96	6.24
H9	6.17	6.43	5.91	6.21	6.16	6.52	NA
H10	5.03	5.52	4.73	5.03	5.22	NA	5.60
H(T2, P2)	NA	NA	NA	NA	NA	7.00	7.26
H(T3, P3)	NA	NA	NA	NA	NA	6.86	7.59
H(T4, P4)	NA	NA	NA	NA	NA	6.42	7.15
C1	84.9	88.1	88.1	86.1	78.8	91.9	87.9
C2	68.4	78.1	73.7	72.3	67.4	70.4	73.1
C3	52.1	63.9	61.5	56.9	54.0	52.4	58.4
C4	76.0	79.8	82.0	78.2	74.7	85.3	81.4
C7	138.8	142.3	135.6	137.2	142.4	131.4	136.7
C8	114.3	116.7	113.8	114.2	115.8	115.1	112.2
C9	128.6	128.4	128.5	128.3	127.2	124.0	140.8
C10	103.2	108.5	100.0	102.1	106.5	110.1	94.5

T1(P1)	NA	NA	NA	NA	NA	140.6	144.2
T2(P2)	NA	NA	NA	NA	NA	119.6	126.0
T3(P3)	NA	NA	NA	NA	NA	128.5	128.5
T4(P4)	NA	NA	NA	NA	NA	118.4	126.4

Table 5-2: Structural parameters for **Y_2K_2-biph**, **Sc_2K_2-biph**, **Lu_2K_2-biph**, **Y_2-biph-K_2-crown$_2$**, **Y_2K_2-terph**, and **Lu_2K_2-TPB** derived from X-ray crystallography. Note: *These values contain large errors due to the disorder of C9 and C10 atoms in **Y_2-biph-K_2-crown$_2$**.

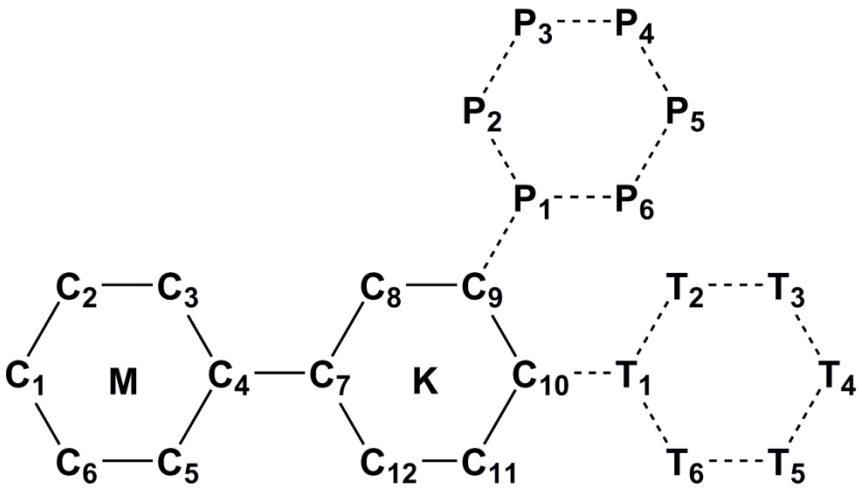

	Y_2	Sc_2	Lu_2	Y_2C	$^tY_2$	$^TLu_2$
C1-C2	1.422	1.436	1.413	1.441	1.420	1.436
C2-C3	1.477	1.474	1.474	1.496	1.476	1.493
C3-C4	1.486	1.481	1.498	1.489	1.484	1.492
C4-C7	1.414	1.418	1.416	1.477	1.411	1.420
C7-C8	1.448	1.444	1.438	1.405	1.444	1.439
C8-C9	1.391	1.390	1.390	1.405	1.372	1.391
C9-C10	1.402	1.405	1.399	1.329*	1.423	1.420
M-C1	2.547	2.367	2.512	2.536	2.569	2.511
M-C2	2.606	2.448	2.599	2.604	2.613	2.599
M-C3	2.487	2.319	2.395	2.453	2.502	2.403
M-C4	2.565	2.516	2.535	2.522	2.568	2.553

K-C(7-12)	3.066 - 3.189	3.064 - 3.344	3.079 - 3.205	NA	3.099 - 3.231	3.156 - 3.279
C10-T1(P1)	NA	NA	NA	NA	1.465	1.493
T1(P1)-T2(P2)	NA	NA	NA	NA	1.412	1.382
T2(P2)-T3(P3)	NA	NA	NA	NA	1.381	1.394
T3(P3)-T4(P4)	NA	NA	NA	NA	1.376	1.379
C8-C7-C12	115	114	115	117	113	115
C3-C4-C7-C8	-5	-8	3	1	4	-5

Table 5-3: ^{89}Y chemical shifts for a series of yttrium compounds (all in THF-d_8, external referenced to YCl_3 in D_2O, ppm). Numbers in red were measured around -45 to -55 °C and those in black measured at 25 °C.

$YBn_3(THF)_3$	**Y-Bn**	**Y-I**	**Y_2K_2-biph**	**Y_2K_2-terph**	**Y-Cp**	**$Cp_3Y(THF)$**
+740	**+436**	**+370 (+370)**	**+189**	**+213**	**+69 (+70)**	**-407**

5.8 References

(1) Faraday, M. *Philos. Trans. R. London* **1825**, *115*, 440.

(2) Chen, Z.; Wannere, C. S.; Corminboeuf, C.; Puchta, R.; Schleyer, P. R. *Chem. Rev.* **2005**, *105*, 3842.

(3) Hückel, E. *Z. Physik* **1931**, *70*, 204.

(4) Heilbronner, E. In *Interscience*; Ginsburg, D., Ed. New York, 1959, p 171.

(5) Lewis, D.; Peters, D. *Facts and Theories of Aromaticity*; Macmillan Press: London, 1975.

(6) Bordwell, F. G. *Acc. Chem. Res.* **1988**, *21*, 456.

(7) Von E.Doering, W.; Knox, L. H. *J. Am. Chem. Soc.* **1954**, *76*, 3203.

(8) Katz, T. J. *J. Am. Chem. Soc.* **1960**, *82*, 3784.

(9) Katz, T. J. *J. Am. Chem. Soc.* **1960**, *82*, 3785.

(10) Zeinstra, J. D.; Nieuwpoort, W. C. *Inorg. Chim. Acta* **1978**, *30*, 103.

(11) Anderson, J. E.; Maher, E. T.; Kool, L. B. *Organometallics* **1991**, *10*, 1248.

(12) Li, J.; Liu, C.-W.; Lu, J.-X. *J. Mol. Struct. (Theochem)* **1993**, *280*, 223.

(13) Chivers, T. *Acc. Chem. Res.* **1984**, *17*, 166.

(14) Banister, A. J. *Nature Physical Science* **1972**, *237*, 92.

(15) Bojes, J.; Chivers, T.; Laidlaw, W. G.; Trsic, M. *J. Am. Chem. Soc.* **1979**, *101*, 4517.

(16) Schmettow, W.; Lipka, A.; von Schnering, H. G. *Angew. Chem. Int. Ed.* **1974**, *13*, 345.

(17) Corbett, J. D.; Prince, D. J.; Garbisch, B. *Inorg. Chem.* **1970**, *9*, 2731.

(18) Cassani, M. C.; Duncalf, D. J.; Lappert, M. F. *J. Am. Chem. Soc.* **1998**, *120*, 12958.

(19) Cassani, M. C.; Gun'ko, Y. K.; Hitchcock, P. B.; Lappert, M. F.; Laschi, F. *Organometallics* **1999**, *18*, 5539.

(20) Diaconescu, P. L.; Arnold, P. L.; Baker, T. A.; Mindiola, D. J.; Cummins, C. C. *J. Am. Chem. Soc.* **2000**, *122*, 6108.

(21) Evans, W. J.; Kozimor, S. A.; Ziller, J. W.; Kaltsoyannis, N. *J. Am. Chem. Soc.* **2004**, *126*, 14533.

(22) Patel, D.; Moro, F.; McMaster, J.; Lewis, W.; Blake, A. J.; Liddle, S. T. *Angew. Chem. Int. Ed.* **2011**, *50*, 10388.

(23) Monreal, M. J.; Khan, S. I.; Kiplinger, J. L.; Diaconescu, P. L. *Chem. Commun.* **2011**, *47*, 9119.

(24) Arnold, P. L.; Mansell, S. M.; Maron, L.; McKay, D. *Nature Chem.* **2012**, *4*, 668.

(25) Diaconescu, P. L.; Cummins, C. C. *Inorg. Chem.* **2012**, *51*, 2902.

(26) Patel, D.; Tuna, F.; McInnes, E. J. L.; McMaster, J.; Lewis, W.; Blake, A. J.; Liddle, S. T. *Dalton Trans.* **2013**, *42*, 5224.

(27) Diaconescu, P. L. *Acc. Chem. Res.* **2010**, *43*, 1352.

(28) Huang, W.; Khan, S. I.; Diaconescu, P. L. *J. Am. Chem. Soc.* **2011**, *133*, 10410.

(29) Kreiter, V. P.; Bonner, W. A.; Eastman, R. H. *J. Am. Chem. Soc.* **1954**, *76*, 5770.

(30) Connelly, N. G.; Geiger, W. E. *Chem. Rev.* **1996**, *96*, 877.

(31) Mortensen, J.; Heinze, J. *Angew. Chem. Int. Ed.* **1984**, *23*, 84.

(32) Stumm von Bordwehr, R. *Ann. Phys. Fr.* **1989**, *14*, 377.

(33) Coles, M. P.; Hitchcock, P. B.; Lappert, M. F.; Protchenko, A. V. *Organometallics* **2012**, *31*, 2682.

(34) Fryzuk, M. D.; Love, J. B.; Rettig, S. J. *J. Am. Chem. Soc.* **1997**, *119*, 9071.

(35) Karle, I. L.; Brockway, L. O. *J. Am. Chem. Soc.* **1944**, *66*, 1974.

(36) Pearson, R. G. *PNAS* **1975**, *72*, 2104.

(37) Sekiguchi, A.; Ebata, K.; Kabuto, C.; Sakurai, H. *J. Am. Chem. Soc.* **1991**, *113*, 7081.

(38) MacKenzie, K. J. D.; Smith, M. E. *Multinuclear solid-state NMR of inorganic materials*; Elsevier Science Ltd: Oxford, 2002.

(39) White, R. E.; Hanusa, T. P. *Organometallics* **2006**, *25*, 5621.

(40) Pierrefixe, S. C. A. H.; Bickelhaupt, F. M. *Chemistry – A European Journal* **2007**, *13*, 6321.

(41) Pierrefixe, S. C. A. H.; Bickelhaupt, F. M. *J. Phys. Chem. A* **2008**, *112*, 12816.

CHAPTER 6: PARAMAGNETIC RARE-EARTH CHEMISTRY: SYNTHESIS OF PARAMAGNETIC RARE-EARTH STARTING MATERIALS AND THE RESULTING BIPHENYL COMPLEXES

6.1 Introduction

The organometallic chemistry of rare-earths not only uncovers rich reactivity but also provides new opportunities for their applications ranging from catalysis to materials.[1] Among organometallic rare-earth complexes, those of scandium, yttrium, lanthanum, and lutetium (group 3 metals) are studied far more in detail due to their diamagnetic nature, which facilitates characterization of their complexes by nuclear magnetic resonance (NMR) spectroscopy. All other rare-earth ions, except for Ce(IV) and Yb(II), have a partially filled 4f shell. Therefore, their complexes are paramagnetic in nature, which complicates the characterization of their complexes by common ^{1}H and ^{13}C NMR spectroscopic techniques, as most are essentially NMR silent due to the huge paramagnetic shifts as well as the line broadening caused by the unpaired 4f electrons.

Although difficult to study, paramagnetic lanthanide chemistry is just as important as group 3 metal chemistry. From a fundamental perspective, since the chemical reactivities of rare-earths depend heavily on the ionic radii of the M(III) ions, it is necessary to fill the knowledge gap between lanthanum and yttrium: the ionic radius of La(III), Y(III), and Lu(III) is 1.03, 0.90, and 0.86 Å, respectively;[2] while the gap between Y(III) and Lu(III) is small at 0.04 Å, the gap between La(III) and Y(III) is large at 0.13 Å. From a general scope, unpaired 4f electrons contribute to the interesting properties and applications of lanthanides. For example, lanthanide luminescence that is indebted to the 4f-4f transition has a constantly increasing number of

applications in industry and medicine.[3,4] The magnetic properties of paramagnetic lanthanides form another area of interest.[5] Neodymium magnets and samarium-cobalt magnets are some of the strongest permanent magnets currently known.[6,7] Lanthanide single-molecule magnets are found to be superior to those of transition metal complexes because of the large single ion anisotropy.[8] However, while a large choice of ancillary ligands has been developed for rare-earth metals recently, few of them have been employed to paramagnetic lanthanide ions.[9,10] The lack of relatively inexpensive and convenient-to-access paramagnetic lanthanide starting materials is probably the main obstacle that restricts the design and synthesis of new such complexes.

Lanthanide trisalkyl complexes are widely used starting materials for organometallic rare-earth chemistry.[11] Methyl, benzyl, and trimethylsilylmethyl are among the most commonly employed alkyl groups. The synthesis of lanthanide trisalkyl complexes is usually achieved by salt metathesis between lanthanide halides and alkali metal alkyl reagents. Although this route has been successfully applied to various compounds, there are still some lanthanide trisalkyl complexes that have not been isolated and/or structurally characterized. This may be attributed to the Schlenk-type equilibrium occurring between the lanthanide trisalkyl complexes and mixed alkyl halide species while in the presence of an alkali metal halide in solution.[12] By introducing N-chelating benzyl ligands, the isolation of trisalkyl complexes was possible for almost all lanthanides despite their ionic size difference.[13-15] In another approach, lanthanide trisalkyl complexes were generated in situ and then protonated by amines or alcohols to form mono- or bisalkyl lanthanide complexes supported by various ancillary ligands.[12,16-18] Recently, by employing lanthanide triiodide (LnI_3) and potassium benzyl ($KCH_2C_6H_5$, KBn), a series of lanthanide trisbenzyl complexes, $Ln(CH_2C_6H_5)_3$, has been successfully synthesized and isolated

for various sizes of lanthanide ions.[19] However, a major drawback of this method is that the starting materials LnI_3 are not readily accessible from lanthanide oxides but instead are obtained from the more expensive lanthanide elements (for instance, the price (on 8/21/2013) listed on us.vwr.com is ca. $1 per gram for La_2O_3 and ca. $10 per gram for the element).[20]

This chapter discusses our efforts in developing a convenient and inexpensive synthetic route for paramagnetic lanthanide trisbenzyls as starting materials for their organometallic chemistry. An *in situ* method to synthesize rare-earth benzyl and iodide complexes supported by a 1,1′-ferrocenediyl diamide ligand (1,1′-fc(NSi^tBuMe_2)$_2$, NN^{TBS}) directly from $MX_3(THF)_y$ (X = Cl or Br) for all rare-earths (except for promethium and europium; ytterbium gave different results than other rare-earths, which will be discussed later in the chapter) is presented. Further contributing to the applicability of these starting materials, all metal halides used were prepared from the less-expensive corresponding oxides. With $(NN^{TBS})MI(THF)_2$ (M = all rare-earths except europium and radioactive promethium) on hand, we synthesized biphenyl tetraanion complexes analogous to those discussed in Chapter 5 and have already got two exciting results: (1) $[(NN^{TBS})Dy]_2[K(OEt_2)]_2$(μ-biphenyl) behaves as a single-molecule magnet; (2) $[(NN^{TBS})Yb]_2[K(OEt_2)]_2$(μ-biphenyl) contains two Yb(II) ions instead of Yb(III) and is structurally different from other rare-earth biphenyl complexes in spite of the same molecular formula.

6.2 Synthesis of rare-earth trisbenzyl complexes from rare-earth oxides

Since 2005, our lab has focused on studying diamagnetic rare-earth metal chemistry.[21-37] We successfully introduced a series of ferrocene-based diamide ligands on scandium, yttrium,

lanthanum and lutetium by using a protonation reaction between the corresponding 1,1′-ferrocene diamine and $M(CH_2Ar)_3(THF)_x$ (for M = Sc and Lu, Ar = 3,5-$C_6H_3(CH_3)_2$ and x = 2; for M = Y and La, Ar = C_6H_5 and x = 3).[21,22] $M(CH_2Ar)_3(THF)_x$ was synthesized from KCH_2Ar and $MX_3(THF)_y$ (for M = Sc, X = Br, y = 2.5; for M = La, X = Br, y = 4; for Ln = Y, X = Cl, y = 3.5; for M = Lu, X = Cl, y = 3),[21,22,38-40] where each metal halide was obtained from the less-expensive corresponding oxide.[21,41,42] In practice, we noticed that the syntheses of $M(CH_2Ar)_3(THF)_x$ from $MX_3(THF)_y$ were not always successful: they suffered from low reproducibility.

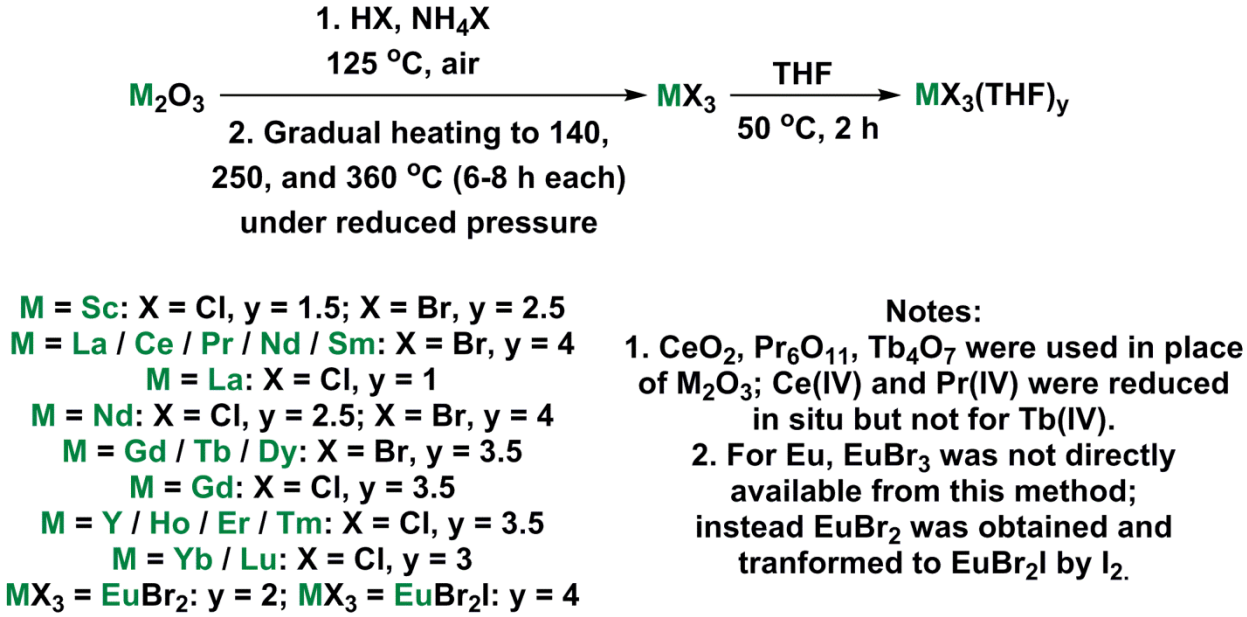

Scheme 6-1: Synthesis of $MX_3(THF)_y$ from rare-earth oxides. This synthetic route required less than four days to complete. Typical scales of the reaction are for 25 or 50 mmol of M_2O_3.[43]

We found that the choice of halide, MCl_3 or MBr_3, and, to a lesser extent, the choice of potassium benzyl, KBn or $K(CH_2C_6H_3Me_2\text{-}3,5)$, is crucial to the success of the rare-earth trisbenzyl synthesis. For example, while $ScBr_3(THF)_{2.5}$ is a good precursor for both $Sc(CH_2C_6H_3Me_2\text{-}3,5)_3(THF)_2$ and $Sc(CH_2C_6H_5)_3(THF)_3$ synthesis, $ScCl_3(THF)_{1.5}$ only works for $Sc(CH_2Ph)_3(THF)_3$ but not for $Sc(CH_2C_6H_3Me_2\text{-}3,5)_3(THF)_2$. These puzzling results were intriguing to us. Therefore, we decided not only to optimize the synthesis of diamagnetic rare-earth trisbenzyls but also to develop a general synthetic route for the synthesis of all rare-earth trisbenzyls.

The first step was to improve our synthesis of rare-earth halides. The synthesis of anhydrous MX_3 from M_2O_3 has been intensely pursued by rare-earth chemists[44] and is now a standard procedure for X = Cl or Br.[42] We followed those procedures to prepare MX_3 (X = Cl or Br) from the readily available rare-earth oxides (for Ce, Pr, and Tb, we used the most common high-valent or mixed-valent oxides CeO_2, Pr_6O_{11}, and Tb_4O_7). As shown in Scheme 6-1, we have successfully prepared MX_3 for all rare-earths. The synthesis is similar with several exceptions: (1) $EuBr_3$ could not be obtained by this method due to its decomposition to $EuBr_2$ and Br_2 at high temperature;[45] instead, the obtained $EuBr_2$ was transformed to $EuBr_2I$ through oxidation by I_2; (2) For CeO_2 and Pr_6O_{11}, the M(IV) species were readily reduced *in situ* by hydrobromic acid; however, for Tb_4O_7 (which may be viewed as $Tb_2O_3 + 2\ TbO_2$), only the Tb(III) species could be transformed into $TbBr_3$, while the Tb(IV) species remained intact and a filtration had to be performed to remove it (although we cannot rule out that prolong heating/refluxing of TbO_2 in concentrated hydrobromic acid may lead to the reduction of TbO_2; we only heated the mixture at 125 °C for ca. 2 h before starting to removing water by constant air flow).

We usually make the THF adduct of MX_3 prior to employing it in the synthesis of the corresponding rare-earth trisbenzyl complex. This enables us to determine the number of THF molecules per rare-earth ion by a simple calculation based on the masses of MX_3 and $MX_3(THF)_y$. The results are listed in Table 6-1. Usually, the calculated number is rounded up to the next half unit. For instance, the value of y for $LaBr_3(THF)_y$ was calculated to be 3.75, so y_0 was assigned to 4.0 and a formula of $LaBr_3(THF)_4$ was used in subsequent synthesis. Besides calculations based on masses, we performed elemental analysis (for C, H, and N) for some of them to verify our assignment on molecular formula of $MX_3(THF)_y$. The results are included in the experimental section of this chapter. Gathering the y_0 values for all MX_3, two trends were observed: (1) For the bromides $MBr_3(THF)_y$, the larger the metal ion size, the larger is the y_0 value ($LaBr_3(THF)_4$, $GdBr_3(THF)_3$, and $ScBr_3(THF)_{2.5}$ represent large, medium, and small rare-earths, respectively). (2) For the chlorides $MCl_3(THF)_y$, the medium rare-earths have the largest y_0 values, such as $GdCl_3(THF)_{3.5}$ and $YCl_3(THF)_{3.5}$, while the small rare-earths have smaller values as indicated by $YbCl_3(THF)_3$ and $LuCl_3(THF)_3$. The most astonishing fact comes from the largest rare-earths, $LaCl_3(THF)_1$ has a y_0 value even smaller than the smallest rare-earth $ScCl_3(THF)_{1.5}$. (3) Combining the trends for the THF adducts of rare-earth bromides and chlorides, it is interesting to note the following facts: (1) for large rare-earths (La and Nd in table 6-1), the bromide has a larger y_0 values than that of chlorides; (2) for medium rare-earths (Gd in table 6-1), the bromide and chloride have similar y_0 values for their THF adducts. These results are counterintuitive: (1) for rare-earths, the larger the cation, the larger is its coordinating number; (2) Br^- is larger than Cl^- so it should be more steric demanding. While all rare-earth bromides are discrete molecules or ion pairs, the rare-earth chlorides are not: for large rare-earths, the

chlorides are polymeric in nature; for medium and small rare-earths, the chlorides are monomeric or ion pairs.[20] The difference between rare-earth bromides and chlorides is likely because of their relative Lewis acidity. Since metal bromides are usually stronger Lewis acid than the corresponding chlorides,[46] all rare-earth bromides are strong enough Lewis acid to form monomeric adducts or ionic pairs with THF; however, only the medium and small rare-earth chlorides are strong enough Lewis acid to form monomeric adducts or ionic pairs with THF. The trends we observed in $MX_3(THF)_y$ synthesis turned out to be crucial to the successful synthesis of rare-earth trisbenzyl complexes.

Table 6-1: Summary of MX_3 and $MX_3(THF)_y$ synthesis

MX_3	Mass of MX_3 (g)	Yield % from oxides	Mass of $MX_3(THF)_y$ (g)	Calculated y	Assigned y_0	Assigned Formula
[1]$ScCl_3$	9.59	63.4	14.58	1.09	1.5	$ScCl_3(THF)_{1.5}$
[1]$ScBr_3$	20.21	70.9	30.31	1.97	2.5	$ScBr_3(THF)_{2.5}$
[1]YCl_3	16.61	85.1	30.89	2.98	3.5	$YCl_3(THF)_{3.5}$
[1]$LaCl_3$	16.64	67.8	20.10	0.71	1.0	$LaCl_3(THF)_1$
[1]$LaBr_3$	26.55	70.1	45.52	3.75	4.0	$LaBr_3(THF)_4$
[2]$CeBr_3$	18.30	96.4	31.41	3.77	4.0	$CeBr_3(THF)_4$
[2]$PrBr_3$	17.69	92.9	30.57	3.85	4.0	$PrBr_3(THF)_4$
[1]$NdCl_3$	19.70	78.6	31.40	2.06	2.5	$NdCl_3(THF)_{2.5}$
[1]$NdBr_3$	27.80	72.4	46.81	3.64	4.0	$NdBr_3(THF)_4$
[2]$SmBr_3$	13.45	69.0	22.50	3.64	4.0	$SmBr_3(THF)_4$
[2]$EuBr_2$	15.25	97.8	31.04	1.64	2.0	$EuBr_2(THF)_2$
*$EuBr_2I$				3.43	4.0	$EuBr_2I(THF)_4$
[3]$GdCl_3$	12.57	89.1	23.02	3.04	3.5	$GdCl_3(THF)_{3.5}$
[1]$GdBr_3$	33.53	84.5	53.23	3.23	3.5	$GdBr_3(THF)_{3.5}$
[2]$TbBr_3$	6.76	33.9	10.36	2.95	3.5	$TbBr_3(THF)_{3.5}$

[2]$DyBr_3$	15.98	79.5	25.22	3.22	3.5	$DyBr_3(THF)_{3.5}$
[2]$HoCl_3$	12.56	92.6	22.74	3.05	3.5	$HoCl_3(THF)_{3.5}$
[1]$ErCl_3$	22.89	83.7	42.44	3.24	3.5	$ErCl_3(THF)_{3.5}$
[2]$TmCl_3$	13.18	95.8	24.51	3.28	3.5	$TmCl_3(THF)_{3.5}$
[1]$YbCl_3$	24.62	88.1	42.82	2.87	3.0	$YbCl_3(THF)_3$
[1]$LuCl_3$	25.45	90.5	42.04	2.54	3.0	$LuCl_3(THF)_3$

Note: [1]Scale of 50 mmol M_2O_3 or 100 mmol based on rare-earths; [2]scale of 25 mmol M_2O_3 or 50 mmol based on rare-earths; [3]scale of 26.7 mmol Gd_2O_3; *synthesized from $EuBr_2$ and 0.5 equiv I_2.

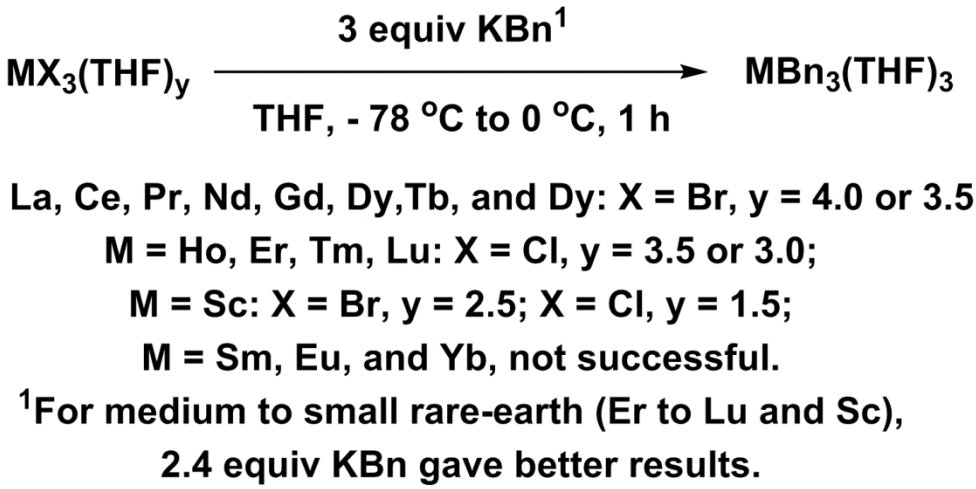

Scheme 6-2: Synthesis of $MBn_3(THF)_3$ (Bn = $CH_2C_6H_5$) from $MX_3(THF)_y$ and KBn. A typical scale is of 2.0 g $MX_3(THF)_y$.

With the rare-earth halides in hand, we pursed the synthesis of the trisbenzyl complexes $MBn_3(THF)_3$. It was found that bromides work better than chlorides in the synthesis of $MBn_3(THF)_3$ for the large to medium rare-earths (La to Gd); for medium to small rare-earths,

both bromides and chlorides served as good starting materials. We attributed the poor reactivity of large to medium rare-earth chlorides to their polymeric nature and insolubility in THF. The use of bromide is particularly important for the synthesis of unstable $MBn_3(THF)_3$. In those cases, chlorides did not yield any isolable products, and the formation of a dark oil indicated the decomposition of rare-earth trisbenzyl complexes.[19] The yields of $MBn_3(THF)_3$ are listed in Table 6-2. It is noteworthy that, for those rare-earths with a stable or semi-stable +2 oxidation state (Eu, Yb, and Sm), the corresponding $MBn_3(THF)_3$ could not be isolated. Upon addition of KBn, the reduction to M(II) occurred, obvious by the indicative color of a divalent species.

Although we were unable to isolate [$YbBn_3$] or [$SmBn_3$] species, the iodides $(NN^{TBS})MI(THF)_2$ (NN^{TBS} = 1,1′-fc(NSi^tBuMe_2)$_2$) were obtained by us for all rare-earths except europium using an *in situ* method that will be discussed below. Another interesting observation was that the use of a sub-stoichiometric amount of KBn gave better overall results for medium to small rare-earths.[21,43] We attributed this to the high tendency of medium to small rare-earths to form $[MBn_4]^-$ species that was also noticed by other researchers.[47]

Since most $MBn_3(THF)_3$ were known and have been characterized by X-ray crystallography and other spectroscopic methods,[19,38,48] the synthesis and characterization of Nd, Gd, Ho, and Er trisbenzyl complexes is discussed in detail as representatives for large, medium, and small rare-earths.[43] Ho and Er trisbenzyl complexes were synthesized from the THF adducts $MCl_3(THF)_{3.5}$ (Scheme 6-2). Holmium trisalkyl complexes were only previously isolated with an N-chelating benzyl ligand,[14] although the corresponding trisphenyl complex is known.[49] The erbium trisneosilyl complex was reported by two groups but without structural characterization,[50,51] while $ErPh_3(THF)_3$ was isolated and structurally characterized.[52] Both Ho

and Er complexes gave pink crystals upon recrystallization. The two compounds were identified as $HoBn_3(THF)_3$ and $ErBn_3(THF)_2$ by X-ray crystallography (Figure 6-1).

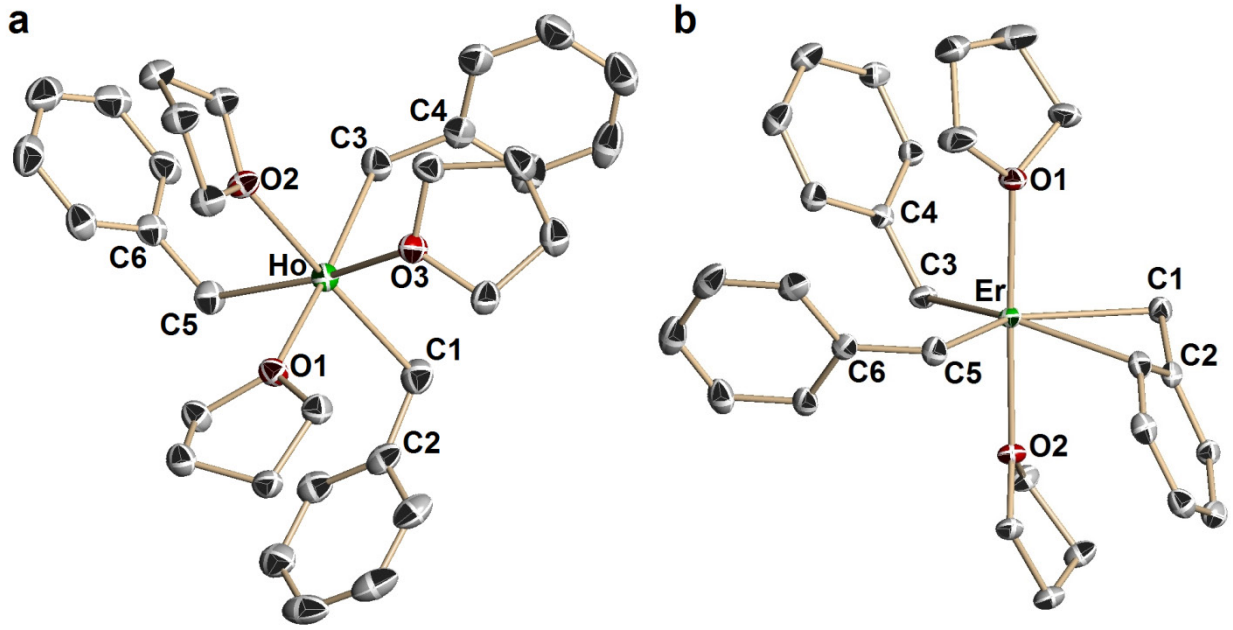

Figure 6-1: Molecular structures of $HoBn_3(THF)_3$ (a) and $ErBn_3(THF)_2$ (b) with thermal ellipsoids drawn at the 50% probability level. Hydrogen atoms were omitted for clarity. Selected distances [Å] and angles [°]: (a) $HoBn_3(THF)_3$: Ho1-C13 2.457(2), Ho1-C20 2.443(3), Ho1-C27 2.453(2), Ho1-O1 2.410(1), Ho1-O2 2.433(2), Ho1-O3 2.401(1), C13-C14 1.470(3), C20-C21 1.465(3), C27-C28 1.470(3), O1-Ho1-O3 78.90(5), O2-Ho1-O3 77.01(5), O1-Ho1-O2 80.33(6), C13-Ho1-C20 92.71(10), C20-Ho1-C27 91.13(9), C27-Ho1-C13 96.26(8), O3-Ho1-C27 166.4(1), O1-Ho1-C20 170.1(1), O2-Ho1-C13 172.1(1). (b) $ErBn_3(THF)_2$: Er1-C1 2.434(2), Er1-C2 2.902(2), Er1-C8 2.416(2), Er1-C15 2.437(2), Er1-O1 2.325(1), Er1-O2 2.311(2), C1-C2 1.461(2), C8-C9 1.468(2), C15-C16 1.472(3), O1-Er1-O2 177.51(4), O1-Er1-C1 87.27(6), O2-

Er1-C1 90.82(6), C1-Er1-C8 121.34(6), C1-Er1-C15 124.48(6), C8-Er1-C15 114.12(6), Er1-C1-C2 92.9(1).

$HoBn_3(THF)_3$ is the first isolated and structurally characterized trisalkyl complex of holmium that does not incorporate the alkyl into a chelating ligand,[14] while $ErBn_3(THF)_2$ is the first structurally characterized erbium trisalkyl complex.[14] $HoBn_3(THF)_3$ is isostructural to $YBn_3(THF)_3$.[14] The holmium atom adopts an octahedral coordination environment with a facial arrangement of the three benzyl groups and three THF ligands, with ∠O−Ho−O ranging from 77.0(1)° to 80.3(1)° and ∠C−Ho−C ranging from 91.1(1)° to 96.3(1)°. The value for ∠Ho−CH_2−C_{ipso} is found from 108.5(1)° to 122.3(1)°, while the long distance of Ho-C_{ipso} between 3.33(1) to 3.45(1) Å indicates that all three benzyl groups coordinate in an η^1 fashion. Single crystals of $ErBn_3(THF)_2$ were obtained from a toluene solution layered with hexanes resulting in the loss of one coordinating THF molecule. A similar phenomenon (loss of one THF) was observed when triturating $MBn_3(THF)_3$ (M = Sc and Lu) in toluene.[11,47] The erbium atom adopts a pseudo-trigonal bipyramidal coordination mode with two THF ligands occupying the two axial positions and the three benzyl groups on the trigonal plane. The angle ∠O−Er−O of 177.5(1)° indicates linearity. The angles ∠C−Er−C ranging from 114.1(1)° to 124.5(1)° indicate a triangular geometry while their sum of 359.9(3)° indicates the co-planarity of the three benzylic carbon atoms and erbium atom. Due to the loss of one THF ligand, one of the benzyl groups coordinates in an η^2 fashion through both the benzylic carbon and the ipso-carbon atom. The small angle ∠Er−CH_2−C_{ipso} of 92.9(1)° compared to the other two ∠Er−CH_2−C_{ipso} of 111.3(1)° and 114.8(1)° and the short Er-C_{ipso} distance of 2.902(2) Å compared to the other two

Er-C_{ipso} distances of 3.274(1) and 3.311(1) Å support the η^2 coordination mode of that benzyl group.[53]

When the same protocol was followed for Nd, only a dark-green oil was obtained and crystals could not be isolated. For Gd, oily blocks could be isolated but elemental analysis indicated that the solid is likely a mixture of halide-benzyl species. Recrystallization attempts did not result in isolable crystals or solid material.

Interestingly, $NdBn_3(THF)_3$ was previously synthesized from $NdBr_3(THF)_{3.5}$ and structurally characterized.[54] In addition, another large-lanthanide trisbenzyl complex, $LaBn_3(THF)_3$, was also obtained from the corresponding bromide,[38] so we attempted the synthesis of neodymium and gadolinium trisalkyl complexes from the metal bromides instead of the chlorides. The preparation of $NdBr_3(THF)_4$ and $GdBr_3(THF)_{3.5}$ was similar to the preparation of other lanthanide halides (Scheme 6-1). Applying the standard protocol and using 3 equiv KBn, $NdBn_3(THF)_3$ and $GdBn_3(THF)_3$ were successfully synthesized in good yield, 66% and 46%, respectively. Single crystals for both compounds were obtained from a THF solution layered with hexanes. A unit cell determination for $NdBn_3(THF)_3$ led to the previously reported metrical parameters.[54] $GdBn_3(THF)_3$ was found to be isostructural to $HoBn_3(THF)_3$ and $ErBn_3(THF)_3$ and the same as the reported values in literature.[19] Both metal trisalkyl complexes were characterized by elemental analysis. $NdBn_3(THF)_3$ was further characterized by ^1H and ^{13}C NMR spectroscopy.

6.3 *In situ* synthesis of $(NN^{TBS})MBn(THF)$ and $(NN^{TBS})MI(THF)_z$ directly from $MX_3(THF)_y$

Since some trisbenzyl complexes are unstable and readily decompose to intractable dark oils,[19,55] and the crystallization of $MBn_3(THF)_3$ usually takes days or even weeks to complete,[43]

we also looked into using the tribenzyl complexes *in situ* for the synthesis of (NN^{TBS})MBn(THF) and (NN^{TBS})MI(THF)$_z$. Previous reports indicate that such compounds may be generated in this fashion and then protonated by a more acidic ligand, such as an amine or an alcohol, to form isolable monoalkyl or bisalkyl complexes.[12,16-18] A similar method was also applied to obtain uranium bisalkyl complexes supported by a 1,1′-ferrocenediyl diamide ligand in our lab.[56] Therefore, we decided to employ the *in situ* method to find out whether (NN^{TBS})MBn(THF) and (NN^{TBS})MI(THF)$_z$ (NN^{TBS} = 1,1'-fc(NSi^{t}BuMe$_2$)$_2$, fc = ferrocenediyl; M = La to Sm, z = 1; M = Gd to Lu and Sc, z = 2) could be generated.

Starting from the THF adducts of metal chlorides and using the *in situ* procedure to generate MBn$_3$(THF)$_3$, 1 equiv (calculated based on the metal, or 0.8 equiv for Er to Lu and Sc that gave better results probably due to the same reason as that for the MBn$_3$(THF)$_3$ synthesis) of H$_2$(NN^{TBS}) was added (Scheme 6-3). Following a regular work-up procedure, (NN^{TBS})MBn(THF) could be isolated in moderate to high yield (47-76%, calculated based on NN^{TBS}). The isolation of (NN^{TBS})MBn(THF), however, was not necessary in order to proceed to the synthesis of (NN^{TBS})MI(THF)$_z$: a toluene solution of 2 equiv Me$_3$SiI (or 1.6 equiv for Er to Lu and Sc) was added to the toluene filtrate of (NN^{TBS})MBn(THF) at 25 °C and the mixture was allowed to stir for 1 h. For large rare-earths (La to Sm), (NN^{TBS})MI(THF) (z = 1) was isolated as a powder after washing the crude products with hexanes in moderate to high yield (see Table 6-2) and the purity was confirmed by ^{1}H NMR spectroscopy, where applicable, and elemental analysis. For medium to small rare-earths (Gd to Lu and Sc), (NN^{TBS})MI(THF)$_2$ were obtained as crystals from a concentrated diethyl ether solution layered with *n*-pentane in moderate to high yield (see Table 6-2). It is important to note that (NN^{TBS})SmBn(THF) and (NN^{TBS})SmI(THF)

could be isolated in moderate yield following the *in situ* method in spite of the incapacity of isolating $SmBn_3(THF)_3$. Moreover, $(NN^{TBS})YbI(THF)_2$ could also be synthesized by the *in situ* method albeit in low yield (ca. 20%). However, $(NN^{TBS})YbBn(THF)$ could not be generated. We attributed the low yield and inability to generate $(NN^{TBS})YbBn(THF)$ to the reduction of Yb(III) to Yb(II) upon addition of KBn. The incapacity to synthesize $YbBn_3(THF)_3$ was also noted by a separate report.[19]

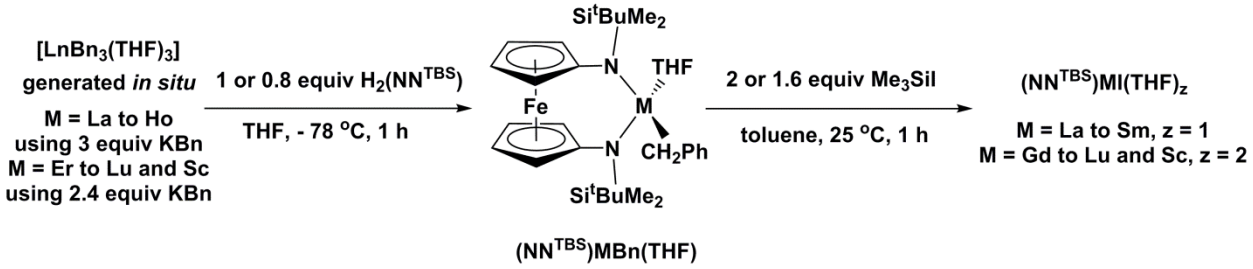

Scheme 6-3: *In situ* synthesis of $(NN^{TBS})MBn(THF)$ and $(NN^{TBS})MI(THF)_z$ from *in situ* generated $[MBn_3(THF)_3]$ (M = La to Sm and Gd to Lu and Sc, with the exception of Yb, see text for details).

The *in situ* synthetic protocol was straightforward and expedient. The synthesis of the final product $(NN^{TBS})MI(THF)_z$ could be achieved in one day. This is a major improvement over the stepwise synthesis used by us previously since the crystallization of $MBn_3(THF)_3$ usually takes several days. More importantly, the yield of $(NN^{TBS})MI(THF)_z$ is high (see Table 6-2). The purity of the compounds obtained by the *in situ* method was confirmed by elemental analysis and ^1H NMR spectroscopy where available.

Our group had been employing 2.4 equivalents of KBn in the synthesis of lanthanide trisbenzyl complexes in order to avoid the formation of ate complexes such as $[K(THF)_6][MBn_4]$.[21] However, the present study provided a better understanding of the synthesis of $MX_3(THF)_y$, and, as a consequence, we realized that it was not always necessary to use sub-stoichiometric amounts of KBn to avoid the formation of undesired byproducts. For the small rare-earths (from Er to Lu and Sc), it was necessary, indeed, to use a sub-stoichiometric amount of KBn to achieve clean formation of $(NN^{TBS})MBn(THF)$ or $(NN^{TBS})MI(THF)_2$, otherwise the products were contaminated by ate complexes $[K(THF)_6][(NN^{TBS})_2M]$ derived from $[K(THF)_6][MBn_4]$. For the large rare-earths (La to Ho), although $[K(THF)_6][MBn_4]$ was isolated using 3 equiv KBn in the $MBn_3(THF)_3$ synthesis, using a sub-stoichiometric amount of KBn was less problematic since ate complexes only formed in a small amount; on the other hand, when using 2.4 equiv KBn, a large quantity of the side-product $[(NN^{TBS})M(THF)(\mu\text{-}Cl)]_2$ was isolated in the synthesis of $(NN^{TBS})MBn(THF)$. Therefore, a different stoichiometry of KBn was employed for large or small rare-earths to achieve the best results in each case. For medium size rare-earths like Ho, similar results were obtained by either stoichiometry of KBn as shown in the experimental section. The advantages of the *in situ* method are more than just convenience. This method is generally more forgiving: (1) although we were unable to isolate $SmBn_3(THF)_3$ and $YbBn_3(THF)_3$, the corresponding $(NN^{TBS})SmBn(THF)$, $(NN^{TBS})SmI(THF)$, and $(NN^{TSB})YbI(THF)_2$ were synthesized in a moderated yield that allowed us to explore the redox non-innocent Sm and Yb chemistry (discussed below); (2) large rare-earth chlorides could not be used to prepare pure trisalkyl complexes,[43] however, they worked just as well as bromides in the *in situ* synthesis of $(NN^{TBS})MBn(THF)$ and $(NN^{TBS})MI(THF)_z$. Since the synthesis of chlorides

and bromides requires a large excess of NH_4Cl/HCl or NH_4Br/HBr, and NH_4Cl/HCl is less expensive than NH_4Br/HBr, the possibility to use rare-earth chlorides is economically attractive. We anticipate that the *in situ* method should work for various ancillary ligands with acidic protons such as alcohols, amines, or terminal alkynes.

Table 6-2: Yields for the synthesis of $MBn_3(THF)_3$ and for the *in situ* synthesis of $(NN^{TBS})MBn(THF)$ or $(NN^{TBS})MI(THF)_z$.

Yield (%)|Rare-earth	La	Ce	Pr	Nd	Sm	Eu	Gd	Tb	Dy	Ho	Er	Tm	Yb	Lu	Y	Sc
MBn_3	56	77	66	66			46		26	76	60	40		76	79	59
$(NN^{TBS})MBn(THF)$				69	54		62			40	50					
$(NN^{TBS})MI(THF)_z$	89	68	65	66	55		63	66	68	70	66	52	15	56	42	44

Note: For M = Er to Sc (except Y), 2.4 equiv KBn was used in the synthesis. The yields were calculated based on the stoichiometry of the limiting reagent.

All the $(NN^{TBS})MBn(THF)$ (where applicable) and $(NN^{TBS})MI(THF)_z$ complexes were characterized by X-ray crystallography. Since most of them were structurally similar, $(NN^{TBS})HoBn(THF)$ is shown and discussed to represent $(NN^{TBS})MBn(THF)$; $(NN^{TBS})ErI(THF)_2$ and $[(NN^{TBS})Nd(THF)(\mu\text{-}I)]_2$ represent medium to small rare-earths and large rare-earths, respectively.

$(NN^{TBS})HoBn(THF)$: The benzyl group in $(NN^{TBS})HoBn(THF)$ (Figure 6-2) is coordinated in an η^2 fashion as evidenced by the short M-C2 distance of 2.695(4) Å and the small M-C1-C2 angle of 82.6(2)°. The Ho-C1 distance of 2.456(4) Å is similar to the average Ho-C distance of 2.45(1) Å in $HoBn_3(THF)_3$. The Fe-Ho distance of 3.234(1) Å is close to the

Fe-Y distance of 3.240(1)Å in the isostructural (NN^{TBS})YBn(THF)[22] and to the sum of covalent radii for iron (low spin) and holmium (3.24 Å).[57]

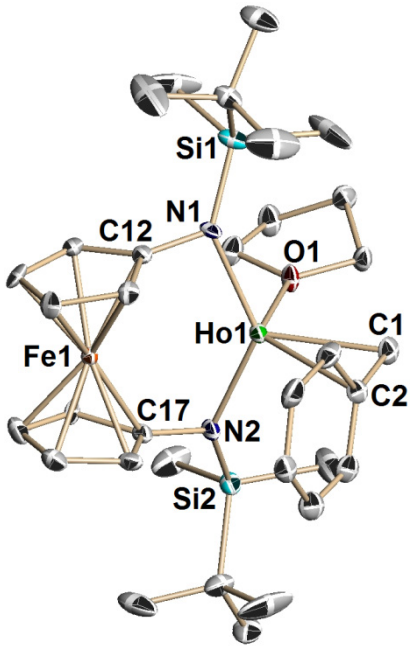

Figure 6-2: Molecular structure of (NN^{TBS})HoBn(THF) with thermal ellipsoids drawn at the 50% probability level. Hydrogen atoms were omitted for clarity. Selected distances [Å] and angles [°]: Ho1-C1 2.456(4), Ho1-C2 2.695(4), Ho1-O1 2.318(3), Ho1-N1 2.218(4), Ho1-N2 2.223(4), Ho1-Fe1 3.234(1), Ho1-C12 2.838(4), Ho1-C17 2.828(4), C1-C2 1.469(6), N1-Ho1-N2 133.4(1), O1-Ho1-C1 90.6(1), Ho1-C1-C2 82.6(2), Ho1-N1-C12 100.9(2), Ho1-N2-C17 99.7(2).

(NN^{TBS})ErI(THF)$_2$ and [(NN^{TBS})Nd(THF)(μ-I)]$_2$: (NN^{TBS})ErI(THF)$_2$ (Figure 6-3a) is isostructural to (NN^{fc})YI(THF)$_2$,[36] while [(NN^{fc})Nd(THF)(μ-I)]$_2$ (Figure 6-3b) adopted a bridging bimetallic structural motif. For a reason not obvious to us, the mononuclear molecular structures show a significant thermal disorder for the iodide ligand as well as the methyl and *tert*-

butyl groups on one silicon substituent. The major diatomic distances of $(NN^{TBS})ErI(THF)_2$ are similar to those of $(NN^{TBS})YI(THF)_2$.[36] The bimetallic structural motif of $[(NN^{fc})Nd(THF)(\mu\text{-}I)]_2$ may be relevant to the weaker Lewis acidity of large rare-earths and their tendency to form polymeric species.[58]

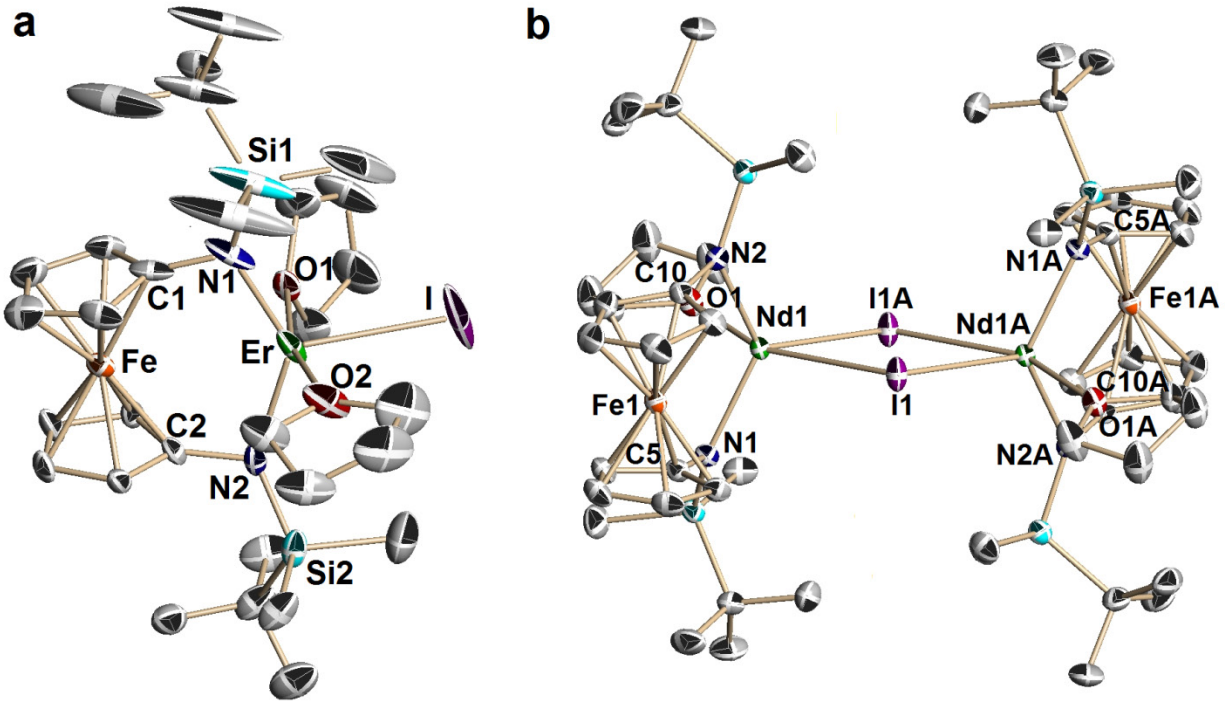

Figure 6-3: Molecular structures of $(NN^{TBS})ErI(THF)_2$ (a) and $[(NN^{TBS})Nd(THF)(\mu\text{-}I)]_2$ with thermal ellipsoids drawn at the 50% probability level. Hydrogen atoms and disordered counterparts were omitted for clarity. Selected distances [Å] and angles [°]: (a) $(NN^{TBS})ErI(THF)_2$: Er1-I1 2.998(1), Er1-N1 2.206(5), Er1-N2 2.200(4), Er1-O1 2.331(3), Er1-O2 2.359(3), Er1-Fe1 3.357(1), Er1-C1 2.897(5), Er1-C6 2.869(4), N1-Er1-N2 132.5(1), O1-Er1-O2 166.7(1). (b) $[(NN^{TBS})Nd(THF)(\mu\text{-}I)]_2$: Nd1-I1 3.213(1), Nd1-I1A 3.235(1), Nd1-N1

2.265(3), Nd1-N2 2.259(3), Nd1-O1 2.469(3), Nd1-Fe1 3.364(2), Nd1-C5 2.917(4), Nd1-C10 2.939(4), N1-Er1-N2 126.1(1), I1-Nd1-I1A 78.24(1), Nd1-I1-Nd1A 101.76(1).

6.4 Biphenyl complexes of paramagnetic rare-earths

With the iodide complexes $(NN^{TBS})MI(THF)_2$ (M = Ce to Sm except Pm, and Gd to Yb) in hand, we pursued the synthesis of biphenyl complexes with the general molecular formula $[(NN^{TBS})M][K(solvent)]_2(\mu\text{-biphenyl})$ (their diamagnetic counterparts are discussed in Chapter 5). Following a similar procedure to $[(NN^{TBS})Y][K(solvent)]_2(\mu\text{-biphenyl})$, all $[(NN^{TBS})M][K(solvent)]_2(\mu\text{-biphenyl})$ (**M_2K_2-biph**) were synthesized in moderate to high yield. Their physical appearance is similar and they are isolated as black powders or small crystals. They are all structurally similar (except for **Yb_2K_2-biph**, which will be discussed later in the text) as determined by X-ray crystallography. As anticipated, they have fascinating physical properties derived from the partially filled 4f shell. Following are two projects currently under investigation: (1) **M_2K_2-biph** as single molecule magnets; (2) the comparison between **Yb_2K_2-biph** and **Sm_2K_2-biph**: evidence for Yb(II) and a biphenyl dianion.

6.4.1 Magnetic study on Dy_2K_2-biph: single-molecule magnet behavior

This project is in collaboration with Jennifer Le Roy (PhD student in Murugesu group) and Professor Muralee Murugesu at the University of Ottawa, Canada. Based on the magnetic data for **Dy_2K_2-biph**, it is apparent that this molecule behaves as a single-molecule magnet with U_{eff} = 53 K, and $t_0 = 1.5*10^{-7}$ s (Figure 6-4). Molecular structures of **Dy_2K_2-biph** and $[K(18\text{-crown-6})(THF)_{1.5}]_2([(NN^{TBS})Dy]_2(\mu\text{-biphenyl}))$ are shown in Figure 6-5.

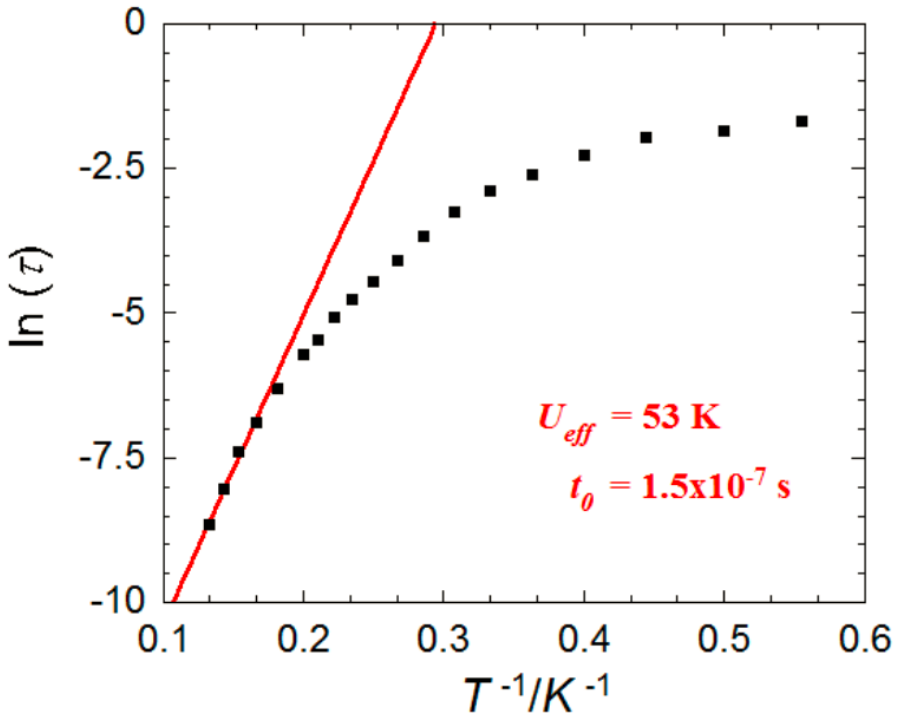

Figure 6-4: Relaxation time of the magnetization ln(τ) *vs.* T^{-1} (Arrhenius plot using AC data) for **Dy_2K_2-biph**. The red solid line corresponds to the fit.

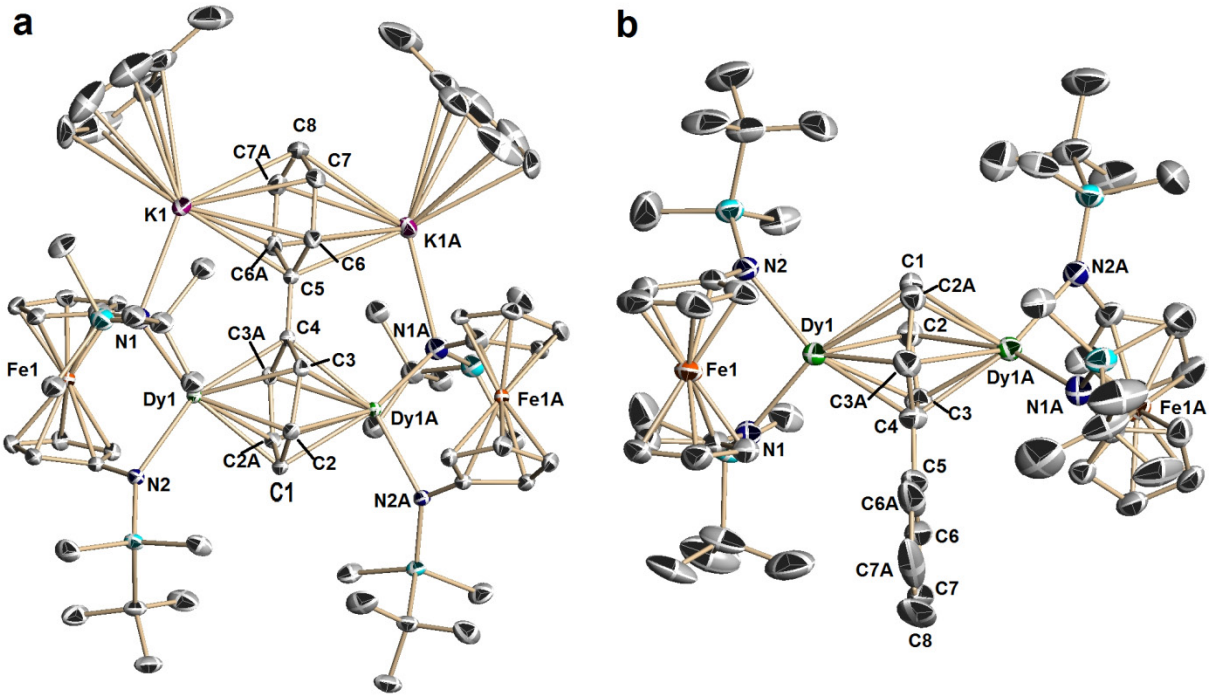

Figure 6-5: Molecular structures of **Dy_2K_2-biph** (a) and [K(18-crown-6)$(THF)_{1.5}]_2$([$(NN^{TBS})Dy]_2$(μ-biphenyl)) (b) with thermal ellipsoids drawn at the 50% probability level. Hydrogen atoms and disordered counterparts are omitted for clarity.

6.4.2 Comparison between Yb_2K_2-biph and Sm_2K_2-biph: evidence for Yb(II) and biphenyl dianion in Yb_2K_2-biph

This project is in collaboration with James R. Gallagher, Guanghui Zhang, Bo Hu (students in Dr. Jeffrey T. Miller's group) and Dr. Jeffrey T. Miller at Argonne National Laboratory, who performed X-ray absorption near edge structure (XANES) spectroscopy on a series of ytterbium and samarium complexes in order to determine the oxidation state of Yb and Sm in **Yb_2K_2-biph** and **Sm_2K_2-biph**, respectively.

Table 6-3: Summary of Yb L3 edge energy

Sample	Edge energy (eV)	Oxidation state
Yb_2O_3	8943.8	III
$(\eta^5\text{-}C_5H_5)_3Yb$	8944.8	III
YbI_2	8936.7	II
$(NN^{TBS})YbBn(THF)$	8943.9	III
$(NN^{TBS})Yb(\eta^5\text{-}C_5H_5)(THF)$	8944.5	III
$(NN^{TBS})YbI(THF)_2$	8944.5	III
$[K(THF)_6][(NN^{TBS})_2Yb]$	8944.2	III
Yb_2K_2-biph	8937.1	II

Table 6-4: Summary of Sm L3 edge energy

Sample	Edge Energy (eV)	Oxidation State
Sm_2O_3	6719.7	III
$SmBr_3(THF)_4$	6720.2	III
$(\eta^5\text{-}C_5H_5)_3Sm$	6720.5	III
SmI_3	6720.1	III
SmI_2	6712.7	II
$(NN^{TBS})SmBn(THF)$	6720.0	III
$(NN^{TBS})Sm(\eta^5\text{-}C_5H_5)(THF)$	6719.8	III
$(NN^{TBS})SmI(THF)$	6720.1	III
Sm_2K_2-biph	6720.0	III

For both Yb and Sm, there was a large shift in the edge energy (ca. 8 eV) depending on the oxidation state of the metal (Table 6-3 and Table 6-4). This allowed an unambiguous assignment of the oxidation states of Yb and Sm in **Yb_2K_2-biph** and **Sm_2K_2-biph** as Yb(II) and Sm(III), respectively. This assignment is consistent with the data derived from X-ray crystallography (Figure 6-6). While **Sm_2K_2-biph** was structurally similar to the previously

characterized **M_2K_2-biph**, the structural parameters of **Yb_2K_2-biph** differed significantly: (1) the coordination mode of biphenyl changed: in **Yb_2K_2-biph**, the ytterbium ions coordinate to different phenyl rings, while in all other **M_2K_2-biph**, the metal ions always coordinate to the same phenyl ring; (2) the C-C distances within the biphenyl fragment are different from those of other **M_2K_2-biph** but are close to the C-C distances in the yttrium coordinated biphenyl dianion $[(P_2N_2)Y]_2(\mu_2\text{-}\eta^6\text{:}\eta^{6'}\text{-}(C_6H_5)_2)$ (P_2N_2 = $(PhP[CH_2(SiMe_2)N(SiMe_2)CH_2]_2PPh)$;[59] (3) the shortest Yb-N distance of 2.31 Å is 0.12 Å longer than the Yb-N distances in $(NN^{TBS})YbI(THF)_2$ (average 2.19 Å); the 0.12 Å difference is close to the 0.15 Å difference between the ionic radius of Yb(II) and Yb(III).[2] In addition to the data derived from XANES and X-ray crystallography, the ^{1}H NMR spectrum of **Yb_2K_2-biph** showed that all peaks were in the diamagnetic region (δ between 0 to 10 ppm), which is typical for Yb(II)-containing complexes. We are currently investigating the electronic structures of both compounds and their chemical reactivity.

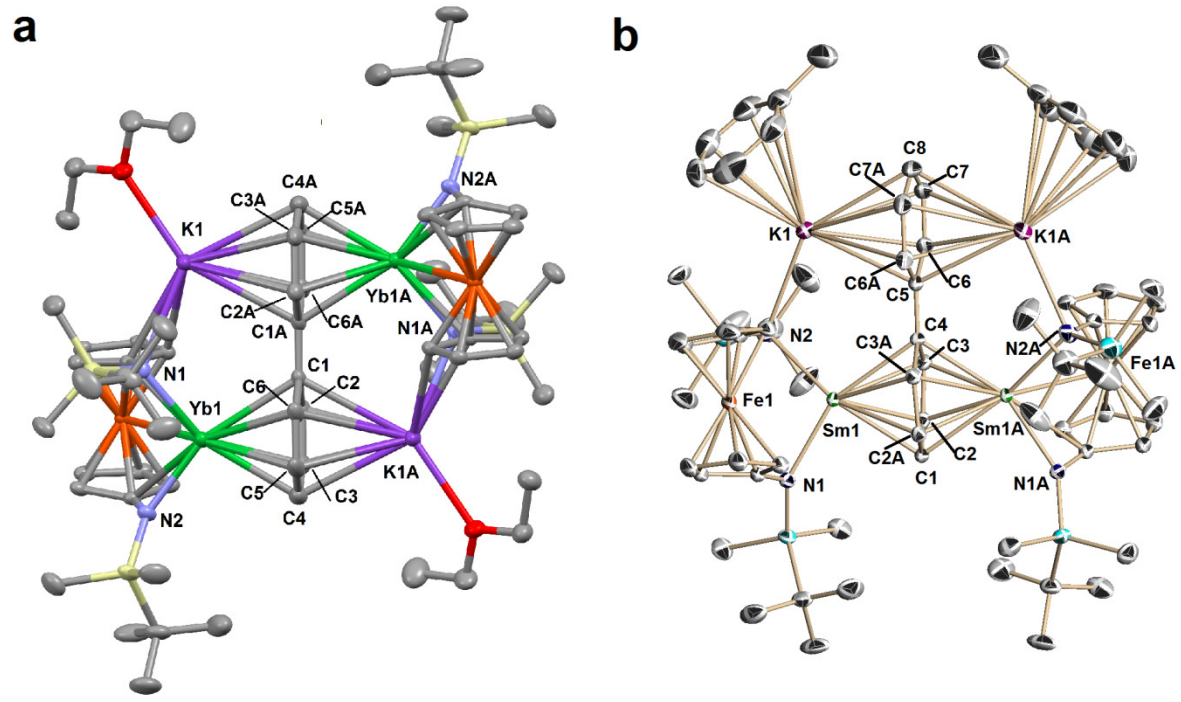

Figure 6-6: Molecular structures of **Yb_2K_2-biph** (a) and **Sm_2K_2-biph** (b) with thermal ellipsoids drawn at the 50% probability level. Hydrogen atoms are omitted for clarity. Selected distances [Å]: (a) **Yb_2K_2-biph**: Yb1-N1 2.392(3), Yb1-N2 2.310(3), Yb1-C1 2.861(4), Yb1-C2 2.816(4), Yb1-C3 2.797(4), Yb1-C4 2.774(4), Yb1-C5 2.779(4), Yb1-C6 2.802(4), Yb1-Fe1 3.098(1), C1-C1A 1.395(7), C1-C2 1.473(5), C1-C6 1.474(5), C2-C3 1.382(6), C3-C4 1.420(7), C4-C5 1.420(7), C5-C6 1.385(6). (b) **Sm_2K_2-biph**: Sm1-N1 2.339(3), Sm1-N2 2.452(3), Sm1-C1 2.618(3), Sm1-C2 2.641(4), Sm1-C3 2.573(4), Sm1-C4 2.622(3), Sm1-C2A 2.574(4), Sm1-C3A 2.642(4), Sm1-Fe1 3.225(1), C1-C2 1.426(5), C2-C3 1.468(5), C3-C4 1.478(4), C4-C5 1.414(7), C5-C6 1.448(5), C6-C7 1.398(7), C7-C8 1396(8).

6.5 Experimental section

Table 6-5: Elemental analysis results for some $MX_3(THF)_y$.

$MX_3(THF)_y$	Molecular weight	Calculated C / H / N	Found C / H / N
$ScCl_3(THF)_{1.5}$	259.476	27.77 / 4.66 / 0	20.93 / 3.29 / <0.1
$ScBr_3(THF)_{2.5}$	464.936	25.83 / 4.34 / 0	22.80 / 3.22 / <0.1
$YCl_3(THF)_{3.5}$	447.640	37.56 / 6.30 / 0	35.79 / 5.95 / <0.1
$LaBr_3(THF)_4$	667.046	28.81 / 4.84 / 0	24.33 / 3.70 / <0.1
$NdCl_3(THF)_{2.5}$	430.868	27.88 / 4.68 / 0	23.53 / 3.42 / <0.1
$GdCl_3(THF)_{3.5}$	515.984	32.59 / 5.47 / 0	28.62 / 4.56 / <0.1
$HoCl_3(THF)_{3.5}$	523.664	32.11 / 5.39 / 0	27.79 / 3.92 / <0.1
$ErCl_3(THF)_{3.5}$	525.992	31.97 / 5.37 / 0	29.39 / 4.52 / <0.1
$LuCl_3(THF)_3$	497.647	28.96 / 4.86 / 0	25.52 / 4.15 / <0.1

Synthesis of $HoBn_3(THF)_3$ by using 2.4 equiv KBn. To 1.500 g $HoCl_3(THF)_{3.5}$ (2.86 mmol) placed in a 100 mL round bottom flask was added 80 mL of THF. The flask was placed in a -78 °C dry ice/acetone or isopropanol bath for at least 15 min. 0.895 g KBn (6.87 mmol, 2.4 equivalents) was weighed in a scintillation vial, dissolved in 15 mL of THF, and cooled down in a -78 °C bath. The KBn solution was added drop-wisely to the $HoCl_3(THF)_{3.5}$ slurry at -78 °C with stirring. The red color of KBn disappeared immediately after mixing. The reaction mixture was allowed to stir in a 0 °C ice bath for 30 min and then filtered through Celite on a coarse frit. The flask and coarse frit were washed with 10 mL of THF. The volatiles were removed under reduced pressure. The resulting oily solid was dissolved in a minimum amount of THF (ca. 12 mL), transferred to a vial, and layered with 8 mL hexanes. Pink crystals were formed after three

days of storing in a -35 °C freezer along with some grey precipitate. The mother liquor and grey precipitate were decanted and the pink crystals were washed with hexanes and dried under reduced pressure. Yield: 0.552 g, 36.8% (29.4% based on Ho). Single crystals of $HoBn_3(THF)_3$ were obtained by recrystallization of the aforementioned pink crystals from a dilute THF solution layered with hexanes. ^{1}H NMR (300 MHz, C_6D_6, 25 °C) δ, ppm: 39.9 (br s), 16.1 (s), 1.6 (br s), and -76.1 (br s). The compound was paramagnetic and most peaks were too broad to get reasonable integrations. Therefore, there was not sufficient data to make assignment on the peaks. Anal. (%): Calcd. for $C_{33}H_{45}O_3Ho$, M_w = 654.650: C, 60.55; H, 6.92; N, 0. Found: C, 59.86; H, 6.70; N, <0.1.

Synthesis of $HoBn_3(THF)_3$ using 3 equiv KBn: Scale: 1.489 g $HoCl_3(THF)_{3.5}$ (2.84 mmol) and 1.111 g KBn (8.53 mmol). The procedure was the same as using 2.4 equiv KBn. Yield: 1.416 g, 76.1%.

General method for *in situ* synthesis of (NN^{TBS})MBn(THF): Using (NN^{TBS})HoBn(THF) and 2.4 equiv KBn as an example, the protocols for the other (NN^{TBS})MBn(THF) or using 3 equiv KBn were similar unless otherwise specified. To 1.0000 g $HoCl_3(THF)_{3.5}$ (1.91 mmol) placed in a 100 mL round bottom flask was added 70 mL of THF. The flask was placed in a -78 °C dry ice/acetone or isopropanol bath for at least 15 min. 0.5967 g KBn (4.58 mmol, 2.4 equivalents) was weighed in a scintillation vial, suspended in 10 mL of THF and cooled down in a -78 °C bath. The KBn solution was added drop-wisely to the $HoCl_3(THF)_{3.5}$ slurry at -78 °C with stirring. The red color of the KBn solution disappeared shortly after mixing. The reaction mixture was allowed to stir at 0 °C in an ice bath for 30 min and then filtered through Celite on a coarse frit. The flask and coarse frit were washed with 10

mL THF and the washings combined with the previous filtrate. The resulting light pink solution was transferred to a clean 100 mL round bottom flask and placed in a -78 °C dry ice/acetone or isopropanol bath for at least 15 min. 0.6792 g $H_2(NN^{TBS})$, (1.53 mmol, 0.8 equiv) was weighed in a scintillation vial, dissolved in 10 mL THF and cooled down in a -78 °C bath for 5 min. The $H_2(NN^{TBS})$ solution was added drop-wisely to the aforementioned light pink solution at -78 °C with stirring. The solution color turned to pale yellow upon addition. The reaction mixture was allowed to stir at -78 °C for 30 min. The volatiles were removed under reduced pressure. The resulting yellow solid was extracted with 20 mL of toluene and filtered through Celite on a coarse frit. The volatiles were removed under reduced pressure. Recrystallization from a concentrated toluene solution layered with *n*-pentane gave (NN^{TBS})HoBn(THF) as yellow crystals after three days of storing in a -35 °C freezer. Yield: 0.2093 g. The mother liquor was dried under reduced pressure to yield a yellow solid which was washed with 15 mL of *n*-pentane and collected on a medium frit to give a 2nd crop as a yellow powder: 0.4142 g. Total yield: 0.6235 g, 53.0% (based on $H_2(NN^{TBS})$ and 42.4% based on Ho). Single crystals of (NN^{TBS})HoBn(THF) were obtained from a dilute toluene solution layered with hexanes. ^{1}H NMR (300 MHz, C_6D_6, 25 °C) δ, ppm: 299.5 and 210.1 (br s, 12H, SiCH_3), 169.6 (br s, 18H, C(CH_3)$_3$), -59.9 (br s), -71.8 (br s), -126.4 (br s), -137.1 (br s), -159,5 (br s), -171.2 (br s), -211.4 (br s), and -306.1 (br s). The compound was paramagnetic and most peaks (except for 299.5, 210.1, and 169.6) were too broad to get reasonable integrations. Therefore, there was not sufficient data to make assignment on those peaks. Anal. (%): Calcd. for $C_{33}H_{53}N_2OFeHoSi_2$, M_w = 770.747: C, 51.43; H, 6.93; N, 3.63. Found: C, 50.91; H, 7.63; N, 4.32.

Synthesis of (NN^{TBS})HoBn(THF) using 3 equiv KBn and 1 equiv $H_2(NN^{TBS})$. Scale: 0.800 g $HoCl_3(THF)_{3.5}$ (1.53 mmol), 0.597 g KBn (4.58 mmol), and 0.679 g $H_2(NN^{fc})$ (1.53 mmol). The procedure was the same as using 2.4 equiv KBn. Yield: 1st crop 0.258 g, 2nd crop 0.211 g, total 39.8%.

General method for *in situ* synthesis of (NN^{TBS})MI(THF)$_x$. Using (NN^{TBS})HoI(THF)$_2$ as an example, the protocols for the other (NN^{TBS})MI(THF)$_z$ or using 3 equiv KBn were similar unless otherwise specified. To 1.300 g $HoCl_3(THF)_{3.5}$ (2.48 mmol) placed in a 100 mL round bottom flask was added 70 mL of THF. The flask was placed in a -78 °C dry ice/acetone or isopropanol bath for at least 15 min. 0.781 g KBn (6.00 mmol, 2.4 equiv) was weighed in a scintillation vial, dissolved in 10 mL of THF, and cooled down in a -78 °C bath. The KBn solution was added drop-wisely to the $HoCl_3(THF)_{3.5}$ slurry at -78 °C with stirring. The red color of the KBn solution disappeared shortly after mixing. The reaction mixture was allowed to stir at 0 °C in an ice bath for 30 min and then filtered through Celite on a coarse frit. The flask and coarse frit were washed with 10 mL of THF and the washings combined with the previous filtrate. The resulting light pink solution was transferred to a clean 100 mL round bottom flask and placed in -78 °C dry ice/acetone or isopropanol bath for at least 15 min. 0.883 g $H_2(NN^{TBS})$ (1.99 mmol, 0.8 equiv) was weighed in a scintillation vial, dissolved in 10 mL of THF and cooled down in -78 °C bath for 5 min. The $H_2(NN^{TBS})$ solution was added drop-wisely to the aforementioned light pink solution at -78 °C with stirring. The solution color turned to pale yellow upon addition. The reaction mixture was allowed to stir at -78 °C for 30 min. The volatiles were removed under reduced pressure. The resulting yellow solid was extracted with 15 mL toluene and filtered through Celite on a coarse frit. The toluene filtrate was transferred to a

scintillation vial. 0.8559 g Me_3SiI (4.28 mmol, 1.73 equiv) was added drop-wisely as a toluene solution (2 mL) at ambient temperature and the reaction mixture was allowed to stir for 1 h. At the end of the reaction, 5 mL of THF was added to quench the extra Me_3SiI. The volatiles were removed under reduced pressure. The resulting yellow solid was dissolved in a minimum amount of Et_2O layered with *n*-pentane. Yellow crystals as $(NN^{TBS})HoI(THF)_2$ formed after three days of storing in a -35 °C freezer. Yield: 0.818 g. After decanting, the mother liquor was concentrated and stored in a -35 °C freezer to give a 2nd crop: 0.351 g. Total yield: 1.169 g, 68.4% (based on $H_2(NN^{fc})$, 54.7% based on Ho). Single crystals of $(NN^{TBS})HoI(THF)_2$ were obtained from an Et_2O solution layered with hexanes. ^1H NMR (300 MHz, C_6D_6, 25 °C) δ, ppm: 315.7 (br s, 12H, SiCH_3), 199.6 (br s, 18H, C(CH_3)$_3$), -137.4 (br s), -142.5 (br s), and -223.6 (br s). The compound was paramagnetic and most peaks (except for 315.7 and 199.6) were too broad to get reasonable integrations. Therefore, there was not sufficient data to make assignment on those peaks. Anal. (%): Calcd. for $C_{30}H_{54}N_2O_2FeIHoSi_2$, M_w = 878.625, with 0.25 molecules of *n*-pentane: C, 41.86; H, 6.41; N, 3.12. Found: C, 41.75; H, 6.34; N, 3.08.

Synthesis of $(NN^{TBS})HoI(THF)_2$ using 3 equiv KBn and 1 equiv $H_2(NN^{TBS})$. Scale: 0.800 g $HoCl_3(THF)_{3.5}$ (1.53 mmol), 0.597 g KBn (4.58 mmol), 0.679 g $H_2(NN^{TBS})$ (1.53 mmol), and 0.611 g Me_3SiI (3.05 mmol). The procedure was the same as using 2.4 equiv KBn. Yield: 1st crop 0.520 g, 2nd crop 0.380 g, total 67.0%.

Experimental details for magnetic measurements on Dy_2K_2-biph: A magnetic analysis was performed on crushed polycrystalline samples of **Dy_2K_2-biph**, wrapped in a polyethylene membrane sealed in a glove box to prevent any sample degradation. The direct current (dc) magnetic susceptibility measurements were obtained using a Quantum Design

Superconducting Quantum Interference Device (SQUID) magnetometer MPMS-XL7 operating between 1.8 and 300 K for dc-applied fields ranging from −7 to 7 T. Alternating current (ac) susceptibility measurements were carried out under an oscillating ac field of 3 Oe and ac frequencies ranging from 1 to 1500 Hz. Diamagnetic corrections were applied for the sample holder and the core diamagnetism from the sample (estimated with Pascal constants).

Experimental details on XANES measurements: X-ray absorption measurements were acquired on the bending magnet beam line of the Materials Research Collaborative Access Team (MRCAT) at the Advanced Photon Source, Argonne National Laboratory. The data was collected in transmission step scan mode. Photon energies were selected using a water-cooled, double-crystal Si(111) monochromator, which was detuned by approximately 50% to reduce harmonic reflections. The ionization chambers were optimized for the maximum current with linear response (~10^{10} photons detected/sec) with 10% absorption in the incident ion chamber and 70% absorption in the transmission and fluorescent X-ray detector. Mn foil and Cu foil was used to calibrate the energy for Sm and Yb measurements, respectively.

Air sensitive samples were prepared in a glove box diluted with boron nitride. The edge energy was determined from the inflection point in the edge, i.e., the maximum in the first derivative of the XANES spectrum. Background and normalization procedures were carried out using the Athena software package using standard methods.

6.6 References

(1) Kagan, H. B. *Chem. Rev.* **2002**, *102*, 1805.

(2) Shannon, R. *Acta Cryst.* **1976**, *A32*, 751.

(3) Binnemans, K. *Chem. Rev.* **2009**, *109*, 4283.

(4) Bünzli, J.-C. G. *Chem. Rev.* **2010**, *110*, 2729.

(5) Sorace, L.; Benelli, C.; Gatteschi, D. *Chem. Soc. Rev.* **2011**, *40*, 3092.

(6) Rinehart, J. D.; Fang, M.; Evans, W. J.; Long, J. R. *J. Am. Chem. Soc.* **2011**, *133*, 14236.

(7) Tuna, F.; Smith, C. A.; Bodensteiner, M.; Ungur, L.; Chibotaru, L. F.; McInnes, E. J. L.; Winpenny, R. E. P.; Collison, D.; Layfield, R. A. *Angew. Chem. Int. Ed.* **2012**, *51*, 6976.

(8) Woodruff, D. N.; Winpenny, R. E. P.; Layfield, R. A. *Chem. Rev.* **2013**, *113*, 5110.

(9) Edelmann, F. T.; Freckmann, D. M. M.; Schumann, H. *Chem. Rev.* **2002**, *102*, 1851.

(10) Marks, T. J. *Organometallics* **2013**, *32*, 1133.

(11) Zimmermann, M.; Anwander, R. *Chem. Rev.* **2010**, *110*, 6194.

(12) Bambirra, S.; Perazzolo, F.; Boot, S. J.; Sciarone, T. J. J.; Meetsma, A.; Hessen, B. *Organometallics* **2008**, *27*, 704.

(13) Harder, S. *Organometallics* **2005**, *24*, 373.

(14) Harder, S.; Ruspic, C.; Bhriain, N. N.; Berkermann, F.; Schürmann, M. *Z. Naturforsch. B: Chem. Sci.* **2008**, *63b*, 267

(15) Zhang, W.-X.; Nishiura, M.; Mashiko, T.; Hou, Z. *Chem. Eur. J.* **2008**, *14*, 2167.

(16) Bambirra, S.; Bouwkamp, M. W.; Meetsma, A.; Hessen, B. *J. Am. Chem. Soc.* **2004**, *126*, 9182.

(17) Bambirra, S.; Meetsma, A.; Hessen, B.; Bruins, A. P. *Organometallics* **2006**, *25*, 3486.

(18) Bambirra, S.; van Leusen, D.; Tazelaar, C. G. J.; Meetsma, A.; Hessen, B. *Organometallics* **2007**, *26*, 1014.

(19) Wooles, A. J.; Mills, D. P.; Lewis, W.; Blake, A. J.; Liddle, S. T. *Dalton Trans.* **2010**, *39*, 500.

(20) Izod, K.; Liddle, S. T.; Clegg, W. *Inorg. Chem.* **2003**, *43*, 214.

(21) Carver, C. T.; Monreal, M. J.; Diaconescu, P. L. *Organometallics* **2008**, *27*, 363.

(22) Carver, C. T.; Diaconescu, P. L. *J. Am. Chem. Soc.* **2008**, *130*, 7558.

(23) Carver, C. T.; Benitez, D.; Miller, K. L.; Williams, B. N.; Tkatchouk, E.; Goddard, W. A.; Diaconescu, P. L. *J. Am. Chem. Soc.* **2009**, *131*, 10269.

(24) Carver, C. T.; Diaconescu, P. L. *J. Alloys Compd.* **2009**, *488*, 518.

(25) Williams, B. N.; Huang, W.; Miller, K. L.; Diaconescu, P. L. *Inorg. Chem.* **2010**, *49*, 11493.

(26) Miller, K. L.; Williams, B. N.; Benitez, D.; Carver, C. T.; Ogilby, K. R.; Tkatchouk, E.; Goddard, W. A.; Diaconescu, P. L. *J. Am. Chem. Soc.* **2010**, *132*, 342.

(27) Diaconescu, P. L. *Comments Inorg. Chem.* **2010**, *31*, 196

(28) Diaconescu, P. L. *Acc. Chem. Res.* **2010**, *43*, 1352.

(29) Jie, S.; Diaconescu, P. L. *Organometallics* **2010**, *29*, 1222.

(30) Miller, K. L.; Carver, C. T.; Williams, B. N.; Diaconescu, P. L. *Organometallics* **2010**, *29*, 2272.

(31) Wong, A. W.; Miller, K. L.; Diaconescu, P. L. *Dalton Trans.* **2010**, *39*, 6726.

(32) Huang, W.; Carver, C. T.; Diaconescu, P. L. *Inorg. Chem.* **2011**, *50*, 978.

(33) Broderick, E. M.; Thuy-Boun, P. S.; Guo, N.; Vogel, C. S.; Sutter, J.; Miller, J. T.; Meyer, K.; Diaconescu, P. L. *Inorg. Chem.* **2011**, *50*, 2870.

(34) Williams, B. N.; Benitez, D.; Miller, K. L.; Tkatchouk, E.; Goddard, W. A.; Diaconescu, P. L. *J. Am. Chem. Soc.* **2011**, *133*, 4680.

(35) Huang, W.; Khan, S. I.; Diaconescu, P. L. *J. Am. Chem. Soc.* **2011**, *133*, 10410.

(36) Huang, W.; Diaconescu, P. L. *Chem. Commun.* **2012**, *48*, 2216.

(37) Huang, W.; Diaconescu, P. L. *Inorg. Chim. Acta* **2012**, *380*, 274.

(38) Bambirra, S.; Meetsma, A.; Hessen, B. *Organometallics* **2006**, *25*, 3454.

(39) Miller, K. L.; Williams, B. N.; Benitez, D.; Carver, C. T.; Ogilby, K. R.; Tkatchouk, E.; Goddard, W. A.; Diaconescu, P. L. *J. Am. Chem. Soc.* **2009**, *132*, 342.

(40) Carver, C. T.; Williams, B. N.; Ogilby, K. R.; Diaconescu, P. L. *Organometallics* **2010**, *29*, 835.

(41) Edleman, N. L.; Wang, A.; Belot, J. A.; Metz, A. W.; Babcock, J. R.; Kawaoka, A. M.; Ni, J.; Metz, M. V.; Flaschenriem, C. J.; Stern, C. L.; Liable-Sands, L. M.; Rheingold, A.

L.; Markworth, P. R.; Chang, R. P. H.; Chudzik, M. P.; Kannewurf, C. R.; Marks, T. J. *Inorg. Chem.* **2002**, *41*, 5005.

(42) Meyer, G.; Garcia, E.; Corbett, J. D. In *Inorganic Syntheses*; John Wiley & Sons, Inc.: 2007, p 146.

(43) Huang, W.; Upton, B. M.; Khan, S. I.; Diaconescu, P. L. *Organometallics* **2013**, *32*, 1379.

(44) Reed, J. B.; Hopkins, B. S.; Audrieth, L. F.; Selwood, P. W.; Ward, R.; Dejong, J. J. In *Inorganic Syntheses*; John Wiley & Sons, Inc.: 1939, p 28.

(45) Haschke, J. M. *J. Chem. Thermodynamics* **1973**, *5*, 283.

(46) Plumley, J. A.; Evanseck, J. D. *J. Phys. Chem. A* **2009**, *113*, 5985.

(47) Meyer, N.; Roesky, P. W.; Bambirra, S.; Meetsma, A.; Hessen, B.; Saliu, K.; Takats, J. *Organometallics* **2013**, *32*, 3427.

(48) Meyer, N.; Roesky, P. W.; Bambirra, S.; Meetsma, A.; Hessen, B.; Saliu, K.; Takats, J. *Organometallics* **2008**, *27*, 1501.

(49) Bochkarev, L. N.; Zheleznova, T. A.; Safronova, A. V.; Drozdov, M. S.; Zhil'tsov, S. F.; Zakharov, L. N.; Fukin, G. K.; Khorshev, S. Y. *Russ. Chem. Bull.* **1998**, *47*, 165.

(50) Atwood, J. L.; Hunter, W. E.; Rogers, R. D.; Holton, J.; McMeeking, J.; Pearce, R.; Lappert, M. F. *J. Chem. Soc., Chem. Commun.* **1978**, 140.

(51) Schumann, H.; Müller, J. *J. Organomet. Chem.* **1978**, *146*, C5.

(52) Bochkarev, L. N.; Stepantseva, T. A.; Zakharov, L. N.; Fukin, G. K.; Yanovsky, A. I.; Struchkov, Y. T. *Organometallics* **1995**, *14*, 2127.

(53) Edwards, P. G.; Andersen, R. A.; Zalkin, A. *Organometallics* **1984**, *3*, 293.

(54) Döring, C.; Kempe, R. *Z. Kristallogr. NCS* **2008**, *223*, 397.

(55) MacDonald, M. R.; Bates, J. E.; Fieser, M. E.; Ziller, J. W.; Furche, F.; Evans, W. J. *J. Am. Chem. Soc.* **2012**, *134*, 8420.

(56) Duhovic, S.; Khan, S.; Diaconescu, P. L. *Chem. Commun.* **2010**, *46*, 3390.

(57) Cordero, B.; Gomez, V.; Platero-Prats, A. E.; Reves, M.; Echeverria, J.; Cremades, E.; Barragan, F.; Alvarez, S. *Dalton Trans.* **2008**, 2832.

(58) Tsuruta, H.; Imamoto, T.; Yamaguchi, K. *Chem. Commun.* **1999**, *0*, 1703.

(59) Fryzuk, M. D.; Love, J. B.; Rettig, S. J. *J. Am. Chem. Soc.* **1997**, *119*, 9071.

CHATPER 7: SUMMARY AND OUTLOOK

By utilizing an electronically and geometrically flexible ferrocene diamide ligand (NN^{TBS} = 1,1′-fc(NSi^tBuMe_2)$_2$) in the reduction chemistry of rare-earths, unprecedented reactivity was discovered together with the synthesis and characterization of a series of rare-earth metal arene complexes. Highlights include: (1) the discovery of a new aromatic C-H/F bond activation mechanism for rare-earth metals; (2) the synthesis of the first scandium naphthalene complex and its reactivity toward P_4 activation; (3) the isolation and characterization of a 6C, 10π-electron aromatic system stabilized by coordination to rare-earth metal ions (as shown in the figure below).

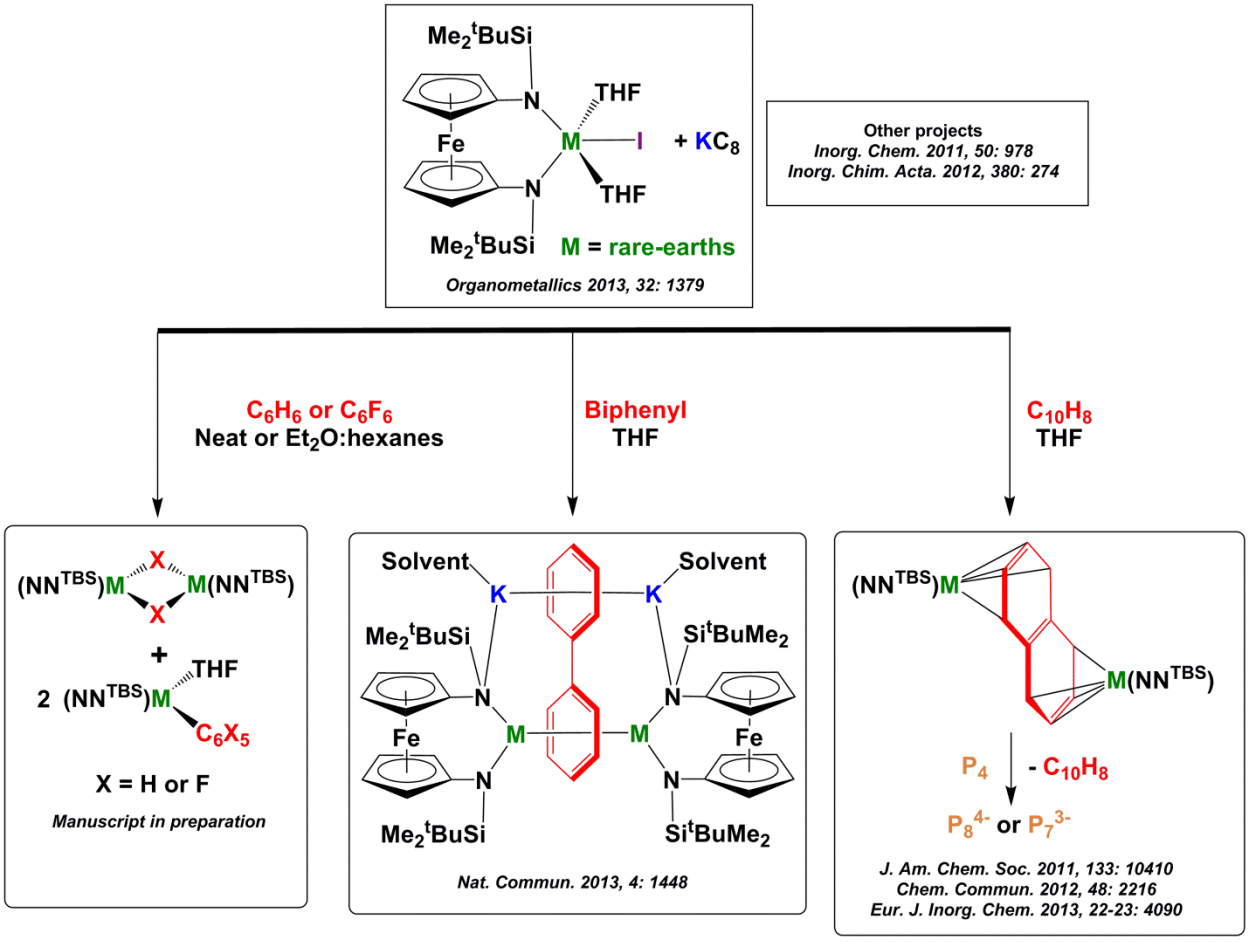

Reductive cleavage of aromatic C-H and C-F bonds: Our initial target was to achieve dinitrogen reduction with the $(NN^{TBS})ScI(THF)_2/KC_8$ system. However, when treating $(NN^{TBS})ScI(THF)_2$ with KC_8 in benzene, no $(N_2)^{x-}$ complexes were observed; instead, $[(NN^{TBS})Sc]_2(\mu\text{-}H)_2$ and $(NN^{TBS})Sc(C_6H_5)(THF)$ were formed in a 1:1 molar ratio per scandium. This C-H bond activation mode is unprecedented for group 3 metal complexes. Since the reaction was carried out under reducing conditions, the term "reductive cleavage" was coined to describe it. Inter- and intramolecular kinetic isotope effects, regio-selectivity for toluene, and C-H bond activation from the isolated $[(NN^{TBS})Lu]_2(\mu\text{-}C_{10}H_8)$ were consistent with the proposed mechanism: a bridging benzene dianion intermediate was formed upon reduction that quickly led to C-H bond cleavage to give a metal hydride and a metal phenyl species; the reaction is driven by the high Lewis acidity of rare-earth metals. The mechanism was further supported by DFT calculations (collaboration with Dr. Cantat at CEA, France). This reaction mode could be extended to C-F bond activation. When treating $(NN^{TBS})ScI(THF)_2$ with 5 equiv of C_6F_6 and 3 equiv of KC_8 in a mixture of solvents (Et_2O : hexanes = 3:1), clean C-F bond cleavage occurred and led to the formation of $[(NN^{TBS})Sc]_2(\mu\text{-}F)_2$ and $(NN^{TBS})Sc(C_6F_5)(THF)$ in a 1:1 molar ratio per scandium. Other rare earth metals, such as lutetium, yttrium, and erbium, were found to behave similarly.

Fused arene complexes and white phosphorus (P_4) activation: A bridging benzene dianion was proposed to be the key intermediate in the reductive cleavage of aromatic C-H bonds; however, its isolation was not possible due to its high reactivity. Consequently, more redox accessible fused arene anions were targeted as an alternative. Scandium, yttrium, lanthanum, and lutetium naphthalene and anthracene complexes were readily accessible from the reaction of $(NN^{TBS})MI(THF)_2$, KC_8, and the fused arene. $[(NN^{TBS})M]_2(\mu\text{-}C_{10}H_8)$ were found to

be excellent two electron reductants toward various substrates, such as 2,2′-bipyridine and pyridine. More prominently, P_4 activation was achieved by these complexes under mild conditions in a controlled fashion to form polyphosphides P_8^{4-} and P_7^{3-} complexes in high yield. It was found that rare-earth metal arene compounds combine the advantages of alkali metal reagents and transition metal complexes by showing both high reactivity and high selectivity toward small molecule activation.

Biphenyl tetraanion in $[(NN^{TBS})M]_2)[K(solvent)]_2(\mu$-biphenyl): Since fused (naphthalene) and non-fused arenes (benzene) behaved differently under reducing conditions, the reactivity of the weakly conjugated biphenyl became of great interest. Regardless of the stoichiometry, the reaction of $(NN^{TBS})YI(THF)_2$, KC_8, and biphenyl in tetrahydrofuran led to the same product, $\{[(NN^{TBS})Y]_2(\mu\text{-biphenyl})\}[K(solvent)]_2$. X-ray crystallography established that the complex contained a biphenyl ligand with the yttrium ions coordinated to the same ring and two potassium ions to the other phenyl ring. The potassium ions were not required to maintain the rigid structure and no significant geometric change was observed upon removal of potassium ions by addition of 18-crown-6. A variable temperature ^1H NMR spectroscopic study confirmed that the solution structure was similar to the solid state structure with no fluxional behavior. The molecular structure and multi-nuclear (^1H, ^{13}C, and ^{89}Y) NMR spectroscopic data suggested that the biphenyl was reduced by four electrons and the four negative charges were mainly localized on the phenyl ring bridging the two yttrium ions, indicating an unprecedented 6C, 10π-electron aromatic system. Further evidence was collected to support this interpretation. X-ray absorption near edge structure spectroscopy (collaboration with Dr. Miller at Argonne National Laboratory) confirmed the oxidation state of the metals: Y(III) and Fe(II). DFT calculations agreed with a biphenyl tetraanion: HOMO and HOMO-1 were mainly the π^* orbitals of the phenyl ring with

some overlap to yttrium d orbitals and minimum conjugation to the adjacent phenyl ring (collaboration with Dr. Cantat at CEA, France). Subsequently, we found that the biphenyl tetraanion was able to mediate electronic and magnetic communication between two metal ions. Recently, we extended the reduction chemistry from diamagnetic group 3 metals to paramagnetic lanthanides in order to explore their magnetic properties. Preliminary results show that $[(NN^{TBS})Dy]_2[K(OEt_2)]_2$(μ-biphenyl) behaves as a single molecule magnet with U_{eff} = 53 K and $t_0 = 1.5*10^{-7}$ s (collaboration with Professor Murugesu at University of Ottawa). In addition, $[(NN^{TBS})Yb]_2[K(OEt_2)]_2$(μ-biphenyl) was found to be different from other rare-earth biphenyl complexes in its electronic structure (collaboration with Dr. Miller at Argonne National Laboratory).

In summary, the fruitful reduction chemistry of rare earth metals, featuring reductive cleavage of aromatic C-X (X = H and F) bonds and novel rare-earth arene complexes, was made possible by utilizing a ferrocene diamide ligand platform. Future work is directed toward studying in depth the electronic structure and the reactivity of the biphenyl complexes. Rare-earth complexes of the biphenyl tetraanion have a promising future in fundamental research, for the understanding of bonding to rare-earths, as well as in applications, a result of their unique physical properties.